

Volume 2 Year 2022

ADVANCED ENGINEERING SCIENCE



ADVANCED ENGINEERING SCIENCE

Aim and scope

Advanced Engineering Science (ADES) is a multidisciplinary journal and covers all fields of basic science and engineering. The Journal is involved in both experimental and theoretical studies on the subject area of basic science and engineering. The Journal is a multidisciplinary journal and covers all fields of basic science and engineering. It is the main purpose of the Journal that to convey the latest development on science and technology towards the related scientists and to the readers. The Journal is also involved in both experimental and theoretical studies on the subject area of basic science and engineering. ADES is a fully free journal, which does not take any article processing charge from authors.

Advanced Engineering Science (ADES) is a multidisciplinary journal and covers all fields of basic science and engineering

- Aerospace Engineering
- Environmental Engineering
- Civil Engineering
- Geomatics Engineering
- Mechanical Engineering
- Geology Science and Engineering
- Mining Engineering
- Chemical Engineering
- Metallurgical and Materials Engineering
- Electrical and Electronics Engineering
- Mathematical Applications in Engineering
- Computer Engineering
- Food Engineering

Editor

Prof. Dr. Murat Yakar

Mersin University, Department of Geomatics Engineering (myakar@mersin.edu.tr)

Advisory Board

Prof. Dr. Mehmet Cihan AYDIN, BITLIS EREN UNIVERSITY (mcaydin@beu.edu.tr)

Associate Professor Ercan IŞIK, BITLIS EREN UNIVERSITY (eisik@beu.edu.tr)

Associate Professor Ümit BUDAK, BITLIS EREN UNIVERSITY (ubudak@beu.edu.tr)

Associate Professor. Mehmet Baran, Ankara Yıldırım Beyazıt University (mehmet.baran@ybu.edu.tr)

Associate Professor. Memduh Kara, Mersin University (memduhkara@mersin.edu.tr)

Associate Professor. Cafer Erkın Koyuncu, Mersin University (ckoyuncu@mersin.edu.tr)

Asst. Prof Atta-ur-Rahman, University of Peshawar (atta-ur-rehman@uop.edu.pk)

Dr. Mehmet Levent Ağırđır, Konya Technical University, Konya/ Turkey (mلاغirdir@ktun.edu.tr)

Dr. Fazal Raziq, King Abdullah University Science and Technology, Saudi Arabia (fazal.raziq@kaust.edu.sa)

Abdell Aziiz Fatthii Abdell Aziiz Ellfadally, Basilicata University / Italian National Research Councils / National Authority for Remote Sensing and Space Sciences (abdelaziz.elfadaly@narss.sci.eg) / (abdelaziz.elfadaly@imaa.cnr.it)

Lec. Mustafa Buber, Selçuk University (mbuber@selcuk.edu.tr)

Technical support: Research Assistant Aydın Alptekin aydinalptekin@mersin.edu.tr

RESEARCH ARTICLES

Volume 2

Determination and modelling of PM2.5 level in summer time in Selcuk University Shopping Centre Konya, Turkey Sukru Dursun, Mina Naseer Qasim	1-8
Investigation of emission control efficiency with gasoline vapor recovery units Ece Kalay, Hasan Sarioğlu, İskender Özkul	9-14
Importance of electrode type and configuration on reaction kinetics in removal of tetracycline antibiotic by electrocoagulation Bahadır K. Körbahti, Meltem Gökteş	15-20
Investigation of failed node method to support healthy communication for linear wireless sensor networks Musa Çibuk, Davut Arı, Fikri Ağgün, Ümit Budak	21-26
PM2.5 concentration measurements and mapping at Gokusagi Mall for autumn 2018, in Konya, Turkey Sukru Dursun, Mina Naseer Qasim	27-34
Geological factors in solid waste landfill site selection Omer Kagan Arici	35-43
Effect of fiber content on the liquefaction potential of improved soils Özgür Lütfi Ertuğrul, Fatma Dülger Canoğulları	44-51
Adsorption of Astrazon red GTLN (AR) with volcanic tuff Bayburt Stone Beyhan Kocadağistan, Erdem Kocadağistan	52-59
Energy dissipation potential of flow separators placed in spillway flip bucket Ali Emre Ulu, Mehmet Cihan Aydın, Ercan Işık	60-66
Modelling of supercapacitor by using parameter estimation method for energy storage system Gökhan Yüksek, Yusuf Muratoğlu, Alkan Alkaya	67-73
Geotechnical examination of Ermenek District in the Province of Karaman Fevzi Sevimli, İsa Kul	74-79
Comparison of infill wall effects in reinforced-concrete frames over different parameters Ercan Işık, Mehmet Cihan Aydın, Ali Emre Ulu	80-86
Evaluation of the soil conditions in Alikahya Region (Izmit) Talas Fikret Kurnaz	87-92
Assessment of the artificial fiber contribution on the shear strength parameters of soils Özgür Lütfi Ertuğrul, Furkan İnal	93-100
Determination of water quality in Hadim District of Konya (Turkey) and the investigation of disinfection efficiency Sukru Dursun, Abdurrahman Sarcan	101-108
The effects of the EU Green Deal harmonization policies in Turkey Aziz Cumhur Kocalar	109-117
On behalf of an intelligent approach based on 3D CNN and multimodal remote sensing data for precise crop yield estimation: Case study of wheat in Morocco Khadija Meghraoui, Imane Sebari, Saloua Bensiali, Kenza Ait El Kadi	118-126
Gabion structures and retaining walls design criteria Esra Uray	127-134



Determination and modelling of PM2.5 level in summer time in Selcuk University Shopping Centre Konya, Turkey

Sukru Dursun ^{*1}, Mina Naseer Qasim ²

¹Konya Technical University, Environmental Engineering Department, Türkiye, sdursun@ktun.edu.tr; mineenviro@gmail.com

Cite this study: Dursun, S., & Naseer Qasim, M. (2022). Determination and modelling of PM2.5 level in summer time in Selcuk University Shopping Centre Konya. *Advanced Engineering Science*, 2, 01-08

Keywords

Air quality
Indoors
Measuring
Modelling
Particulate matters
PM2.5
Shopping centers

Research Article

Received: 05.01.2022
Revised: 11.02.2022
Accepted: 19.02. 2022
Published: 14.03.2022



Abstract

Most of the people spend their most more the time in closed environments during their life. The quality of living atmosphere is really important because of this long contact time period. In inhaled respiration air is contain particle matters pollutant sources in the atmospheric environment, like volatile organic compounds, dusts and different sizes of particulate matters. The health impact of these substances has been investigated in recent years on may scientifically research. In this investigation, particulate matter PM2.5 size dimension, which is one of the indoor air pollutants, was carried out in Selcuk University public shopping center and the data were compared according to seasons, weekday and weekends. For the preparing 3-dimensional mapping, Surfer v.16 computer packed program was used and data modelling was investigated. Certain intervals were measured during three seasons. The measured shopping center is located in the Alaeddin Keykubat campus of Selcuk University. Measurement PM2.5 values in the center of Gökkuşığı shopping center exceed the standards of WHO, and it was observed that summer values were lower than winter seasons. Higher values were observed in the winter season. In terms of measurement area, higher PM concentrations were found in Gökkuşığı shopping center than in similar shopping malls.

1. Introduction

Many of the epidemiological studies on particulate matter in the world have shown that the high air pollution caused by these substances, respiratory tract diseases, cardio vascular system and lung problems are great importance on human health [1]. The fact that people generally spend about 90% of their time indoors is clear how important the air quality of these environments is. However, most of the studies to determine the amount of particulate matter in the world have been carried out outdoors, and the studies carried out in closed environments are limited [2]. Particulate matter, which is a mixture of organic and inorganic compounds, is defined as an important source of air pollution. These particles, which are generally divided into two groups in terms of mass; defined as coarse particles (above 10 μm) and fine particles (below 2.5 μm). The residence time of the particles in the air depends on the particle size, the smaller the size of the particles, the longer the residence time in the air [3].

While coarse particles (>2.5 μm) are mostly formed as a result of mechanical processes, fine particles (<2.5 μm , PM2.5) and ultrafine particles (<0.1 μm) can also be formed as a secondary pollutant as a result of chemical reactions of gases and fuels, for example diesel. It is the direct discharge of fuels to the environment as a result of combustion [4]. Concentration levels of indoor particles, the main source of which are activities in indoor

environments and outdoor pollution, generally vary due to factors such as the change rate of air, indoor activities, outdoor PM level, aerodynamic diameters of particles released into the environment [5]. Smoking, ventilation mechanisms, heating, cooking and other indoor activities in indoor environments can cause the dispersion of dusts and particles in the indoor environment. When the activities that can cause the dispersion of these particles do not occur, normal activities of people, cleaning activities, moving, skin rashes, dust particles precipitated from fabric and paper fibres may cause the dispersal of dust particles to the environment again [6]. Today, due to the prevalence of research on air pollution and the health problems it causes, it is carried out with the data of outdoor air quality. However, since people spend 87% of their time indoors and these environments have poor air quality, indoor data should be examined instead of outdoor data in order to evaluate the impact of the air in the environment on health.

It is expressed as the air contained in buildings such as workplaces, residences, shopping and living centres, interior spaces of transportation vehicles (bus, car, ship, train, etc.), schools and offices indoor air. Indoor air pollution is the presence of substances that can harm health in the above-mentioned environments. The amount and concentration of these substances in the environment differ according to the characteristics of the environment, the building and interior materials used in the construction of the building, and the behaviour of the individuals in it. For example, the increase in dust and particulate matter rates in the corridors caused by the movements of the students in a school building, as well as the equipment such as printing machine and photocopying machine used in a stationery shop, caused the spread of various volatile organic compounds to the environment. It is a known fact that human performance is affected by indoor air quality. For human comfort and productivity, the indoor environment must be at 19-20°C and the humidity of the air he breathes must be 30-50% [7].

The presence of pollutants in the air by being directly discharged from the source to the atmosphere is called primary particles. Volcanic, soil dust, particles detached from leaf surfaces are all natural main sources of primary particles. Steam generators, traffic, construction and agricultural activities, heating processes are anthropogenic sources. Particles smaller than 1 µm in diameter are usually formed from combustion sources, while particles larger than 1 µm in diameter are formed from natural sources. Secondary particles are the particles formed as a result of the condensation of the primary particles dispersed in the atmosphere with other species in the air, adsorption to the surface and some reactions.

PM_{2.5} exposure threshold has not been defined to provide an unequivocally safe and complete level of protection against all adverse health effects [8]. However, in order to limit the health effects of fine particle pollution, the World Health Organization (WHO) has proposed guidelines for annual and short-term (24 hours) human exposure to PM_{2.5}. In addition to these global standards, WHO encourages governments to define and implement national standards [9]. Along with the guideline levels, WHO has defined three intermediate exposure levels to gradually reduce PM_{2.5} concentrations. In addition, WHO recommends an annual average, with priority over the 24-hour average, as high PM_{2.5} events are generally less harmful than annual exposure to high PM_{2.5} levels. The current WHO's annual average air quality guide (AQG) is 10 µg/m³. Australia and the Canadian province of British Columbia are national jurisdictions that introduced a lower standard of 8 µg/m³ [10, 11].

2. Material and Method

The variation of the levels of air pollutant concentrations between regions in big cities is shaped by the characteristics of the regions [12]. In this study, which was started on the basis of shopping centres located in Selçuklu district of Konya province, it was chosen as the appropriate location for measurements. This place, which was chosen by paying attention to its indoor environment, is located on the campus of Selçuk University.

Social facilities serving students and staff in Selçuk University Alâeddin Keykubat Campus were deemed suitable as a location for carrying out measurements and collecting data. Rainbow is located in front of the medical faculty, approximately 400 meters from the campus entrance. This building, which covers an area of approximately 13000 m², consists of 63 stores, stationery, bookstores and restaurants.

In the northern part of the building, there are two corridors with a width of approximately 2 m on the east and west sides, and the entrances of some shops are within those corridors, the air pollutants circulating in these corridors, which consist of low ceilings, are trapped in a narrow area, causing them to be close to the respiratory level.

Although the shops have their own ventilation systems, they are not available in the common areas. As a result of the fact that the areas with an air blowing system were out of use due to technical failures, a suspended ceiling was built and completely closed. Although the Gökkuşuğu shopping center, which was built and put into operation in 1999, underwent simple renovations over time, no general restoration was carried out from its opening to the working period. 13 points were determined for the measurements to be made in the rainbow (Figure 1).



Figure 1. Selcuk University Alaeddin Keykubat Campus Gökkuşağı shopping centre sampling points (edited from [13])

2.1. Particulate matter meter measurement device

The measurement methods of dust and particles in the air vary according to the volume of the particles and the desired results in the study. Thanks to electronic recording, the data can be displayed numerically in a laser particle counter and dust measuring device “Particle Counter PCE-PC01” configured to determine the concentration of particles in the air. This device is used in clean rooms, indoor air quality, exposure to exhaust, tobacco or cigarette smoke and other harmful air pollutants, and for monitoring airborne dust levels.

The particle counter was developed to precisely determine the pollution level. The device measures 6 different particle sizes (0.3 μm , 0.5 μm , 1.0 μm , 2.5 μm , 5.0 μm , 10 μm), measurements (more than 5000 measurements) can be saved in the internal memory, A large colour LCD with backlight, for image and video recording other features include a built-in camera, air temperature, dew point and relative humidity sensors, displaying the temperature in $^{\circ}\text{C}$ or $^{\circ}\text{F}$. This device, which is deemed suitable for taking measurements at different points in terms of its easy portability, should be charged and prepared before going to the measurement site and zeroed by calibration in a dust-free standard environment before measurement.

The device also has 3 different sampling modes: cumulative, differential (differential) and concentration. The desired mode must be selected before measuring. In addition to these features, the date and time, language and screen brightness can be adjusted optionally from the system settings. In these studies, it is of great importance that the data obtained depending on the sampling and measurement period are constantly (if possible, daily checked) from the memory card of the device to the computer environment in order to avoid data loss.

2.2. Modelling and graphics program Surfer-16

This software, produced by Golden software company, consists of a 3D graphics system. It is used for gridding scattered data recorded in different environments, creating contour maps and obtaining 3D images [14]. Since 1984, more than 100,000 scientists and engineers worldwide have benefited from Surfer. The program's exceptional shaping capabilities make it the preferred software for working with X,Y,Z data. It shows high performance to visualize X,Y,Z data with stunning clarity and accuracy. This program, which transforms the collected data into information, visualizes the data in high quality while preserving its accuracy and precision. Along with Surfer's extensive modelling tools, interpolation and grating parameters can be adjusted, define errors and breaks, or perform grid calculations such as volumes, transformations, smoothing or filtering [15].

It consists of map types such as contour, calculation, 3D surfaces, colour relief, etc., and provides tools to visualize and model all types of data. The type of map obtained in this study is contour map. After making all the statistical calculations by turning the 3D data loaded on the worksheet into a grid, the map is created by selecting the desired map type. In order to make the map more meaningful and readable, the map can be personalized with various customization options, thanks to the window in the lower left corner of the screen. These options include sections, magnifiers, scale bars and edits such as multi-axis, linear or logarithmic color scales, combining multiple maps, text, line, fill, and symbol properties [15].

2.3. Particulate matter PM2.5 measurement method

In the researches carried out to determine the particulate matter concentrations, the pollutant sources in the external environment were examined. By comparison, there is little information on indoor particulate matter pollution, its concentrations, sources, and exposure levels to people who spend most of their time in various indoor environments [16]. In this study, which was started to determine the effect of seasonal changes on particulate matter, summer, autumn and winter seasons were selected to take measurements, and two-day measurements were made on weekdays and weekends. The total measurement period was completed as 4 days in each period.

In all three seasons when the measurements were made, the daily measurement program lasted for 10 hours, depending on the working hours of the venues. Measurements were repeated 6 times a day with an interval of 2 hours. After taking the coordinates of the measurement points, the data collected at the end of each season are listed in the Excel program in such a way that daily, weekly and hourly averages are taken. X and Y coordinates and Z coordinate represented the measured PM_{2.5} values. A worksheet was created by transferring X,Y coordinates and measurement values to the SURFER-16 program. Statistical calculations were made by converting the prepared data into tables. Then, contour map is selected from the map options in order to show the contour lines. The customization window is used to clearly show high and low concentrations and dispersion lines on the map.

3. Results and Discussion

Particulate matter measurements were carried out in three different seasons in the rainbow shopping center of Selçuk University Alaeddin Keykubat campus, an important shopping center in Konya. The sampling period was carried out between 21.05.2018 - 03.06.2018. During the measurement periods, measurements were made for one week. Weekly average distributions of particulate matter PM_{2.5} were prepared with Surfer 16 by measuring 6 times a day.

Within the scope of the research, it was arranged to be close to the opening and closing hours of the shopping center between the hours of weekdays and weekends (09.00 - 19.00). As a result of the study, the average values of PM_{2.5} obtained from the examination of all data during the week and at the weekend are shown in Table 1.

Table 1. This is the example of table formatting

Sampling period	Weekday average PM _{2.5} µg/m ³	Weekend average PM _{2.5} µg/m ³
Summer	600	528

According to the summer period data, the average of PM_{2.5} at 9:00 in the morning was 580 µg/m³ on weekdays and 720 µg/m³ on weekends. While the most intense point of pollution was at point B on weekdays, it was seen intensely at points B and C on weekends. point B; it is in a narrow and closed corridor with cooking stoves, hairdressers, tailors and locksmiths. Thanks to these shops that are actively working, there is not much difference between weekday and weekend values. Point C, on the other hand, corresponds to the aforementioned corridor in the shopping mall, on the west side of the building. There is a restaurant material entrance area, a medical equipment sales point and a clothing store door opening to this corridor. The value seen over the weekend appears to have increased due to the material loading in the corridor. The modelling results are shown in Figure 2.

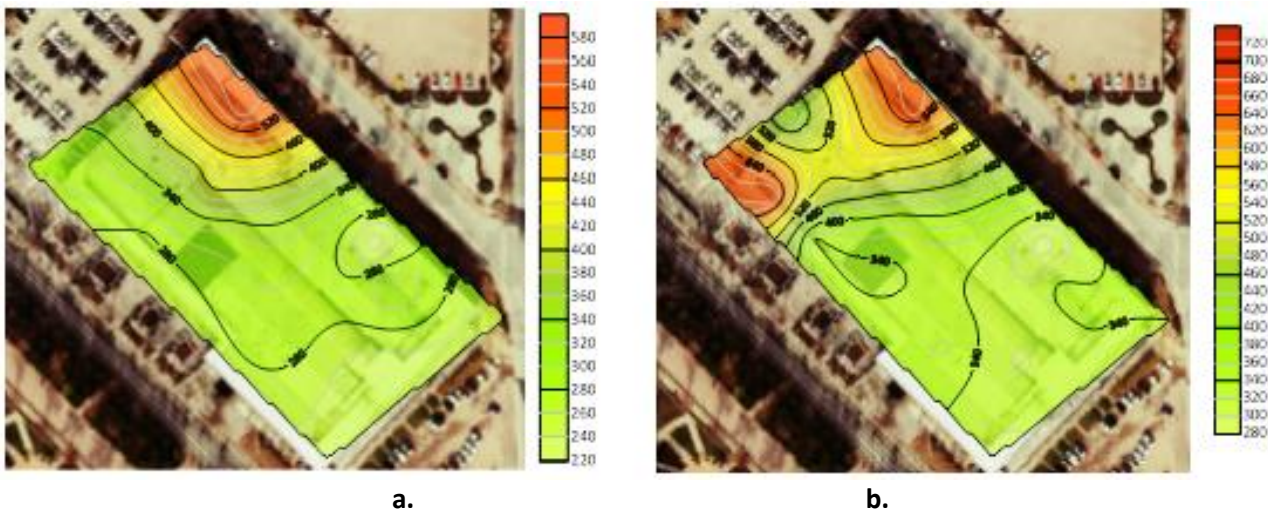


Figure 2. Summer season at Gökkuşuğu Mall at 9:00 a.m. a-Weekdays, b-Weekend average

As the middle of the day approaches, the values increase slightly and the measurements made around 11:00 reflect the modelling in both weekday and weekend averages. The average of PM_{2.5} at 11 o'clock was found to be 1040 µg/m³ on weekdays, and very close values were obtained as 1050 µg/m³ at the end of the week. The intense

pollution zone seen on weekdays exactly coincides with the middle parts of the building, some of the corridors and restaurants (Figure 3).

With the campus staff and students taking a lunch break around this time, the number of people inside the Rainbow Shopping Centre increases significantly. In this time period, PM_{2.5} concentration also increases in direct proportion to the increase in the number of people. PM_{2.5} is higher than weekdays, but PM_{2.5} is higher at the weekend. A. This spot is located at the north entrance of the building and is mostly open. Other parts of the building have normal PM_{2.5} values, and it is thought to be high in the north door entrance and PM_{2.5} as a source of pollutants originating outside. Modelling results for 11:00 am measurements are shown in Figure 3.

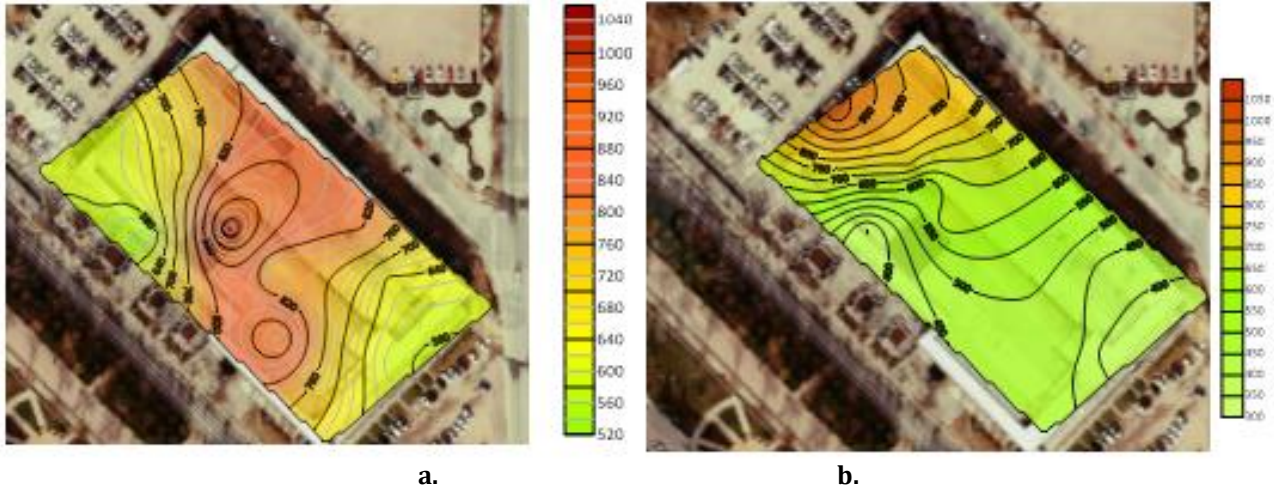


Figure 3. Summer season at Gökkuşuğu Mall at 11:00 am. (a-Weekdays, b-Weekend average)

The high values of the weekend compared to the weekdays gave similar results at the average of 13:00. Weekday average was 720 µg/m³ and weekend average was 740 µg/m³. As a result of the dispersal of the majority (students and school personnel) who entered the shopping mall after the lunch break time was over, a decrease was observed in the values of PM_{2.5} in the indoor environment. In addition, it causes PM_{2.5} dilution in the indoor environment due to the ventilation activities carried out by doors and windows in the indoor environments in summer. The results at time 13.00 are shown in Figure 4.

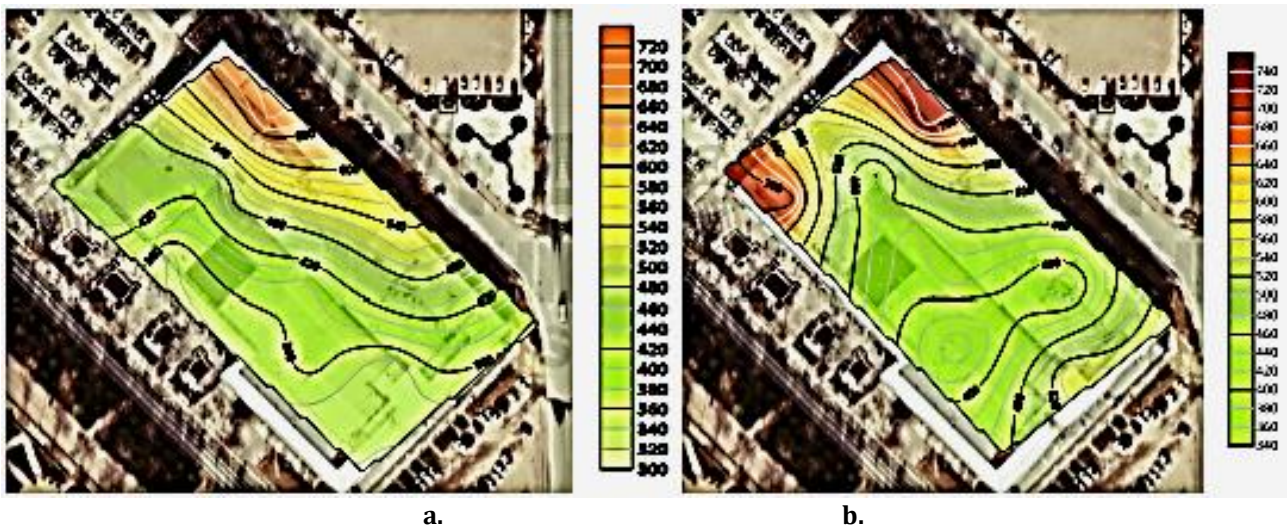


Figure 4. Summer season at Gökkuşuğu Mall at 13:00 (a-Weekdays, b-Weekend average)

The average of 15.00 µg/m³ on weekdays during the summer period was found to be 1700 µg/m³, when we look at the PM_{2.5} values, PM_{2.5} concentrations between 900-1,700 µg/m³ along the B, F, G, H, I, J, K points correspond to the end of working hours. This indicates an increase in the number of visitors and a crowd in the shopping mall. This is especially true where these points (corridors and dining areas) are located. As the crowd increases in closed environments, there is an increase in particulate matter in direct proportion. This is a situation that can be seen even in the case of ventilation in the summer season. As the human activity rate increases, PM_{2.5} concentrations increase.

Weekend PM_{2.5} results were 900 µg/m³, half the weekday average. Although the points where the values are high are the same, the concentration of particulate matter is lower due to the decrease in the number of visits to the shopping mall after 15:00 on the weekend. The results at 3:00 PM are shown in Figure 5.

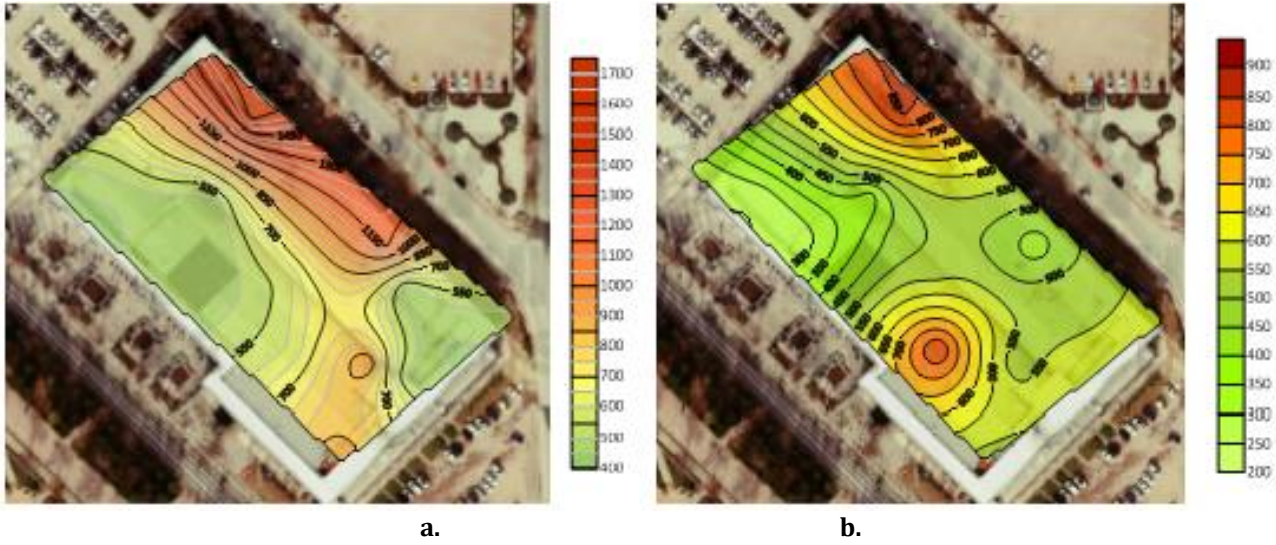


Figure 5. Summer season at Gökkuşuğu Mall at 3:00 pm (a-Weekdays, b-Weekend average)

In general, point B of the rainbow with the highest PM_{2.5} value was observed at 17.00 with a high average of 1550 µg/m³ on weekdays. Looking at this result, PM_{2.5} is seen at high values in the north and north east parts of the building. In the western part of the building, a lower value (around 600 µg/m³) was found throughout. The values rising again in the south-easter part of the building indicate the presence of the pollutant source entering the interior with the door open to the outside environment. Along with the decrease in the number of people on the campus towards the evening hours on weekends, the number of people coming to the shopping mall also decreases. It shows that this situation is observed at the weekend values at 17.00 hours and the average concentration decreased to 800 µg/m³. Figure 6 shows the weekday and weekend results at 17:00.

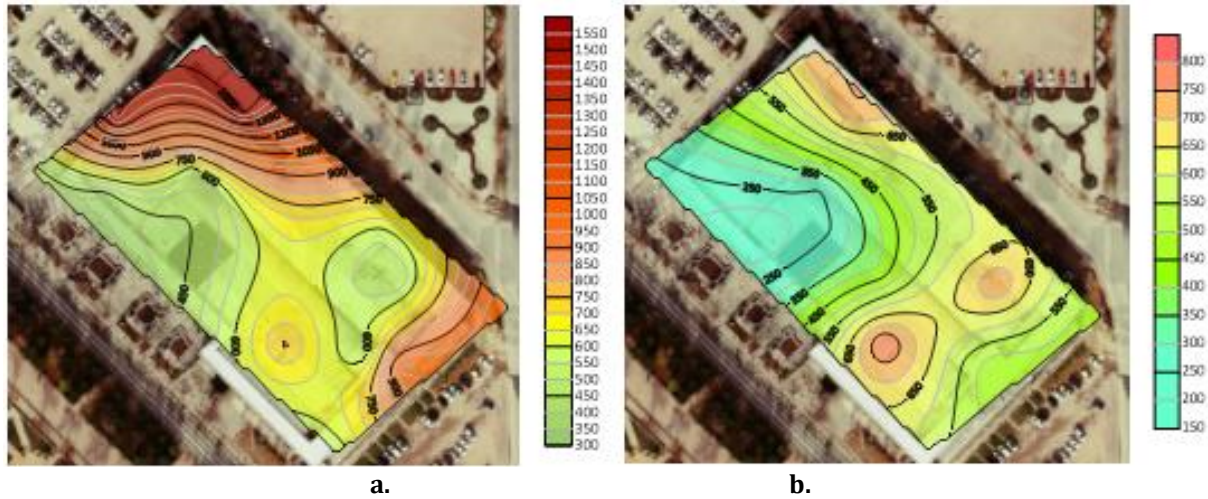


Figure 6. Summer season at Gökkuşuğu Mall at 5:00 pm (a-Weekdays, b-Weekend average)

PM_{2.5} level at 19.00, when the last measurement of the day was made, was 1,550 µg/m³ on weekdays and 370 µg/m³ on weekends. At 19.00, it coincides with the patient visiting hours of the Selcuk University Medical Faculty Hospital, located on the west side of the Rainbow Mall. With this said, most of the visitors who come to the hospital at that hour stop by the shopping mall for food or shopping. On the contrary, PM_{2.5} level was found to be very low compared to weekdays due to the fact that there were very few people on the campus at the weekend. Figure 7 shows the modelling results of the last measurement at 19:00 in the rainbow shopping mall in summer.

With a general interpretation, as a result of the measurements made in the summer period, the lowest PM_{2.5} value is 370 µg/m³. This value exceeds the hourly 25 µg/m³ limit set by WHO, EEA and EPA for PM_{2.5}. In the outdoor air quality assessment management and regulation updated in 2008 in Turkey, the standard value for PM_{2.5} is 200 µg/m³. While the indoor air should be lower than these values, the results obtained exceed the HKDYY limit value.

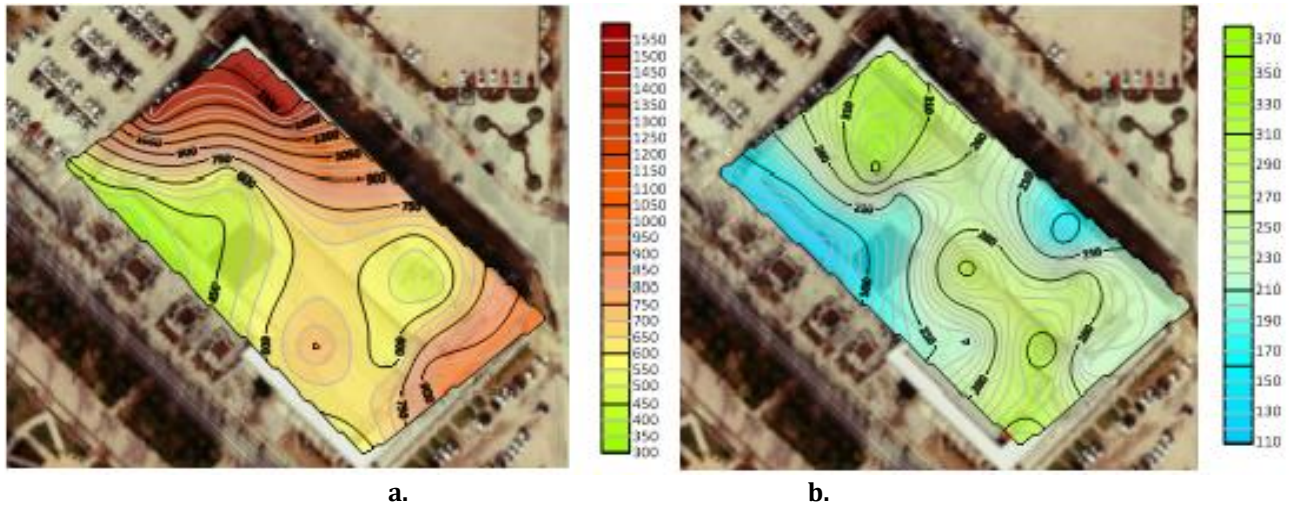


Figure 7. Summer season at Gökkuşağı Mall at 5:00 pm (a-Weekdays, b-Weekend average)

4. Conclusion

In this study, indoor air quality, the importance of which has started to be noticed in Turkey in recent years, has been examined. In this study, which was started in Konya, one of the most important industrial cities of the country, based on shopping centers, particulate matter PM_{2.5} measurements, which carry serious risk factors on human health and which is in the second rank among air pollutants by the World Health Organization, were made. Two different environments were selected for the measurements. Rainbow shopping center located on Selçuk University Alaeddin Keykubat campus was chosen as the first location for measurements. Measurements were made in three separate periods. Sampling was carried out during the summer season between 09:00 and 19:00 between 21.05.2018 – 03.06.2018. When investigated how particulate matter PM_{2.5} affects indoor air quality throughout the season and what causes it. The results were mapped and modelled using the Surfer 16 program. While modelling, the results were interpreted as weekday and weekend averages. As a result, measurement PM_{2.5} values in the center of Gökkuşağı Mall did not exceed WHO's standards [17].

It is thought that the fact that the building structure of Gökkuşağı shopping center is older has an effect on the results. In addition, the central ventilation system in the building was not repaired and closed for use years ago as a result of deterioration, resulting in insufficient air circulation inside. Thanks to the stationery, photocopiers, restaurants, clothing, tailors and cafes in the building, there are only 3 exit doors so that the pollutants dispersed in the indoor environment can mix with the outside environment. The number of daily visitors also had an effect on the high values observed especially at noon. In addition to the lack of ventilation, the absence of a ban on smoking caused the corridors in the northern part of the building to be exposed to the highest PM_{2.5} pollution. It is thought that the old building materials and the unrepaired structure also affect the pollution level. Since the measurements took place on campus, higher values were obtained during the week, except for some exceptional cases. This building, which is located right across the medical faculty hospital in terms of its location, caused an increase in PM_{2.5} pollution in the shopping mall in direct proportion to the patient visit hours of the hospital.

5. Recommendation

In order to breathe healthy air in closed living spaces where people spend most of their time, these environments and existing ventilation systems, devices and vehicles must be maintained by constantly monitoring and controlling in terms of quality atmosphere [18]. For this reason, it is necessary to implement methods that will ensure an acceptable indoor air quality in shopping malls. These methods are respectively;

- Removal of the source affecting the environment,
- Making central ventilation systems according to standards suitable for the environment in which they will be used, using them appropriately and maintaining them at regular intervals,
- It is recommended to take precautions against smoking in closed environments.

Also; universities should organize lectures, symposiums and educational seminars in educational institutions about the importance of indoor air quality and its effects on health. Due to the lack of standards determining indoor air quality in Turkey until today, it is recommended that the relevant institutions take action as soon as possible to establish standard values for this air, which has a direct impact on the health of living things. It should be ensured that the parameters determining the air quality in all provinces of Turkey are measured and modelling maps are created.

Acknowledgement

This paper has been prepared a part of Mina Naseer Qasim's MSc. Thesis and presented 1st Advanced Engineering Days, Mersin, 2021 [19].

Funding

This research has been funded by Selcuk University, Scientific Research Found, Project no:18201117.

Author contributions

Sukru Dursun: Conceptualization, Methodology, -Reviewing and Editing; **Mina Naseer Qasim:** Investigation, Data curation, Writing-Original draft preparation, Modelling.

Conflicts of interest

The authors declare no conflicts of interest.

References

1. Brunekreef, B., & Holgate, S. T. (2002). Air pollution and health, *The Lancet*, 360 (9341), 1233-1242.
2. Karakaş, B. (2015). Assessment of Particulate Matter (PM10, PM2.5 and PM1) Concentrations in Indoor and Outdoor Environments. Master Sc. Thesis, Hacettepe University, Ankara
3. Kaya, D. & Öztürk, H. H. (2013). Hava Kalitesi Yönetimi, Ankara, Umuttepe Yayınları, Izmit. ISBN: 978-605-5936-84-6, pp. 352.
4. Xing, Y-F., Xu, Y-H., Shi, M-H., & Lian, Y-X. (2016). The impact of PM2.5 on the human respiratory system. *Journal of Thoracic Disease*. Jan; 8(1), E69-E74.
5. Braniš, M., Řezáčová, P. & Domasová, M., (2005). The effect of outdoor air and indoor human activity on mass concentrations of PM10, PM2. 5, and PM1 in a classroom. *Environmental research*, 99 (2), 143-149.
6. Fromme, H., Twardella, D., Dietrich, S., Heitman, D., Schierl, R., Liebl, B., Rüdén, H., (2007). Particulate matter in the indoor air of classrooms-exploratory results from Munich and surrounding area. *Atmospheric Environment*, 41 (4), 854-866.
7. Alyüz, B., & Sevil, V. (2006). İç ortam havasında bulunan uçucu organik bileşikler ve sağlık üzerine etkileri. *Trakya Üniversitesi Fen Bilimleri Dergisi*, 7 (2), 109-116.
8. Kiesewetter, G., Schoepp, W., Heyes, C. & Amann, M. (2015). Modelling PM2. 5 impact indicators in Europe: health effects and legal compliance. *Environmental Modelling & Software*, 74, 201-211.
9. WHO, (2013). World Health Organization (2013). Review of evidence on health aspects of air pollution.
10. British Columbia Branch, (2009). British Columbia ambient air quality objectives, ambient air quality objectives. <https://www2.gov.bc.ca> [02.12.2021].
11. Hyde, J. C., Yedinak, K. M., Talhelm, A. F., Smith, A. M., Bowman, D. M., Johnston, F. H., ... & Tinkham, W. T. (2017). Air quality policy and fire management responses addressing smoke from wildland fires in the United States and Australia. *International Journal of Wildland Fire*, 26(5), 347-363.
12. Cindoruk, S. S., (2018). Havadaki NO ve NO₂ parametrelerinin Marmara temiz hava merkezi ölçümleri kapsamında incelenmesi, *Ömer Halisdemir Üniversitesi Mühendislik Bilimleri Dergisi*, 7 (2), 600-611.
13. URL-1, (2021). <https://earth.google.com/>
14. Polat, O. (2002). Golden software surfer v.8 kullanım ile ilgili notlar.
15. URL-2, (2021). Golden software products. <https://www.goldensoftware.com/products>
16. Challoner, A. & Gill, L. (2014). Indoor/outdoor air pollution relationships in ten commercial buildings: PM2.5 and NO₂. *Building and Environment*, 80, 159-173.
17. Dursun, Ş., Ayturan, Z., Kunt, F., Ulusoy, Ç., & Mesutoğlu, Ç. (2017). Selçuk Üniversitesi Yerleşkesi Açık Alanlarda Ortam PM2.5 Seviyesinin Belirlenmesi, VII. ulusal hava kirliliği ve kontrolü sempozyumu, 190-202.
18. Kiesewetter, G., Schoepp, W., Heyes, C., & Amann, M. (2015). Modelling PM2.5 impact indicators in Europe: health effects and legal compliance. *Environmental Modelling & Software*, 74, 201-211.
19. Dursun, S., & Qasim, M. N. (2021). Determination and modelling of PM2. 5 level in summer time in Selcuk University Shopping Centre Konya, Turkey. *Advanced Engineering Days (AED)*, 1, 69-71.





Investigation of emission control efficiency with gasoline vapor recovery units

Ece Kalay ^{*1}, Hasan Sarioğlu ¹, İskender Özkul ²

¹Ergil Group and Aager GMBH, Research and Development Department, Mersin, Türkiye, ece.kalay@aager.de, hasan.sarioglu@aager.de

²Mersin University, Engineering Faculty, Mechanical Engineering Department, Mersin, Türkiye, iskender@mersin.edu.tr

Cite this study: Kalay, E., & Sarioğlu, H., & Özkul, İ. (2022). Emission control with vapor recovery systems. *Advanced Engineering Science*, 2, 9-14

Keywords

Volatile organic compounds
Vapor recovery units
Emission control
Storage tank

Research Article

Received:06.01.2022
Revised: 11.02.2022
Accepted:19.02.2022
Published:14.03.2022



Abstract

Increasing environmental regulations and the widespread use of gasoline vapor recovery systems have become a current issue. The development of technology and equipment for the gasoline vapor recovery industry is also growing rapidly and the demands on the relevant technical standards are increasing. Depending on the domestic and international development of the gasoline vapor recovery technology and standard, the purpose of this study will be to examine the VRU systems developed to control the emissions of gasoline-sourced volatile organic compounds. Analysis of the relevant terminology will be carried out through a literature review.

1. Introduction

Gasoline consists of organic compounds obtained by the distillation of petroleum and enriched with various additives. Approximately 71 liters of gasoline can be obtained from 159 liters of crude oil. Gasoline used in industry and transportation has a significant impact both locally and globally. Gasoline can also be released into the environment from leaks and processes during production, transportation, and delivery, from storage tanks, spills, and combustion as liquid and vapor [1].

Volatile organic compounds (VOCs) are among the most common air pollutants emitted by the chemical industries and include hydrocarbons such as olefins, paraffin, and aromatics. VOCs adversely affect air quality and therefore human health. During the distribution and storage of gasoline, VOCs are emitted into the atmosphere by evaporation. The evaporation rate is a parameter dependent on vapor pressure, turbulence, and temperature. VOC emissions are not only an environmental hazard but also a loss of money. For this reason, systems are developed to minimize the amount of evaporation from bulk storage tanks and storage tanks in stations [2].

Gasoline vapor recovery systems are widely used in Europe and the USA. However, these systems have not been given the desired level of importance in Turkey. It is planned that the emissions released to the environment will be controlled by the Industrial Air Pollution Control Regulation. This will increase the need for steam recovery systems [3].

This study will be to examine the vapor recovery systems used for the control of gasoline-derived volatile organic compounds emissions. Evaluation of the relevant terminology will be carried out through a literature review.

2. Material and Method

Gasoline is a worldwide commodity. Carbon dioxide, nitrogen oxides, and hydrocarbons are released as a result of gasoline burning. Emissions from hydrocarbons occur due to evaporation during the storage and distribution of gasoline. Some compounds are released during the storage and distribution of gasoline. These compounds are called volatile organic compounds (VOCs). VOCs constitute an important class of air pollutants and contain different organic compounds. They are pure hydrocarbons, partially oxidized hydrocarbons, chlorine, sulfur, and nitrogen-containing organics. Most VOCs are toxic and or carcinogenic [4].

In the United States, VOCs are defined as any carbon compound that participates in an atmospheric photochemical reaction except carbon monoxide, carbon dioxide, carbonic acid, carbonates, ammonium carbonate. The United Nations Economic Commission for Europe (UNECE) classifies VOCs according to their photochemical ozone generating potential (POCP). POCP is defined as the change in ozone production due to the change in the emission of the VOC [5].

In sunlight, VOCs react with nitrogen oxides to form photochemical oxidants such as ozone. Ground-level ozone is a well-known greenhouse gas. It is an important component of air pollution. Smoke also adversely affects human health and vegetation. Although VOCs and nitrogen oxides occur naturally, anthropogenic sources have greatly increased the concentration in the atmosphere. The sources of VOC emissions are shown in Table 1.

Table 1. Percentage of emission [1]

Emission Sources	%
Industrial and domestic	40
Exhaust gases from motor vehicles	25
Evaporation losses from motor vehicles	10
Gasoline distribution	3
Vehicle refueling	2
Oil refining	3
Others	17

Gasoline distribution and vehicle refueling account for only 5% of total VOC emissions. These emissions are concentrated in gasoline storage stations where people are densely populated. A typical gasoline distribution system is shown in Figure 1.

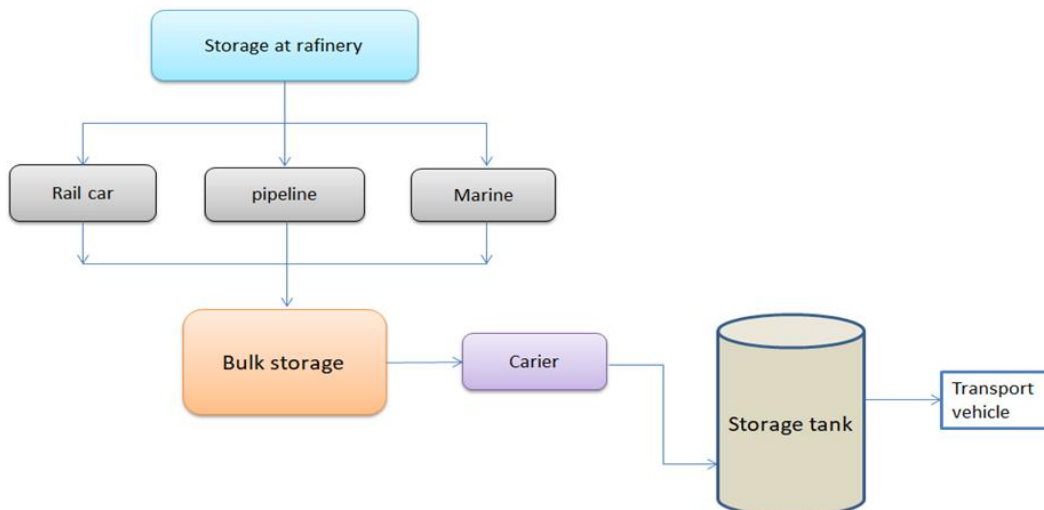


Figure 1. Gas storage and distribution system

The control of emissions from gas storage facilities during the transportation of the final product to the consumer consists of three stages. (Figure 2):

- Stage 1 - Includes the control of emissions at facilities when road tankers are loaded.

- Stage 2 - Includes control of emissions when road tankers are discharged into service station storage tanks
- Stage 3 - It includes the control of emissions generated during vehicle refueling.

During each of these steps, evaporation losses occur as shown in Figure 2 [6]. A product loss occurs unless the resulting vapor contains a VOC / air mixture. The VOC composition is a mixture of compounds with different boiling points of lower molecular weight than gasoline in shown Table 2.

Table 2. Only VOC Typical gasoline vapor composition [2]

Compounds	Volume
Isobutene	8%
n-Butane	10%
Propane	1.5%
Pentane	14%
Benzene	5000 ppm
Hexane and others	6%
Ethane	Traces

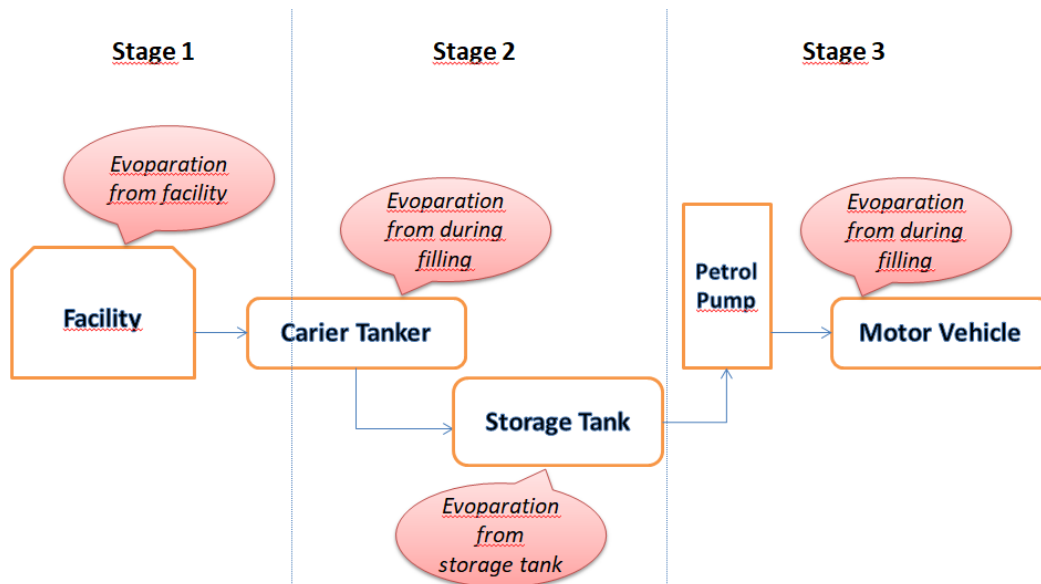


Figure 2. Evaporation emission from petrol storage systems

3. Types of emissions in gasoline storage tanks

Displacement emissions occur in underground storage tanks due to vapor displacement emissions from storage facilities as well as from fixed roof storage facilities. Total emission loss is 0.56% by volume.

Filling emissions result from changes in tank content, temperature, and barometric pressures that cause the liquid and vapor in the tank to expand and contract. Discharging emissions occur when gasoline is pumped out of a storage tank, causing air intake through pressure/vacuum relief valves. The incoming air will dilute the VOC / air mixture previously in the tank, causing an increase in evaporation to restore equilibrium. Filling and discharge emissions from storage tanks account for 0.02% of total emission losses and 0.01% of emissions from station storage tanks.

While refueling a motor vehicle, the incoming gasoline replaces the gasoline vapor in the fuel tank and causes it to escape into the atmosphere. These emissions account for 0.18% by volume of total emissions from gasoline storage and distribution systems [3].

4. Vapor recovery systems for emission control

In this section, steam recovery systems that can be applied to the terminals are examined. The efficiency, reliability, safety, and production capacity of these systems were evaluated.

4.1. Absorption - Compression-Refrigeration Systems (ACR)

ACR works on the principle that gasoline vapor is absorbed under pressure. The first unit in ACR systems conditions the steam entering the absorber. It increases absorber efficiency, reduces heat losses, and increases system safety. Firstly, the inlet vapors are saturated to eliminate explosiveness. Cooling and compression processes are performed before partially saturated vapors enter the absorber. Then the compressed vapors are sucked in contact with the cooled gasoline. Air containing a small number of hydrocarbons passes through the absorber into the atmosphere. Gasoline enriched with light tips is drawn from under the absorber and returned to the fuel storage tanks. The operating conditions in the absorber vary according to the manufacturers. The ambient temperature is -23°C and working pressures are between 3.10 – 14 bars. These values vary depending on terminal operating conditions and vapor storage capacity. The outlet hydrocarbon concentration is determined according to the absorber operating conditions. When the results of the field tests are examined, it has been determined that the values between 1% and 4.5% by volume. Auxiliary compressors can be needed to achieve 90% steam recovery from ACR systems [7].

4.2. Condensation - Compression - Refrigeration Systems (CCR)

The CCR systems work on the principle of condensation of hydrocarbon vapors by compression and cooling. Inlet vapors are saturated above the flammability range in the first stage and then the saturated vapors are compressed. Condensate is drawn from the intercooler. The compressed vapors, together with the condensation coming from the intercooler, pass through the condenser and return to the gasoline storage tank. Hydrocarbon-free air is sent to the condenser. Each manufacturer has slight differences from this basic flow diagram. The operating conditions of the system are temperatures ranging from -23.3°C to -1°C and pressures ranging from 5.8 bars to 28.26 bars. These values vary depending on the terminal operating programs and steam storage capacity. Manufacturers report that the recovery rate of the system will increase up to 94% with the equipment to be added according to the operating conditions. The flow diagram of the system is as shown in Figure 3.

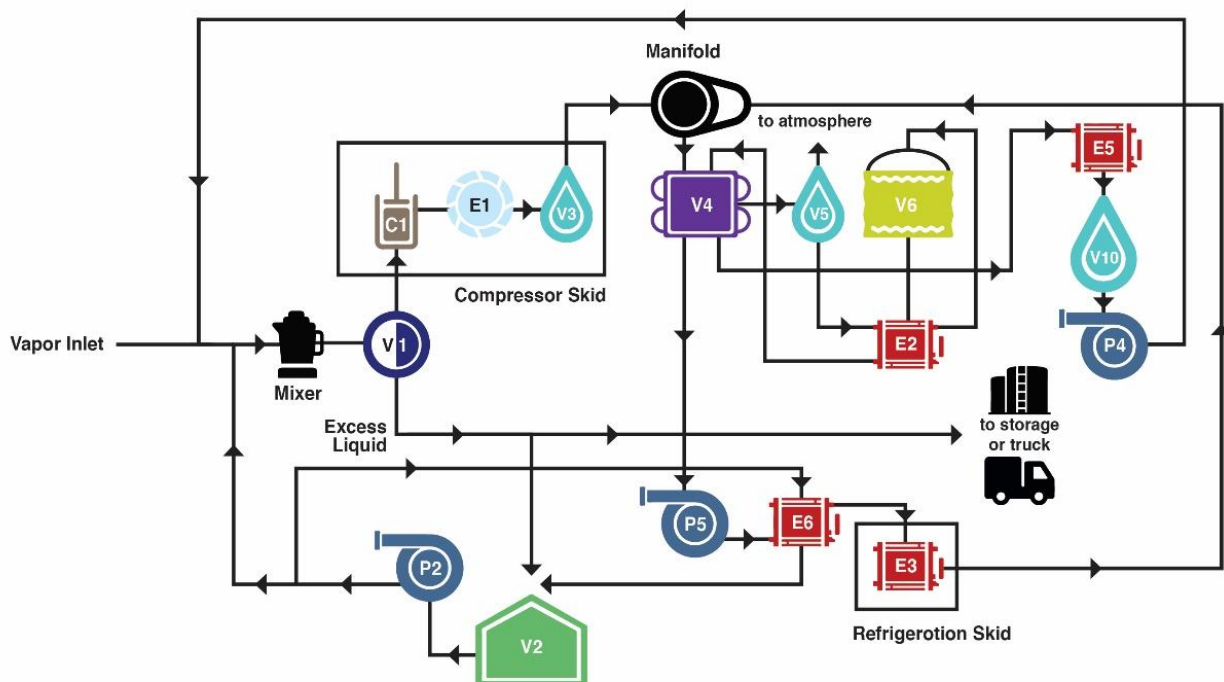


Figure 3. CCR system flow diagram [8]

4.3. Refrigeration Systems (RS)

RS systems work on the principle of condensation of gasoline vapors by cooling under atmospheric pressure. The outlet vapors enter the horizontal finned condenser for cooling to -73°C . Air containing a low proportion of hydrocarbons is sucked from the bottom of the condenser. The remaining air is released from the top of the condenser to the atmosphere. Cooling for the condenser coils is provided by a methyl chloride reservoir. A two-

stage cooling unit is used to cool the stored brine solution between -76 °C and 51 °C. The vapor recovery efficiency depends on the hydrocarbon concentration of the vapors inlet the system. The field tests data of a system with a capacitor temperature of -73.3 were examined. It was found that the hydrocarbon concentration of 0.6% to 2.6% by volume was stabilized by temperature. With these systems, recovery rates of hydrocarbons vary between 99% and 97% [9].

4.4. Lean Gasoline absorption systems (LGA)

LGA systems work on the principle of absorption of gasoline vapors into lean gasoline. The gasoline vapors are displaced along with the packed absorbent columns. The absorbed air is expelled from the top of the absorbent column. Enriched gasoline is recycled. The lean gasoline for the absorber is produced by heating and evaporating the gasoline in the tank. The separated hydrocarbons are condensed and sent back to the warehouse. The lean gasoline is stored separately for use in the absorption column [10].

4.5. Membrane Systems

MS is a simple and small vapor recovery system for a lower cost separation of gasoline from the vapor mixture. In recent years, several hundred gas stations have used these systems to clean tank vents. The air distributed from the station is collected and sent to the storage tank. When the pressure to be created in the tank reaches a predetermined value, the pressure switch activates the compressor to absorb the excess steam. Some of the hydrocarbon vapors condense and are returned in liquid form to the tank. The remaining hydrocarbon vapors are sent back to the tank as concentrated vapors. Air separated from 96%-98% hydrocarbons is discharged [11].

5. Results

Vapor recovery systems are units with high operational safety. The reliability of these technologies has been proven over two decades of use. Companies using ACR and CCR systems regularly report that the maintenance period is approximately one week a year. Freezing problems have occurred in systems exposed to temperatures below 0°C. Water vapor freezes in the system, preventing the heat transfer of the lines. The solutions for this are as follows [12].

- During closed periods, a part of the system should be turned off and an automatic defroster should be added.
- Methanol can be injected into the system to reduce the freezing point.
- It has been shown that both solutions recommended for the icing problem give effective results. Another important part of ACR and CCR systems is the gasoline vapor compressor.

Safety is of paramount importance in equipment design for working with flammable materials. Vapor recovery equipment manufacturers are aware of this and have included safety features in their designs. Vapor saturators are installed in the systems to prevent the possibility of explosion. The compression ratios and associated off-gas temperatures should be kept at low levels to prevent overheating and spontaneous combustion [13]. Another potential danger in using a vapor recovery system is leaking. Regular maintenance does not cause any security problems [12].

6. Conclusion

Product losses through evaporation create significant losses for companies. At the same time, environmental pollution caused by the uncontrolled release of these vapors is also a potential threat to living things. Reducing material losses, increasing environmental regulations, reducing operational costs and greenhouse gases, and insufficient stocks in the industry and the country have paved the way for the development of products containing various technologies.

Within the scope of this study, the product recovery efficiencies of various vapor recovery systems with different technologies were investigated. Membrane systems have recovery efficiencies of 96-98%, but spare parts, maintenance, and operating costs are high. RS systems provide a recovery rate of up to 99%, while the rate of CCR systems is around 94%. ACR systems provide a 90% recovery rate at high pressures and low temperatures. It has been observed that CCR systems are frequently preferred by businesses, considering the operation, maintenance, investment costs, system control ease, and solutions to the icing problem. It is predicted

that the use of these systems will become widespread especially in our country due to environmental safety and economic factors.

Funding

This research received no external funding.

Author contributions

Ece Kalay: Conceptualization, Methodology, Software, Writing-Original draft preparation **Hasan Sarioğlu:** Data curation, Software, Validation. **İskender Özkul:** Visualization, Investigation, Writing-Reviewing, and Editing.

Conflicts of interest

The authors declare no conflicts of interest.

References

1. Elsamani, M. A., & Elwadie, M. E. (2015). Gasoline Vapour Recovery. University of Khartoum.
2. Hansen, M. (1996). Hydrocarbon vapor emission reduction by recovery. Paper presented at the Danish Days in Ukraine conference.
3. Mulder, T. J. H. E. (2007). VOC recovery systems. 12(6), 37-40.
4. Jo, W.-K., & Song, K.-B. J. S. O. T. T. E. (2001). Exposure to volatile organic compounds for individuals with occupations associated with potential exposure to motor vehicle exhaust and/or gasoline vapor emissions. 269(1-3), 25-37.
5. Jeffery, K. (1998). Bulk Liquids vapour control: IIR Publications Limited.
6. Hadley, P., Devos, F., Esty, W., Gommel, P., Ising, U., Lilie, R., Williams, L. J. S. C. (1978). Hydrocarbon emissions from gasoline storage and distribution systems. 4.
7. Chang, D., Min, J., Moon, K., Park, Y. K., Jeon, J. K., & Ihm, S. K. (2004). Robust numerical simulation of pressure swing adsorption process with strong adsorbate CO₂. Chemical Engineering Science, 59(13), 2715-2725.
8. Sabareesh, R. K., Gobinath, N., Sajith, V., Das, S., & Sobhan, C. B. (2012). Application of TiO₂ nanoparticles as a lubricant-additive for vapor compression refrigeration systems–An experimental investigation. *International Journal of Refrigeration*, 35(7), 1989-1996.
9. Kalinowski, P., Hwang, Y., Radermacher, R., Al Hashimi, S., & Rodgers, P. (2009). Application of waste heat powered absorption refrigeration system to the LNG recovery process. *International journal of refrigeration*, 32(4), 687-694.
10. Junbo, D., Weiqiu, H., Qiuyun, B. J. C. E. O. O., & Gas. (2008). Optimization Research of Absorption Process for Vapor Recovery System
11. Baker, R. W. (2006). Membranes for vapor/gas separation. Membrane Technology and Research, Inc.: Menlo Park, CA, USA.
12. Shi, L., & Huang, W. (2014). Sensitivity analysis and optimization for gasoline vapor condensation recovery. *Process Safety and Environmental Protection*, 92(6), 807-814.
13. Liu, Y., Ritter, J. A., & Kaul, B. K. (2000). Simulation of gasoline vapor recovery by pressure swing adsorption. *Separation and Purification Technology*, 20(1), 111-127.



© Author(s) 2022. This work is distributed under <https://creativecommons.org/licenses/by-sa/4.0/>



Importance of electrode type and configuration on reaction kinetics in removal of tetracycline antibiotic by electrocoagulation

Bahadır K. Körbahti ^{*1}, Meltem Gökteş ¹

¹Mersin University, Department of Chemical Engineering, Türkiye, korbahti@mersin.edu.tr; meltemgoktas969@gmail.com

Cite this study:

Korbahti, B. K., & Gökteş, M. (2022). Importance of electrode type and configuration on reaction kinetics in removal of tetracycline antibiotic by electrocoagulation. *Advanced Engineering Science*, 2, 15-20

Keywords

Tetracycline
Electrocoagulation
Reaction kinetics
Aluminum electrode
Iron electrode

Research Article

Received: 08.01.2022
Revised: 13.02.2022
Accepted: 23.02.2022
Published: 14.03.2022



Abstract

In this study, the effect of Al-Al, Al-Fe and Fe-Fe electrode configurations was investigated on reaction kinetics in removal of tetracycline antibiotic (TCY) by electrocoagulation. Response surface optimized reaction conditions were operated at 800 mg/L tetracycline concentration, 8 mA/cm² current density, 6 g/L NaCl electrolyte and 40°C reaction temperature at 60 min reaction time. The reaction kinetics study was carried out by nonlinear regression of the integral method with 95% confidence level on the basis of tetracycline concentration and COD concentration. The first order reaction rate equation was determined based on tetracycline concentration and reaction rate constants were calculated as 0.3919 min⁻¹, 0.2918 min⁻¹ and 0.2885 min⁻¹ for Al-Al, Al-Fe and Fe-Fe, respectively. The second order reaction rate equation was determined based on COD concentration and reaction rate constants were calculated as 4.67×10⁻⁴ mg⁻¹Lmin⁻¹, 4.32×10⁻⁴ mg⁻¹Lmin⁻¹ and 4.28×10⁻⁴ mg⁻¹Lmin⁻¹ for Al-Al, Al-Fe and Fe-Fe, respectively. The activation energy values based on tetracycline concentration were calculated as 3.020 kJ/mol, 0.866 kJ/mol and 0.805 kJ/mol for Al-Al, Al-Fe and Fe-Fe, respectively. Based on COD concentration, the activation energy values were determined as 9.413 kJ/mol, 10.085 kJ/mol and 9.825 kJ/mol for Al-Al, Al-Fe and Fe-Fe, respectively.

1. Introduction

Antibiotics are chemotherapeutic agents that inhibits or terminates the growth of microorganisms. They can be grouped by their chemical structure or mechanism of action and can be divided into subgroups such as β -lactams, quinolones, tetracyclines, macrolides, sulphonamides and others [1]. Antibiotics are being widely used in human medicine, veterinary medicine and in aquaculture to treat or prevent microbial infections. Wise [2] has been reported the worldwide annual consumption of antibiotics between 100,000 and 200,000 tons. Antibiotics are detected in hospital effluents, in municipal wastewater, and in sea, surface water and groundwater due to their consumption. Since antibiotics can be found in environmental matrices they are recognized as emerging pollutants [3]. Therefore, various processes have been investigated in order to remove the contamination arise from antibiotic sources [1].

Electrocoagulation is an efficient method that has been used for the treatment of many types of wastewaters [4]. Electrocoagulation involves the process of formation of coagulants by electrolytic oxidation of the sacrificial electrode, destabilization of the contaminants, particulate suspension, breaking of emulsions and aggregation of the destabilized phases to form flocs [5].

In electrocoagulation, Fe²⁺ and Al³⁺ ions generate with iron or aluminum sacrificial anodes and these ions immediately undergo spontaneous reactions to produce hydroxides and polyhydroxides [5,6]. The reactions with Fe and Al anodes are given in Equations 1-9, respectively. Fe²⁺ ions generated by electrochemical oxidation of Fe anode may form monomeric ions and polymeric hydroxy complexes depending on the pH of the solution [5,6]. Fe(OH)₂ precipitates remaining in equilibrium with Fe²⁺ at pH > 5.5 up to pH 9.5 or with monomeric species such as Fe(OH)⁺, Fe(OH)₂ and Fe(OH)₃⁻ at higher pH values [6].



In the presence of dissolved O₂ gas, insoluble Fe(OH)₃ is generated and released protons can be directly reduced to H₂ gas at the cathode [6].



Fe(OH)₃ precipitate can be in equilibrium with soluble monomeric species like Fe³⁺, Fe(OH)²⁺, Fe(OH)₂²⁺, Fe(OH)₃ and Fe(OH)₄⁻ depending on the pH range [6]. The polymeric hydroxy complexes may be Fe(H₂O)₆³⁺, Fe(H₂O)₅(OH)²⁺, Fe(H₂O)₄(OH)₂⁺, Fe₂(H₂O)₈(OH)₂⁴⁺ and Fe₂(H₂O)₆(OH)₄⁴⁺ [5].

Al³⁺ ions generated by electrochemical oxidation of Al anode may form monomeric species such as Al(OH)²⁺, Al(OH)₂⁺ and Al(OH)₃ in acidic medium and Al(OH)₄⁻ in alkaline medium [5,6]. Al³⁺ ions on hydrolysis may generate Al(H₂O)₆³⁺, Al(H₂O)₅OH²⁺, Al(H₂O)₄(OH)₂⁺ and the hydrolysis products may form many monomeric and polymeric species such as Al(OH)²⁺, Al(OH)₂⁺, Al₂(OH)₂⁴⁺, Al(OH)₄⁻, Al₆(OH)₁₅³⁺, Al₇(OH)₁₇⁴⁺, Al₈(OH)₂₀⁴⁺, Al₁₃O₄(OH)₂₄⁷⁺, Al₁₃(OH)₃₄⁵⁺ over a wide pH range [5,6].



The reactions involving chlorine ions in Equations 10-12 could also occur in the presence of NaCl supporting electrolyte [7]:



In electrocoagulation, the pollutants can be removed by insoluble flocs of Fe(OH)₃ and Al(OH)₃ by surface complexation or electrostatic attraction [5,6]. The excess amount of aluminum and iron ions in the solution also feasible by anodic corrosion with Cl⁻ ions [6]. In this study, the effect of Al-Al, Al-Fe and Fe-Fe electrode configurations was investigated on reaction kinetics in removal of tetracycline antibiotic (TCY) by electrocoagulation in the presence of NaCl supporting electrolyte in a batch electrochemical reactor. The reaction kinetic models were developed with the nonlinear regression of the integral method on the basis of tetracycline concentration and COD concentration.

2. Material and Method

Tetracycline hydrochloride (Sigma-Aldrich), mercury sulfate (Merck), sodium chloride (Merck) and acetonitrile (Merck) were received in extra pure grade. Double distilled water was produced in our laboratory. Batch electrochemical system was equipped with jacketed electrochemical reactor, Ametek Sorensen XFR 60-46 programmable DC power supply, Lauda RE 620S refrigerated circulating water bath with thermostat control, Heidolph RZR 2021 mechanical mixer, Heidolph PD 5206 peristaltic pump and thermometer. Aluminum and iron

electrodes were obtained from local sources and used as anode and cathode with 120 cm² surface area. The reaction volume was 600 mL and mechanically stirred at 500 rpm. Samples were taken from the reaction medium at regular intervals for HPLC and chemical oxygen demand (COD) analysis. HPLC analysis were done using Inertsil ODS-3 column (5 mm, 4.6×250 mm) in a Shimadzu Prominence LC-20AD Liquid Chromatography. Gradient mobile phase was acetonitrile and water (50/50) (v/v) at a flow rate of 1.5 mL/min. UV/Vis detection wavelength of tetracycline antibiotic was at 254 nm. Column temperature was set at 40°C. Injection volume was 40 mL. Merck Spectroquant® TR 420 thermoreactor and Nova 60 photometer were used for the COD analysis.

3. Results and Discussion

The response surface optimized reaction conditions were operated at 800 mg/L tetracycline concentration, 8 mA/cm² current density, 6 g/L NaCl electrolyte and 40°C reaction temperature at 60 min reaction time in order to determine the reaction kinetics in removal of tetracycline antibiotic by electrocoagulation. The reaction kinetics study was carried out by nonlinear regression of the integral method based on tetracycline concentration and COD concentration. Nonlinear regression is the modeling of the observational data by a function which is a nonlinear combination of the model parameters and depends on one or more independent variables. The experimental reaction kinetics data were processed for the nonlinear models using CurveExpert Professional 2.7 software.

The nth order reaction kinetics can be expressed in Equation 13 [8,9] and by integrating with the boundary conditions in Equation 14, the solutions of first order and second order reaction kinetics can be obtained in Equations 15 and 16, respectively.

$$\frac{dC_A}{dt} = -kC_A^n \quad (13)$$

$$\begin{aligned} @ t = 0 & \Rightarrow C_A = C_{A0} \\ @ t = t & \Rightarrow C_A = C_A \end{aligned} \quad (14)$$

The solution of first order reaction kinetics for n=1:

$$C_A = C_{A0}e^{-kt} \quad (15)$$

The solution of second order reaction kinetics for n=2:

$$C_A = \frac{C_{A0}}{1 + C_{A0}kt} \quad (16)$$

The reaction rate constant, k, is strongly dependent on the reaction temperature and this temperature dependence could be correlated by Arrhenius equation with the activation energy of the reaction as in Equation 17 [8,9]. The activation energy of the reaction is defined as the minimum energy that must be possessed by reacting molecules before the reaction will occur [8].

$$k = k_0 e^{\frac{-E_a}{RT}} \quad (17)$$

In Equation 17, k₀ is pre-exponential constant, R is gas constant as 8.314 J/(mol.K), T is absolute temperature in K and E_a is the activation energy in J/mol. The nth order reaction rate can be obtained in Equation 18 by substituting Equation 17 in terms of activation energy. Finally, the solutions of first order and second order reaction kinetics can be obtained in Equations 19 and 20, respectively.

$$\frac{dC_A}{dt} = -\left(k_0 e^{\frac{-E_a}{RT}}\right) C_A^n \quad (18)$$

The solution of first order reaction kinetics with activation energy (n=1):

$$C_A = C_{A0} e^{-\left(k_0 e^{\frac{-E_a}{RT}}\right)t} \quad (19)$$

The solution of second order reaction kinetics with activation energy (n=2):

$$C_A = \frac{C_{A0}}{1 + C_{A0} \left(k_o e^{-\frac{E_a}{RT}} \right) t} \quad (20)$$

Equations 19 and 20 were solved by nonlinear regression using CurveExpert Professional 2.7 software and the kinetic model results with the experimental reaction kinetics data were demonstrated in Figure 1 and Figure 2 for tetracycline removal and COD removal by electrocoagulation with Al-Al, Al-Fe and Fe-Fe electrode configurations, respectively. Tetracycline removal and COD removal was achieved with the insoluble flocs of Fe(OH)₃ and Al(OH)₃ by surface complexation or electrostatic attraction as well as by indirect oxidation due to the formation of HOCl/OCl⁻ redox oxidants in the aqueous medium by Cl₂ discharge on the anode. The initial electrochemical degradation rate of tetracycline antibiotic was found higher than the COD removal. This result showed that the formation of intermediates and by-products were removed at a much lower reaction rate.

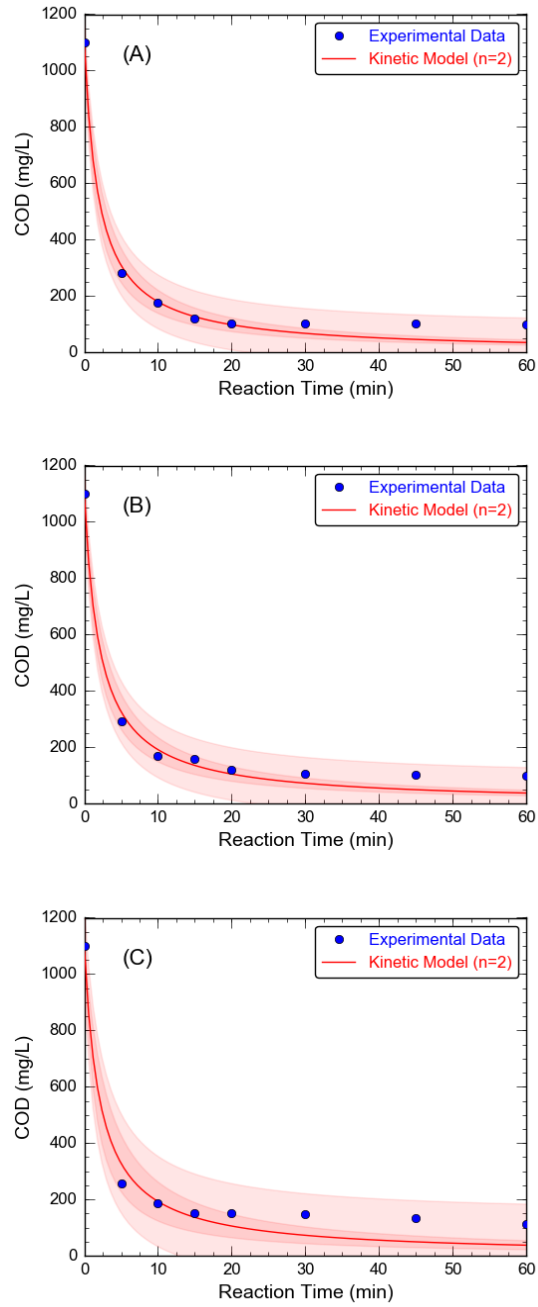
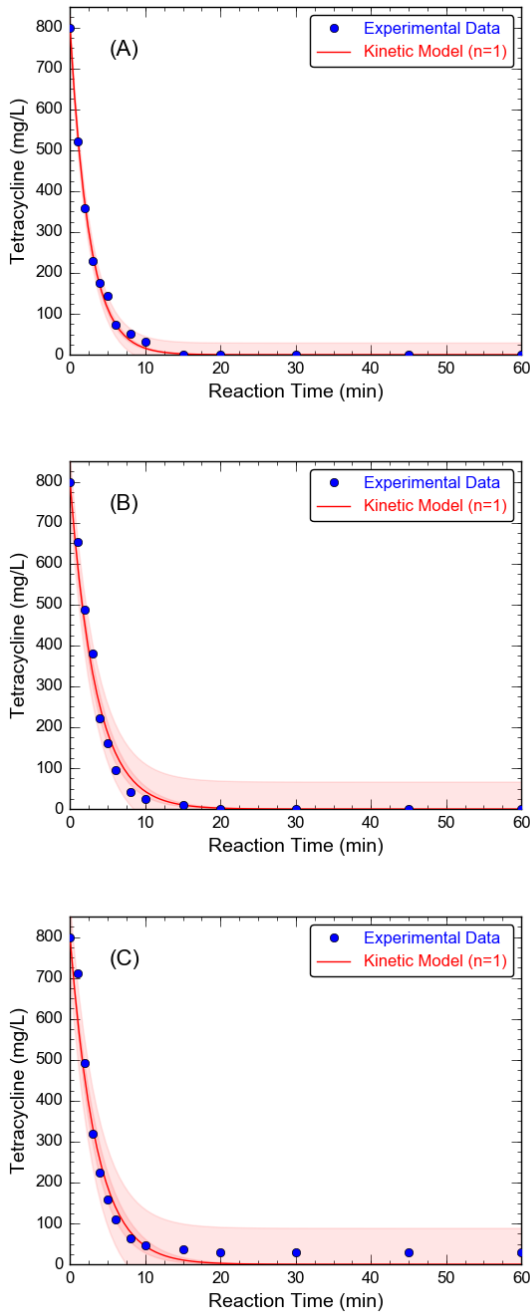


Figure 1. Tetracycline removal by electrocoagulation with (a) Al-Al electrodes, (b) Al-Fe electrodes, (c) Fe-Fe electrodes ([TCY]₀=800 mg/L)

Figure 2. COD removal by electrocoagulation with (a) Al-Al electrodes, (b) Al-Fe electrodes, (c) Fe-Fe electrodes ([COD]₀=1100 mg/L)

The reaction order and the reaction rate constant values were found by nonlinear regression of the integral method with 95% confidence level as outlined in Table 1. The reaction order was determined as 1 for tetracycline removal and as 2 for COD removal. The relationships developed between the parameters were in very good agreement according to the regression coefficients.

Table 1. Reaction order and reaction rate constant values for removal of tetracycline antibiotic by electrocoagulation with Al-Al, Al-Fe and Fe-Fe electrode configurations

Parameter	Electrode configuration	Reaction order	Reaction rate constant	R ²
Tetracycline removal	Al-Al	1	0.3919 min ⁻¹	0.9970
	Al-Fe	1	0.2918 min ⁻¹	0.9872
	Fe-Fe	1	0.2885 min ⁻¹	0.9764
COD removal	Al-Al	2	4.67×10 ⁻⁴ mg ⁻¹ Lmin ⁻¹	0.9888
	Al-Fe	2	4.32×10 ⁻⁴ mg ⁻¹ Lmin ⁻¹	0.9877
	Fe-Fe	2	4.28×10 ⁻⁴ mg ⁻¹ Lmin ⁻¹	0.9665

The first order reaction rate constants based on tetracycline concentration were calculated as 0.3919 min⁻¹, 0.2918 min⁻¹ and 0.2885 min⁻¹ for Al-Al, Al-Fe and Fe-Fe, respectively. Based on COD concentration, the second order reaction rate constants were determined as 4.67×10⁻⁴ mg⁻¹Lmin⁻¹, 4.32×10⁻⁴ mg⁻¹Lmin⁻¹ and 4.28×10⁻⁴ mg⁻¹Lmin⁻¹ for Al-Al, Al-Fe and Fe-Fe, respectively. The second order behavior can be attributed to the existence of an energized and unstable form for the reactant [9]. It is known that reaction rate constants drastically affect the rate of the reactions. According to these results, the reaction rates with electrode configurations were found as Al-Al > Al-Fe > Fe-Fe for both tetracycline removal and COD removal. It can be concluded that Al(OH)₃ flocs more rapidly destabilize the pollutants in the solution than Fe(OH)₃ flocs. In addition, the use of hybrid configuration was increased the reaction rate slightly than using single Fe electrodes in the electrocoagulation.

The activation energy values were obtained in Table 2 by nonlinear regression of the experimental reaction kinetics data with 95% confidence level. The activation energy values based on tetracycline concentration were calculated as 3.020 kJ/mol, 0.866 kJ/mol and 0.805 kJ/mol for Al-Al, Al-Fe and Fe-Fe, respectively. Based on COD concentration, the activation energy values were determined as 9.413 kJ/mol, 10.085 kJ/mol and 9.825 kJ/mol for Al-Al, Al-Fe and Fe-Fe, respectively. It was reported that fast reactions generally have small activation energy values and E_a is typically less than 40 kJ/mol for diffusion-controlled homogeneous reactions [10-12]. The activation energy values of COD removal are higher than the values of tetracycline removal confirming that COD removal is much more difficult than tetracycline removal due to the recalcitrant nature of the degradation products. The activation energy values with electrode configurations were found as Fe-Fe < Al-Fe < Al-Al for tetracycline removal and Al-Al < Fe-Fe < Al-Fe for COD removal. The results indicated the requirement of Fe-Fe electrode configuration in tetracycline removal and Al-Al electrode configuration in COD removal for the minimum activation energy.

Table 2. Activation energy and pre-exponential constant values for removal of tetracycline antibiotic by electrocoagulation with Al-Al, Al-Fe and Fe-Fe electrode configurations

Parameter	Electrode configuration	Activation energy (kJ/mol)	Pre-exponential constant	R ²
Tetracycline removal	Al-Al	3.020	1.2505 min ⁻¹	0.9970
	Al-Fe	0.866	0.4071 min ⁻¹	0.9872
	Fe-Fe	0.805	0.3931 min ⁻¹	0.9764
COD removal	Al-Al	9.413	0.0174 mg ⁻¹ Lmin ⁻¹	0.9888
	Al-Fe	10.085	0.0208 mg ⁻¹ Lmin ⁻¹	0.9877
	Fe-Fe	9.825	0.0187 mg ⁻¹ Lmin ⁻¹	0.9665

4. Conclusion

In this study, the effect of Al-Al, Al-Fe and Fe-Fe electrode configurations was investigated on reaction kinetics in removal of tetracycline antibiotic by electrocoagulation in the presence of NaCl supporting electrolyte in a batch electrochemical reactor. The reaction order was determined as 1 for tetracycline removal and as 2 for COD removal with nonlinear regression of the integral method. According to the calculated values of the reaction rate constants, the reaction rates with electrode configurations were found as Al-Al > Al-Fe > Fe-Fe for both tetracycline removal and COD removal. The activation energy values with electrode configurations were determined as Fe-Fe < Al-Fe < Al-Al for tetracycline removal and Al-Al < Fe-Fe < Al-Fe for COD removal. The results showed that Fe-Fe electrode configuration is feasible in tetracycline removal and Al-Al electrode configuration is feasible in COD removal for the minimum activation energy. Al(OH)₃ flocs more rapidly destabilize the pollutants in the solution than Fe(OH)₃ flocs. The use of hybrid configuration was increased the reaction rate slightly than using single Fe electrodes in the electrocoagulation.

Acknowledgement

The authors gratefully acknowledge Mersin University Scientific Research Projects Center (MEÜ BAP) for the financial support.

Funding

This study was supported by Mersin University Scientific Research Projects Center (MEÜ BAP) with Grant No. 2019-3-TP2-3823.

Author contributions

Bahadır K. Körbahti: Conceptualization, Methodology, Writing-Reviewing and Editing. **Meltem Göktepe:** Investigation, Data collection, Writing-Original draft preparation.

Conflicts of interest

The authors declare no conflicts of interest.

References

1. Kümmerer, K. (2009). Antibiotics in the aquatic environment-A review-Part I. *Chemosphere*, 75, 417-434.
2. Wise, R. (2002). Antimicrobial resistance: priorities for action. *Journal of Antimicrobial Chemotherapy*, 49, 585-586.
3. Homem, V. and Santos, L. (2011). Degradation and removal methods of antibiotics from aqueous matrices-A review. *Journal of Environmental Management*, 92, 2304-2347.
4. Khandegar, V. and Saroha, A.K. (2013). Electrocoagulation for the treatment of textile industry effluent-A review. *Journal of Environmental Management*, 128, 949-963.
5. Mollah, M.Y.A., Morkovsky, P., Gomes, J.A.G., Kesmez, M., Parga, J. and Cocke, D.L. (2004). Fundamentals, present and future perspectives of electrocoagulation. *Journal of Hazardous Materials*, B114, 199-210.
6. Brillas, E. and Martínez-Huitle, C.A. (2015). Decontamination of wastewaters containing synthetic organic dyes by electrochemical methods. An updated review. *Applied Catalysis B: Environmental*, 166-167, 603-643.
7. Chen, G. (2004). Electrochemical technologies in wastewater treatment, *Separation and Purification Technology*, 38, 11-41.
8. Fogler, H.S. (1992). *Elements of Chemical Reaction Engineering*, Prentice Hall International Editions, USA.
9. Levenspiel, O. (1999). *Chemical Reaction Engineering*. John Wiley & Sons, USA.
10. Körbahti, B.K. and Demirbüken, P. (2017). Electrochemical Oxidation of Resorcinol in Aqueous Medium Using Boron-Doped Diamond Anode: Reaction Kinetics and Process Optimization with Response Surface Methodology. *Frontiers in Chemistry*, 5, 75.
11. Körbahti B.K. and Artut, K. (2010). Electrochemical oil/water demulsification and purification of bilge water using Pt/Ir electrodes. *Desalination*, 258, 219-228.
12. Samet, Y., Chaabane Elaoud, S., Ammar, S. and Abdelhedi, R. (2006). Electrochemical degradation of 4-chloroguaiacol for wastewater treatment using PbO₂ anodes. *Journal of Hazardous Materials*, B138, 614-619.





Investigation of failed node method to support healthy communication for linear wireless sensor networks

Musa Çibuk*¹, Davut Ari¹, Fikri Ağgün¹, Ümit Budak²

¹Bitlis Eren University, Department of Computer Engineering, Türkiye, mcibuk@beu.edu.tr dari@beu.edu.tr; faggun@beu.edu.tr

²Bitlis Eren University, Department of Electricity - Electronic Engineering, Türkiye, ubudak@beu.edu.tr

Cite this study: Çibuk, M., Ari, D., Ağgün, F., & Budak, Ü. (2022). Investigation of failed node method to support healthy communication for linear wireless sensor networks. *Advanced Engineering Science*, 2, 21-26

Keywords

WSN
LWSN
MAC Protocol
Linear Topology
Failed Node

Research Article

Received: 09.01.2022

Revised: 13.02.2022

Accepted: 23.02.2022

Published: 14.03.2022



Abstract

Wireless Sensor Networks (WSNs) are used extensively in many natural environment research and observation applications in the world, and their popularity is increasing day by day. In parallel with these studies, Linear Wireless Sensor Network (LWSN), which is a type of WSNs application, is frequently encountered for reasons such as meeting the security requirements of highways, bridges, pipelines, and border lengths, determining the needs, and observing. In the network structure of LWSNs, the nodes are lined up sequentially and the communication environment is created in a linear order. In this type of wireless networks, communication is carried out with Media Access Control (MAC) protocols, and it is important to design these protocols in accordance with linear array characteristics. Because, as the number of nodes in the network increases, the end-to-end delay of the packets increases and the data traffic of the nodes close to the coordinator node reaches very high levels. Although the increasing number of nodes in linear topology increases the possibility of collision and congestion, it is also important that the network connections of the nodes are not broken and the communication continues in a healthy way. Therefore, protocols developed for linear topologies are expected to have characteristics that can be connected seamlessly and transmit data to the center without error. For this purpose, within the scope of a project, a new MAC protocol has been designed by us, which is effective in minimizing LWSN problems and can ensure the continuity of the network connection in difficult physical conditions. With the failed node method, which is the main subject of our article and introduced in the protocol in question, an important study has been put forward to avoid situations that will disrupt the data transmission of the network.

1. Introduction

Nowadays, developments in electronic technologies make it possible to produce low-cost, high-processing, and small-sized sensor nodes (LN). As a result of these important developments, possibilities have emerged that allow the implementation of Linear Wireless Sensor Network (LWSN) applications, which can consist of many sensor nodes and are used along linear lines, easily. LWSN is a specialized type for WSN applications that require linear topology characteristic as seen in [Figure 1](#). Thanks to its linear array feature, operations such as installation, maintenance, and routing are very easy. However, there are difficulties to be solved in such networks, such as end-to-end latency, excessive data traffic at end nodes, network reliability, node failure, and link failure [1]. The linear nature of such networks can be an important motivation for designing custom protocols to increase reliability, efficiency, energy savings and network lifetime [2,3].

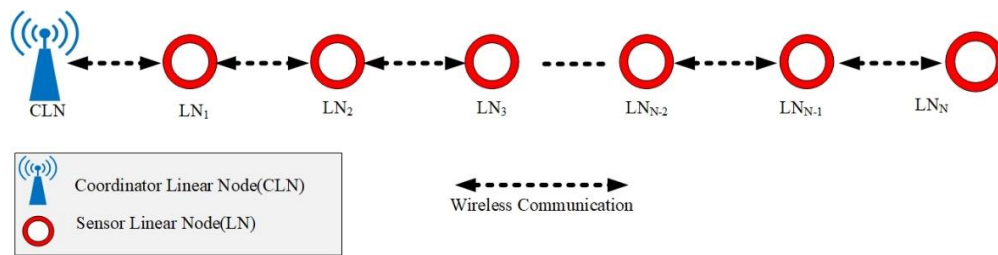


Figure 1. An example LWSN scheme structure

A MAC protocol that can be used in LWSNs and provides effective, healthy, and lossless communication has been put forward by us. A new method has been proposed, aiming to prevent the interruption of the communication of the nodes in the network with each other, which will be activated in case the nodes in the network fall from the network and contribute to the continuity of the network, even though the node named as the Failed Node is disconnected from the network. The success of the proposed method was demonstrated by the simulation and network model application. The performance analysis of the proposed MAC protocol was performed. The results show that the method that is activated in the node failure scenario in the proposed MAC protocol is a very effective method that can eliminate the disconnection in the network and continue the communication without any problems.

When all these developments are evaluated, it is thought that the method in the proposed MAC protocol will have an important place in the literature.

Karveli et al. [4] proposed a protocol that guarantees collision-free communication between sensor nodes distributed on a linear line and running synchronized with each other, which they called Directional Scheduled MAC (DiS-MAC). Thanks to the use of directional antennas; higher gains were obtained, signal transmission was provided to longer distances between nodes, and noise and collisions were eliminated as a result of the transmission of radio waves in a certain direction. In DiS-MAC, a single channel is used for data transmission and other operations.

In the LC-MAC [5] protocol, Fang et al. proposed a mechanism that pre-books relay nodes and transmits it in a burst to reduce end-to-end delivery delay in a long-chain sensor network without sacrificing energy efficiency.

The study named WiWi [6] can be said to be an advanced version of DiS-MAC. In particular, both protocols avoid interference between simultaneous transmissions by using alternate transmission based on sequencing between neighboring nodes.

LWSN networks continue to increase in popularity day by day. Well-designed MAC protocols, and the methods and methods used in these protocols have an important place among the most important factors affecting the efficient use of resources by sensor nodes with limited resources with low features. MAC layer in a layered WSN architecture; It is the layer where delays are tried to be reduced, possible collisions are prevented to reduce packet losses, and energy efficiency is tried to be increased with minimum packet traffic.

The MAC protocol developed within the scope of this study; has been designed by taking into account the control and energy saving issues, especially in roadside lighting in urban and intercity highways. In addition, different operating modes (ToSlave, ToMaster, and 2Way) have been introduced in order to overcome energy efficiency and worst-case scenarios in the network. An uncontested approach has been established in the proposed MAC protocol.

LWSN is formed by arranging sensor nodes one after another along a line. In fact, as the number of nodes increases, many network parameters such as end-to-end latency, network connection success, energy saving, and network lifetime are adversely affected. In this respect, many researchers have focused their attention on topology optimization, and many studies have been and continue to be made on this subject [7-11]. Considering all these, topology optimization is among the attractive research topics in the LWSN literature.

Energy-efficient node placement research is among the main design considerations for all WSNs, and especially for large-area LWSNs [3]. Li and Shunjie [11] investigated two different node placement strategies to maximize network lifetime and optimize network load balance in LWSNs.

In our study, it is thought that the proposed method to optimize the topology and feel the network disconnection as little as possible will take its place by supporting the topology optimization approach.

With these aspects, it is thought that the method in the proposed protocol will make an effective contribution to the literature.

2. Material and Method

The Failed Node method, which is included in the developed MAC protocol and maintains the communication in the network even if the nodes are disconnected from the network by ensuring the continuity of the network,

and which significantly affects the protocol performance in this respect, has the mechanism whose diagram is given in Figure 2.

Thanks to this structure defined in the MAC protocol, the node, which decides that its neighbor has dropped from the network, increases its coverage area, scans the distance of two hops instead of one hop, and communicates with its neighbor at two hops distance and can ensure the continuation of the network over themselves. Thus, this mechanism ensures continuity of the communication line. In the example simulation scenarios, in the first case, neighboring nodes communicate in the area with a radius of 125m. In case of a node failure, that is, if the node drops from the network for any reason, if the node that will transmit the packet cannot receive the negative-addressed reflection packet for a certain period of time, it concludes that there is no node within the scope of the packet in the relevant forward direction. In this case, it expands its coverage area, in other words, it increases the signal strength to cover the area with a radius of 225m. Thus, it switches to a 2-hop communication mode and reaches the two next nodes, and the communication of the network continues without interruption. Within the scope of this study, only one node disconnected from the network was studied, and the behavior in case of disconnection in more than one consecutive node was not discussed.

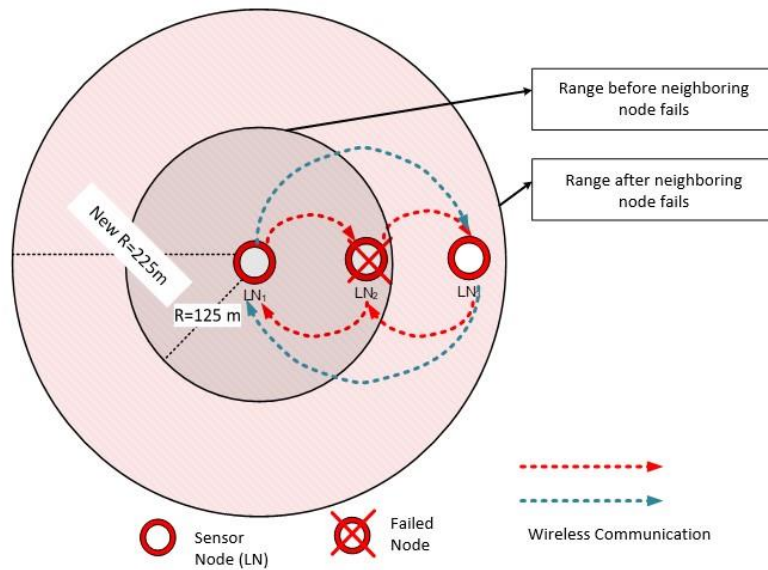


Figure 2. Behavior Mechanism of Failed Nodes

The Riverbed Modeler program was preferred for the performance evaluation of the MAC protocol proposed within the scope of this project. There are three types of nodes in the prepared Network Project environment. There are 10 standard nodes (LN, Sensor Node), 2 CLN (Coordinator Node) and 1 SINK node. The radio propagation range is 125m - 225m. The simulation parameters are given in Table 1.

Table 1. Simulation Parameters

Items	Value(s)
Radio propagation delay model	dra_propdel
Modulation	bpsk
Radio propagation Range	125m & 225m
Transmit Power	SR_tx = 0.027w
Receive Power	Sr_rx = 0.0366w
LN Count	10, 20, 30, 40, 50
CLN Count	2
Sink Count	1
Node Layout	Linear
Used Channel Count	1
Distance Between Nodes	100m
Simulation time	25s

Connection Continuity Analysis of the Nodes has been done under the above-mentioned network environment conditions, and the success status has been obtained.

3. Results

It is of great importance in terms of network performance that LWSN nodes connect to the network and perform their duties without disconnecting from the network. In fact, the failure of a node can affect the entire network from the linear topology feature. Under this title, the reactivity and behavior of the protocol, due to the relevant method, in case if a node drops (breaks off) from the network for any reason, has been examined. Within the scope of the project, single node falls on the line are considered. A consecutive large number of node failure (error burst) cases are left as a subject for further studies and are not covered in this study. The example scenario applied to show the response of the nodes and the continuation status of the network in case of node failure is shown in Figure 3.

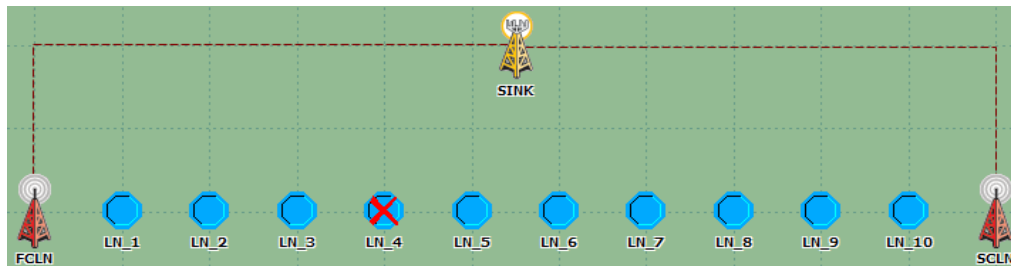


Figure 3. Failed node example scenario

As can be seen in the figure, a node (LN4) in the network was disconnected from the network in a certain time period and after a while, the disconnected node was allowed to join the network again. Against this situation, the total number of active nodes in the network is shown in the graph in Figure 4.

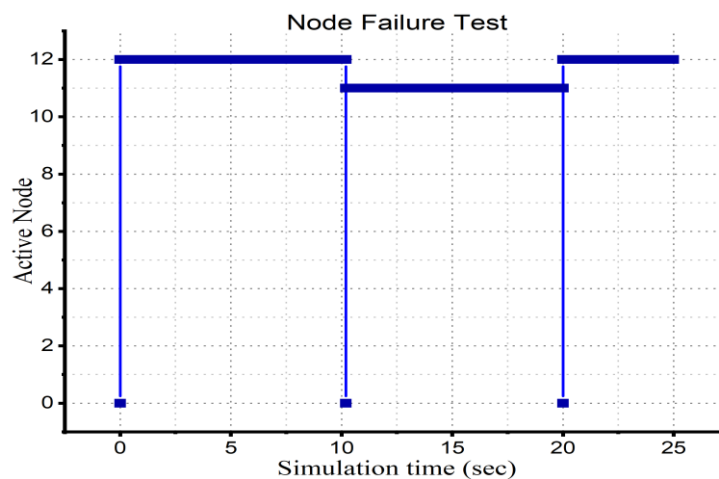


Figure 4. Failed node graphic

In Figure 4, it can be seen that the number of nodes decreases by 1 when one of the nodes is dropped from the network. If packet mobility continues in the network, it can be said that the broken node does not affect the network communication. When Figure 5 is examined, the packet mobility situation is observed in the above graph, although the number of nodes is missing 1 for a while and after a certain period of time, it rejoins the network and completes the number of nodes.

4. Discussion

When Figure 5 is examined, it is seen that although a node is disconnected from the network, data packet communication continues in that process. In this case, with the node falling from the network, neighboring nodes doubled their coverage area, and continued communication and connection continuity was ensured in the network. It is seen that the same number of packets reached the destination in all three data transmission models. The results show that the failed node method in the proposed protocol works, and the transmission continues without packet loss in the network, proving the success of the method.

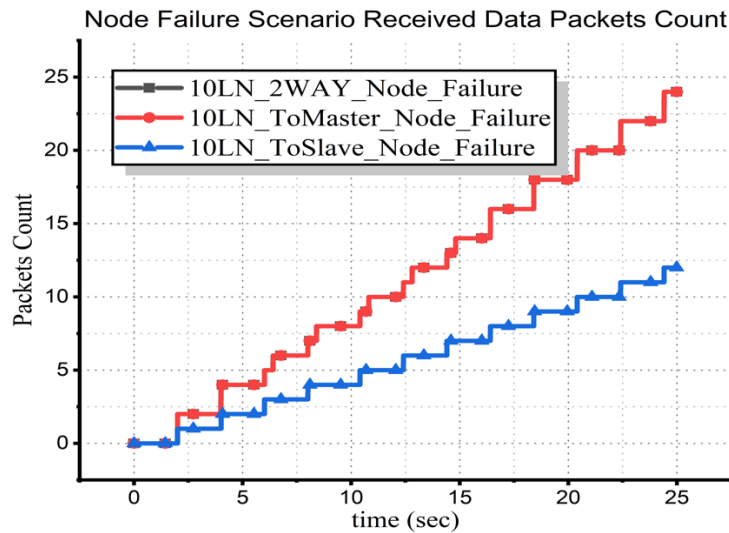


Figure 5. Number of data packets transmitted in case of failed node

5. Conclusion

LWSN application simulation shows that the proposed protocol in the simulation environment and the node failure method in the protocol work successfully, and this success also shows that our proposed method has an important place among the precautions to be taken against breaks in the network.

In the node failure method, the node that has fallen from the network performs its task by expanding the coverage area of the neighboring node, and the continuity of data communication is ensured without disrupting the communication of the network.

Within the scope of this study, only one node disconnected from the network is studied, and the behavior in case of disconnection in more than one consecutive node is left for later studies.

Funding

This project study was supported by Bitlis Eren University Scientific Research Projects Unit with project number BEBAP2019.006. We would like to thank Bitlis Eren University Scientific Research Projects Unit for their contribution and support.

Acknowledgement

This study is an extended version of the study titled "Investigation of failed node method to support healthy communication for linear wireless sensor networks" presented at the 1st Advanced Engineering Days (AED) held on Thursday, December 23, 2021 in Mersin/Turkey [12].

Author contributions

Musa Çibuk and **Davut Ari**: Conceptualization, Methodology, Software. **Fikri Ağgun**: Data accuration, Writing-Original draft preparation, Software, Validation. **Ümit Budak**: Visualization, Investigation, Writing-Reviewing and Editing.

Conflicts of interest

There is no conflict of interest between the authors.

References

1. Chen, H., Chi, K. T., & Feng, J. (2009). Impact of topology on performance and energy efficiency in wireless sensor networks for source extraction. *IEEE Transactions on Parallel and Distributed Systems*, 20(6), 886-897.
2. Jawhar, I., & Mohamed, N. (2009, April). A hierarchical and topological classification of linear sensor networks. In *2009 Wireless Telecommunications Symposium* (pp. 1-8). IEEE.
3. Varshney, S., Kumar, C., & Swaroop, A. (2015, May). Linear sensor networks: Applications, issues and major research trends. In *International Conference on Computing, Communication & Automation* (pp. 446-451). IEEE.
4. Karveli, T., Voulgaris, K., Ghavami, M., & Aghvami, A. H. (2009, October). DiS-MAC: A MAC protocol for sensor networks used for roadside and highway monitoring. In *2009 International Conference on Ultra Modern Telecommunications & Workshops* (pp. 1-6). IEEE.
5. Fang, C., Liu, H., & Qian, L. (2011, April). Lc-mac: An efficient mac protocol for the long-chain wireless sensor networks. In *2011 Third International Conference on Communications and Mobile Computing* (pp. 495-500). IEEE.
6. De Caneva, D., & Montessoro, P. L. (2010). A synchronous and deterministic MAC protocol for wireless communications on linear topologies. *Int'l J. of Communications, Network and System Sciences*, 3(12), 925-933.
7. Xie, W., Zhang, X., Chen, H., (2007). Wireless sensor network topology used for road traffic. *IET Conf. Publ.* 2007, 285-288.
8. Wu, C. H., & Chung, Y. C. (2007, May). Heterogeneous wireless sensor network deployment and topology control based on irregular sensor model. In *International Conference on Grid and Pervasive Computing* (pp. 78-88). Springer, Berlin, Heidelberg.
9. Alfayez, F., Neill, I., (2016). Topology-based Optimization of Linear Wireless Sensor Networks. *Proc. - 2015 Eur. Intell. Secur. Informatics Conf. EISIC 2015 2016*, 183.
10. Fu, X., Pace, P., Aloï, G., Yang, L., Fortino, G., (2020). Topology optimization against cascading failures on wireless sensor networks using a memetic algorithm. *Comput. Networks*, 177, 107327.
11. Hong, L., Xu, S., (2010). Energy-Efficient Node Placement in Linear Wireless Sensor Networks. *2010 Int. Conf. Meas. Technol. Mechatronics Autom.* March 2010, 104-107.
12. Çıbuk, M., Arı, D., Ağgün, F., & Budak, Ü. (2021). Investigation of failed node method to support healthy communication for linear wireless sensor networks. *Advanced Engineering Days (AED)*, 1, 41-44.



© Author(s) 2022. This work is distributed under <https://creativecommons.org/licenses/by-sa/4.0/>



PM_{2.5} concentration measurements and mapping at Gokusagi Mall for autumn 2018, in Konya, Turkey

Sukru Dursun ^{*1}, Mina Naseer Qasim ¹

¹Konya Technical University, Environmental Engineering Department, Konya, Türkiye, sdursun@ktun.edu.tr; mineenviro@gmail.com

Cite this study: Dursun, S., & Naseer Qasim, M. (2022). PM_{2.5} concentration measurements and mapping at Gokusagi Mall for summer 2018, in Konya, Turkey. *Advanced Engineering Science*, 2, 27-34

Keywords

Air quality
Indoors
Measuring
Modelling
Particulate matters
PM_{2.5}
Shopping centers

Research Article

Received: 10.01.2022
Revised: 14.02.2022
Accepted: 24.02.2022
Published: 14.03.2022



Abstract

The majority of people living in urban areas spend a significant part of their lives indoors such as homes, schools and workplaces. Therefore, the air quality of indoor or indoor environments is very important. As in Turkey, while improving the outdoor air quality first, regulations on indoor air quality have started to be developed recently, or lower pollutant concentrations are determined by lowering the air quality standards by certain ratios for acceptable limit values for indoor environments. Ventilation systems and air quality are very important especially for Shopping Centers, which are visited by people from different walks of life and have many different business lines. Gökkuşuğu Shopping Center also causes thousands of patients and their relatives to visit because of the fact that the Faculty of Medicine has more than 100 personnel, together with around 100 thousand students belonging to Selçuk University. Gökkuşuğu Shopping Center, which was established to meet the needs of these people, serves around 100 people with its cafes, restaurants and many workplaces. This service is concentrated at certain hours, especially when there is a need for food. In this study, which was carried out during the university education period, the measurements of the particle size (PM_{2.5}) pollution reaching the human lungs and remaining there to a large extent were made at 6 different hours between the opening-closing hours of the shopping mall. The distribution of the pollutant in the space was modelled using the Surfer16 package program and the distribution map was drawn. The values obtained in the measurements were above the international standards.

1. Introduction

Industrialized societies also want a modern living space in modern life and living spaces. These vehicle demands bring along motor vehicles and industrialization close to city centres and this poses a danger to human and environmental health. Gases belonging to air sources, and their life span in nature and nature are important due to their nature. A person breathes an average of 13,000–16,000 liters of air per day, or 400–500 million liters of air in a lifetime. Therefore, clean and polluted air is important for humanity [1]. Among the world climate, one of the world's weathers has been determined in relation to the world climate in 1992. Indoor air circuit from 2 main sources. Designs consisting of interior design and design, interior designs consisting of interior designs.

Indoor PM uses are affected by drinking, cooking, home, etc., first of all, outdoor-indoor atmosphere-indoor ventilation such as resuspension and ventilation, and removal from outdoor-indoor air such as hand precipitation [2-4]. Certain indoor environments in homes are expressed in time, outdoor environments indoor PM_{2.5} levels approximately 75% PM₁₀ levels approximately 66%. Since there are important indoor types in homes, it is understood that the contribution of outdoor air to indoor PM₁₀ and PM_{2.5} levels is still around 55-60% [5].

No PM_{2.5} exposure threshold has been defined to provide an unequivocally safe and complete level of protection against all adverse health effects [6]. However, in order to limit the health effects of fine particle pollution, the World Health Organization (WHO) has proposed guidelines for annual and short-term (24 hours) human exposure to PM_{2.5}. In addition to these global standards, WHO encourages governments to define and implement national standards [7].

Smoking, ventilation mechanisms, heating, cooking and other indoor activities in indoor environments can cause the dispersion of dusts and particles in the indoor environment. When the activities that can cause the dispersion of these particles do not occur, normal activities of people, cleaning activities, moving, skin rashes, dust particles precipitated from fabric and paper fibres may cause the dispersal of dust particles to the environment again [8]. Today, due to the prevalence of research on air pollution and the health problems it causes, it is carried out with the data of outdoor air quality. However, since people spend 87% of their time indoors and these environments have poor air quality, indoor data should be examined instead of outdoor data in order to evaluate the impact of the air in the environment on health.

In this study, PM_{2.5} concentrations were measured at different times during the day in the closed environment of the closed social area Gökkuşuğu Shopping Centre at Selçuk University, one of the campuses with the highest number of students in Turkey, and three-dimensional pollution maps were obtained by modelling the indoor distribution.

2. Material and Method

2.1. Study area

In this study, which was started on the basis of shopping centres located in Selçuklu district of Konya province, suitable measurement points were determined for making measurements. This place, which was chosen by paying attention to its indoor environment, was chosen as the place where people visit the most on the campus of Selçuk University.

It was carried out in the social facilities that serve students-employees and those who come to the hospital in the Alâeddin Keykubat campus of Selçuk University, and the locations for the data were determined. The details of the study area are given in Naseer Qasim [9].

There are two corridors with a width of approximately 2 m in the north, east and west parts of the shopping centre. Some business entrances lead to these corridors. These corridors, which consist of a ceiling structure that cannot be high as a structure, cause the air pollutants circulating in a narrow area to be trapped in a narrow area and close to the respiratory level.

Although existing workplaces have ventilation systems, they are not sufficient in common areas. In previous years, the air blowing system was out of use due to technical malfunctions. Although the Gökkuşuğu Shopping Center, which was built and put into operation in the past years, has undergone simple renovations over time, there has not been sufficient improvement from its opening to the working period. 13 measurement points were determined to represent the space for your measurements in the rainbow (Figure 1).



Figure 1. Selçuk University Alaeddin Keykubat Campus Gökkuşuğu shopping centre sampling points [10]

2.2. Atmospheric Particulate Matter Measurement Method

Atmospheric particulate matter measurement methods vary according to the size and purpose of the particles. Thanks to electronic systems, a laser particle counter and dust measuring device "Particle Counter PCE-PC01"

configured to determine the concentration of particles in the atmosphere can be determined. This device is used in non-polluted environments, indoor air quality or exposure to cigarette smoke and other harmful air pollutants, and for monitoring dust levels in the air. Detailed information for measurement can be obtained from [9] and [11].

In a study conducted by Stranger et al., [12] in 18 homes and 27 schools, it was determined that cigarette smoke was the most effective reason for the presence of PM_{2.5} and PM₁₀ pollutants. In the study by Lee *et al.*, [13] at 14 different points (restaurants, libraries, shopping malls, gyms, parking lots), it was determined that there are traffic emissions and roads as PM₁₀ pollutant sources and this is reflected in the indoor environment. A total of 14 different points were used as indoor environment in the study conducted in. Indoor / outdoor ratios for PM₁₀ were found to be due to the high infiltration rate and the presence of indoor air pollutants. The indoor / outdoor ratio for PM₁₀ is 4 times higher, respectively, in smoking areas than in non-smoking areas [13]. In the indoor air PM measurements made at a University in Istanbul, measurements were made in the canteen, dean's office, financial office and classrooms. and EPA limit values of 35 µg/m³ are only exceeded in the canteen and workshop [14].

2.3. Modelling and graphics program Surfer-16

Golden software 16 is a program capable of modelling and creating a 3D graphic preparation system that includes basic statistics. It is used for creating contour maps and obtaining 3D images by processing complex data obtained from different processes and making grids [15, 16]. Since the eighties, more than 100,000 scientists and engineers around the world This program, which transforms the collected data into information, visualizes the data in high quality while preserving its accuracy and precision [17]. Along with Surfer's extensive modelling tools, interpolation and grating parameters can be adjusted, define errors and breaks, or perform grid calculations such as volumes, transformations, smoothing or filtering [18].

2.4. Particulate matter PM_{2.5} measurement method

In the researches carried out to determine the particulate matter concentrations, the pollutant sources in the external environment were examined. By comparison, there is less information about indoor particulate matter pollution, its concentrations, sources, and exposure levels to people who spend most of their time in various indoor environments [19]. In order to determine the interaction of particulate matter values with seasonal changes, studies are carried out in different seasons to take measurements in the study. In this study, autumn was chosen as the opening period of schools, and in the study, two-day measurement intervals were determined on weekdays and weekends. The periodical measurement period was completed as 4 days.

The daily measurement program, in which the measurements were made, lasted 10 hours depending on the working hours of the places. Measurements were repeated in 6 periods per day with an interval of 2 hours. After the measurement points and coordinates were determined, the final data were collected and the Excel table was arranged and listed in such a way that daily, weekly and hourly averages were taken. X and Y coordinates and Z coordinate represented the measured PM_{2.5} values. A worksheet was created by transferring X Y coordinates and measurement values to the SURFER 16 program. Statistical calculations were made by converting the prepared data into tables. Then, contour map is selected from the map options in order to show the contour lines. The customization window is used to clearly show high and low concentrations and dispersion lines on the map.

3. Results and Discussion

Particulate matter 2.5 micro meter size measurements were carried out in the autumn period in the rainbow shopping centre of Selçuk University Alaeddin Keykubat campus, which is one of the important shopping centres in Konya. The sampling period, the second sampling period, was carried out between 24.09.2018 - 07.10.2018. During the measurement period, measurements were made for one week. Weekly average distributions of particulate matter PM_{2.5} were prepared for Surfer 16 by measuring 6 times a day.

Within the scope of the research, it was arranged to cover the opening and closing hours of the shopping centre between the hours of weekdays and weekends (09.00 - 19.00) at the Gokkusagi AVM at the university. As a result of the study, the average values of PM_{2.5} obtained from the examination of all data during the week and at the weekend are shown in Table 1.

Table 1. Autumn season weekday and weekend particulate matter PM_{2.5} averages in Rainbow shopping mall.

Sampling period	Weekday average PM _{2.5} µg/m ³	Weekend average PM _{2.5} µg/m ³
autumn	693	496

Average PM_{2.5} concentrations in the autumn 2018 period were found to be 693.65 µg/m³ and 495.75 µg/m³ on weekdays. Measurement times were made between 09.00-19.00 hours. The 7-day measurement period, which started right after the official semester registration of Selçuk University, started on 24.09.2018 and continued until 30.09.2018.

The weekday average was found to be 1400 µg/m³ even in the early hours of the day thanks to the pollution that occurred at point F (west entrance gate) and exceeded 1000. It affects the entrance point of the restaurant

chimneys located on both sides of the entrance door. Values not exceeding $700 \mu\text{g}/\text{m}^3$ were observed during weekdays in other parts of Gökkuşağı Shopping Center.

Low PM_{2.5} concentration was found to be $760 \mu\text{g}/\text{m}^3$, resulting from quieter weekends and fewer visits. The modelling results of the first average PM_{2.5} concentration of the study period at 09:00 are shown in Figure 2.

The values at 11:00 am found to be quite high and the PM_{2.5} value was found to be $2900 \mu\text{g}/\text{m}^3$. Here, the particle pollution formed at point B started from the north-eastern part of Gökkuşağı Shopping Center and spread towards the centre. PM_{2.5} concentration was found to be at least $1300 \mu\text{g}/\text{m}^3$ at points J and K where cooking restaurants are located. Cooking activities have been ranked 2nd by EPA as the indoor PM_{2.5} formation source [20].

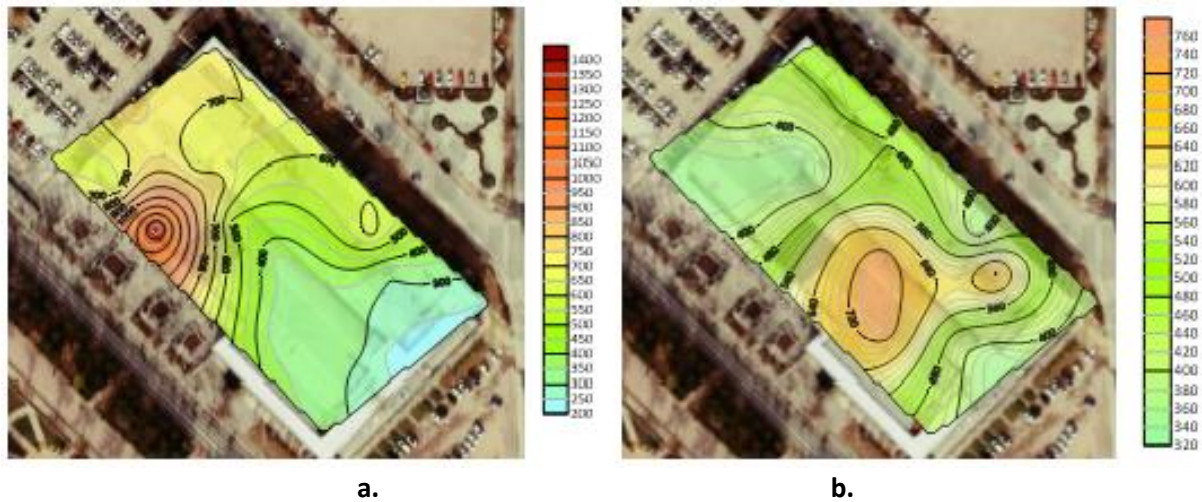


Figure 2. Gokkusagi Shopping Center at 9:00 a. Weekdays, b. Weekend average

A comfortable and healthy indoor environment in restaurants increases the visual appearance and protects the health of customers and employees against harmful air pollutants [21]. Weekend Particulate matter pollution is $1350 \mu\text{g}/\text{m}^3$ by showing its effect only at the point where it occurs. In other parts of the mall, concentrations during the weekend did not generally exceed $300\text{-}400 \mu\text{g}/\text{m}^3$. Figure 3 shows the modelling results at 11:00.

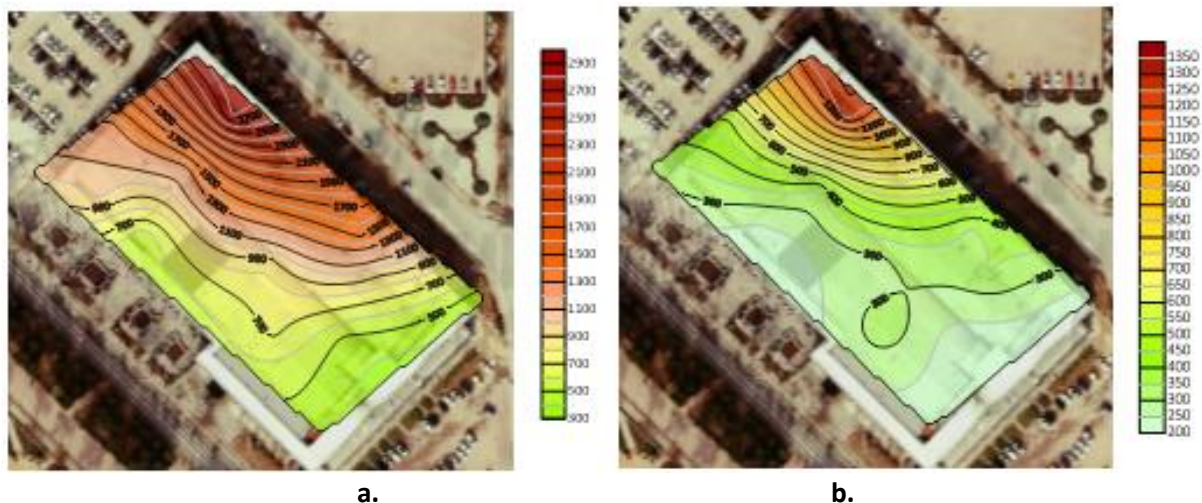


Figure 3. Gokkusagi Shopping Center at 11:00 a. Weekdays, b. Weekend average

Looking at the pollution map prepared for 13.00, it is seen that the PM_{2.5} concentration shows a similar distribution to 11:00. While values are found as $1300 \mu\text{g}/\text{m}^3$ in the northern part of Gökkuşağı Shopping Center, they do not exceed $650 \mu\text{g}/\text{m}^3$ in the central and southern parts. At the weekend, lower concentrations dominated the building, while the maximum PM_{2.5} value was found to be $700 \mu\text{g}/\text{m}^3$. Maps are presented in Figure 4 to show PM_{2.5} concentrations at 13:00 on weekends and weekdays.

Looking at the results obtained from the 15.00 hours sampling, the average PM_{2.5} values at the weekend were found to be higher than the weekday values, with a value of $2600 \mu\text{g}/\text{m}^3$, showing that the region with the most pollution corresponds to the J point. The fact that the restaurant has a wide front façade causes all the pollutants and PM_{2.5} particles formed in the case of using the stoves at the back, to spread directly to that area. Weekday average was found to be $2100 \mu\text{g}/\text{m}^3$. Weekday results were higher at point B, similar to the 13.00-hour average. The mean concentrations at 15.00 hours are shown in Figure 5.

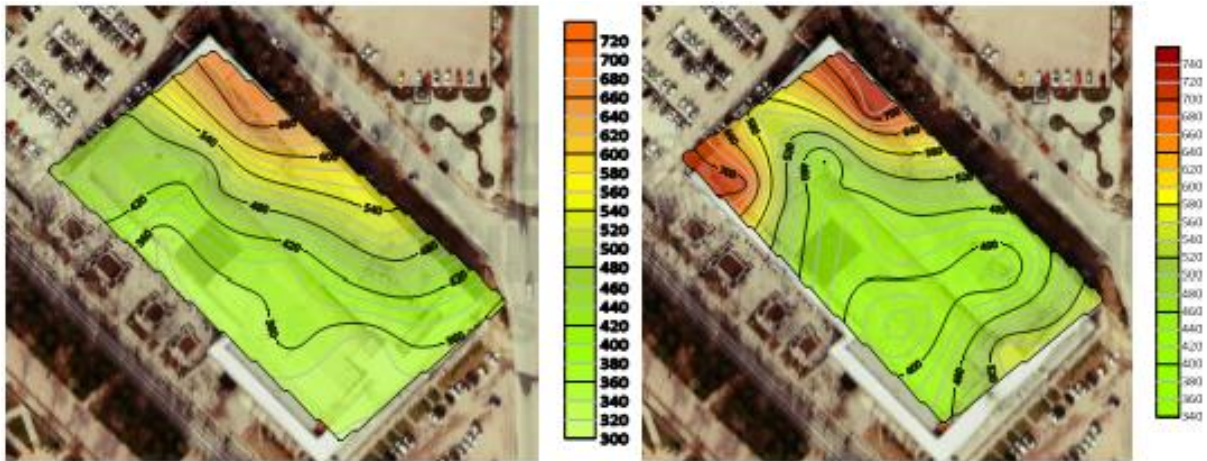


Figure 4. Gokkusagi Shopping Center at 13:00 (a-Weekdays, b-Weekend average)

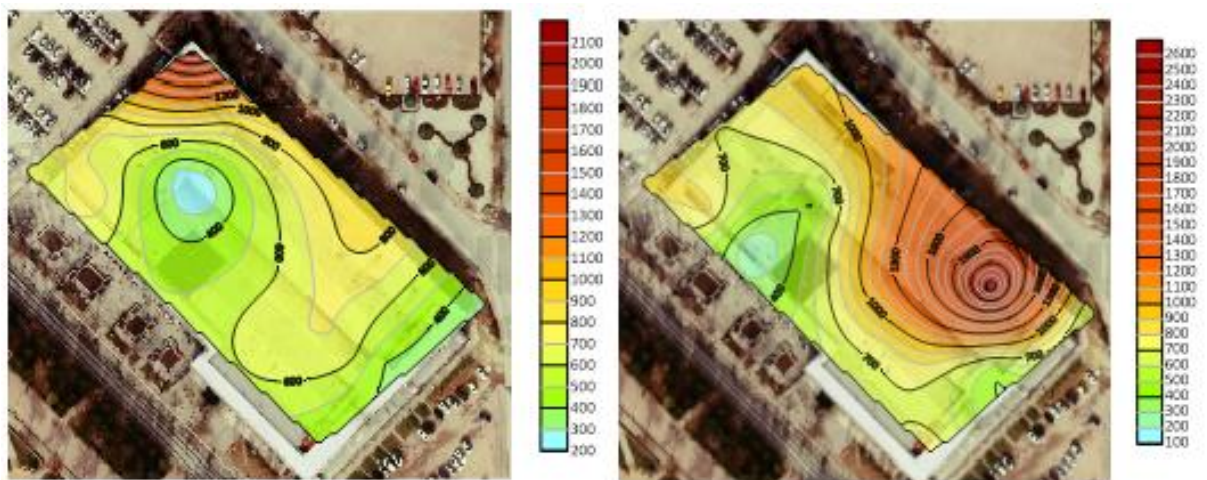


Figure 5. Gokkusagi Shopping Center at 15:00 (a-Weekdays, b-Weekend average)

At 17.00, PM_{2.5} values were found to be 950 µg/m³ on weekdays and weekends with equal concentrations. However, the areas where the pollution is visible are different from each other. While the distribution of pollution during the week is distributed from the north-eastern part of the Rainbow Shopping Centre to other regions, on the weekend map, on the contrary, there is a distribution in the south-eastern part of the building. It is estimated that the pollution originating from the outside environment has penetrated into the indoor environment thanks to the south entrance door located there. The results are shown in [Figure 6](#).

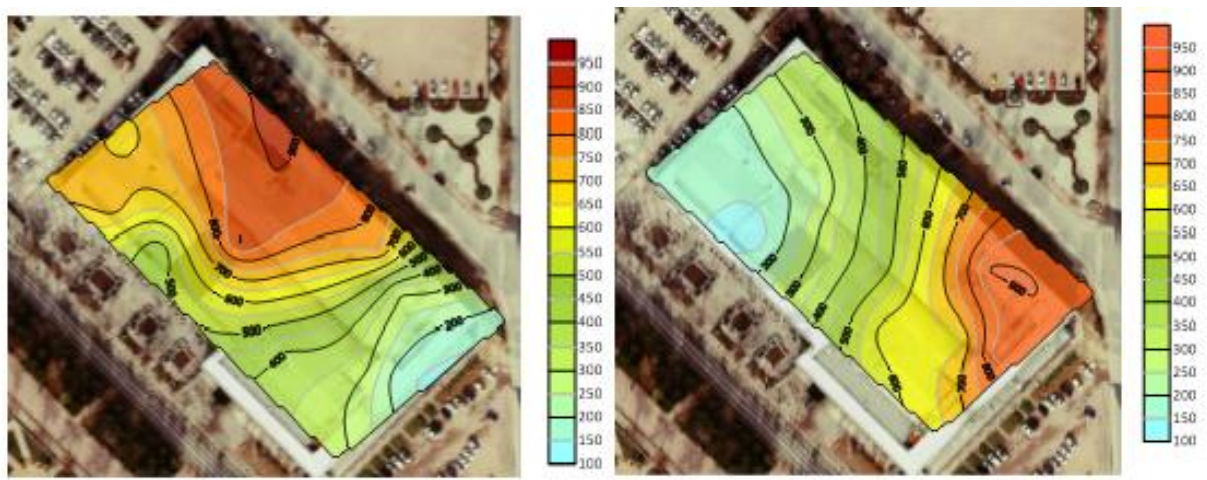


Figure 6. Gokkusagi Shopping Center at 17:00 (a-Weekdays, b-Weekend average)

Particulate matter PM_{2.5} pollution level further reduced the values at 19.00, when the last measurement of the day was made, and concentrations close to each other were observed throughout the building on weekdays and the average was found to be 660 µg/m³. At the weekend, this value decreased further and the lowest average concentration of the autumn season was found as 540 µg/m³. It is the explanation of why such low PM_{2.5} levels are encountered in Gökkuşağı Shopping Centre at the last measurement hour of the day on the weekend, with staff, students and staff leaving the campus. Weekend and weekday maps of the PM_{2.5} distribution at 19.00 are shown in Figure 7.

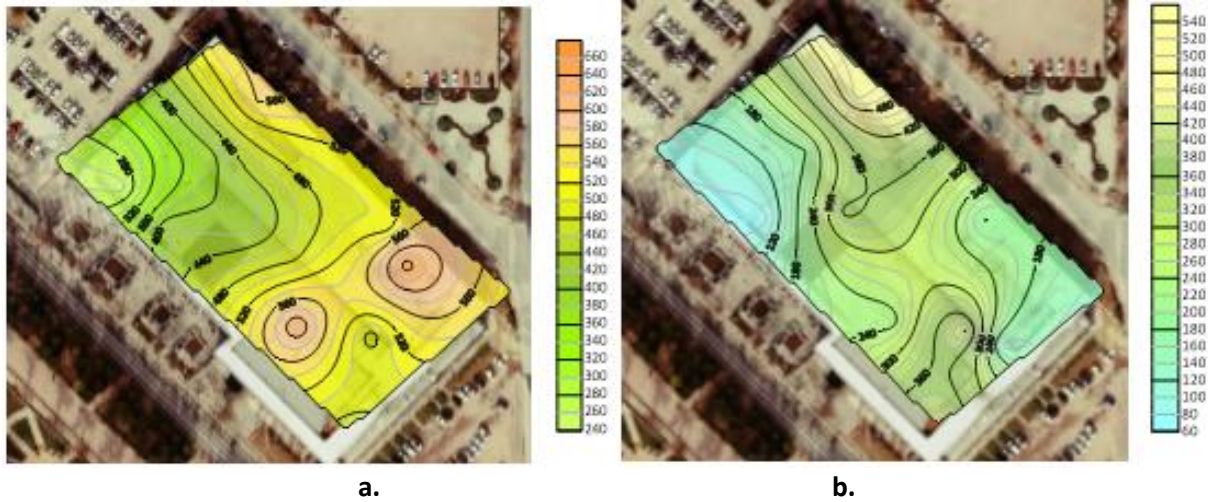


Figure 7. Gokkusagi Shopping Centre at 19:00 (a-Weekdays, b-Weekend average)

When the measurements made during the study period are examined, the lowest PM_{2.5} value is 540 µg/m³. This value exceeds the hourly 25 µg/m³ limit set by WHO, EEA and EPA for PM_{2.5} [22, 23]. In Turkey, the standard value for PM_{2.5} in the air quality outdoor assessment management and regulation, which was last updated in 2008, is much higher than 200 µg/m³. The results obtained should be much lower than the HKDYD limit value [24], but exceed these values.

4. Conclusion

In this study, indoor PM_{2.5} air quality, a breathable air pollutant, which is an important environmental problem in Turkey as in the world, has been examined. Although air pollution is a major problem in Konya, one of the most important industrial cities of Turkey, this study for indoor environment is based on shopping malls, the particulate matter PM_{2.5}, which carries serious risk factors on human health and is ranked second among air pollutants by the World Health Organization. measurements and modeling were done. In order to make the measurements, it was preferred to make the measurements at the Gökkuşağı Shopping Center located on the Selçuk University Alâeddin Keykubat campus. The sampling period for the measurements was carried out between 24.09.2018 and 07.10.2018. Sampling hours at Gökkuşağı Shopping Center were held between 09:00 and 19:00. How particulate matter PM_{2.5} affects indoor air quality throughout the period and what causes it are examined. The results were mapped and modeled using the Surfer 16 program. While modeling, the results were interpreted as weekday and weekend averages. As a result, measurement PM_{2.5} values in Gökkuşağı Shopping Center did not exceed WHO's standards.

It is thought that the fact that the building structure of Gökkuşağı shopping center is older has an effect on the results. In addition, the central ventilation system in the building was not repaired and closed for use years ago as a result of deterioration, resulting in insufficient air circulation inside. Thanks to the stationery, photocopiers, restaurants, clothing, tailors and cafes in the building, there are only three exit doors so that the pollutants dispersed in the indoor environment can mix with the outside environment. The number of daily visitors also had an effect on the high values observed especially at noon. In addition to the lack of ventilation, the absence of a ban on smoking caused the corridors in the northern part of the building to be exposed to the highest PM_{2.5} pollution. It is thought that the old building materials and the unrepaired structure also affect the pollution level. Since the measurements took place on campus, higher values were obtained during the week, except for some exceptional cases. This building, which is located right across the medical faculty hospital in terms of its location, caused an increase in PM_{2.5} pollution in the Gökkuşağı Shopping Center in direct proportion to the patient visiting hours of the hospital.

5. Recommendation

In order for people to spend most of their time in their homes, workplaces, indoor living areas such as public transportation vehicles and shopping malls and to breathe healthy air, these environments and existing ventilation systems, devices and vehicles must be constantly monitored and controlled in terms of quality atmosphere. For this reason, it is necessary to implement methods that will ensure an acceptable indoor air quality in shopping malls. These methods are respectively;

- Removal of the pollutant source that affects the air quality,
- In order to reduce the pollution concentration, the ventilation systems should be made according to the conditions suitable for the environment in which they will be used, using them correctly and maintaining them at routine intervals,
- It is recommended to take precautions against smoking in closed environments.

Also; Universities should organize lectures, symposiums and educational seminars in educational institutions about the importance of indoor air quality and its effects on health. Due to the lack of standards determining indoor air quality in Turkey until today, it is recommended that the relevant institutions take action as soon as possible to establish standard values for this air, which has a direct impact on the health of living things. It should be ensured that the parameters determining the air quality in all provinces of Turkey are measured and modeling maps are created.

Acknowledgement

This paper has been prepared a part of Mina Naseer Qasim's MSc.Thesis and presented at 1st Advanced Engineering Days, Mersin, 2021 [25].

Funding

This research has been funded by Selcuk University, Scientific Research Found, Project no: 18201117

Author contributions

Sukru Dursun: Conceptualization, Methodology, -Reviewing and Editing; **Mina Naseer Qasim:** Investigation, Data curation, Writing-Original draft preparation, Modelling.

Conflicts of interest

The authors declare no conflicts of interest.

References

1. Yurtseven, E., (2008). İki farklı bölgedeki ilköğretim okullarında iç ortam havasının insan sağlığına etkileri yönünden incelenmesi, PhD. Thesis, İ.Ü. Sağlık Bilimleri Enstitüsü. İstanbul.
2. Quackenboss, J. J., Lebowitz, M. D., & Crutchfield, C. D. (1989). Indoor-outdoor relationships for particulate matter: exposure classifications and health effects. *Environment International*, 15, 353–360.
3. Thatcher, T. L. & Laytol, D. W., (1995). Deposition, re-suspension and penetration of particles within a residence. *Atmospheric Environment*, 29, 1487–1497.
4. Moriske, H.-J., Drews, M., Ebert, G., Menk, G., Scheller, C., Schondube, M., & Konieczny, L. (1996). Indoor air pollution by different heating systems: coal burning, open fire place and central heating. *Toxicology Letters*, 88, 349–354.
5. Monn C. (2001). Exposure assessment of pollutant: a review on spatila heterogeneity and indoor/outdoor/personel exposure to suspended particulate matter, nitrogen dioxide and ozone. *Atmospheric Environment* 35, 1-32.
6. Kiesewetter, G., Schoepp, W., Heyes, C., & Amann, M. (2015). Modelling PM_{2.5} impact indicators in Europe: health effects and legal compliance, *Environmental Modelling & Software*, 74, 201-211.
7. WHO (2013). World Health Organization. Review of evidence on health aspects of air pollution. https://www.euro.who.int/__data/assets/pdf_file/0004/193108/REVIHAAP-Final-technical-report-final-version.pdf [Retrieved December, 2021]
8. Fromme, H., Twardella, D., Dietrich, S., Heitma, N, D., Schierl, R., Liebl, B., & Rüdén, H. (2007). Particulate matter in the indoor air of classrooms—exploratory results from Munich and surrounding area, *Atmospheric Environment*, 41 (4), 854-866.
9. Naseer Qasim, M. (2019). Determination and modelling of ambient particle material level in shopping centres. M.Sc. Thesis, The Graduate School of Natural and Applied Science of Selçuk University, Konya, Turkey.
10. URL-1, (2021). <https://earth.google.com/>

11. URL-2 (2021). https://www.pce-instruments.com/english/measuring-instruments/test-meters/particle-counter-pce-instruments-particle-counter-pce-pco-1-det_516316.htm
12. Stranger M., Potgieter-Vermaak S. S., & Van Grieken R. (2007). Comparative overview of indoor air quality in Antwerp, Belgium, *Environment International* 33 789–797.
13. Lee S. C., Chan L. Y., Chiu M. Y. (1999). Indoor and outdoor air quality investigation at 14 public places in Hong Kong. *Environment International*, 25(4), 443-450.
14. Onat B., Şahin Ü. (2008). İç Ortam Havasında Partikül Madde Seviyesinin Belirlenmesi. Ulusal Hava Kalitesi Sempozyumu. Konya.
15. Polat, O. (2002), Golden software surfer v.8 kullanım ile ilgili notlar
16. URL-3 (2021). <https://www.goldensoftware.com/>
17. Bresnahan, T., & Dickenson, K. (2002). Surfer 8 self-paced training guide, Golden Software Inc.
18. URL-4, (2021). Golden software products, <https://www.goldensoftware.com/products>:
19. Challoner, A., & Gill, L. (2014). Indoor/outdoor air pollution relationships in ten commercial buildings: PM2. 5 and NO₂, *Building and Environment*, 80, 159-173.
20. Lai, A. & Ho, Y. (2008). Spatial concentration variation of cooking-emitted particles in a residential kitchen, *Building and Environment*, 43 (5), 871-876.
21. Lee, S. C., Li, W.-M., & Chan, L. Y. (2001). Indoor air quality at restaurants with different styles of cooking in metropolitan Hong Kong. *Science of the Total Environment*, 279 (1-3), 181-193.
22. URL-5, (2021). Agency, U.E.P. Smoke-free Homes, <http://www.epa.gov/smokefree/healtheffects.html#What:>
23. URL-6, (2018). International Monetary Fund (2018). Report for selected countries and subjects., <http://www.imf.org/external/pubs/ft/weo/2017/02/weodata/weorept.aspx>:
24. ÇOB (2008). Hava Kalitesi Değerlendirme ve Yönetimi Yönetmeliği - Resmi Gazete. Sayı: 26898. 6 Haziran 2008. <https://www.resmigazete.gov.tr/eskiler/2008/06/20080606-6.htm>
25. Dursun, S., & Qasım, M. N. (2021). PM2. 5 Concentration Measurements and Mapping at Gökuşağı Mall for Autumn 2018, in Konya, Turkey. *Advanced Engineering Days (AED)*, 1, 72-74.



© Author(s) 2022. This work is distributed under <https://creativecommons.org/licenses/by-sa/4.0/>



Geological factors in solid waste landfill site selection

Ömer Kağan Arıcı*¹ 

¹Selcuk University, Environmental Protection Control Department, Türkiye, omerkagan@gmail.com

Cite this study: Arıcı, Ö. K. (2022). Geological factors in solid waste landfill site selection. Advanced Engineering Science, 2, 35-43

Keywords

Storage areas
Hydrogeological
Hydraulic
Geological
Solid waste

Research Article

Received: 10.01.2022
Revised: 13.02.2022
Accepted: 25.02.2022
Published: 14.03.2022



Abstract

It is possible to define all kinds of substances and materials that become useless as a result of human activities and do not contain enough liquid to be fluid, as "solid waste". This definition includes all sweepings and garbage generated in houses, streets, parks and institutions, solid wastes and wastes resulting from commercial agricultural and industrial activities, and sludge produced in water and wastewater treatment plants. Problems arising from solid wastes, which is one of the important environmental problems of our country, are increasing in parallel with the increasing population, and the necessity of landfills has gained importance in terms of environmental and human health. Solid wastes are generally disposed of through incineration, composting, recycling or landfill. The landfill is an integrated management system that includes the transportation of domestic solid wastes in accordance with the legislation, regular storage, sterilization of medical wastes, leachate treatment and storage gas disposal, and incineration system components. Many criteria are taken into consideration when selecting solid waste landfill sites. During the site selection, the preparation of thematic maps by examining the geological, hydrogeological, and hydrological characteristics of the area in detail is included in the field of geology. Within the scope of the investigation, the importance of geological factors in the selection of solid waste landfill sites was examined and their importance was stated within the scope of sustainable environmental protection.

1. Introduction

Solid wastes are collected in two main groups as medical and chemical wastes which consist of toxic substances and products, and domestic wastes (garbage). The disposal of solid wastes consisting of toxic chemical products requires very special scientific studies and legal regulations. Since storing and isolating them may cause new problems, rendering them harmless by incineration and chemical processes is seen as the most rational approach. Domestic solid wastes consist of domestic wastes from houses in residential areas, plant wastes from parks, gardens, and green areas, treatment sludge obtained from domestic wastewater treatment plants, excavation soil, and construction debris [1].

From ancient times to the present, people have used natural resources to sustain their lives. The disposal of wastes generated in this way did not pose a significant problem for a long time, since the population was low and the land required for the wastes to be absorbed in their natural environment was sufficient [2-6]. Problems related to the disposal of waste have emerged with the gathering of people in large and small communities such as tribes and villages, and the accumulation of waste, which is a part of life [7].

In the 1900s, waste was stored and burned at random places. With urbanization, industrialization, and rapid population growth, the negative effects of waste collection and incineration on the environment and human health have begun to be seen. As a result, methods such as incineration, composting, recycling, or landfilling have been developed for the disposal of solid wastes. Methods, except the last one, are not exact methods for eliminating all the waste. These methods aim to provide economic benefit from wastes. Landfilling is the only way to get rid of the waste completely. All kinds of solid waste can be safely stored in Regular Solid Waste (Garbage) Landfills built in accordance with technical standards. For this reason, there must be at least one Solid Waste Storage Area in all settlements. If the Solid Waste Storage Areas are not selected correctly and built-in accordance with the standards, it may cause irreparable problems in the future (Figure 1). Especially if the wastes come into contact with the groundwater, the effects can continue for 30 to 40 years even if the contact has disappeared. For this reason, the landfill site selection should be made after a serious examination and the Storage Facility should be built in a way that includes the issues specified in the Solid Waste Regulations [8-9].



Figure 1. The view of the problems that arise during the construction of a landfill area in pictures a, b, c, d [9]

The first and most important step in the regular storage of Solid Wastes begins with the selection of the appropriate location. The issues that need to be carefully considered in the selection of the appropriate place are as follows:

- A. It should not be in the recharge basin of water collection centers for drinking, use, or irrigation purposes.
- B. Groundwater should not approach the water table floor level more than 10 meters.
- C. The drainage system should be an outward-facing area, where surface water accumulates at least.
- D. It should not be an active fault, debris, landslide, avalanche, overflow, and erosion risk areas.
- E. The ground should consist of solid, less permeable rocks that geologically and geotechnically suitable.
- F. The traffic density should be low, especially away from the main artels.
- G. It should be at least visible from the surrounding area, away from the main recreation areas of the city.
- H. The storage capacity should be at a level to meet the city's minimum 30-year needs.
- I. There should be an area where the clay raw material to be used to seal the top and bottom of the wastes can be easily obtained.
- J. It should be open to main air currents in accordance with meteorological conditions.
- K. An Environmental Impact Assessment report should be available according to the storage capacity (ONEIA if it is less than 100 tons per day, EIA if it is larger).

Today, most of the garbage collected by the municipalities is haphazardly piled up on the fields created without any precautions and thrown away. While the municipalities, which allocate 40% of their budgets to cleaning expenses, fulfill the duties assigned to them in solid waste management in collecting and transporting, they do not show the necessary importance in evaluation and disposal. Especially the mistakes made in the selection of the "Wild Storage" fields for disposal and the negativities in the operating conditions cause growing problems day by day [10].

The rapidly increasing population and changing living standards make it difficult to control and manage wastes by increasing the volume of waste and diversifying the waste composition. Solid waste management is becoming increasingly important and complex due to the current and potential risks of solid wastes, the reduction of natural

resources, economic and other reasons. For this reason, it is necessary to know the elements of integrated solid waste management that include all stages from waste generation to final disposal and their relations with each other (Table 1) [11-12].

Table 1. Suggested methods for determining solid waste storage areas

Karaguzel and Mutluturk [13]	Costa and Ryan [14]	Dörhöfer and Siebert [15]
1. Waste Inventory a. Characteristics of trash to be stored b. Waste amount c. Disposal method 2. Location Selection a. Geology of the Site b. Hydrogeology of the Site c. Drilling d. Permeability tests e. Meteorological Condition f. Aquifers and Aquitares g. Ground-water 3. Control Systems 4. Storage Technique	1. Geology of the Region 2. Industry a. Liquid Waste Production b. Liquid Effect c. Environment d. Geomorphology and Hydrology e. Geology f. Hydrogeology 3. Soil and Water Pollution Studies 4. Field Studies a. Field Work Program b. Waste Zones c. Waterways	1. Site Selection Process a. Geological Studies b. Hydrogeological Studies c. Mapping positive and negative areas 2. Regional Planning Process a. Geological Routing Surveys b. Selection of Alternative Region / or Regions c. Effective Environmental Studies, Conferences 3. Permission Process a. Detailed geological study of the area b. Ground-Water studies c. Climate d. Environment 4. Geological Planning Surveys

The importance of geological factors cannot be overlooked in the conditions of suitable site selection mentioned above. Geological factors such as surface and underground waters, rock structure, active fault, debris, landslide, avalanche, flood, and erosion risk are particularly important in the selection of solid waste storage areas. Examining these factors and specifying their importance in choosing a suitable site constitute the basis of the research scope.

2. Wastes and Geological Factors

Solid waste occurs as a natural consequence of human life. In parallel with the increasing population and developing technology all over the world, there has been a serious increase in the amount of waste produced by people. Primitive methods applied for the disposal of these wastes threaten human health directly or indirectly. It has become a necessity to use modern technologies in order to minimize the damages caused by solid wastes to humans and nature [13].

Solid waste landfill site selection studies consist of three stages in geological terms. In the first stage, thematic maps are prepared by examining the geological, hydrogeological, and hydrological characteristics of the study area in detail. Since the storage facility is planned to be designed to meet the needs of the region for 50 years, a population projection and waste inventory are prepared to determine the area that will be needed in the construction of the facility. Conservation areas and land use status maps of the basin are also prepared and overlaid with other thematic maps in the computer simulation to obtain a synthesis map showing the regions that are suitable and unsuitable for the construction of facilities belonging to the basin. Alternative areas are determined on the synthesis map prepared in the second stage, taking into account the morphological features suitable for the placement of the facility units. In the third stage, the most suitable area for storage is determined among the alternative areas.

Table 2. Evaluation of alternative areas in solid waste landfill site selection

Criteria	Coefficients	The goodness of the Field		The score of the Field		
		Relativity	increasing goodness	1st Field	2nd Field	3rd Field
	5= most important	3	↑			
	1= least important	2				
		1				
Sample:						
Ground-water depth		3		15		
		2			10	
		1				5

These coefficients range from 1 to 5 and are graded as 1: least important, 2: less important, 3: important, 4: very important, 5: most important. In addition, alternative fields are ranked as 1, 2, 3 relatively to each other according to their goodness for each criterion (3: best, 2: less good, 1: least good). The score of each field from any criterion is determined by the product of the field's number in the ranking and the relevant criterion coefficient. Alternative fields are scored in this way according to each criterion. The alternative area with the highest total score is selected as the most suitable area for storage. In the last stage of the study, engineering geology studies are carried out for the design of the storage facility [16-17].

Table 3. Criteria used in solid waste landfill site selection and their coefficients

Assessment Criteria	Coefficients
Geological Suitability	
- Structural Feature	
- Fault Status	5
- Seismic Impact Zone	4
- Stratigraphic Feature	3
- Contact Relations	3
- Availability of impermeable cover materials	4
Hydrogeological Compatibility	
(Distance to inland surface waters from which drinking and utility water is supplied)	
Distance to lake	5
Distance from streams, springs, etc.	4
Floodplain	4
Geotechnical Compatibility	
Properties of the bedrock	4
Permeability of the soil	5
Ground type	5
Sensitivity of the area	3
Environmental Conditions	
Availability of sufficient space for plant construction and expansion if needed	5
Land use status	3
Protected areas	4
Distance to settlements	4
Suitability of topography	4
Airport security	2
Wind direction	4
Aesthetic	4
Economic Conditions	
Leveling Cost	3
Availability of roads for transportation	3
Distance to waste source	3
Ownership status of the land	2
Infrastructure status	2

2.1. Geological Criteria

Geological conditions are the most important factor in determining the environmental suitability of a storage area. Using geological survey maps and regional geological information is especially important in the initial identification of alternative sites. It is very important to determine the three-dimensional distribution of the natural unit underground, which will form the ground of solid waste landfills. Geological sections should be drawn by determining the distribution of bedrock by drilling.

In geological studies, potential groundwater flow, flow direction, and groundwater level measurements can be made with drillings. Interpretation of aerial photography is also often of great benefit. Flood, avalanche, landslide and erosion zones, floodplains, earthquake-affected zones, marshes, fault zones should be investigated very well with geological studies [18].

2.2. Earthquake Condition

The stability of landfills is an important issue since they are complex structures. Stable landfill design is possible by understanding mechanisms such as settlement, slope stability, and seismic behavior. Storage sites in earthquake zones must be safe against landslides not only under static conditions but also under seismic conditions. Deformations in clay pavements or geosynthetic pavements will cause leaching and thus groundwater contamination. At the same time, fractures or ruptures in the leachate collection pipes and gas collection pipes reduce the usage performance of the landfill. Due to the heterogeneous nature of the waste, settlement, slope stability, and seismic behavior are different and more complex than the ground. Mechanical properties of ECCs,

such as strength and compressibility, depend on the composition of the waste, the mechanical properties of the components of the stored material, the water content, and the effect of degradation [19].

The distance of the alternative areas to the active faults, the earthquake history of these areas, and the intensity of the possible earthquakes should be investigated very well. As much as possible, solid waste storage areas should not be built in earthquake-active areas. The solid waste storage area built in such a region may cause serious environmental problems and are very difficult to remove after the earthquake.

2.3. Geotechnical Conditions (Soil Conditions)

In addition to regional and terrestrial geology, determining the kind of material and the method to work within geotechnical conditions is an indispensable work. Research pits and core drilling wells should be performed at the points determined by the observations made from a geological study. Thus, the three-dimensional distribution of the floor that will form the warehouse floor can be determined.

Disturbed and undisturbed samples will be taken from the underground material through pits and drillings, and all necessary experiments will be carried out on these samples in the laboratory. In addition, it is possible to conduct various experiments in drilling and research pits, in the field, and at the wellhead.

These experiments are;

Field Tests: SPT Test, Pressurized water test, Vane Test, Plate loading test, etc.

Laboratory Tests: Unit Volume Weight (dry, wet and normal) Test, Specific Gravity Test, Atterberg Limits (liquid, plastic and shrinkage limit) Test, Sieve Analysis, Uniaxial Compressive Strength, Triaxial Compressive Strength, Shear Box Test, Permeability Test, Consolidation Test, and Compaction Tests. The necessary and appropriate ones among these tests should be performed.

The type, bearing capacity, settlement amount, compressibility, and other physical properties of the soil will be determined by the experiments. Parameters found in these tests will be used when necessary for slope stability analysis. In addition, necessary laboratory tests should be carried out on the soil sample that is intended to be used as a covering material [20].

In general, a waste collection plant suitable for engineering consists of natural and synthetic mattresses, cover layers, and other removal systems that cover natural soil and waste. Fine-grained soils that occur naturally in waste storage can be used as mattresses, and the important thing here is the permeability of the floor mattresses. The permeability of the compressed floor mattresses should be at the rate of 10^{-5} – 10^{-7} cm/sec, depending on the stored material content. Clay floors are widely used as natural mattresses. Commonly used clay groups are the montmorillonite clay group with very low permeability. Ideally, the natural ground under the storage area is sufficiently impermeable to work as a protective barrier layer. If the ground under the facility does not have sufficient engineering properties, then the natural ground should be replaced with an impermeable clay floor and clay mattresses should be made on the floor of the warehouse. In addition, the facility should be covered with an impermeable cover layer [21].

2.3.1. Clay Mattresses

Clay mattresses are used as foundation and slope mattresses or hydraulic barrier layer (impermeable) in units containing waste, or similarly as cover lining. Compressed clay mattresses are usually made from natural clay materials. The permeability of the compressed clay varies depending on the clay mineral, the void structure, the water content at the time of compression, and the compaction method. In order to obtain a lower impermeability, the water content of the compressed clay should be higher than the optimum water content (ω_{opt}). Soils compressed under optimum water content (ω_{opt}) have a more void structure than soils compressed above optimum water content (ω_{opt}). Therefore, the hydraulic conductivity (k) value also changes as a function of the gap arrangement, and it has been stated that the hydraulic conductivity (k) value gives lower values above the optimum water content (ω_{opt}) [22].

If the clays are compressed at a water ratio higher than the optimum water content (ω_{opt}), the soft and wet grains of the soil are remolded and a smaller void structure is obtained. Thus, lower hydraulic conductivity (k) values are obtained [23].

The following characteristics of the clays to be used as mattresses in solid waste storages will affect the quality of the mattresses to be made; $k \leq 10^{-7}$ cm/sec, low shrinkage and cracking properties when dried, having sufficient shear strength, ≥ 39 -50 percentage of dry weight passing through no.200 sieve, the plasticity index (I_p) (ASTM D4318) should be ≥ 7 -10% and the dry weight remaining on the 4th sieve should be $\leq 20\%$ [24].

2.3.2. Synthetic Mattresses

There are many geosynthetics used for different purposes in waste warehouses. These are synthetics such as geomembrane, geotextile, geonet, or geogrid. Geomembrane is used to provide impermeability in clay mattresses. Geomembranes used in liquid and vapor insulation are flexible, polymer sheets with very low permeability. In

landfills, geomembranes are typically used as a ground/foundation or covering layer on their surface, in addition to low permeability mattresses. In order not to pollute the ground and groundwater from the wastewater that will occur in the waste, or to reduce the damage of the wastewater, the ground/foundation mattresses are placed under the waste material. Polyethylene (PE) geomembranes are most commonly used in the foundation and coating systems of waste warehouses. These geomembranes have important properties especially in terms of chemical resistance and durability. High-density polyethylene (HDPE) geomembranes are used in foundation coating systems [25]. However, due to the large accumulations that may occur in the waste, a more flexible geomembrane is needed in the coating systems. For this reason, very low-density polyethylene (VLDPE) is generally used in these applications. It is stated that this material is more flexible and adapts more easily to settlements in the waste without puncturing [24]. Apart from these, there are different geomembranes used in storage units and other impermeability structures.

Apart from geomembranes as mattresses, geotextiles are also used in waste disposal facilities. Geotextiles are widely used as a filter, separation, support, cushion, and drainage material. A relatively new application for geotextiles is as an alternative log coating for waste. Apart from geotextiles, geonet and geopipe can be used in drainage systems. Geogrids are also used in case of carrying capacity problems in storage units. In waste management systems, geogrids can be used to support stratification systems on the weak ground surface or cover mattresses on overhead waste slopes [24-25].

2.3.3. Geosynthetic Clay Mattresses

In recent years, design engineers prefer the use of geosynthetic clay mattresses as an alternative to clay mattresses in covering and covering systems in waste storage due to very low permeability and cost. Geosynthetic clay mattresses are very low permeability insulating materials consisting of powdery bentonite or weak granular layers that can adhere chemically or mechanically to a geotextile or geomembrane. Geosynthetic clay mattresses (Geosynthetic Clay Liner, GCL) are usually made by placing them on top of each other in the field. These are often used as an alternative to compacted clay silts and GCLs have some advantages over compacted clay silts. These are materials that are more flexible, can hold themselves to some extent, and are easier to place. They may be preferred for low construction costs in the fields where low permeability clays are not readily available [26-28].

2.4. Hydrological Condition

The irregular storage of solid wastes causes soil, water, and air pollution. Solid waste and leaking wastewater pollute surface and underground waters, and as a result, they pose threat to human health and the environment. Detailed geological studies in the determination of suitable storage locations and the examination of soil properties, as well as the study of the hydrogeological properties of the region, are important in this respect.

The boundaries and characteristics of the recharge basin in which the storage area is located, the precipitation area, underground seepage, and runoff should be examined, and necessary drainage measures should be taken [29]. The hydrogeological and permeability properties of existing and potential aquifers and lithological units should be described in detail. Structural and surface properties that affect the flow of groundwater and the resistance properties of the material at the bottom of the storage area against deterioration should be determined [30]. Groundwater level should be measured, chemical analysis of water should be done, water reserve and hydraulic slope should be calculated [31]. Due to the spreading and accelerating effect of possible contamination, soils with high permeability values and fissured and soluble carbonate lithological units in which contamination can spread should be avoided [32].

The selected storage location should be outside the protection zone of drinking and thermal water resources, the groundwater level should be at least 3 meters or deeper, and it should not be in the flood and earthquake zone. In order to prevent contamination of ground and surface waters, soil and nutrients, impermeability must be provided for both the ground and the surface [33].

Hydrology is very important in determining the existing natural drainage and flow characteristics. Centennial flood limits should be defined. The waste storage built in the 100-year-old floodplain should be designed by defining the characteristics of the basin very well in order to reduce the temporary water holding capacity of the flood basin and not to interrupt the flow when transporting the solid waste that will harm human health and the environment.

In geological and geotechnical studies, drillings can be used to measure the potential groundwater flow, flow direction, and groundwater level. In addition, all necessary hydrogeological characteristics of the unit forming the floor of the solid waste storage area should be determined in the field, wellhead, or laboratory. Drinking water areas should be determined very well and the interaction with these areas should be examined [31].

2.5. Measures Against Ground and Surface Water Pollution

As long as there are suitable areas in the landfill method, the negative effects on the environment are minimized, while the wastes are decomposed under control and converted into stable substances [34]. While the leachate is filtered through the solid wastes, it is polluted with some chemical, physical and biological events and contains elements and compounds arising from the solid waste content. The source of the leachate is the water content in the stored solid waste and the water entering the tank from outside. The water entering the tank from the outside is formed by the leakage of rainwater over the tank and the entry of surface and underground waters into the tank. Factors affecting the formation of garbage leachate in solid waste storage areas are precipitation, surface flow, groundwater inflow, irrigation, waste degradation, evapotranspiration (temperature, wind, humidity, atmospheric pressure, cover humidity, vegetation, solar radiation), infiltration, moisture of waste holding capacity and permeability [35]. Waste leachate formation in solid waste landfills increases in direct proportion to the amount of precipitation, surface runoff, and groundwater entering the area. In order to minimize leachate formation and to prevent environmental damage of leachate, hydrological and hydrogeological water inflows to the storage area should be prevented. For this, solid waste storage areas should be selected from regions with low rainfall, the top cover should be made and grassed, surface drainage should be made and solid waste should be subjected to adequate compression [36]. Apart from these;

A. In order to prevent the accumulation of rainwater, which is the most effective factor in water pollution, in the storage area, the surface of the tank should be covered with an impermeable clay layer and its surface should be sloped %3.

B. The bottom of the landfill should be made impermeable and the leachate should be drained and collected at a specific point so that the leachate does not mix with the groundwater.

C. The collected leachate should be discharged after being treated in a way that does not pollute the environment [37-38].

3. Conclusions and Recommendations

Mainly geological, hydrogeological, and geotechnical factors play an important role in the selection and evaluation of landfill sites for waste disposal. These factors include not only the physical properties of rocks but also their stratigraphic and structural properties and engineering properties such as permeability, strength, and usability. It is important to consider these factors in selecting sites suitable for any use. The depth of geological information obtained from the surface in site selection can be improved by geophysical studies and drilling. In addition, issues such as the current use of the projected place, distance from settlements, transportation, types and amounts of hazardous wastes are also extremely important. It has been supported by many studies that it would be important and beneficial not to limit the studies to the only surface and subsurface studies, and to pay due attention to shallow and deep researches.

According to the results obtained from environmental protection studies, it has been proven and understood by the studies that the efforts are successful and it is possible to create living environments where the environment is intact or less affected. Therefore, it should be taken into account that environmental protection does not only consist of problems that appear on the ground but that there are/may be ongoing problems underground as well. In addition, reduction at source, recovery, recycling, and composting efforts should be encouraged to reduce the volume of waste. However, source reduction, recycling, and composting can result in a significant portion of the urban waste stream being diverted to landfills. The economic viability of incinerators, on the other hand, depends on the revenue from the sale of energy produced by incineration of waste. International criteria must be used in the classification and disposal of wastes.

Funding

This research received no external funding.

Conflicts of interest

The authors declare no conflicts of interest.

References

1. Baran, S. (1995). Some Main Issues in Selection and Construction of Solid Waste (Cop) Storage Sites. Geological Engineering, Special Environmental Protection Agency Presidency, Ankara, 46, 82-154.
2. Horasan, B. Y., & Arık, F. (2019). Assessing heavy metal pollution in the surface soils of Central Anatolia Region of Turkey. *Carpathian Journal of Earth and Environmental Sciences*, 14, 1, 107 – 118. <http://doi.org/10.26471/cjees/2019/014/063>
3. Horasan, B. Y. (2020). The environmental impact of the abandoned mercury mines on the settlement and agricultural lands; Ladik (Konya, Turkey) *Environmental Earth Sciences* 79, 1-13. <https://doi.org/10.1007/s12665-020-08985-6>
4. Ozturk, A., & Arici, O. K. (2021). Carcinogenic-potential ecological risk assessment of soils and wheat in the eastern region of Konya (Turkey). *Environmental Science and Pollution Research*, 28(12), 15471-15484. <https://doi.org/10.1007/s11356-020-11697-w>
5. Horasan, B. Y., Ozturk, A. & Tugay, O. (2021). Nb–Sr–Pb isotope analysis in soils of abandoned mercury quarry in northwest Black Sea (Turkey), soil and plant geochemistry, evaluation of ecological risk and its impact on human health. *Environ Earth Sciences*, 80(15), 488. <https://doi.org/10.1007/s12665-021-09775-4>
6. Horasan, B. Y. (2021). Evaluation of geological properties of solid waste landfill. International Symposium for Environmental Science and Engineering Research (ISESER) Tirana, Albania, June 11-13, 2021 ISBN: 978-605-83522-3-0
7. Beyhan, M. (1997). Investigation of the potential of recyclable materials from Isparta domestic and commercial solid wastes. Yıldız Technical University, Institute of Science, Environmental Engineering Department, Master's Thesis, Istanbul.
8. Tahtasızoğlu, B. (2010). Investigation of design criteria of solid waste storage areas. Marmara University Institute of Science, Environmental Sciences Department Master's Thesis, Istanbul.
9. Özel, S. (2010). Investigation of underground leachate dispersion in sivas solid waste landfill by geophysical methods. Cumhuriyet University, Institute of Science and Technology, Ph.D. thesis, Sivas, 148s.
10. Akdoğan, A. & Güleç S. (2007). A research on sustainable solid waste management and analysis of the attitudes and thoughts of managers in municipalities on solid waste management. *Hacettepe University Journal of the Faculty of Economics and Administrative Sciences*, 25(1), 39-69.
11. Kemirtlek, A. (2005). Integrated Solid Waste Management. İSTAÇ A.Ş., Istanbul.
12. Şimşek, C. & Filiz, S. (2005). Investigation of geological and hydrogeological characteristics of Torbalı (İzmir) Landfill Site. *Dokuz Eylül University Faculty of Engineering Science and Engineering Journal*, 7(2), 39 – 56.
13. Karagüzel, R. & Mutlutürk, M. (2005). Selection of site in solid waste landfill: The Case of Isparta. *International Engineering Geology Turkish National Committee, Engineering Geology Bulletin*, p. 21:19-33.
14. Costa C., & Ryan C. J. (2001). Site investigation on heavy metals contaminated ground in Estorjea. *Engineering Geology*, 45(37-39), Springer-Verlag.
15. Dörhöfer G. & Siebert H. (1998). The search for landfill sites requirements and implementation in lower Saxony. *Environmental Geology*, 35(1), Springer-Verlag.
16. Veeken, J. & Bilijam, K., (2000). Checklist with site selection criteria for landfills. DHV Consultants BV, The Netherlands, R & R Scientific and Technical Services Ltd. Şti., (Prepared for the Ministry of Environment and Forestry)
17. Karagüzel, R., Özçelik, H., Mutlutürk, M., Güldal, V., Tokgözlü, A., Beyhan, M., et al. (2003). Investigation report on site selection and environmental impact for solid waste of Manavgat–Antalya Municipality. Suleyman Demirel University, Turkey, unpublished report (pp 134).
18. Borat M., (2006). Storage site location selection, design, necessary equipment and structures. solid waste landfill & wild landfill rehabilitation training, Training Project, 3-11.
19. Jessberger H. L., & Kockel R. (1995). Determination and assessment of the mechanical properties of waste materials. In: *Proceedings Sardinia 93, 4th international landfill symposium*, S. Margherita di Pula, Cagliari, Italy, October 1993, 1383–1392.
20. Çağlar S., & Yılmaz T. (2006). Preparation of infrastructure in landfills, construction of roads and platforms, storage of wastes by celling method. regular storage of solid wastes & rehabilitation of wild landfills, training project, 13-20.
21. Akbulut, S. (2002). Geotechnical Design of Solid Waste Storage Areas. Atatürk University, Department of Civil Engineering, Erzurum, p. 42.
22. Olsen, H. W. (1962). Hydraulic Flow-Through Saturated Clay. *Clay Miner*, 9(2), 131-161
23. Daniel D. E. (1993). *Geotechnical Practice for Waste Disposal*. Chapman & Hall Pub. London, UK.
24. Sharma, D. H. & Lewis, P. S. (1994). *Waste Containment Systems, Waste Stabilization, and Landfills, Design and Evaluation, Waste Characterization and Solid-Waste Interaction*. Jhon Wiley & Sons INC., pp 26-35, New York.
25. Koerner, R. M. (1993). *Geomembrane Liners. Geotechnical Practice for Waste Disposal*, Chapman & Hill Pub., pp. 164-186, London, UK.

26. Lake, C. B., & Rowe, R. K. (2000). Diffusion of sodium and chloride through geosynthetic clay liners, geotextiles and geomembranes. 18, 103-131.
27. Shackelford, C. D, Benson, C. H, Katsumi, T., Edil, TB, Lin, L. (2000). Evaluating the hydraulic conductivity of gcls permeated with non- standard liquids. Geotextiles and Geomembranes, 18, 133-161.
28. Vangpaisal, T., & Bouazza, A. (2001). Gas permeability of three needle punched geosynthetic clay liners. In *Geoenvironment* (pp. 373-378). Australian Geomechanics Society Inc. (Newcastle Chapter).
29. Tchobanoglous, G., Theisen, H. and Vigil, S. (1993). *Integrated Solid Waste Management Engineering Principles and Management Issues*, McGraw Hill, Inc., New York.
30. Freeze R. A. & Cherry J. A. (1979). *Groundwater*. United Kingdom.
31. Jewell, C. M., Hensley P. J., & Barry, D. A. (1993). Site investigation and monitoring techniques for contaminated sites and potential waste disposal sites. *Geotechnical Management of Waste and Contamination*. Rotterdam, pp. 9-23.
32. USEPA (1973). United States Environmental Protection Agency. An Environmental Assessment of Potential Gas a Leachate Problems at Land Disposal Sites. Report 110, pp. 1-33.
33. Erdin, E. (1995). Solid Wastes and EIA. Environmental Impact Assessment Training Course Papers. DEU and TMMOB Environmental Eng. Chamber, Izmir, p. 151-187.
34. Yıldız Ş., Tüylüoğlu B.S. & İskenderoğlu, A. (1999). Solid waste management and disposal practices in Istanbul. Urban Management, Human and Environmental Problems Symposium, Istanbul Metropolitan Municipality, İSTAÇ AŞ., Volume 3.
35. Yıldız, Ş., & Goncaloğlu, B. (2001). Leakage water management in solid waste landfills. *Groundwater and Environment Symposium*, İzmir, p. 437-443.
36. Christensen, T. H., Cossu, R., & Stegmann, R. (1998). Problems and strategies in leachate management. International Training Seminar Management of MSW Landfill Leachate, Venice, Italy.
37. Apaydın, S., Ertuğrul T., Berktaş, A. (2002). Pre-Treatment of Young Leachate of Solid Waste Landfill. Selçuk University Environmental Engineering, Konya, 4.
38. Yıldız, Ş. (2006). Leachate Water and Landfill Gas Management in Landfills. Regular Storage of Solid Wastes & Rehabilitation of Wild Landfills Training, Training Project, 2-5.



© Author(s) 2022. This work is distributed under <https://creativecommons.org/licenses/by-sa/4.0/>



Effect of fiber content on the liquefaction potential of improved soils

Özgür Lütfi Ertuğrul*¹, Fatma Dülger Canoğulları²

¹ Mersin University, Civil Engineering Department, Türkiye, ertugrul@mersin.edu.tr

² Toros University, Civil Engineering Department, Türkiye, fatma.dulger@toros.edu.tr

Cite this study: Ertuğrul, O. L. & Canoğulları, F. (2022). Effect of fiber content on the liquefaction potential of improved soils. *Advanced Engineering Science*, 2, 44-51

Keywords

Fibers
CSR
Reinforced soil
Liquefaction

Research Article

Received: 11.01.2022

Revised: 15.02.2022

Accepted: 25.02.2022

Published: 14.03.2022



Abstract

The use of randomly distributed fibers as soil reinforcement has recently become popular as a result of more satisfactory performance compared with those of the conventional reinforcements. Most previous investigations have focused on the strength and deformation characteristics of fiber-reinforced soil. The liquefaction behavior of fiber reinforced soils has recently received interest since fiber addition is currently considered as a new way of soil improvement to prevent soil liquefaction. Studies indicate that when soils are reinforced with synthetic or natural fibers, a reduction is observed in the number of cycles required to initiate liquefaction under undrained loading conditions. In this study, a regression analysis was performed by using the results of the previous studies. The obtained formula is able to capture the effect of fiber percentage and relative density of the cohesionless soil on the cyclic stress ratio values with a good agreement.

1. Introduction

Soil liquefaction can cause landslides, collapse of foundations, damage to soil structures, and lateral movement of structures standing on the ground. Therefore, it is important to consider the liquefaction potential of dams, embankments, slopes, foundation structures.

The liquefaction of saturated loose sands is defined as the loss of soil strength due to excessive pore pressures under seismic waves. During earthquakes, liquefaction causes reductions in the bearing capacity of soils and causes excessive settlements [1]. Basic liquefaction scheme is shown in Figure 1.

The occurrence of liquefaction has encouraged the interest of many investigators and remarkable work has been carried out to evaluate liquefaction susceptibility. Properties of soil could be improved by using reinforcement materials to eliminate the liquefaction hazard [2].

It has been revealed that the use of fiber in soils increases the shear strength of the soil, improves the flexible behavior and reduces the strength loss observed after the highest strength is reached. Recently, static liquefaction studies have investigated the possibility of fiber reinforcement to improve the liquefaction resistance of sand, these studies indicated that lateral spreading can be prevented by using fiber reinforcement.

Soil reinforcement with randomly distributed fibers was investigated by researchers in last few years and results showed that mixing fibers with granular soils improved liquefaction resistance and shear modulus of the soils.

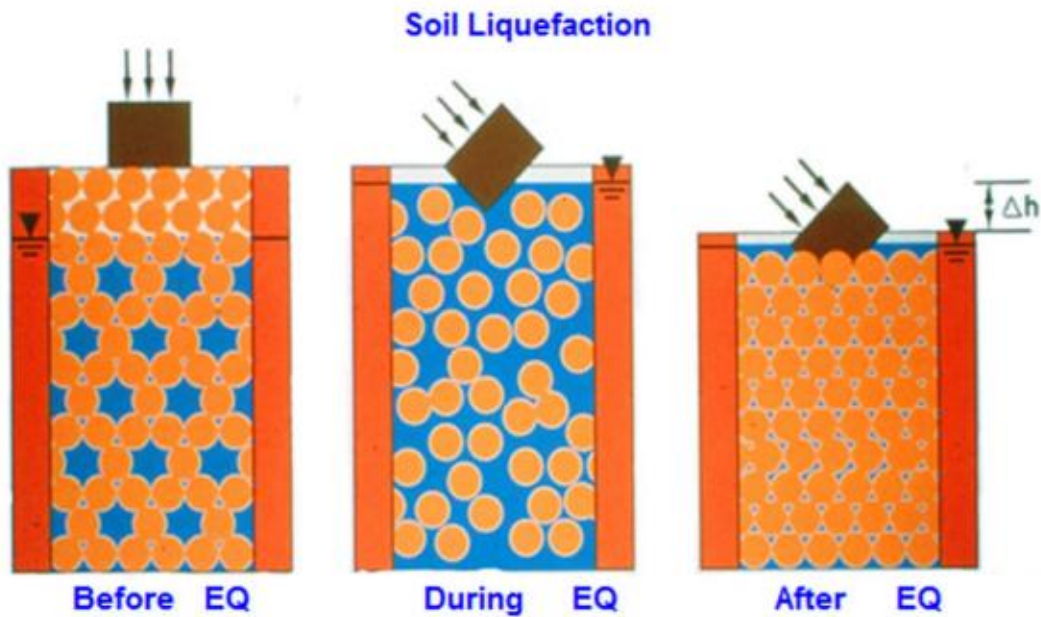


Figure 1. Liquefaction scheme [3]

2. Material and Method

It has been frequently used in recent years to obtain a homogeneous and clean soil with improved engineering properties, by randomly mixing the fibers produced from natural sources or artificially, which is a soil improvement method first researched in the laboratory and then used in practical engineering applications.

Soil reinforcement with fibers has some advantages compared to traditional soil reinforcement techniques. For example; mixing fibers with the soils is relatively easy with current soil mixing techniques and if homogeneous mixing is achieved, the fibers provide isotropic strength gain in the soil [4].

Basically, in this technique, which is developed by considering the contribution of plant fibers or roots to the stability of the soil, the fiber-soil mixture can reach very high shear strength values compared to the nonreinforced soil. Because, the fibers have higher tensile strength compared to the soil. For this reason, it is thought that the fibers will be efficient especially in soils near to the surface where the effective stresses and accordingly the shear strength are low.

Additionally, fibers mechanically change the failure mechanisms of cracks that may occur due to tensile stresses in the soil and prevent serious strength loss in the soil [5].

Although there are various investigations about strength and deformation characteristics of fiber-reinforcement soils under static loads, the studies on under cyclic loading are very limited in the literature.

In order to understand the liquefaction behavior of fiber reinforced soil, a series of ring-shear tests and a series of cyclic triaxial tests have been carried out on soil samples with different fiber content and sand density.

3. Literature Review

Jin Liu et al. [6], carried a series of undrained ring shear tests on saturated samples with different fiber content and sand density percentages to understand the effect of fiber content and sand density on the liquefaction behavior of fiber-reinforced sand. Fiber-free and fiber-reinforced samples were prepared using a moist compression technique. This technique is widely used in laboratory studies of fiber-reinforced sand and allows control of sample density while preventing fiber separation.

To analyze the results of shear tests on fiber-reinforced saturated sand, the samples were separated three groups as loose, medium dense and dense samples.

In loose samples, fiber addition did not significantly affect the undrained shear behavior, but samples without fiber added after shear showed a completely collapsed structure, while reinforced samples retained structural stability even after removal of the top ring. This situation is shown in Figure 2.



Figure 2. Liquefied loose specimens after shearing: (a) Sand; (b) fiber 0.4% [6].

As seen in [Figure 3](#) and [Figure 4](#), the presence of fibers obviously affected the undrained behavior of medium density and dense samples.

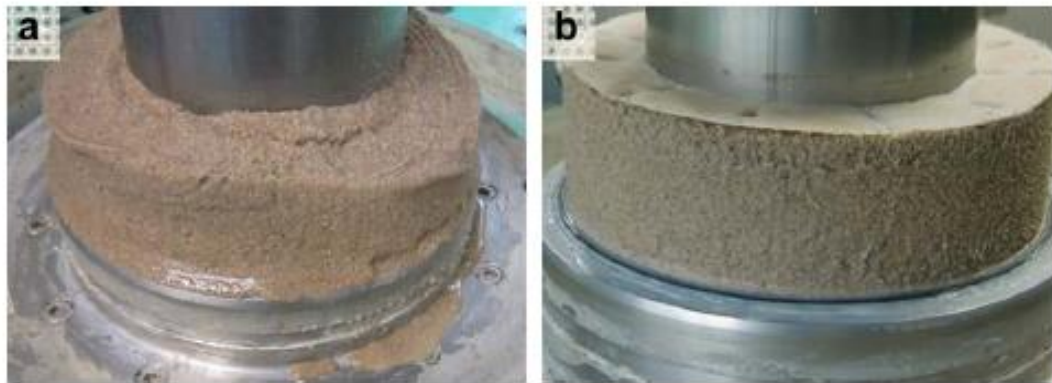


Figure 3. Liquefied medium dense samples after shearing: (a) Sand; (b) fiber 0.4% [6].



Figure 4. Liquefied dense samples after shearing: (a) Sand; (b) fiber 0.4% [6].

The results indicated that tests on sand samples showed a continuous decrease in shear strength after the sand was sheared, while samples with added fiber showed fluctuations even after shearing. This fluctuation is further strengthened by increasing fiber content. All reinforced medium density and dense samples retained structural stability, while the medium density sample without added fiber showed a partially collapsed structure and the dense sample showed little structural stability.

Noorzad et al. [7], aimed to characterize the liquefaction resistance and shear modulus of the sand-fiber mixture using cyclic triaxial experiments. The effects of test parameters and fiber properties on the liquefaction resistance and shear modulus of non-fiber and fiber-added samples were investigated.

As a result of the experiments, it is seen that the number of cycles required for liquefaction to occur increases with the increase in fiber content. By adding the fibers to the sand soil, the soil grains are better interlocked and at the same time, an easy homogeneous distribution is achieved.

An increase in fiber length has been found to increase the number of cycles required for liquefaction to occur, although the fibers are less effective during the initial cycles. In this case, the probability of slippage in the fibers decreased with increasing fiber length, resulting in better performance of the fibers in the ground.

Sonmezer [8] investigated the liquefaction potential of sandy soil reinforced with 0.25-1.00% polypropylene fiber using a stress-controlled cyclic shear test and an energy-based approach.

6, 12 and 19 mm long polypropylene fibers were used to reinforce the soil. The fibers used have a diameter of 0.031 mm, a specific density of 0.9, a tensile strength of 400 MPa and a modulus of elasticity of around 1000-2500 MPa.

The aim of the study was observing the effect of fiber reinforcement in loose sand layers saturated with water and with high liquefaction potential during an earthquake, mostly samples with 30% relative density were tested. However, to investigate the effect of relative density, tests were also conducted on a few samples with 50% relative density.

In the tests, the cumulative energy values of the fiber reinforced sand samples were obtained until the beginning of the liquefaction occurrence.

As a result of the tests, the area under the curve decreased as the number of cycles increased. The reason for this decrease was explained as the increase in excessive pore water pressure, and at the time of liquefaction, the area under the loop was greatly reduced and the hysteresis loop took an almost flat shape.

When the results of the study are examined, the cumulative energy, depending on the increase in fiber length as well as fiber content; increased with increasing number of cycles until liquefaction occurred.

It was observed that the liquefaction resistance of fiber-reinforced samples increased significantly with the increase in fiber content and length, especially when compared to non-fiber-reinforced samples. This increase is thought to be due to the increase in the shear strength of the soil sample due to the presence of fibers. This showed that fibers mixed with sand clearly had a significant effect on the liquefaction susceptibility of sandy soil.

In addition, the presence of fibers strongly influenced the evolution of pore water pressure. In other words, the increase in excess pore pressure in the presence of fibers is very slow. The same result is valid for both the increase in fiber content and the increase in fiber length. This is thought to be due to the fact that the fiber is an extensible material, increasing the energy absorption capacity of the sand.

Karakan et al. [9], aimed to determine the liquefaction resistance of fiber reinforced sand samples and the development of pore water pressure by applying cyclic triaxial tests. The effect of fibers in improving the liquefaction resistance of poor grade sand was investigated with a series of dynamic tests. The test sets contain samples with 0%, 0.25%, 0.5% and 1% polypropylene fiber content and two different fibers (6 mm and 12 mm) lengths. The relative density of the samples was 30%, 50% and 70%, representing different hardness states of the soil, and the samples were consolidated under a confined pressure of 100 kPa. In addition, a cyclic loading frequency of 0.1 Hz was applied to the samples.

When the experimental results were examined, an increase in fiber length increased the number of cycles that would trigger liquefaction for samples with a relative density of 30%. Additionally, the lowest liquefaction resistance for samples with 50% relative density and 6 mm fiber length was obtained from samples with 0.25% fiber ratio.

Moreover, the highest liquefaction resistance was obtained in samples containing 1% fiber. For samples with a relative density of 50% and a fiber length of 12 mm, the liquefaction resistance of the fiber-free samples showed a liquefaction resistance varying in a narrow band of 0.25% and 0.5%. The most remarkable improvement against liquefaction was obtained in samples with 1% fiber content.

Muley et al. [10], in their work; the effect of natural fiber, namely coconut fiber, on the liquefaction susceptibility of Solani River fine sand was investigated using tension-controlled undrained cyclic triaxial tests performed in accordance with ASTM D3999. The tests were carried out with samples prepared at 35% relative density and different fiber contents (0%, 0.25%, 0.50% and 0.75%). The inclusion of fibers significantly affected the results, and the specific gravity values of the mixed soil decreased continuously due to the increase in fiber content, while the maximum and minimum void ratio increased.

Chegenizadeh et al. [11], investigated the effect of fibers on the liquefaction resistance of low plasticity silt by performing a series of dynamic triaxial tests on fiber-reinforced and non-fiber-reinforced samples. The results showed that increasing the fiber content and length increased the liquefaction resistance of the samples, whereas

with an increase in the relative density (D_r), the liquefaction resistance of the fiber-reinforced sample became more marked than that of the unreinforced sample.

Vercueil et al. [12], performed an experimental study (cyclic triaxial tests) of the liquefaction resistance of Hostun sand reinforced with geosynthetics. The results showed that the liquefaction resistance considerably decreases with fiber addition.

Bhandari and Han [13], carried out studies on the behavior of the geotextile and the soil under a cyclic wheel load using discrete element method. They reported that the geotextile has a major effect on the degree of interaction between the geotextile and the soil.

Altun et al. [14], conducted several stress-controlled cyclic torsional shear tests to investigate the effect of geosynthetics in increasing the resistance to liquefaction of Toyoura sand. The results showed that the liquefaction resistance of sand deposits can be remarkably improved by geosynthetic reinforcement.

Maher and Woods [15], studied the dynamic response (i.e., shear modulus and damping) of sand reinforced with randomly distributed fibers using resonant-column and torsional shear tests. They reported that the addition of fibers enhances the dynamic modulus of cohesionless soils.

Ibraim et al. [16], investigated the static liquefaction behavior of fine sand reinforced with discrete crimped polypropylene fibers in both triaxial compression and triaxial extension tests. They found that the presence of fibers diminishes the potential of liquefaction.

Chen and Loehr [17], studied the behavior of fiber reinforced soil in the triaxial experimental setup under with and without drainage. They found that the soil strengths of the fiber-reinforced specimens under drained conditions exceeds the respective values of the same specimens under undrained conditions at low deformation levels.

Makiuchi et al. [18], reported that the strength and ductility of fiber-reinforced soils are properties that help build earthquake-resistant structures. They also proposed a method using synthetic fiber in their study.

Ashmawy and Bourdeau [19] explored the effect of geotextile reinforcement on the stress-strain and volumetric behavior of sand subjected to monotonic and cyclic loading. They conducted a series of drained triaxial tests on saturated sand samples reinforced with woven and nonwoven geotextiles. The results showed that the presence of reinforcement resulted in a significant increase in monotonic shear strength and ductility of sand and a reduction in cyclic deformability. Furthermore, under both monotonic and cyclic loading, a reduction in volume change potential was observed by the geotextile reinforcement.

Krishnaswamy and Isaac [20], observed that the inclusion of fiber significantly increased liquefaction resistance of sands. Authors used polypropylene, needle-punched and natural fiber as reinforcing material. It was observed that the reinforcement effect was more pronounced at lower densities.

Sharma and Kumar [21], reported that the strength and bearing capacity of the fiber-reinforced soil increased considerably with an increase in the relative density. Moreover, the previous researchers reported that the fibers can increase the ductility and liquefaction resistance of the soil.

The tests carried by Sadek et al. showed that a 0.5 to 1.5 % fiber content in the soil increases the shear strength values of the specimens [22].

Erken et al. [23] carried that the dynamic strength values of sand specimens saturated to water increase with increasing fiber ratio.

Shuai-dong and Xiang-juan [24] studied the cyclic behavior of reinforced silty sand by performing consolidated undrained cyclic triaxial tests. The dynamic elastic modulus of reinforced soil was reported to increase due to reinforcement, confining pressure, and consolidation stress ratio, as to the unreinforced soil.

4. Results and Discussion

The studies on the behavior of soils reinforced with randomly distributed elements under cyclic loading is very limited in the literature since the studies are about the strength properties of fiber reinforced soils. Investigators noted that that the number of cycles causing liquefaction increased with an increase in fiber ratio and CSR values increased with the increase of fiber length. Since, application of dynamic triaxial and torsional shear tests are significantly difficult, a regression analysis were performed in the current study by using the results of the previous studies. A sample of the used data is depicted in [Table 1](#).

Table 1. A summary of the results derived from previous studies

Fiber Percent (%)	Dr (%)	Fiber Length (mm)	CSR
1	30	6	0.336
0.5	30	6	0.288
0.25	30	6	0.244
0	30	6	0.221
1	30	12	0.351
0.5	30	12	0.296
0.25	30	12	0.266
0	30	12	0.221
1	50	6	0.399
0.5	50	6	0.323
0.25	50	6	0.264
0	50	6	0.316
1	50	12	0.409
0.5	50	12	0.344
0.25	50	12	0.335
0	50	12	0.316

Based on the multiple variate regression analyses, the following equation was obtained.

$$CSR = a + bF_p + cD_r + d\left(\frac{F_p}{D_r}\right) + e(\exp(F_p^3 D_r^3)) \tag{1}$$

In this equation, CSR represents the Cyclic Stress Ratio whereas F_p , and D_r denotes fiber percent and soil relative density, respectively. The constant parameters of a , b , c , d and e will be taken as: 0.5481, 0.2832, 0.2328, -0.04756, -0.4001, respectively. The graphical representation of the multivariate regression analysis was shown in Figure 5. The coefficient of determination is found as 0.90 for the suggested formula.

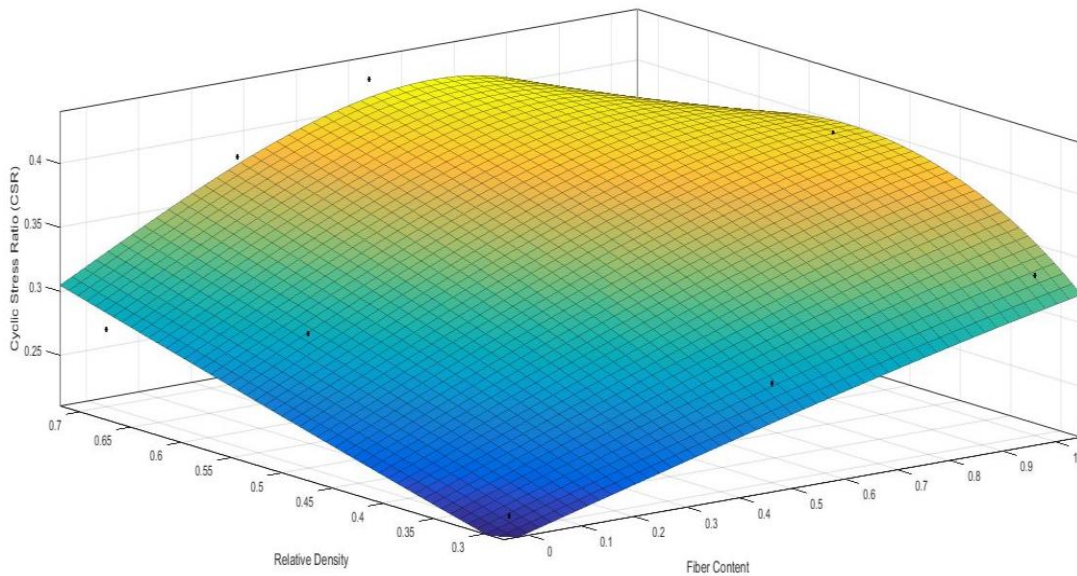


Figure 5. Graphical depiction of the multivariate nonlinear regression modeling results

5. Conclusion

Fiber reinforcement is an efficient method in limiting or even preventing the occurrence of the lateral movement of the sandy soils due to liquefaction. The presence of fibers affects the behavior of sand in cyclic compression by increasing the cyclic strength therefore liquefaction hazards or deformations appear to diminish. The cyclic test results showed that the addition of randomly distributed polypropylene fibers increases significantly the liquefaction resistance of sands at low relative densities. Since, application of dynamic triaxial and torsional shear tests are significantly difficult, a regression analysis were performed in the current study by using the results of the previous studies. The obtained formula is able to capture the effect of fiber percentage and relative density of the cohesionless soil on the cyclic stress ratio values with a good agreement ($R^2=0,90$).

Acknowledgement

This paper was partly presented in 1st Advanced Engineering Days (AED) held on Thursday, December 23, 2021 in Mersin/Turkey [25].

Funding

This research received no external funding.

Author contributions

Özgür Lütfi Ertuğrul: Data curation, Validation, Writing-Reviewing and Editing. **Fatma Dülger Canoğullari:** Investigation, Writing- draft preparation.

Conflicts of interest

The authors declare no conflicts of interest.

References

1. Towhata, I. (2008). Geotechnical Earthquake Engineering. Berlin Heidelberg: Springer-Verlag; (698 pp.).
2. Maher, M. H. & Gray, D. H. (1990). Static response of sand reinforced with randomly distributed fibers. *Journal of Geotechnical Engineering* 116 (11), 1661–1677.
3. Nath, S.K. (2011). Seismic microzonation manual and handbook. Geoscience Division, Ministry of Earth Sciences, Govt. of India, New Delhi.
4. Darvishi, A. (2014). Behavior of Fiber Reinforced Sand Under Static Load. MSc Thesis, İstanbul Technical University, İstanbul, Turkey.
5. Sarğın, S. (2012). Cyclic Behavior and Liquefaction Resistance of Unreinforced and Polypropylene Fiber-Reinforced Loose Sands, MSc Thesis, İstanbul Teknik Üniversitesi.
6. Liu, J., Wang, G., Kamaı, T., Zhang, F., Yang, J., & Shi, B. (2011). Static liquefaction behavior of saturated fiber-reinforced sand in undrained ring-shear tests. *Geotextiles and Geomembranes*, 29(5), 462-471.
7. Noorzad, R., & Amini, P. F. (2014). Liquefaction resistance of Babolsar sand reinforced with randomly distributed fibers under cyclic loading. *Soil Dynamics and Earthquake Engineering*, 66, 281-292.
8. Sonmezer, Y. B. (2019). Investigation of the liquefaction potential of fiber-reinforced sand. *Geomechanics and Engineering*, 18(5), 503-513.
9. Karakan, E., Eskişar, T., & Altun, S. (2018). The liquefaction behavior of poorly graded sands reinforced with fibers. *Advances in Civil Engineering*.
10. Muley, P., Maheshwari, B. K., & Paul, D. K. (2015). Effect of coir fiber on liquefaction resistance of solani sand. In *6th International Geotechnical Symposium on Disaster Mitigation in Special Geo-environmental Conditions, IIT Madras, India* (pp. 141-144).
11. Chegenizadeh, A., Keramatikerman, M., & Nikraz, H. (2018). Liquefaction resistance of fibre reinforced low-plasticity silt. *Soil Dynamics and Earthquake Engineering*, 104, 372-377.
12. Vercueil, D., Billet, P., & Cordary, D. (1997). Study of the liquefaction resistance of a saturated sand reinforced with geosynthetics. *Soil Dyn Earthq Eng* 16 (7-8), 417-25.
13. Bhandari, A., & Han, J. (2010). Investigation of geotextile–soil interaction under a cyclic vertical load using the discrete element method. *Geotextiles and geomembranes*, 28(1), 33-43.

14. Altun, S., Göktepe, A.B., & Lav, M.A. (2008). Liquefaction resistance of sand reinforced with geosynthetics. *Geosynth International*, 15(5), 322–332.
15. Maher, M. H., & Woods, R. D. (1990). Dynamic response of sand reinforced with randomly distributed fibers. *Journal of Geotechnical Engineering*, 116(7), 1116-1131.
16. Ibraim, E., Diambra, A., Wood, D. M., & Russell, A. R. (2010). Static liquefaction of fibre reinforced sand under monotonic loading. *Geotextiles and Geomembranes*, 28(4), 374-385.
17. Chen, C. W., & Loehr, J. E. (2008). Undrained and drained triaxial tests of fiber-reinforced sand. Proceedings of the 4th Asian Regional Conference on Geosynthetics, Shanghai, China.
18. Makiuchi, K., & Minegishi, K. (2001). Strain-induced toughness and shearing characteristics of short fiber reinforced soils, International Symposium on Earth Reinforcement, Fukuoka, Japan, November, 14-16.
19. Ashmawy, A. K., & Bourrdeau, P. L. (1998). Effect of geotextile reinforcement on the stress–strain and volumetric response of sand. 6th international conference on geosynthetics, Atlanta, 2, 1079–1082.
20. Kirshnaswami, N. R. & Isaac, N. L. (1994). Liquefaction resistance of reinforced sand. *Geotextiles and Geomembranes*, 13, 23-41.
21. Sharma, V., & Kumar, A. (2017). Influence of relative density of soil on performance of fiber-reinforced soil foundations. *Geotextiles and Geomembranes*, 45(5), 499-507.
22. Sadek, S, Najjar, S. S. & Freiha, F. (2010). Shear strength of fiber reinforced sands. *Journal of Geotechnical and Geoenvironmental Engineering*, 136(3), 490-499.
23. Erken, A., Torabi, M., Sargin, S. & Darvishi, A. (2015). Liquefaction resistance of reinforced sands. Proceedings of the 6th International Geotechnical Symposium on Disaster Mitigation in Special Geoenvironmental Conditions, Chennai, India, January.
24. Yang, S. D., & Yu, X. J. (2011). The experimental study on the dynamic behavior of reinforced silty sand. International Conference on Electric Technology and Civil Engineering (ICETCE), pp. 2745–2750.
25. Ertuğrul, Ö. L., & Canoğulları, F. D. (2021). Effect of fiber content on the liquefaction potential of improved soils. *Advanced Engineering Days (AED)*, 1, 108-110.



© Author(s) 2022. This work is distributed under <https://creativecommons.org/licenses/by-sa/4.0/>



Adsorption of Astrazon red GTLN (AR) with volcanic tuff Bayburt Stone

Beyhan Kocadağistan*¹, Erdem Kocadağistan¹

¹Ataturk University, Department of Environmental Engineering, Türkiye, beyhank@atauni.edu.tr; kocadagistan@atauni.edu.tr

Cite this study: Kocadağistan, B., & Kocadağistan, E. (2022). Adsorption of Astrazon red GTLN (AR) with volcanic tuff Bayburt Stone. *Advanced Engineering Science*, 2, 52-59

Keywords

Adsorption
Volcanic tuff
Removal efficiency

Research Article

Received: 12.01.2022
Revised: 15.02.2022
Accepted: 25.02.2022
Published: 14.03.2022



Abstract

The discharge of dyestuffs originating from the textile industries pollutes the natural waters. Therefore, the adsorption which used to remove dyestuffs from wastewater, is an effective, economical and successful method. Adsorption is a very effective, widespread, easy and inexpensive method used for textile dye removal from wastewater. Bayburt stone powders were used as adsorbent and Astrazon Red GTLN textile dye was used as adsorbate. According to the results of the study, the optimum pH value was 10, the initial dye concentration was 10 mg/L, the mixing speed was 200 rpm and the adsorbent amount was 10 g/L. Langmuir, Freundlich and Temkin isotherms were used to evaluate the adsorption dynamics. Langmuir isotherm was best fit and Astrazon Red removal efficiency was found to be 85% by using Bayburt stone under optimum conditions.

1. Introduction

With industrialization, the textile industry is also developing rapidly. Finishing processes such as dyeing, printing, washing and drying are commonly used in textile fabrics. Since textile dyes have the potential to pollute the receiving water environment, they are in the group of wastewaters that must be treated before discharge [1]. For this purpose, various treatment methods such as coagulation, flocculation, electrochemical processes, chemical oxidation, reverse osmosis, electrochemical filtration, aerobic and anaerobic treatment are used for textile dye removal from wastewaters. More economical and more suitable operating conditions are preferred in terms of the applicability and efficiency of the treatment methods used in dyestuff removal [2]. The adsorption of methylene blue dyestuff in aqueous solutions with pumice powder was investigated and it was revealed that as the amount of adsorbent and time increased, the adsorption increased, and the adsorption rate of the basic dye decreased with increasing concentration [3]. Wastewaters containing dyestuffs generally have a dark different colour and wide pH range, high temperature, COD (Chemical Oxygen Demand), BOD (Biological Oxygen Demand), total dissolved solids and high conductivity. Both physical, chemical and visual pollution occur in the discharge of dye-containing wastewater. The colour and density of wastewater containing dyestuffs may differ according to the type of dyestuff [4].

Adsorption is a frequently used, inexpensive and good method for the treatment of dyestuff-containing wastewater. Adsorption studies are carried out by altering the conditions such as different organic and inorganic materials and different pH, temperature, concentration, adsorbent amounts to optimise the conditions for adsorption. Adsorption continues until a balance that established between the concentration of the substance deposited on the surface of the adsorbent and the concentration of the substance remaining in the solution. At this equilibrium time, the relationship between the amount of substance adsorbed at constant temperature and the

equilibrium pressure or concentration is called "adsorption isotherm" and gives information about the characterization of the experiment. In the study in which rice husk was used as adsorbent, it was observed that the adsorption process reached equilibrium at pH 7.87 and within 90 minutes [5]. In another study, the removal of ethylene blue dye from aqueous solutions with pine-magnetite composite as adsorbent was studied and its effects on the removal of methylene blue dyestuffs were investigated at different temperatures, adsorbent dose, adsorbate concentration and different temperatures [6].

2. Material and Method

The Bayburt stone used in this study is extracted from the provincial borders of Bayburt and brought to the laboratory in relatively large sizes to be used in the study. It was first grinded and cleaned by washing several times with the help of distilled water and left to dry in an oven at 105 °C for 24 hours and then ground into powder. Detailed technical analyse values of yellow Bayburt stone are given in Table 1 [7].

Table 1. Technical analysis values of Bayburt stone

MgO, %		0.5
SiO ₂ , %		4.80
CaO, %		7.30
Fe ₂ O ₃ , %		2.45
Specific gravity, g/cm ³		2.71
Unit volume weight, g/cm ³		1.84
Water absorption at atmospheric pressure	By weight (%)	13.0
	By volume (%)	24.0
Apparent porosity, %		24.0
Pressure resistance, kgf/cm ²		282
Porosity degree, %		32.2
Average wear resistance, cm ³ /50 cm ²		63.6

In order to investigate the zeta potential values, potential measurements were made at different pH values between 2 and 12 and the maximum value was obtained at pH 10 as -29.8 mV (Figure 1).

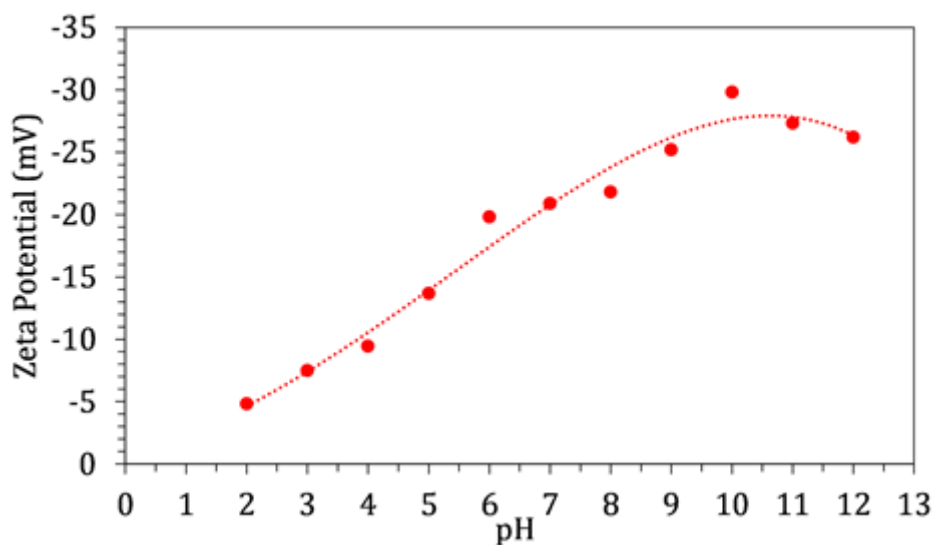


Figure 1. Zeta potential values versus pH

The wastewater used in the study was prepared synthetically with Astrazon Red GTLN textile dye. Astrazon Red GTLN textile dye has the chemical formula of C₁₉H₂₅ClN₅O₂. The chemical structure of it is given in Figure 2.

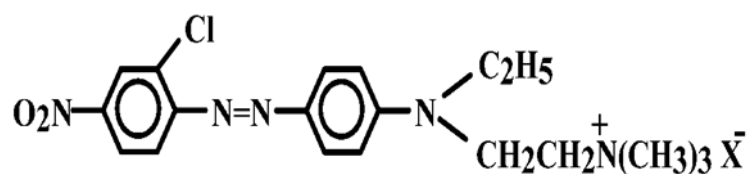


Figure 2. Chemical formula of Astrazon Red GTLN

In the study, different inlet dye concentration, adsorbent amount, contact time and different temperature values were tried to determine the adsorption efficiency for dyestuff removal in laboratory conditions.

1 N hydrochloric acid (HCl) and 1 N sodium hydroxide (NaOH) solution were used to bring the pH value to the desired values. The dyestuff stock solution prepared at 1000 ppm was diluted in the range of 10-200 mg/L and placed in 250 ml bottles and adsorbent was added in the range of 0.1-10 g/L. After centrifugation, it was heated and stirred at constant temperature for a certain period of time. The samples were filtered and read in the spectrophotometer.

Devices used in conducting experimental studies are in Atatürk University Environmental Engineering Department Laboratories. Axis 220 brand analytical balance was used for precision weighing, MikrotestTT104 brand oven and desiccator were used for the preparation of the samples, batch trials were carried out in Edmund Bühler Incubator HoodTH15 brand heater mixer. pH measurement was made with a CrisonpH25+ brand pH meter. Nuve NF 1200 R brand centrifuge device was used for solid-liquid separation. The concentrations of the samples were determined with the help of Merck Spectroquant prove 300-mark spectrophotometer device.

At the end of the experiment the adsorbent was separated from the solution with the help of filtration and then viewed with the Daytam ZEISS SIGMA 300 brand Scanning Electron Microscope (SEM) device. SEM photographs of Bayburt stone before and after adsorption are shown in [Figures 3 and 4](#).

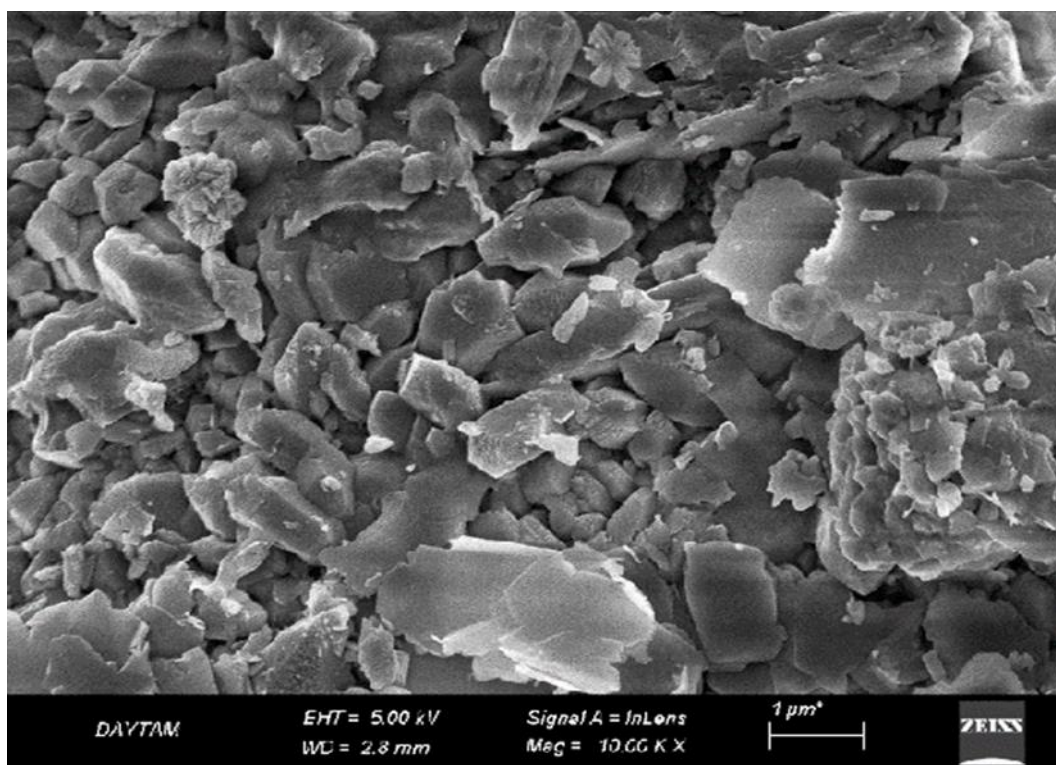


Figure 3. Before adsorption

Different inlet concentration, temperature and contact time values were tried to determine the optimum conditions.

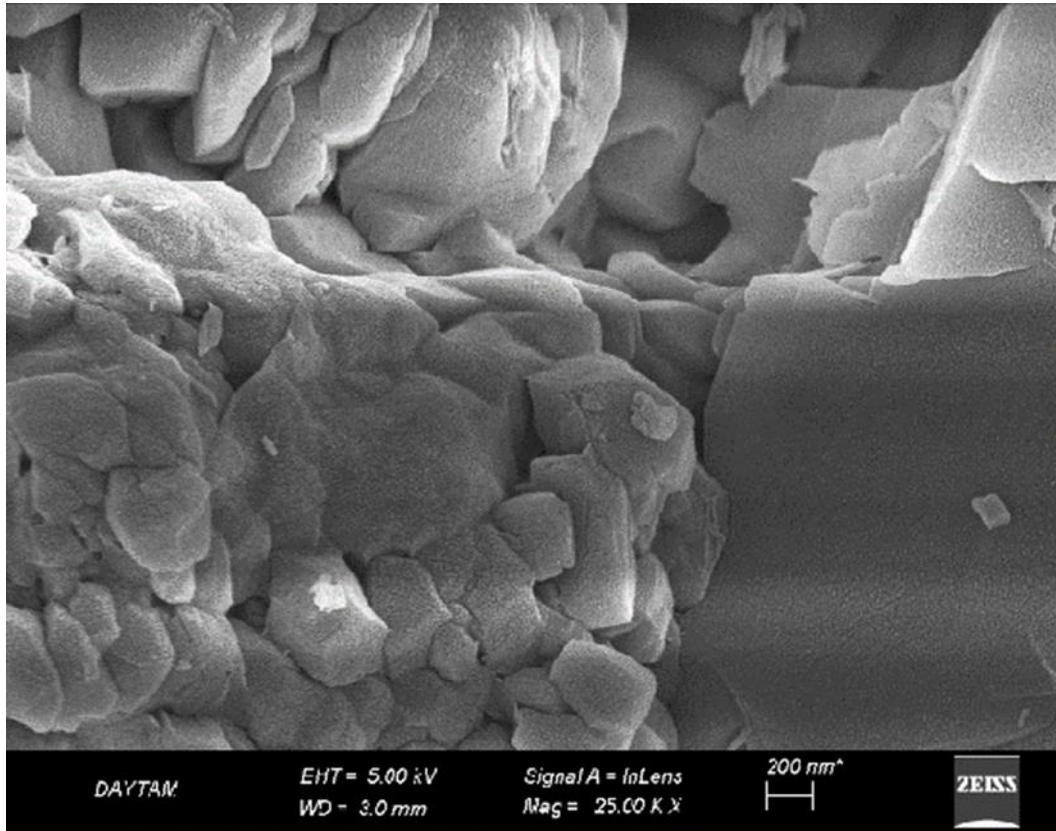


Figure 4. After adsorption

In order to calculate the adsorption efficiency for dyestuff removal in laboratory conditions, the adsorbent amount is taken as the basis in the inlet and equilibrium state, and the concentration and volume. The equilibrium amount of adsorbed substances (q_e) and removal efficiency was calculated with the Equations (1) and (2):

$$q_e = \frac{C_0 - C_e}{m} * V \quad (1)$$

$$\%R = \frac{C_0 - C_e}{C_0} * 100 \quad (2)$$

where C_0 and C_e are the liquid-phase concentrations of dye (mg/L) at initial and equilibrium state, respectively, V is the volume of the solution (L) and m is the mass of dry sorbent(g) [8].

3. Results

Adsorption experiments were carried out by using 250 mL Erlenmeyer flasks. Sorbent and Astrazon Red GTLN solutions were added to the flasks for each experiment. Flask content temperatures stabilized before the test within a range between 25 °C and 35 °C.

Adsorbed Astrazon Red GTLN amount onto per unit weight of adsorbent (mg/g) is calculated with Equation 1. Langmuir [9], Freundlich [10] and Tempkin [11] isotherm model equations are given below with the Equations of 3, 4 and 5, respectively.

$$\frac{1}{q_e} = \left(\frac{1}{K_L \cdot q_m} \right) \left(\frac{1}{C_e} \right) + \left(\frac{1}{q_m} \right) \quad (3)$$

where q_m is the maximum adsorbate uptake capacity (mg/g) and K_L is the Langmuir constant related to the energy of adsorption (L/mg).

$$\ln(q_e) = \ln K_F + \frac{1}{n} \ln C_e \quad (4)$$

where K_F is Freundlich constant related to biosorption capacity (L/g) and $1/n$ is the heterogeneity factor.

$$q_e = B \ln A + B \ln C_e \quad (5)$$

where $B = RT/b$, b is the Temkin constant related to heat of sorption (J/mol), A is the Temkin isotherm constant (L/g), R is the gas constant (8.314 J/mol.K) and T is the absolute temperature (K) of solution.

Langmuir, Freundlich and Tempkin isotherms were tested. Graphs are given in Figure 5.

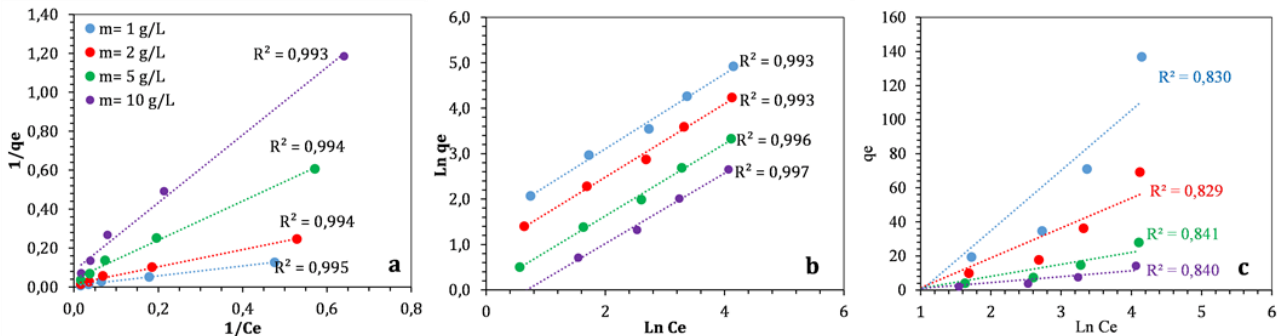


Figure 5. Langmuir (a), Freundlich (b) and Tempkin (c) isotherm model plots

The isotherm model constants are given in Table 2.

The study was carried out at 25°C, 30°C, 35°C conditions. In the study, the adsorption efficiency for dyestuff removal was calculated under different temperature laboratory conditions and it was observed that the adsorption rate increased with temperature. According to the results of the adsorption study, it was determined that the highest dye removal efficiency was at 35°C (Figure 6).

Table 2. Isotherm model constants

Temp.	m(g)	Langmuir			Freundlich			Temkin			
		qm	B	R ²	K _F	n	R ²	A	B	b	R ²
25°C	1	75,864	0,055	0,973	4,143	1,312	0,987	0,347	29,935	86,931	0,809
	2	39,086	0,055	0,973	2,148	1,312	0,992	0,358	15,131	171,982	0,822
	5	17,266	0,050	0,980	0,891	1,308	0,995	0,369	6,158	422,619	0,843
	10	8,420	0,058	0,977	0,483	1,320	0,995	0,397	3,114	835,616	0,841
30°C	1	91,649	0,049	0,982	4,436	1,266	0,991	0,371	32,892	79,116	0,816
	2	45,533	0,051	0,981	2,305	1,272	0,993	0,384	16,497	157,741	0,821
	5	17,641	0,060	0,978	1,037	1,306	0,994	0,425	6,522	399,000	0,834
	10	9,506	0,057	0,981	0,531	1,290	0,996	0,434	3,358	774,912	0,841
35°C	1	147,833	0,027	0,995	4,298	1,214	0,993	0,362	35,360	73,593	0,830
	2	63,240	0,036	0,994	2,383	1,239	0,993	0,395	17,554	148,245	0,829
	5	24,920	0,040	0,994	1,047	1,261	0,996	0,428	6,994	372,054	0,841
	10	11,730	0,049	0,993	0,591	1,292	0,997	0,478	3,475	748,875	0,840

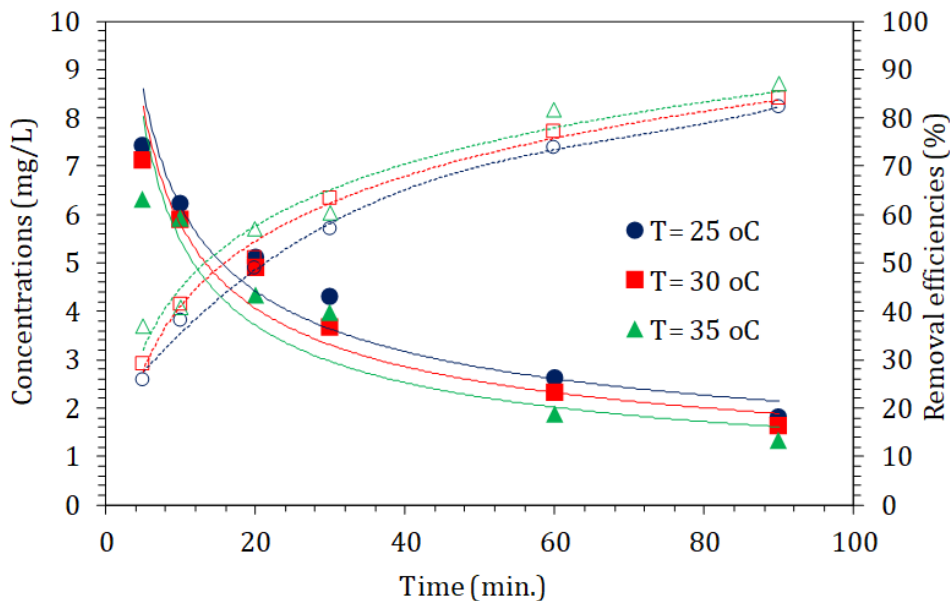


Figure 6. Concentrations with time for different temperatures

It was observed that as the inlet dye concentration increased, the removal efficiency decreased as it exceeded the adsorption capacity. Similarly, in a study which is on the removal of methylene blue, used pine leaves as adsorbent, it was observed that while the concentration was increased from 10 to 90 mg/L, the removal efficiency decreased from 96.5 to 40.9% [2].

The following experiments were carried out under different temperature and inlet concentration conditions and the dye removal efficiencies were investigated. It was observed that the adsorption efficiency decreased as the inlet concentration increased (Figure 7). In order to determine the adsorption efficiency and concentration behaviours in the adsorption process, experiments were carried out up to 90 minutes but the first 30 minutes were found to be the effective time.

The adhesion and contact of the dyestuff to be removed in the adsorbent substance yellow Bayburt stone surface area and pores should be homogeneously ensured. Therefore, since the mixing speed is effective in adsorption, the diffusion of the entire substance cannot fully adhere to the adsorbent surface in a low-speed mixing process. High mixing speed disrupts the adsorption mechanism and makes it difficult for adsorption to reach equilibrium [12]. In addition, when the mixing energy cost is considered, the mixing speed becomes even more important.

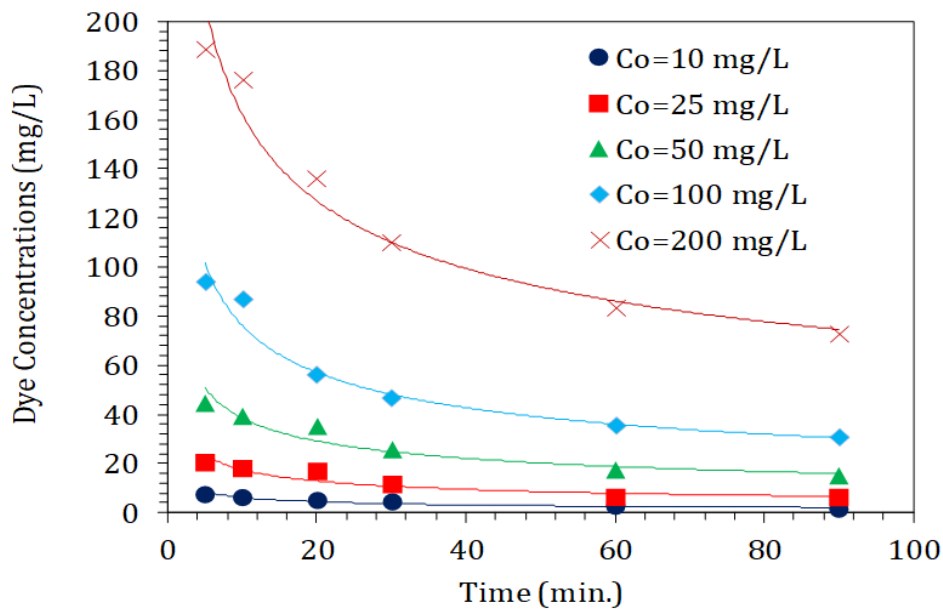


Figure 7. Concentrations with time for different initial dye concentrations

As can be seen in Figure 8, when the dye removal efficiency values were examined against different initial concentrations, the adsorption efficiency decreased as the concentration value increased.

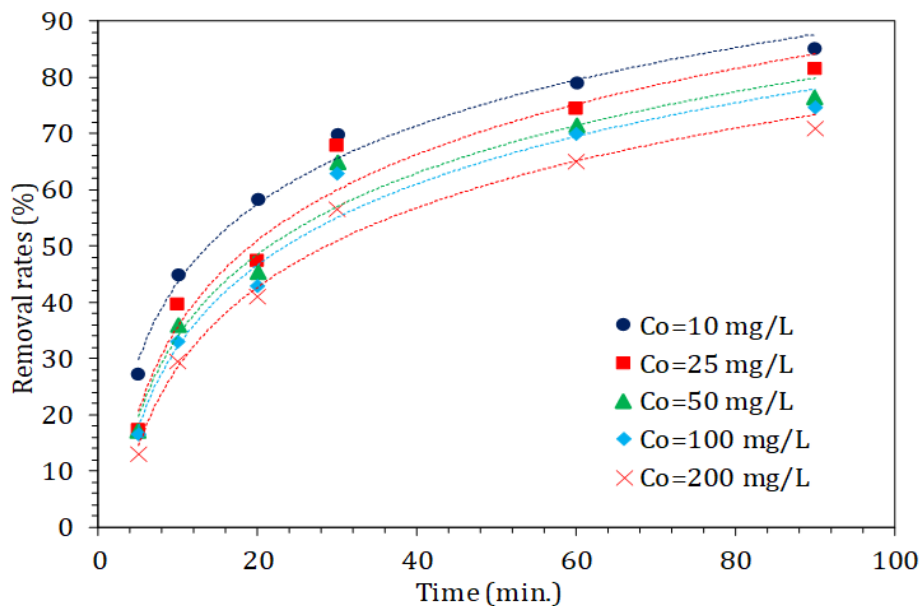


Figure 8. Removal rates for different initial dye concentrations

Considering these experimental data, it is seen that increasing the amount of Bayburt stone increases the adsorbing efficiency of the dyestuff. Since the surface area of the adsorbent will increase with the increase of the amount used, the amount of adsorbate adsorbed in the pores of the adsorbent also increases. Because the adsorption efficiency and intensity will increase proportionally with the increase in surface area, this ratio has been proven [13].

4. Conclusion

By using the yellow type of Bayburt stone, in this study, the removal of dyestuff in the aqueous solution, which is used in dyeing products in the textile industry, by adsorption method was investigated. In terms of parameters affecting adsorption, the effects of contact time, inlet adsorbate substance concentration, adsorbent substance dosage, mixing speed and temperature were investigated in batch system experiments. The results obtained in this study revealed that Bayburt stone, which is very cheap and easy to find, is an effective adsorbent material.

In order to determine the optimum dye concentration, experiments were carried out with concentrations of 10 mg/L, 25 mg/L, 50 mg/L, 100 mg/L and 200 mg/L. As the initial dye concentration increased, the removal efficiency decreased and the optimum value was determined as 25 mg/L. In addition, 1 g/L, 2 g/L, 5 g/L and 10 g/L adsorbent amounts were used to determine the most suitable adsorbent amount, and it was determined that 10 g/L adsorbent substance amount was the most appropriate. In order to determine the effective mixing speed in adsorption, studies were carried out at different mixing speeds. Stirring speeds of 100 rpm, 200 rpm and 300 rpm were tried. The optimum mixing speed was determined as 200 rpm. In the study; 85% adsorption efficiency was obtained by taking the temperature 35°C, inlet dye concentration 10 mg/L, stirring speed 200 rpm and adsorbent concentration 10 g/L. As a result, the results of the study showed that Bayburt stone is an economical, effective and suitable adsorbent that can be used in the adsorption method.

Acknowledgement

This research study was carried out at the laboratory of Ataturk University Engineering Faculty, Environmental Engineering Department laboratories. This paper was partly presented in 1st Advanced Engineering Days (AED) held on Thursday, December 23, 2021 in Mersin/Turkey [14].

Funding

This research received no external funding.

Author contributions

Erdem Kocadağistan: Writing-Original drafting, Software, Validation. **Beyhan Kocadağistan:** Visualization, Analysis, Writing-Review and Editing.

Conflicts of interest

The authors declare no conflicts of interest.

References

1. Gazigil, L., (2014). Investigation of dyestuff removal by sunflower kernel shell from low-cost industrial wastes. Master's Thesis, Institute of Science and Technology, Atatürk University, Erzurum
2. Yagub, M. T., Sen, T. K. Afroze, S. & Ang, H. M. (2014). Dye and its removal from aqueous solution by adsorption: A review. *Advances in Colloid and Interface Science*, 209, 172-184.
3. Akbal, F. (2005). Adsorption of basic dyes from aqueous solution onto pumice powder. *Journal of Colloid and Interface Science*, 286(2), 455-458.
4. Babuşcu, F. (2007). Dyestuff Adsorption Using Modified and Crude Zeolite. Master's Thesis, Graduate School of Natural and Applied Sciences, Gebze Institute of Technology, Gebze.
5. Sawasdee, S. Jankerd, H. & Watcharabundit, P. (2017). Adsorption of dyestuff in households dyeing onto rice husk. *Energy Procedia*, 138, 1159-1164.
6. Mtshatsheni, K. N. G. Ofomaja, A. E. & Naidoo E. B. (2019). Synthesis and optimization of reaction variables in the preparation of pine-magnetite composite for removal of methylene blue dye. *South African Journal of Chemical Engineering*, 29, 33-41.
7. Stone mine limited company, (2018). (Bayburt Natural Stone Potential Mining Geology Report-MTA)

8. Nsami, J. N., & Mbadcam, J. K. (2013). Adsorption efficiency of chemically prepared activated carbon from cola nut shells by ZnCl₂ on methylene blue. *Journal of Chemistry*, 469170, 7.
9. Zhang, J., Shao, J., Jin, Q., Li, Z., Zhang, X., Chen, Y., Zhang, S., & Chen, H. (2019). Sludge-based biochar activation to enhance Pb (II) adsorption. *Fuel* 252: 101-108.
10. Nuri, O. S., Irannajad, M., & Mehdilo, A. (2019). Reagent adsorption on modified mineral surfaces: isotherm, kinetic and thermodynamic aspects. *Journal of Molecular Liquids*, 291, 111311.
11. Ghasemi, N., Ghasemi, M., Moazeni, S., Ghasemi, P., Alharbi, N. S., Gupta, V. K., ... & Tkachev, A. G. (2018). Zn (II) removal by amino-functionalized magnetic nanoparticles: Kinetics, isotherm, and thermodynamic aspects of adsorption. *Journal of industrial and engineering chemistry*, 62, 302-310.
12. Kul, Z. E., Nuhoglu, Y., Kul, S., Nuhoglu, Ç., & Torun, F. E. (2016). Mechanism of heavy metal uptake by electron paramagnetic resonance and FTIR: enhanced manganese (II) removal onto waste acorn of *Quercus ithaburensis*. *Separation Science and Technology*, 51(1), 115-125.
13. Kahraman, H. T. & Edebali, S. (2016). The use of organo-modified nanoclay as an alternative adsorbent for Cr (VI) removal from wastewater. *Selcuk University Journal of Engineering Science and Technology*, 4(3), 173-181
14. Kocadağistan, B., & Kocadağistan, E. (2021). Adsorption of Astrazon red GTLN (AR) with volcanic tuff Bayburt Stone. *Advanced Engineering Days (AED)*, 1, 60-62.



© Author(s) 2022. This work is distributed under <https://creativecommons.org/licenses/by-sa/4.0/>



Energy dissipation potential of flow separators placed in spillway flip bucket

Ali Emre Ulu^{*1}, Mehmet Cihan Aydın¹, Ercan Işık¹

¹Bitlis Eren University, Engineering and Architecture Faculty, Department of Civil Engineering, Bitlis, Türkiye, aliemreulu@gmail.com; mcaaydin@gmail.com; ercanbitliseren@gmail.com

Cite this study: Ulu, A. E., Aydın, M. C., & Işık, E. (2022). Energy dissipation potential of flow separators placed in spillway flip bucket. *Advanced Engineering Science*, 2, 60-66

Keywords

Spillway
CFD
Energy dissipater
Flow separator

Research Article

Received: 13.01.2022
Revised: 17.02.2022
Accepted: 25.02.2022
Published: 14.03.2022



Abstract

The design of the energy dissipating pools at the downstream of the spillway is an important issue in terms of controlling the downstream flow regime, jet velocities and the scour problem that may occur in this region. In this context, there are many designs for flip-bucket pools for both energy dissipation and minimizing scour problems. In this study, the energy dissipation performance of a flow separator structure placed in an energy dissipation pool was investigated numerically by increasing the shear stresses. As a remarkable result, it has been observed that flow separators are able to reduce flow velocities by up to 55%, while the downstream trajectory increases significantly.

1. Introduction

Spillways are water structures that are widely used in hydraulic engineering. These structures are used to safely transfer the excess water accumulated in the dam reservoirs to the downstream part. After the body part of the dams, they are the most important structures for a dam. Ogee style weirs are also the most important water intake structures from the past to the present. In these weirs, which are known as classical crests, the water taken from the reservoir is passed over an inclined body and delivered to a flip bucket to break its energy. This structure, which resembles a bucket, absorbs the energy it gains during the fall of the flow, and it is important to prevent possible damage to the downstream of the structure. In cases where the spillway design is not done correctly, at the downstream some problems may occur due to scouring, cavitation and energy breakdown at the downstream of the spillway and regulator [1-2]. In this respect, their designs have many differences or shapes, obstacles and sizes that increase the energy breaking potential. There are a number of experimental and numerical studies in the literature for investigating the energy of the high-speed flow that occurs just downstream of the spillway structures [3-7].

Two important problems in spillway chute channels subject to high discharges and velocities are cavitation that may occur on the chute and scour in the downstream. In order to prevent these, measures such as reducing the flow velocities on the chute channels and throwing the water jet away from the downstream are taken. Flip-bucket type chute channels create a jet of water, allowing downstream scours to occur away from the dam body. Thus, the stability of the dam body is not affected. In this case, there are two situations; the first is to reduce the maximum flow velocities in the chute, and the second is to increase the downstream jet trajectory. Although these two situations do not seem possible since they are directly proportional to each other, in this study, these two elements will be examined by using a flow separator. In this study, flow velocities, downstream jet trajectory and

the energy dissipation potential of a flow separator structure placed in the flip bucket of a 2D Ogee-style spillway structure was investigated numerically. Possible sediment scour in the downstream region was not taken into account in the study.

2. Material and method

FLOW-3D, a powerful computational fluid dynamics (CFD) program, was used as a method in the study. Flow-3D is a widely used reliable method that can simulate fluid motions [8]. The program determines fluid motion by solving equations such as conservation of mass and momentum. The mass conservation equation used in Flow-3D is presented below [9].

$$V_F \frac{\partial \rho}{\partial t} + \frac{\partial}{\partial x}(\rho u A_x) + R \frac{\partial}{\partial y}(\rho v A_y) + \frac{\partial}{\partial z}(\rho w A_z) + \xi \frac{\rho u A_x}{x} = R_{DIF} + R_{SOR}$$

Where;

V_F : Volume ratio of the fluid,

ρ : Density of the fluid,

R_{dif} : Turbulent diffusion term,

R_{sor} : Mass source,

u, v, w are the velocity components in the coordinate directions (x, y, z).

Momentum equation of fluid motion:

$$\begin{aligned} \frac{\partial u}{\partial t} + \frac{1}{V_F} \left\{ u A_x \frac{\partial u}{\partial x} + v A_y R \frac{\partial u}{\partial y} + w A_z \frac{\partial u}{\partial z} \right\} - \xi \frac{A_y v^2}{x V_F} &= -\frac{1}{\rho} \frac{\partial p}{\partial x} + G_x + f_x - b_x - \frac{R_{SOR}}{\rho V_F} (u - u_w - \delta u_s) \\ \frac{\partial v}{\partial t} + \frac{1}{V_F} \left\{ u A_x \frac{\partial v}{\partial x} + v A_y R \frac{\partial v}{\partial y} + w A_z \frac{\partial v}{\partial z} \right\} + \xi \frac{A_y u v}{x V_F} &= -\frac{1}{\rho} \left(R \frac{\partial p}{\partial y} \right) + G_y + f_y - b_y - \frac{R_{SOR}}{\rho V_F} (v - v_w - \delta v_s) \\ \frac{\partial w}{\partial t} + \frac{1}{V_F} \left\{ u A_x \frac{\partial w}{\partial x} + v A_y R \frac{\partial w}{\partial y} + w A_z \frac{\partial w}{\partial z} \right\} &= -\frac{1}{\rho} \frac{\partial p}{\partial z} + G_z + f_z - b_z - \frac{R_{SOR}}{\rho V_F} (w - w_w - \delta w_s) \end{aligned}$$

Where;

(G_x, G_y, G_z) : Mass acceleration,

(f_x, f_y, f_z) : Viscous accelerations,

(b_x, b_y, b_z) : It expresses flow losses in porous media.

3. Numerical modeling and analysis

In the study, a two-dimensional ogee type spillway with a crest elevation of $H = 5.28$ m and a flip-bucket diameter of 2.0 m was used. Flip bucket design with 3 different types of geometry is used. Type 1 consists of a classic ogee weir without the use of a flow separator. In Type 2 and Type 3 models, a flow separator is placed at $\alpha=10$ cm and $\alpha=20$ cm above the flip bucket, respectively (Figure 1). The weir length (B) is taken as 7.7 m. The height of the flip bucket (c) is 80 cm.

In the study, hexahedral 0.05 m cell size was used. Total mesh count is calculated as 130,000 (Figure 2a). Analyzes were continued until the flow became completely stable (120 seconds). Fluid elevation change over time is given in Figure 2b. Analyzes performed using the Renormalized Group (RNG) turbulence model were solved by giving fluid elevation. As the initial fluid elevation, the water level started from 5.38 m and the elevation was increased by 0.1 m till 6.38 m. Since analyzes were carried out in two dimensions, the channel boundary conditions were determined as Symmetry. The channel floor boundary condition has been assigned as Wall, and the inlet and outlet parts have been assigned as Specified Pressure. 1 m downstream water inlet is defined in order to provide downstream conditions and to observe hydraulic jump.

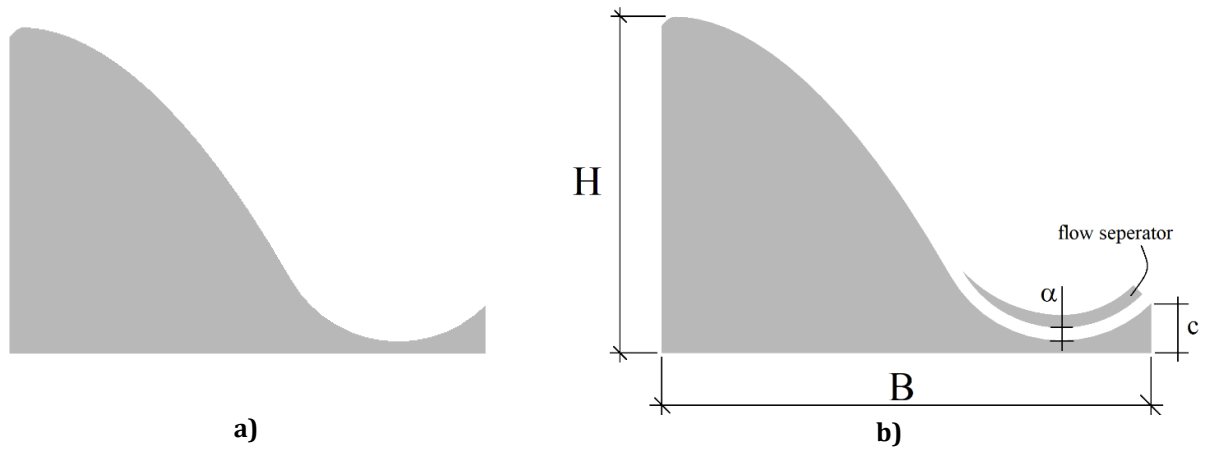


Figure 1. Geometry of the spillway; a) Type1 b) Type 3

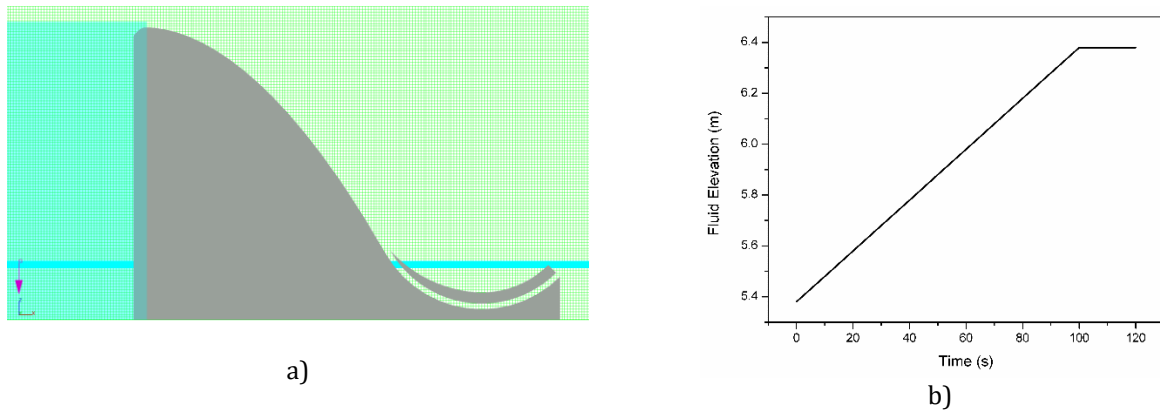
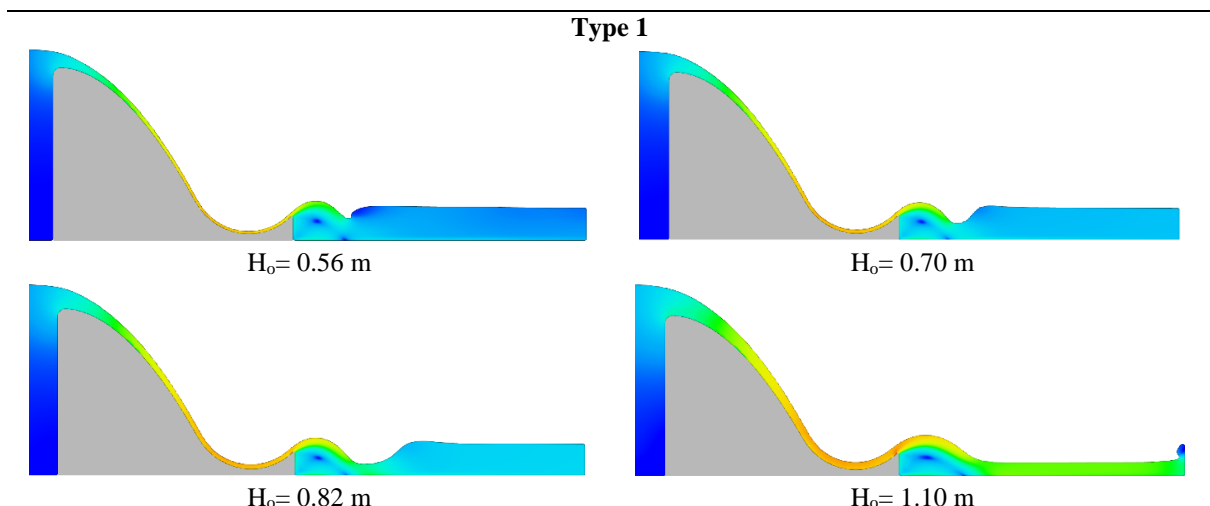


Figure 2. a) Mesh structures of the models (Type 2), b) Fluid elevation versus time

3. Results and discussion

In the study, the performance of a flow separator structure placed to increase the energy breaking potential of the spillway flip bucket at different upstream water heads was investigated in a developed CFD software. From analysis results obtained, velocity and pressure contours of some water heads belong to Type 1, Type 2 and Type 3 were presented in Figure 3 and 4, respectively.



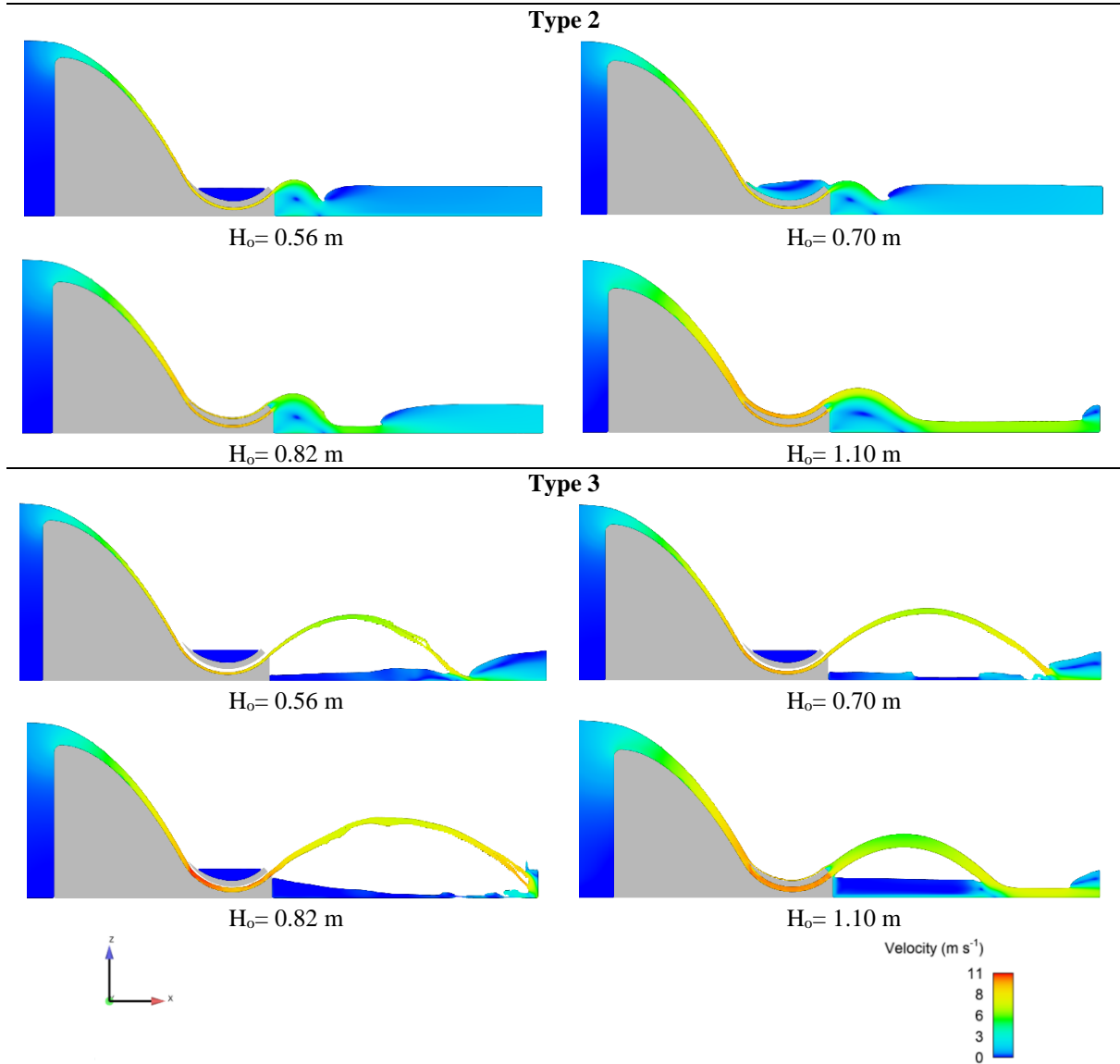
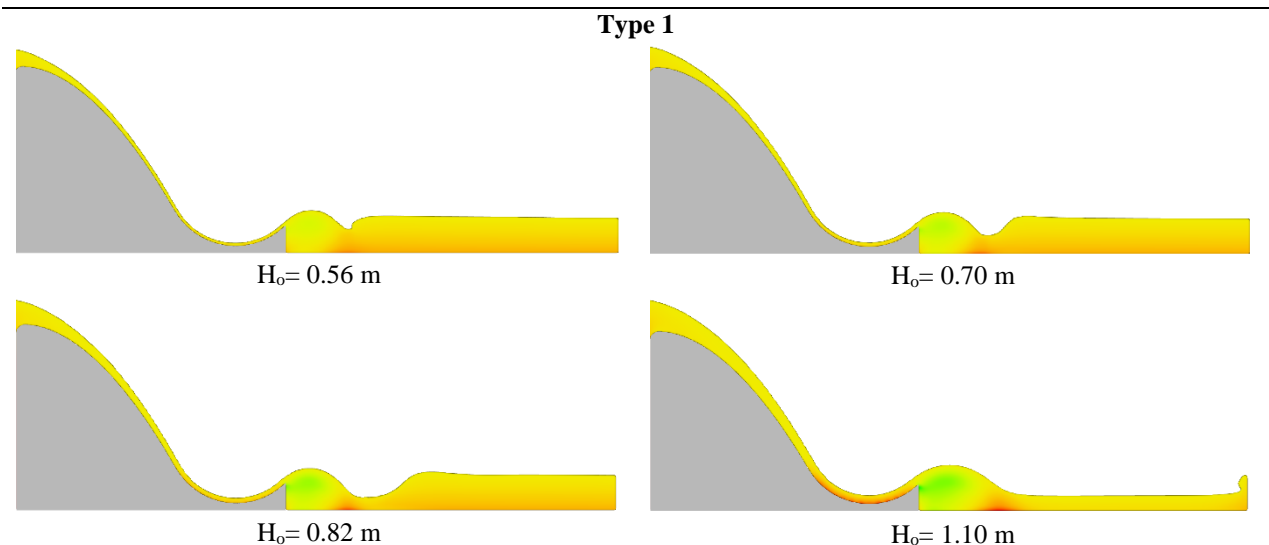


Figure 3. Velocity profiles of the flow



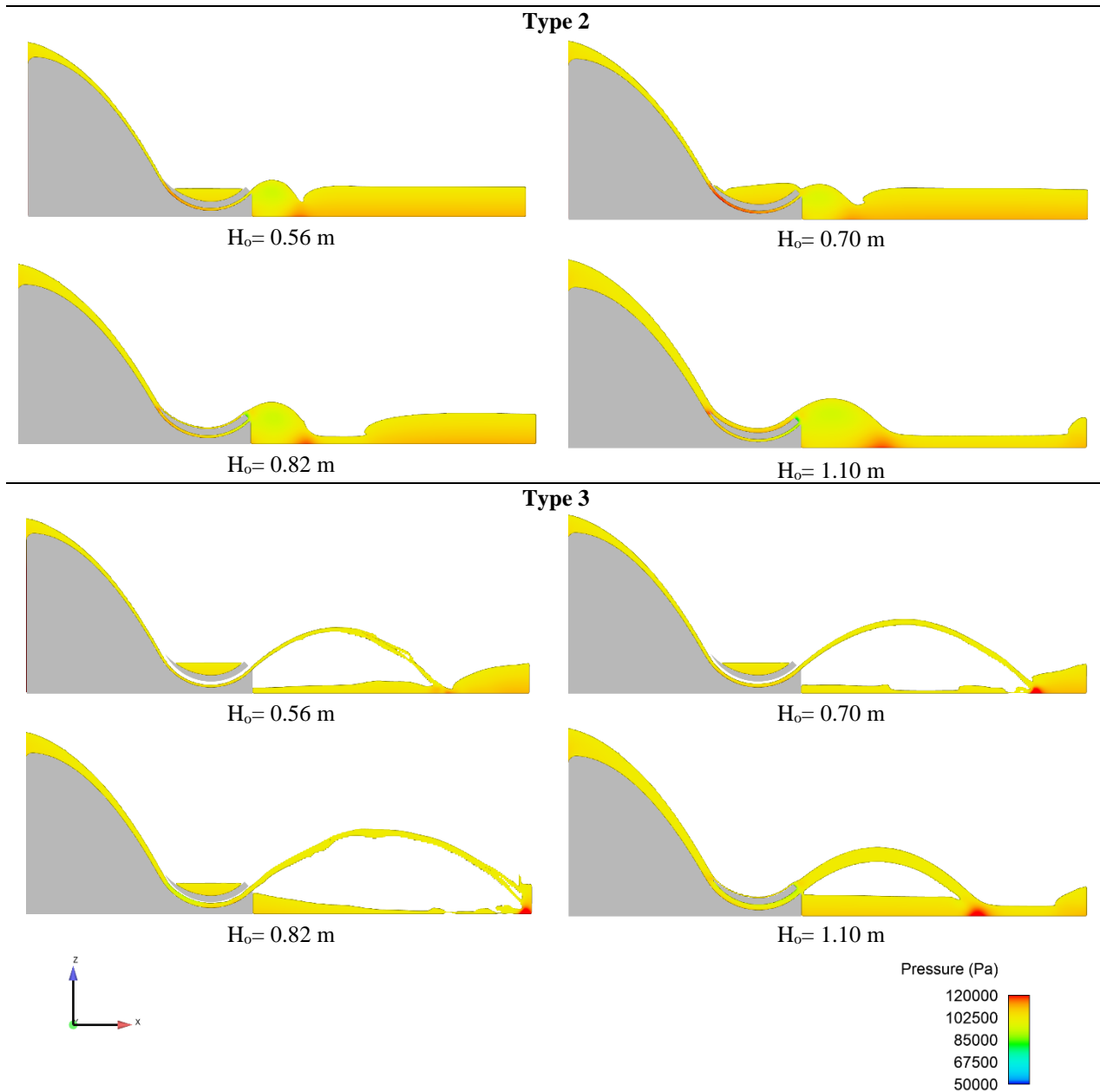


Figure 4. Pressure profiles of the flow

From the figures obtained, it is noticed that similar downstream conditions are obtained in cases of Type 1 and Type 2. However, it is clearly seen that Type 3 is very different from the other two models, it has been observed that the flow is jetted from the flip bucket in all water heads. However, it has been observed that the flow velocity of the Type 3 model, especially at the starting point of the flow separator, is higher in high water heads than in other models. At this point where the velocity increased, it was noticed that the pressure decreased in the Type 3 with $H_o = 0.82$ m. In this case, it was observed that the flow splash to the farthest point among the Type 3 states. At heads above $H_o = 0.82$ m, the pressure drop shifted towards the end of the bucket. Also, it is observed that at low water heads of Type 2, the pressure is high at the beginning of the flow separator, but the pressure is balanced as the water head continues to increase.

In the study, how different models affect the flow on the weir was also investigated. For this reason, the average velocity values of the sections A-A and B-B shown in Figure 5a were obtained. In Figure 5b, the velocity distribution of the types for the B-B section is presented. According to the velocity values taken, it was observed that the velocities were very close to each other at each cross-sectional point of the flow in Type 1, which is the model without a flow separator. According to the velocity values taken, it was observed that the velocities were very close to each other at each cross-sectional point of the flow in Type 1, which is the model without a flow separator. The velocity values of Type 1 are the highest values among the investigated models. As can be seen from Table 1, this value is 9.55 m/s. It is seen that the velocities decrease in this section in the models using a flow separator. The lowest average velocity was found in Type 2 with a value of 6.17 m/s.

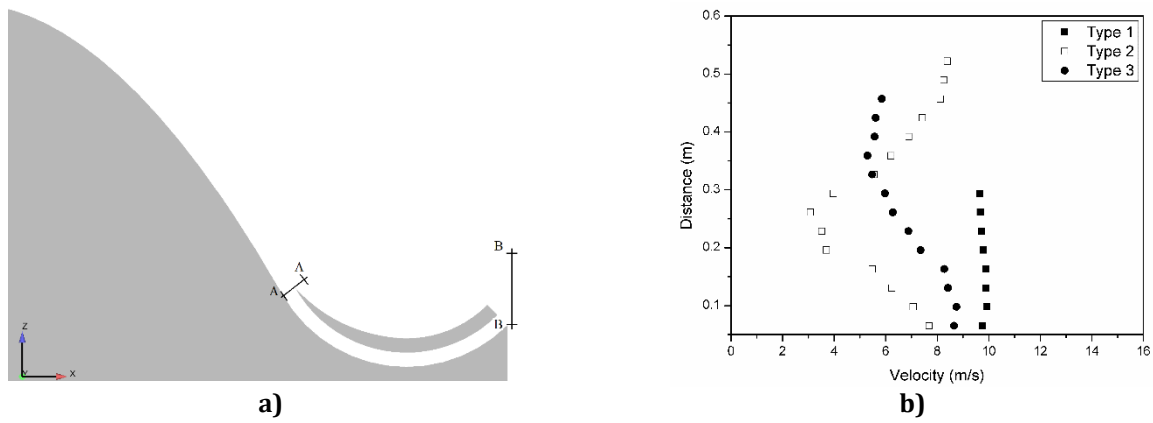


Figure 5. a) Velocity point sections, b) Velocities at the B-B section

It is understood from the Froude numbers in Table 1 that the flow has super-critical flow conditions in the A-A section in all three models. It has also been observed as a result of the numerical study that the flow separator has the effect of slowing down the flow passing through this section. This effect was observed mostly in Type 2.

Table 1. Characteristics of the flow

Models	h_{A-A} (m)	V_{avr} (m/s)		$F_{r,A-A}$
		$V_{avr,A-A}$	$V_{avr,B-B}$	
Type 1	0.275	9.24	9.55	5.813
Type 2	0.408	8.71	6.17	3.084
Type 3	0.358	9.02	6.87	3.668

The results showed that the launch significantly increased the jet trajectory, even though the flow separator (Type 3) adjusted at a certain opening reduced the exit velocities (compared to the Type 1). This situation also causes a decrease in the Froude number in the A-A section of the spillway. This will reduce the energy of the flow and increase the length of the water jet formed at the downstream, thus contributing positively to possible cavitation on the surfaces and scours downstream. The reason for this is thought to be due to the changes in pressures under the jet separator, as well as the effect of the flow separator on the shear stresses on the flow (hence the friction resistance / drag coefficient) and the development of the boundary layer. In order to better examine the subject, it is recommended to support it with experimental studies and to analyze it in more detail.

4. Conclusion

In the data obtained from the study, it has been observed that the flow rises by jumping from the flip-bucket structure in the Type 3 model using a flow separator at all investigated water heads. At low head loads, a hydraulic jump has occurred just after the jet throwing region of the models with the flow separator. This situation was not observed in the models without the separator. It has been observed that flow separators reduce flow velocities by up to 55%, especially at the point where the flow leaves the weir structure. The most essential reason for this is that flow separators increase frictional resistance.

In the study, the effect of a flow separator placed in the energy breaking pools (flip bucket) of the spillway structures, which has an important place in the field of hydraulic engineering, on the flow velocities and energy dissipation status was investigated. In future studies, the performance of the flow separator can be evaluated by comparing the different dimensions, the cavitation risk it will create and how it will behave in case of a possible scour in the downstream region compared to the normal situation.

Acknowledgement

This paper was partly presented in 1st Advanced Engineering Days (AED) held on Thursday, December 23, 2021 in Mersin/Turkey [10].

Funding

This research received no external funding.

Author contributions

Ali Emre Ulu: Methodology, Software **M. Cihan Aydın:** Model design, Validation. **Ercan Işık:** Visualization, Writing-Reviewing and Editing.

Conflicts of interest

The authors declare no conflicts of interest.

References

1. Aydın, M. C., Ulu, A. E., & Karaduman, Ç. (2017). Investigation of Energy Dissipation and Sediment Scour Over a Regulator Using CFD. CEPPIS 2017, Poland.
2. Aydın, M. C., & Ulu, A. E. (2018). Effects of different shaped baffle blocks on the energy dissipation and the downstream scour of a regulator. Bitlis Eren University Journal of Science and Technology, 8(2), 69-74.
3. Yavuz, C., Dincer, A. E., & Aydın, I. (2016). Head Loss Estimation for Water Jets from Flip Buckets. The International Journal of Engineering and Science (IJES), 5(11), 48-57.
4. Daneshfaraz, R., & Ghaderi, A. (2017). Numerical investigation of inverse curvature ogee spillway. Civ Eng J, 3(11), 1146-1156.
5. Chatila, J., & Tabbara, M. (2004). Computational modeling of flow over an ogee spillway. Computers & structures, 82(22), 1805-1812.
6. Daneshfaraz, R., Ghaderi, A., Akhtari, A., & Di Francesco, S. (2020). On the effect of block roughness in ogee spillways with flip buckets. Fluids, 5(4), 182.
7. Hurtig, K., Croockewit, J., & Vasquez, J. A. (2013). Verification of CFD simulations of flip bucket spillway performance using physical model results. Canadian Dam Association 2013 Annual Conference, Montréal, Québec, Canada.
8. Aydın, M. C., & Işık E. (2015). Using CFD in Hydraulic Structures. International Journal of Scientific and Technological Research. 1(5):7-13.
9. Flow 3D, (2014). Manual, Sediment Scour Model. Flow-3D User Manual, v11.0.3. Flow Science, Inc.
10. Ulu, A. E., Aydın, M. C., & Işık, E. (2021). A study on the flow velocities and energy dissipation potential of flow separator placed in spillway flip bucket. *Advanced Engineering Days (AED)*, 1, 38-40.



© Author(s) 2022. This work is distributed under <https://creativecommons.org/licenses/by-sa/4.0/>



Modelling of supercapacitor by using parameter estimation method for energy storage system

Gökhan Yüksek¹, Yusuf Muratoğlu², Alkan Alkaya¹

¹Mersin University, Department of Electrical and Electronics Engineering, Türkiye, gyuksekm@mersin.edu.tr;
alkanalkaya@mersin.edu.tr

²Toros University, School of Occupational Higher Education, Mechatronics, Türkiye, yusuf.muratoglu@toros.edu.tr

Cite this study: Yüksek, G., Muratoglu, Y., & Alkaya, A. (2022). Modelling of supercapacitor by using parameter estimation method for energy storage system. *Advanced Engineering Science*, 2, 67-73

Keywords

Supercapacitor
Parameter Estimation
Renewable Energy
Modelling
Energy Storage

Research Article

Received: 14.01.2022

Revised: 20.02.2022

Accepted: 26.02.2022

Published: 14.03.2022



Abstract

Researches to increase efficiency in renewable energy systems are increasing the interest in high power density (HPD) energy storage units' day by day. HPD units form a hybrid energy storage system (HESS) when used together with a high energy density (HED) energy storage system. Supercapacitors are the most frequently used storage units among HPD with their features such as low cost, low self-discharge rate and high lifecycle. When systems need high power, supercapacitors which is used to support HED units to ensure that the transmitted power's stability, efficiency, and high quality. The use of supercapacitors in HESS with the exact timing has a significant impact on its performance. For this reason, supercapacitors must be modeled correctly and well-integrated with the system. In this study, parameter estimation was made by using the data obtained from the simulation study and the supercapacitor was modeled. The supercapacitor model has been tested for charging and discharging at different currents and successful results have been obtained.

1. Introduction

According to the National Energy Agency, if energy consumption habits continue as they are today, it is estimated that fossil fuel consumption will be up to 1.7 times in 40 years. Under these conditions, it is predicted that the carbon emission rate will increase by 1.3 times and the global temperature will increase by 6 degrees [1]. Renewable energy sources (RES's) are seen as the greatest alternative to fossil fuels' depletion and environmental impacts [2]. It is anticipated that RES's will play a major role in the energy world of the future, as they offer sustainable and environmentally friendly energy [3]. However, in addition to these advantages, it has disadvantages such as not being continuous and insufficient in terms of power quality. Photovoltaic systems, which are one of the most preferred types among RES types, can't produce energy at night times and cloudy days. In addition, being affected by atmospheric conditions negatively affects production. Similarly, wind energy systems operate directly depending on atmospheric conditions [3]. RES are used with energy storage systems to ensure continuity, power quality and load monitoring. In order to overcome this situation, RES's are used in integration with energy storage systems [4].

Energy storage systems are divided into two categories: high energy density and high-power density. High energy density storage units can provide continuous but low power. Pump hydro energy storage (PHES), compressed air energy storage (CAES), fuel cell (FC) and majority of batteries are in this category. High power density storage units, on the other hand, can provide short-term but high power. Superconducting magnetic energy storage (SMES), supercapacitor (SC), flywheel, and high power batteries can be count in this category [5-6]. The storage technologies in the literature, when used alone, cannot meet both power density and energy density due to the limitations of their chemical and physical structures [7]. By using the advantages of these two different types together, hybrid energy storage systems (HESS) are obtained [8].

SC are the most commonly used storage systems that provide high power density [9]. SC are used as secondary or backup storage on HESS, due to their higher power density and faster dynamic response. Also SC has very long life cycle and lower self-discharge rate [10]. A comparison of different ESS types is given in Table 1. As can be seen in the Table 1, SCs have obvious advantages in terms of power density and life cycle.

Table 1. Properties of different type of ESS [11-12]

Storage Type	Power Density (W/l)	Energy Density (Wh/l)	Cycle Life	Efficiency (%)	Discharge Time	Self Discharge (%)	Power Rate (kW)
Lead Acid Battery	90-700	3-15	250-1500	75-90	s-h	0.1-0.3	0-20000
Lithium Ion Battery	1300-10000	5-100	600-1200	65-75	min-h	0.1-0.3	0-100
Flywheel	5000	20-80	104-107	80-90	s-h	100	0-250
Fuel Cell	0.2-20	600	103-104	34-44	s-h	0	0-50000
SMES	2600	6	-	75-80	ms-s	10-15	0-300
Supercapacitor	40000-120000	10-20	500000	85-98	ms-min	20-40	100-10000

A model is needed to know in advance how the SC will behave in different operating conditions [13]. Also, while using in hybrid energy storage systems, the use of SC at the right time is of great importance in terms of system performance and efficiency. To decide the right time while designing the energy management system, the exact mathematical model of the SC must be known by designer. There are different SC modelling techniques in the literature.

One of the modeling types to improve the accuracy in SC modeling is the fractional order modeling method [14]. Fractional order models include non-integer differential equations and have proven to have higher accuracy compared to equivalent circuit models with integer orders. However, the cost is high due to the high mathematical computational load [15].

In intelligence-based SC modeling, artificial intelligence, fuzzy logic or learning methods are approached against complex and non-linear structures [16-17]. With the use of large amounts of data in training, very high accuracy modeling can be performed. Since it contains a much heavier mathematical load than the fractional order modeling method, its cost is much higher.

Equivalent circuit models consisting of capacitors and resistors are designed to imitate the behavior of supercapacitors exactly. Thanks to the capacitor it contains, it can be expressed with differential equations and has the feature of easy application in this way [18-19]. In against to intelligent based methods and fractional order methods, mathematical complexity is low. Simple equivalent circuit [20], classical equivalent circuit [21], debye polarization equivalent circuit [22], zubieta equivalent circuit [23], faranda equivalent circuit [24], ladder equivalent circuit [25], voltage dependent equivalent circuit [26] methods were used in the literature on the past decade.

In this study, debye polarization equivalent circuit model was used because of its simplicity and non-complicated mathematical theory. The estimation of the model parameters was determined in the MATLAB/Simulink parameter estimation toolbox. Validation of method was proved by working under different current conditions.

2. Material and Method

In the literature, many equivalent circuit models have been proposed for supercapacitors. The proposed circuits include the simplest models as well as models containing many parameters such as leakage current, adsorption capacity, pulse load and slow discharge. The supercapacitor equivalent circuit models proposed in the literature are shown in Figure 1.

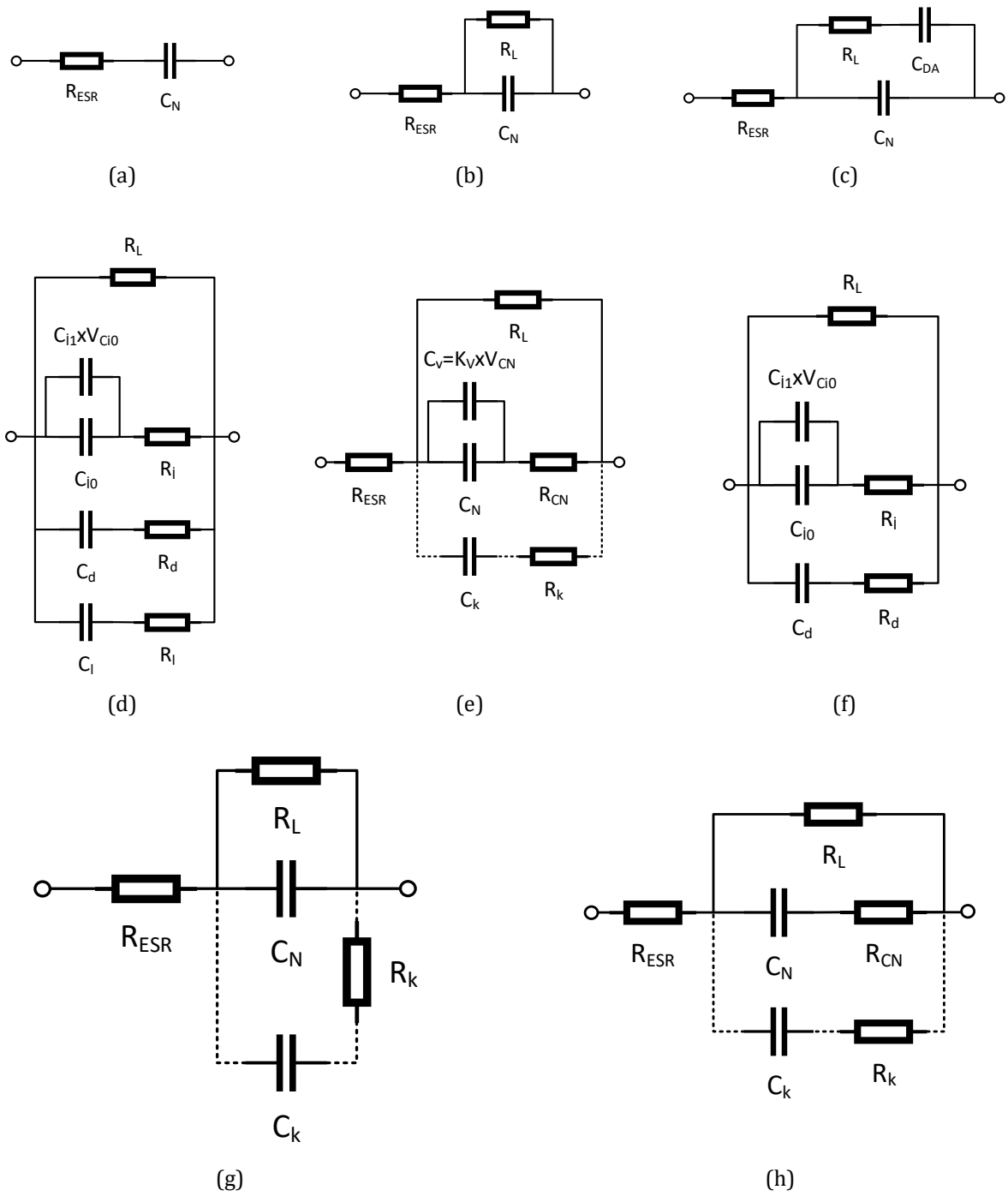


Figure 1. The supercapacitor equivalent circuit models. (a) Simple Equivalent Circuit, (b) Classical Equivalent Circuit, (c) Debye Polarization Equivalent Circuit, (d) Zubieta Equivalent Circuit, (e) Voltage Dependent Equivalent Circuit, (f) Faranda Equivalent Circuit, (g) Ladder Equivalent Circuit, (h) Voltage Independent Equivalent Circuit

2.1. Equivalent Circuit Model

In this study, supercapacitor model, given in Figure 1, is constructed using Debye polarization equivalent circuit. The Debye polarization equivalent circuit includes the leakage current and adsorption capacity parameters.

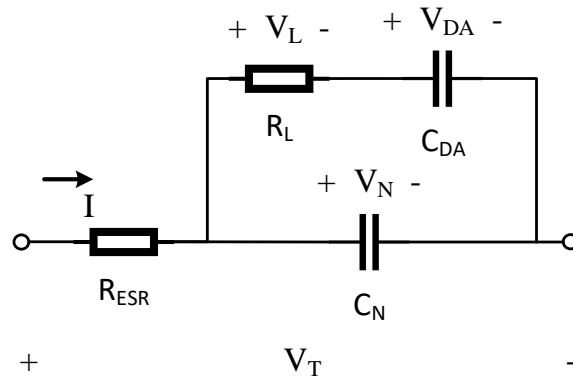


Figure 2. Debye polarization equivalent circuit model

where R_{ESR} is the equivalent series resistor, R_L is the leakage current resistance, C_{DA} is the Debye adsorption capacitance, and C_N is the nominal capacitance. The electrical behavior of the Debye polarization equivalent circuit model can be expressed as Equations 1-3:

$$\frac{dV_{DA}}{dt} = -\frac{1}{R_L C_{DA}} V_{DA} + \frac{1}{R_L C_{DA}} V_N \quad (1)$$

$$\frac{dV_N}{dt} = -\frac{1}{R_L C_N} V_{DA} + \frac{1}{R_L C_N} V_N - \frac{1}{C_N} I \quad (2)$$

$$V_T = V_N - IR_{ESR} \quad (3)$$

2.2. MATLAB/Simulink Model

The supercapacitor was modeled in MATLAB/Simulink using mathematical expressions of the Debye polarization equivalent circuit as seen in the Figure 3.

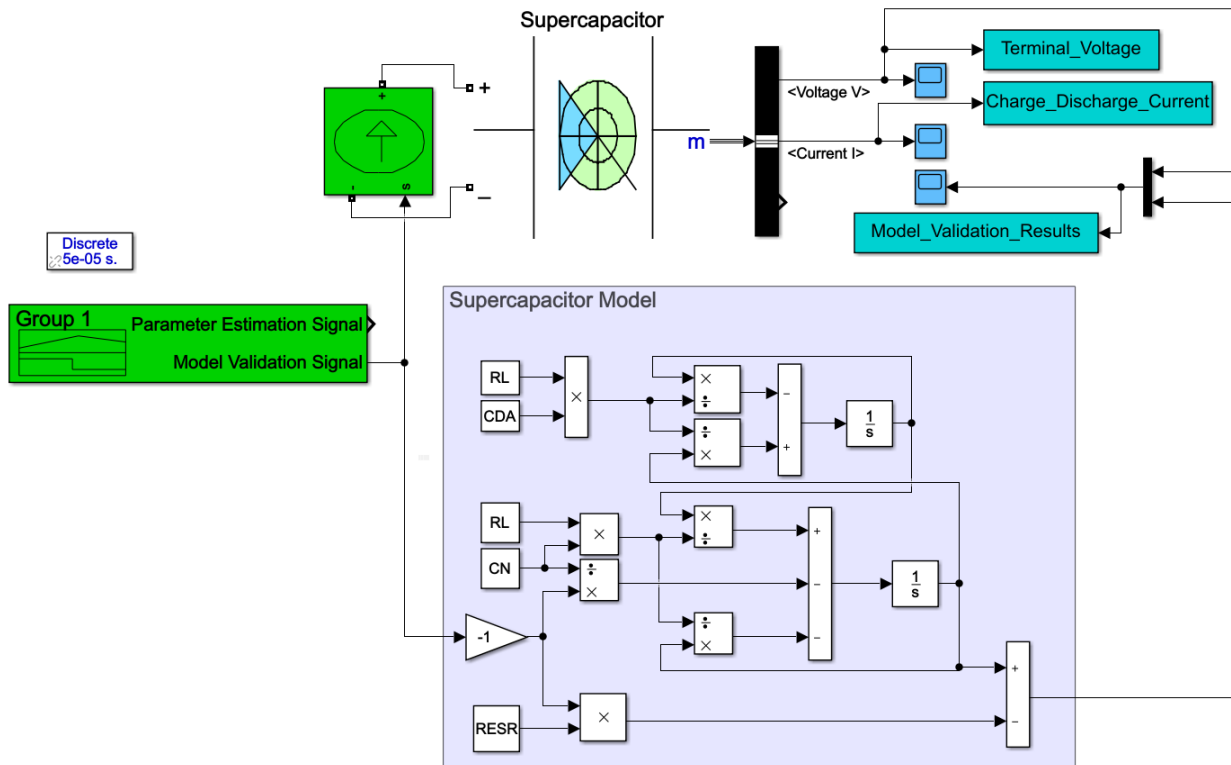


Figure 3. Validation of Debye polarization equivalent circuit model in MATLAB/Simulink

The Simulink model includes a real supercapacitor and a Debye polarization equivalent circuit model. The same input signal is applied to the model and the terminal voltages are observed for comparison. The model performance is verified by calculating the comparison errors of the terminal voltages.

3. Results

Nonlinear Least Square method based on Trust Region Reflective algorithm was used for estimation of equivalent parameters. The input current given in Figure 3(a) was applied to the circuit model for parameter estimation. Comparison of model and actual terminal voltages as a result of parameter estimation is given in Figure 3(b). The estimation result was confirmed with a mean squared error of 1.7520×10^{-4} .

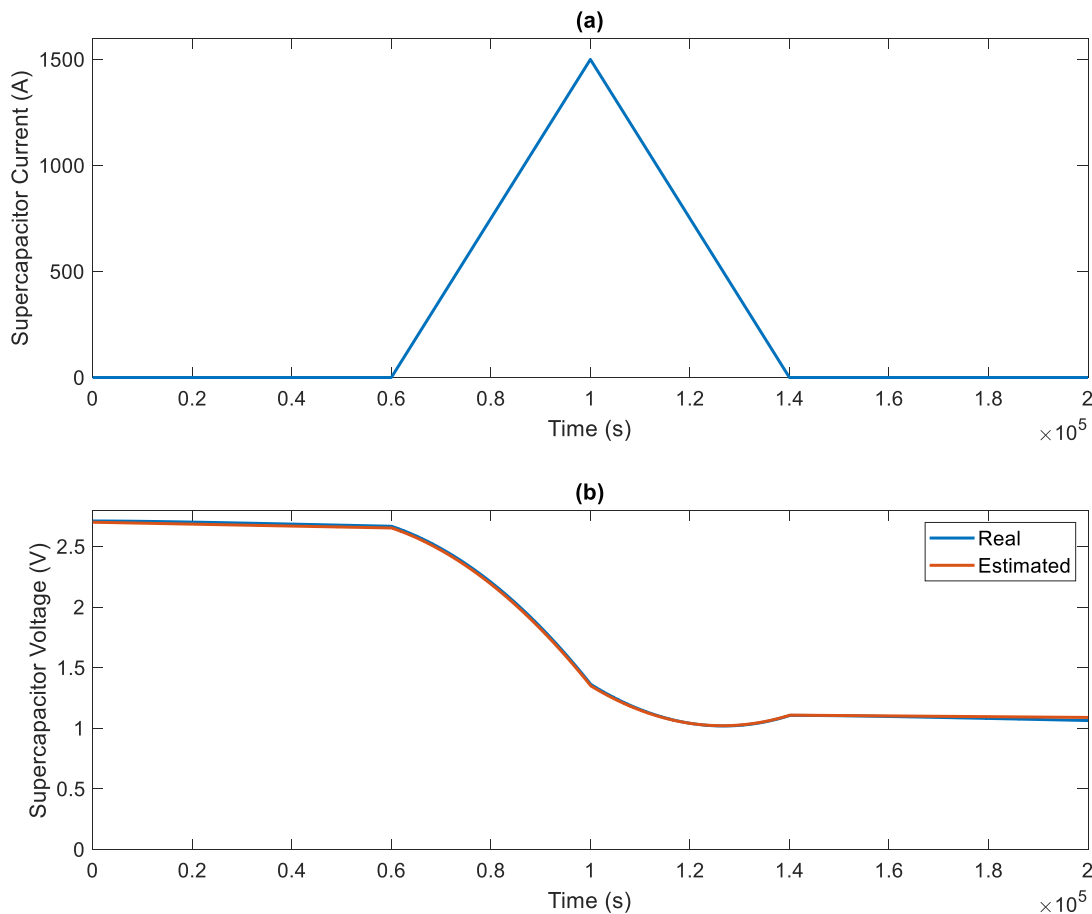


Figure 4. Parameter estimation results, (a) input current of Supercapacitor, (b) output voltage comparison

Different charge and discharge currents were used to validate the equivalent circuit model. The current values given as input to the model created in Figure 4(a) are given. Comparison of actual and model terminal voltage with respect to this given input matched as seen in Figure 4(b).

The mean square error was calculated for the comparison of terminal voltages. The generated supercapacitor model accuracy was verified with a mean square error of 0.0028 in the comparison.

4. Conclusion

In this study, supercapacitor's mathematical model was determined by debye polarization equivalent circuit. The estimation of the model parameters was determined in the MATLAB/Simulink parameter estimation toolbox with a maximum error rate of 0.17%. The accuracy of the model has been proven with a maximum error of 0.28% under different operating currents.

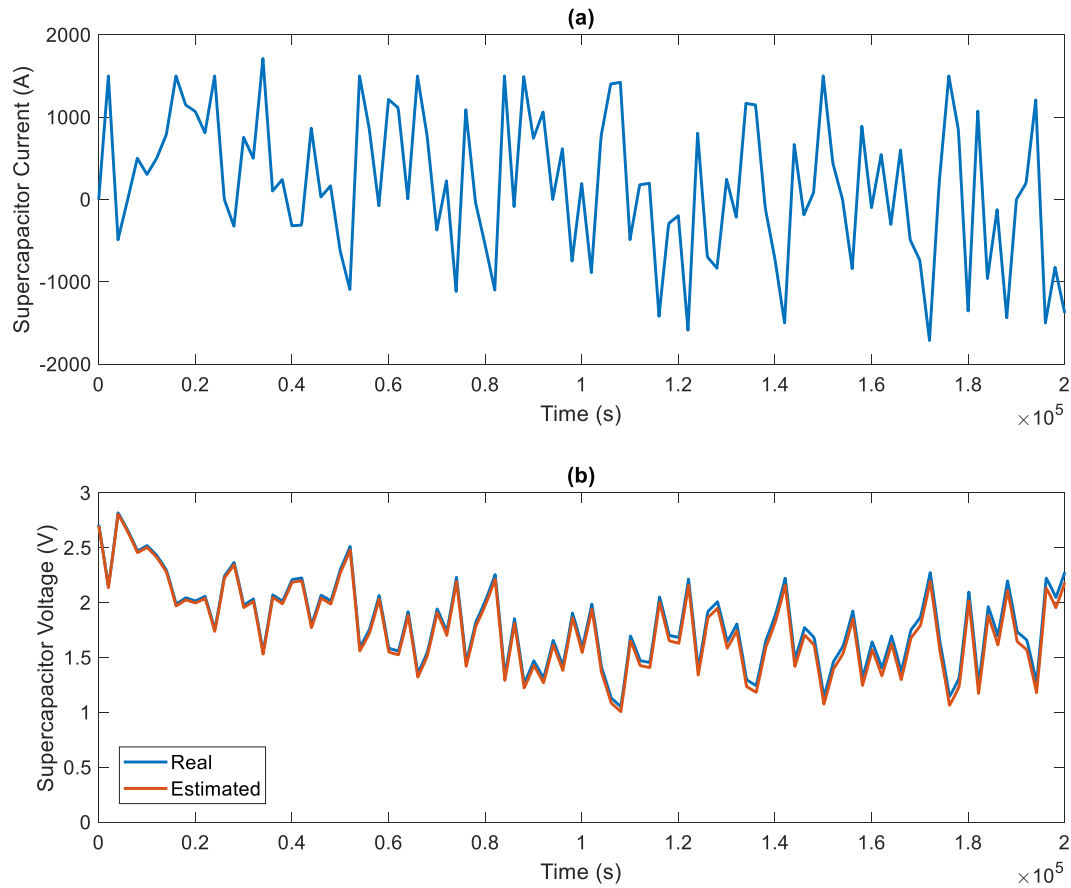


Figure 5. Model validation results, (a) input current of Supercapacitor, (b) output voltage comparison

Acknowledgement

This paper was partly presented in 1st Advanced Engineering Days (AED) held on Thursday, December 23, 2021 in Mersin/Turkey [27].

Funding

This research received no external funding.

Author contributions

Gökhan Yüksek: Writing-Original draft preparation, Methodology. **Yusuf Muratoğlu:** Software, Validation. **Alkan Alkaya:** Investigation, Reviewing and Editing.

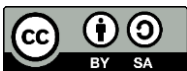
Conflicts of interest

The authors declare no conflicts of interest.

References



1. Aneke, M., & Wang, M. (2016). Energy storage technologies and real life applications–A state of the art review. *Applied Energy*, 179, 350-377.
2. Nair, U. R., & Costa-Castelló, R. (2020). A model predictive control-based energy management scheme for hybrid storage system in islanded microgrids. *IEEE access*, 8, 97809-97822.
3. Blaabjerg, F., Teodorescu, R., Liserre, M., & Timbus, A. V. (2006). Overview of control and grid synchronization for distributed power generation systems. *IEEE Transactions on industrial electronics*, 53(5), 1398-1409.

4. Chong, L. W., Wong, Y. W., Rajkumar, R. K., Rajkumar, R. K., & Isa, D. (2016). Hybrid energy storage systems and control strategies for stand-alone renewable energy power systems, *Renewable and Sustainable Energy Reviews*, Elsevier, 66(C), 174-189.
5. Hemmati, R., & Saboori, H. (2016). Emergence of hybrid energy storage systems in renewable energy and transport applications–A review. *Renewable and Sustainable Energy Reviews*, 65, 11-23.
6. Etxeberria, A., Vechiu, I., Camblong, H., & Vinassa, J. M. (2010, October). Hybrid energy storage systems for renewable energy sources integration in microgrids: A review. In *2010 Conference Proceedings IPEC* (pp. 532-537). IEEE.
7. Zimmermann, T., Keil, P., Hofmann, M., Horsche, M. F., Pichlmaier, S., & Jossen, A. (2016). Review of system topologies for hybrid electrical energy storage systems. *Journal of Energy Storage*, 8, 78-90.
8. Chen, H., Cong, T. N., Yang, W., Tan, C., Li, Y., & Ding, Y. (2009). Progress in electrical energy storage system: A critical review. *Progress in natural science*, 19(3), 291-312.
9. Stippich, A., Van Der Broeck, C. H., Sewergin, A., Wienhausen, A. H., Neubert, M., Schülting, P., ... & De Doncker, R. W. (2017). Key components of modular propulsion systems for next generation electric vehicles. *CPSS Transactions on Power Electronics and Applications*, 2(4), 249-258.
10. Yang, H. (2017). Analysis of supercapacitor charge redistribution through constant power experiments. In *2017 IEEE Power & Energy Society General Meeting* (pp. 1-5). IEEE.
11. Chatzivasileiadi, A., Ampatzi, E., & Knight, I. (2013). Characteristics of electrical energy storage technologies and their applications in buildings. *Renewable and Sustainable Energy Reviews*, 25, 814-830.
12. Zhao, H., Wu, Q., Hu, S., Xu, H., & Rasmussen, C. N. (2015). Review of energy storage system for wind power integration support. *Applied energy*, 137, 545-553.
13. Nikkhoo, M., Farjah, E., & Ghanbari, T. (2016). A simple method for parameters identification of three branches model of supercapacitors. In *2016 24th Iranian Conference on Electrical Engineering (ICEE)* (pp. 1586-1590). IEEE.
14. Martynyuk, V., & Ortigueira, M. (2015). Fractional model of an electrochemical capacitor. *Signal Processing*, 107, 355-360.
15. Xu, J., Mi, C. C., Cao, B., & Cao, J. (2013). A new method to estimate the state of charge of lithium-ion batteries based on the battery impedance model. *Journal of power sources*, 233, 277-284.
16. Soualhi, A., Sari, A., Razik, H., Venet, P., Clerc, G., German, R., ... & Vinassa, J. M. (2013, November). Supercapacitors ageing prediction by neural networks. In *IECON 2013-39th Annual Conference of the IEEE Industrial Electronics Society* (pp. 6812-6818). IEEE.
17. Hu, X., Li, S. E., & Yang, Y. (2015). Advanced machine learning approach for lithium-ion battery state estimation in electric vehicles. *IEEE Transactions on Transportation electrification*, 2(2), 140-149.
18. Hu, X., Li, S., & Peng, H. (2012). A comparative study of equivalent circuit models for Li-ion batteries. *Journal of Power Sources*, 198, 359-367.
19. Kim, S. H., Choi, W., Lee, K. B., & Choi, S. (2011). Advanced dynamic simulation of supercapacitors considering parameter variation and self-discharge. *IEEE Transactions on Power Electronics*, 26(11), 3377-3385.
20. Du, L. (2009, December). Study on supercapacitor equivalent circuit model for power electronics applications. In *2009 2nd International Conference on Power Electronics and Intelligent Transportation System (PEITS)* (Vol. 2, pp. 51-54). IEEE.
21. Ab Rahim, A. H., Ramli, N., Nordin, A. N., Othman, R., Asrar, W., & Sulaeman, E. (2017, November). Classical equivalent circuit characterization for a double-layer capacitor. In *2017 IEEE 4th International Conference on Smart Instrumentation, Measurement and Application (ICSIMA)* (pp. 1-6). IEEE.
22. Nelms, R. M., Cahela, D. R., & Tatarchuk, B. J. (2001). Using a Debye polarization cell to predict double-layer capacitor performance. *IEEE Transactions on Industry Applications*, 37(1), 4-9.
23. Zhang, L., Hu, X., Wang, Z., Sun, F., & Dorrell, D. G. (2018). A review of supercapacitor modeling, estimation, and applications: A control/management perspective. *Renewable and Sustainable Energy Reviews*, 81, 1868-1878.
24. Zou, C., Zhang, L., Hu, X., Wang, Z., Wik, T., & Pecht, M. (2018). A review of fractional-order techniques applied to lithium-ion batteries, lead-acid batteries, and supercapacitors. *Journal of Power Sources*, 390, 286-296.
25. Yang, H. (2018, March). Impact of charge redistribution on delivered energy of supercapacitors with constant power loads. In *2018 IEEE Applied Power Electronics Conference and Exposition (APEC)* (pp. 2686-2690). IEEE.
26. Szewczyk, A., Sikula, J., Sedlakova, V., Majzner, J., Sedlak, P., & Kupařowitz, T. (2016). Voltage dependence of supercapacitor capacitance. *Metrology and Measurement Systems*, 23(3), 403-411
27. Yükses, G., Muratođlu, Y., & Alkaya, A. (2021). Modelling of supercapacitor by using parameter estimation method for energy storage system. *Advanced Engineering Days (AED)*, 1, 29-31.





Geotechnical examination of Ermenek District in the Province of Karaman

Fevzi Sevimli *¹, Isa Kul¹

¹KTO Karatay University, Department of Civil Engineering, Türkiye, fevzisevimli@gmail.com; isa.kul@karatay.edu.tr

Cite this study: Sevimli, F., & Kul, I. (2022). Geotechnical examination of Ermenek District in the Province of Karaman. *Advanced Engineering Science*, 2, 74-79

Keywords

Ermenek
Ground
Carriage
Earthquake
Liquefaction

Research Article

Received: 15.01.2022
Revised: 21.02.2022
Accepted: 27.02.2022
Published: 14.03.2022



Abstract

In recent years, as a result of the increasing interest in construction in our country, the demand for construction areas has also increased. Regarding the buildings we plan to build, we should examine whether the ground being the surface on which the structure will sit or be adjacent, can respond to us positively in terms of strength. As a result, if the soil strength is poor, either the ground must be improved or the property of the structure to be built must be changed. Hence, the building and the ground can not be considered separately. They need to be considered as a whole. In our country, there are not many geotechnical studies which deal with the structure-soil relationship and explain the ground infrastructure of the region, especially in settlements with medium and small populations. Due to this reason, in this study, it is aimed to address the Ermenek district of Karaman from this respect and to eliminate this deficiency of the district. In accordance with this, ground structure of district, various ground survey reports and geophysical reports prepared in recent years were examined. Furthermore, structure class of building planned to be made on that parcel, as well as ground settlement area, number and height of floors, approximate building and foundation loads were calculated with respect to architectural aspects and static and dynamic loads that were formed were brought together and their suitability for the structure, amount of seating that may occur on the ground, and liquefaction situations were examined with respect to bearing capacity of ground. In this way, an infrastructure information bank was created with regards to geotechnical aspects of district.

1. Introduction

Natural disasters occur almost every year in our country and in different parts of the world. These disasters cause situations of loss of life and property. Earthquake, which is one of these disasters, is the most damaging ground movement. About 500,000 earthquakes occur annually in the world whereas 80% of these earthquakes are palpable, and nearly 100 of them are destructive. Unfortunately, earthquakes in urban areas cause physical and socio-economic losses. As an example of this, we are a country that experienced earthquakes in 1999 in Gölçük and Düzce, in 2003 in Bingöl, in 2011 in Van, and in 2020 in Elazığ and İzmir. As a result of these earthquakes, tens of thousands of our citizens lost their lives and were injured, and thousands of families were left homeless and unemployed.

Although it is not possible to prevent the occurrence of earthquakes or to determine when they will occur by using today's technology, it is possible to minimize the damage they will cause. Especially in the settlement areas established on problematic, low-strength floors, the high population increases the danger even more.

Besides, incidents such as "Building-Soil Incompatibility", that is, the construction of a structure on a ground with unsuitable strength for the structure, are often confronted with. This event does not only cause settlement or

swelling in the buildings built over time, but also damages and even collapses the structures situated on the adjacent parcels.

Even though it is not possible to prevent the occurrence of earthquakes or to determine when they will occur with today's technology, it is possible to minimize the damage they will cause, and it is possible to prevent the dangers and damages that will occur by improving the soils with unsuitable strength and by choosing the appropriate construction/manufacturing method.

Ermenek District of Karaman Province, which has been examined regarding this issue, is one of the safest regions in our country in terms of seismicity. No large earthquakes occurred in the mentioned region. Considering the earthquake events of the last 15 years in the region, it is seen that the largest earthquake had a Magnitude of 3. Maybe due to these reasons, no geotechnical studies and investigations covering Ermenek and its surroundings that can be taken as a reference in general terms have been carried out. However, the recent major construction attack in the district, in addition to this, the Ermenek Dam with a crest height of 274 meters that is built on the Ermenek Stream, which passes through the south of the district and feeds the Göksu River, the presence of many regulators on the same brook and the construction of Tekeçatı Regulator on Tekeçatı Stream, which passes through the north of the district constitute the evidence that more interest must be shown on the region with regards to geotechnical aspects.

In the study, geological and geophysical reports previously prepared in province of Ermenek were evaluated, and structures built or planned to be built as per zoning plan were evaluated and required numerical values were calculated and accordingly, bearing capacity of ground, amount of floor seating, liquefaction situation were examined parcel by parcel with certain geotechnical programs. By means of this study, ground status of province has been revealed.

If we would give some other studies similar to this study being conducted as an example;

Alkaya [1] has prepared an excel program to make the preparation of geotechnical reporting in an error-free and fast way. Formulae, tables and figures that were required in this program were revealed in an explanatory manner. In the package programs which are known in the market, either limited calculations are made or the necessary arrangements are not made for the calculation outputs, so a new software has been developed that brings together geotechnical calculations.

Sert et al. [2] mentioned that one of the most important problems of the Sakarya region is the earthquake problem. They emphasized that the North Anatolian Fault Line passes through this region, and large magnetized earthquakes occur in the region for 10–30-year periods. Within scope of their studies, they conducted field and laboratory studies in Arifiye, Geyve and Güneşler locations in the region after the 1999 earthquake. Geotechnical evaluations of the data obtained as a result of these studies were carried out with the help of the Geographical Information System, and the causes of the damage after the earthquake were revealed.

Şahin [3] stated that there are many active fault lines in and around Bursa, where construction is extremely fast. It was stated that the soils in this region were exposed to volumetric changes as a result of earthquake movements. For this reason, he mentioned that if the structure of the soil is suitable, unfortunately, liquefaction may occur in the soils of the region. In the studies he conducted he determined that during the 1999 Kocaeli earthquake, there was liquefaction in fine-grained soils, in addition to sand. He stated that sand, silt, and clay content dominate the region. This situation has added even more importance to his work. In this study, he focused on two parameters for the region and examined the liquefaction potential and bearing capacities of the soils in the general soil evaluation. 140 liquefaction analyzes and 36 carrying capacity calculations were made. As a result of this study, critical values were found in 11 soils. In addition to cohesionless soils, it was observed that the liquefaction potential increased in cohesive soils with low plasticity and low fine grain ratio. It has been determined that soil improvement should be applied in such critical soils.

Kurtulus and Bozkurt [4] conducted geological and geotechnical investigations in the Cayirhan District of Ankara, due to the fact that some lands were opened for construction. In their field work, they had 12 drillings and conducted a SPT experiment at each distance of 1.5 m. UD and Core samples were taken at various depths from the drilling sites. In their studies, they determined the formation of the ground structure, and determined that it consists of vegetative soil in the range of 0.00-1.00 m, followed by silty clay and gravel. No faults were found in the study area. In the laboratory experiments, it was determined that the ground generally has plastic from low to medium value. Geotechnically, it has been determined that the soil has low and medium swelling properties.

Sevimli [5] mentioned in his study that seismic analysis is a field study used in geotechnical earthquake engineering. In his study, he stated that seismic analysis played an important role in the design of many structures. Within the scope of his study, the analysis of seismic movements occurring around the province of Batman from 1900 to the present has been made. The study area covers the region within the circular area with a radius of 100 km from the city center. The study also deals with deterministic and probabilistic methods. Suggestions have been proposed against damages that may occur as a result of seismic movement that can form as the conclusion of his study.

Bayrakçı and Baran [6] examined the geological and geotechnical structure of Osmaniye Province within the scope of their studies. In their study, they have divided the settlement area into regional systems having dimensions of 330 m x 330 m at areas where alluvion unit is observed on geological maps created by MTA and they

divided other observed areas into regional systems having dimensions of 400 m x 400 m. They drilled in the middle of each region. During this work, 15 boreholes were drilled. As a result of the analyzes they made by considering the data of the drilling wells in the regions, different earthquake accelerations and soil elastic spectra were processed on OKM maps.

Ateş et al. [7] revealed the geotechnical properties of the lands by using geological, geophysical and geotechnical methods in order to reveal the soil properties of the lands to be opened for construction in Kaynaşlı District in their study. He has mentioned that Duzce segment being one of the important segments of Kaynasli district Northern Anatolian Faulty zone diving into two branches is within Northern segment zone and that in the district till 1999 earthquake, disordered urbanization took place. Lateral and vertical thickness changes of coarse- and fine-grained alluvial deposition units of approximately 4-12 m thickness of the study area were determined. They drew attention to the fact that the region is close to both the alluvial structure and fault lines. Standard Penetration Test (SPT) and seismic refraction studies were performed at the study sites. They determined the physical-mechanical properties of soil samples with laboratory experiments. Geotechnical map of the region was prepared in line with the obtained geotechnical data.

Tutar [8] wanted to create a data bank for the northeastern region of Şanlıurfa. The geotechnical data of the field were digitized and collected in an environment. 30 ground survey reports have been digitized and the data obtained has been converted into a data bank with Delphi 7 programming language. As a result, he made necessary comments for the study area.

Özaydın and Anlı [9] discussed the geological and geotechnical structure of the south of the Bosphorus and the Golden Horn. They have determined that young tectonic movements are effective in the region and that it has undergone significant morphological changes. They suggested that young sediments were formed in the region as a result of this change, and that these sediments were intertwined laterally and vertically. They mentioned that the movement caused two important topographical irregularities in the offshores of Karaköy and Sarayburnu, and that the sudden change in elevation caused by the fault offshore of Karaköy occurred, and that this fault gradually turned the Golden Horn into a hanging valley with the faults passing near Sarayburnu. They suggested that this caused the young sediments in the Golden Horn to be located deeper in the south of the Bosphorus. In this way, they produced a geotechnical map of the region.

Akdeniz et al. [10] stated that it is a study conducted for the purpose of ground survey and geotechnical survey, determination of the engineering properties of the ground, determination of the groundwater level, and evaluation of the structure to be built on the ground, both with the building ground and the surrounding structures. They mentioned that these surveys were determinant in deciding whether there is need for improvement or not at the ground where structure was based. They said that the survey work will be done in two branches as field and laboratory work. As a matter of fact, in line with these studies, 885 soil survey reports made in Eskişehir from 10 August 2005 until now were handled according to the "Soil and Foundation Study General Format" published by the Ministry of Public Works and Settlement on 10 August 2005. They revealed a general soil structure of the region.

Akyol et al. [11] revealed the effect of geotechnical and some seismic parameters of soils on construction in an area where business and residential buildings are concentrated in Denizli city center. During the study, they have used seismic breakage data of SPT value obtained from geological reports relating with the region. They revealed that the dynamic and geotechnical parameter values are low in the central parts and north of Denizli region, while they are higher in other regions. They have seen that the most common ground period distribution coincides with the 4-7 storey building period when they are based on the period depending on the number of floors in standard reinforced concrete structures. With this result, they revealed that most of the structures in the study area will resonate with the ground in a possible earthquake. As a result, they state that the period values of the ground and the structure should be made suitable for earthquake resistant structure design.

Similar studies have been carried out for different places such as.

As a result of this study, it is aimed to examine whether the structures suitable for the ground are built in this district, where almost no geotechnical studies have been carried out, whether any Soil Improvement is needed for the ground of the structures to be built, and to shed light on the future studies.

2. Material and Method

If we would mention about the district being examined, Ermenek District is located in Karaman province and it is 67 kilometers southeast of Karaman. There is Mut district in the east of the district, Anamur in the south and Balkusan Village in the west, 15.75 km north of the Antalya provincial border. While the land structure of the district varies from north to south, that is, from Tekeçatı Region to Ermenek Dam, between an altitude of 1400 and 700, there is no great difference in elevation from east to west. Geologically, the region is a structure that generally contains limestone, clay, marl, fossiliferous sandstone and even coal. At a distance of 40 km from the district, there are many small faults that are distributed within a zone of 17 km length and 3 km width. This region is named as Mut Fault Zone. The researchers state that the fault is strike-slip with vertical component and possibly alive due to the river valleys and parallel ridges following the faults.

The study was started by obtaining the Geological and Geophysical Report, which was prepared as a result of the Field and Laboratory Test results obtained from the Ermenek Municipality, from more than 40 parcels and more than 100 boreholes built by both state institutions and private companies, and by examining these reports in detail.

Experiments and results of the Geological Surveys on the land, the results of the laboratory experiments made on the samples taken, as well as the results obtained as a result of the Geophysical Surveys and seismic refraction tests carried out on the same plot, were presented in plots. Then, all data were transferred to a Geotechnical Analysis program known as Geotransportation, again separately. In the meantime, the building classes, number of floors, residence areas, estimated foundation models, foundation depths, Groundwater Levels and total building load of the structures built or planned to be built on the parcels were calculated and processed in the same analysis program. As seen below, 5 parcels selected from different regions and neighborhoods are presented in Tables 1-3.

Table 1. The working numbers of the examined parcels and underground water level

Work Number	Quarter	Plot	Parcel	Underground Water Level
1	Seyran	112	33	None
2	Taşbaşı	761	5	None
3	Meydan	460	36	None
4	Güllük	701	1	None
5	Değirmenlik	174	36	-3,00m

Table 2. Earthquake data of the examined parcels

Work Number	Vp Speed	Vs Speed	Vs30 Speed	To	Ss-Fs SDS	S1-F1 SD1	PGA PGV	TA-TB TL	TAD-TBD TLD
1	483	274	564	0,24	0,280-1,30	0,076-1,50	0,127	0,063-0,313	0,021-0,104
	2495	809			0,364	0,114	6,142	6,000	3,000
2	316	192	434	0,30	0,283-1,30	0,076-1,50	0,128	0,062-0,310	0,021-0,103
	1172	723			0,368	0,114	6,179	6,000	3,000
3	719	440	558	0,38	0,286-1,30	0,077-1,50	0,130	0,062-0,311	0,021-0,104
	1190	568			0,372	0,116	6,223	6,000	3,000
4	556	223	401	0,38	0,282-1,30	0,076-1,50	0,128	0,062-0,311	0,021-0,104
	1228	558			0,367	0,114	6,173	6,000	3,000
5	616	223	334	0,59	0,282-1,57	0,076-2,40	0,128	0,0082-0,411	0,027-0,137
	884	354			0,444	0,182	6,167	6,000	3,000

Table 3. Data on the buildings to be built on the examined parcels

Work Number	BF	BS (I)	EN	BHC	Bulding Foundation Depth (m)	Bulding Foundation Type	Bulding Foundation Area (m ²)	Bulding Total Weight (kN)
1	1	1,5	3a	6	-2,00	Raft	1097	104586
2	1	1,5	3a	6	-5,30	Raft	2950	103826
3	3	1	3a	5	-2,00	Continuous	175	34030
4	3	1	3a	6	-3,50	Continuous	1580	32282
5	3	1	3a	5	-2,00	Raft	280	29049

3. Geotechnical Analysis Results

After all the data were entered into the Geotransport Soil Analysis Program separately, the Controls for the Transport Forces, Settlement Amounts and Soil Liquefaction of all processed parcels were made as a result. Here again, the results of the 5 plots I mentioned above are presented in Tables 4-6.

Table 4. Analysis results of geotechnical bearing capacity of inspected parcels

Work Number	Bearing capacity analysis as per TBDY	Results
1	238,578>166	Sufficient
2	1252,286>200	Sufficient
3	2005,714>184	Sufficient
4	788,67>302	Sufficient
5	2331,429>151	Sufficient

Table 5. Analysis results Geotechnically Elastic fit amount and Consolidated fit amount of inspected parcels

Work Number	Elastic fit amount	Results	Consolidated fit amount and Results	Results
1	E.F.A. s=0,010m	Suitable	C.F.A. s=0,088m	Suitable
2	E.F.A. s=0,063m	Suitable	C.F.A. s=0,027m	Suitable
3	E.F.A. s=0,000m	Suitable	C.F.A. s=0,007m	Suitable
4	E.F.A. s=0,000m	Suitable	C.F.A. s=0,001m	Suitable
5	E.F.A. s=0,003m	Suitable	C.F.A. s=0,004m	Suitable

Table 6. Liquefaction Analysis results of inspected parcels

Work number	Liquefaction Analysis	
	Layer 1	Layer 2
1	Layer 1: 4,49>1,1 Suitable	Layer 2: 3,177>1,1 Suitable
2	Layer 1: 0,335<1,1 Suitable (Layer is above UWL)	Layer 2: 2,799>1,1 Suitable
3	Layer 1: 0,331<1,1 Suitable (Layer is above UWL)	Layer 2: 2,769>1,1 Suitable
4	Layer 1: 4,459>1,1 Suitable	Layer 2: 4,49>1,1 Suitable
5	Layer 1: 0,278<1,1 Suitable (Layer is above UWL)	Layer 2: 1,441>1,1 Suitable

4. Conclusion and Suggestions

The soil class determined in the district is mainly ZC class and has a structure mainly composed of limestones. In the analysis made in the examined parcels, it was seen that it has sufficient and suitable properties in terms of Bearing Power, Elastic and Consolidated Settlement Amounts and Liquefaction potential. It has been concluded that there is no need for any ground improvement for these structures planned to be built on the said parcels. In addition, the results of these geotechnical analyzes in higher building loads and multi-storey structures, can be examined and even examination can be made about how far the endpoints can be.

Acknowledgement

The authors thank KTO Karatay University. This study was partly presented in 1st Advanced Engineering Days [12].

Funding

This research received no external funding.

Author contributions

Fevzi Sevimli: Conceptualization, Methodology, Data supply, Writing-Original draft preparation, **İsa Kul:** Writing-Reviewing and Editing.

Conflicts of interest

The authors declare no conflicts of interest.

References

1. Alkaya, D., & Yeşil, B. (2010). Creating Standard Solutions Using Spreadsheet (Ms Excel) Program for Geotechnical Report Preparation. Academic Informatics. Academic Conference Proceedings. Mugla, Turkey.
2. Sert, S., Özocak, A., Arel, E., & Bol, E. (2005). The Effect of Local Soil Properties on Damage Size in Sakarya Region, Arifiye-Geyve-Güneşler Example. Earthquake Symposium. Kocaeli, Turkey
3. Şahin, H. C. (2020). Geotechnical evaluation of Bursa Özlüce Region. Master Thesis, Bursa Uludag University, Institute of Science and Technology, Bursa.
4. Kurtuluş, C., & Bozkurt, A., (2009). Investigation of Soil Properties of Çayırhan District, Ankara, Using Geophysical and Geotechnical Methods. Journal of Applied Earth Sciences, 8(2), 15-27.
5. Sevimli, S. (2019). Evaluation of Batman and its surroundings in terms of geotechnical earthquake engineering. Master Thesis, Batman University Institute of Science and Technology, Batman.

6. Bayrakcı, S., & Baran, T. (2018, October). Evaluation of microzonation maps of Osmaniye city center (OKM) based on geotechnical features. Proceedings of the 3rd International Mediterranean Science and Engineering Congress (IMSEC-2018). In the paper (p. 98-104).
7. Ateş, A., Green, B., & Toprak, B. (2014). Investigation of geotechnical properties of the soils of Kaynaşlı (Düzce) TOKİ settlement area with geophysical and geotechnical methods. *Balıkesir University Journal of Science Institute*, 16(1), 1-13.
8. Tutar, H. (2008). Establishment of a geotechnical data bank of the north east region of Şanlıurfa city center. Doctoral Thesis, Harran University, Institute of Science and Technology, Şanlıurfa.
9. Özaydın, K., & Anlı, A. (1992). Geological Structure and Geotechnical Features of the South of the Bosphorus and the Golden Horn. *Geological Engineering* (4) 5-14.
10. Akdeniz, E., Mutlu, S., Güney, Y., & Özdemir, V. (2012). Evaluation of the Compliance of Soil Survey Reports with the Principles: Example of Eskişehir. *Electronic Journal of Construction Technologies / Electronic Journal of Construction Technologies*, 8(2).
11. Akyol, E., Aydın, A., Alkan, M., & Hazer, G. (2014). The Effects of Seismic and Geotechnical Parameters on Construction: Example of Denizli. *Adıyaman University Journal of Educational Sciences* 4(1), 36-46.
12. Sevimli, F., & Kul, İ. (2021). Geotechnical examination of Ermenek District in the province of Karaman. *Advanced Engineering Days (AED)*, 1, 1-3.



© Author(s) 2022. This work is distributed under <https://creativecommons.org/licenses/by-sa/4.0/>



Comparison of infill wall effects in reinforced-concrete frames over different parameters

Ercan Işık¹, Mehmet Cihan Aydın¹, Ali Emre Ulu*¹

¹ Bitlis Eren University, Department of Civil Engineering, Türkiye, eisik@beu.edu.tr; mcaaydin@gmail.com; aliemreulu@gmail.com

Cite this study: Işık, E., Aydın, M. C., & Ulu, A. E. (2022). Comparison of infill wall effects in reinforced-concrete frames over different parameters. *Advanced Engineering Science*, 2, 80-86

Keywords

Infill
Limit state
RC
Eigen value
Pushover

Research Article

Received: 16.01.2022

Revised: 22.02.2022

Accepted: 28.02.2022

Published: 14.03.2022



Abstract

Infill walls are widely used in reinforced-concrete structures and their contribution to the reinforced-concrete frame can be neglected. The amount of infill wall effect was investigated for a reinforced-concrete frame which has three different openings in this study. For this purpose, five different structural models have been created such as completely filled, gap in the corner, double gap and completely bare on the ground floor. Structural analyses were performed in Seismostruct software by using pushover and eigen value analyses for each structural model, respectively. Only the absence of infill wall was selected as a variable. The limit state of three different damages for performance level, period, base shear force, elastic and effective section stiffness's were obtained separately for each structural model. The study revealed once again that the amount of infill wall contributes significantly to the seismic capacity of the building. Considering the contributions of infill walls will make the structural results much more realistic.

1. Introduction

Infill walls are widely used in buildings to fill frame gaps or to separate residences [1,2]. In the current design of such structures, in most cases only the weight of the infill walls is taken into account and other strength parameters are ignored. The structural behavior of such frames is highly dependent on the dynamic properties of the respective laterally and vertically loaded infill walls, such as stiffness, bearing capacity, period and damping level [3-6]. In-plane and out-of-plane damages are common in reinforced concrete structures after earthquakes [7-13]. For these reasons, the infill wall effect is a subject worth examining.

It has been determined by experimental studies that the values obtained as a result of the calculations will not reflect the truth in cases where the infill walls are not placed appropriately and consciously and are not taken into account [14]. In the literature, the effect of the infill wall was investigated on different parameters by both experimental and numerical modeling. The capacity curves of infill walls, story horizontal displacements, relative displacements, maximum plastic rotations in stories and the distribution of plasticized sections in the system in regular reinforced-concrete structures were compared by Korkmaz and Uçar [15]. In the study conducted by Akyürek et al. [16], the effects of the infill wall change on the capacity curve of the building, the first natural period, the target target displacements, the damage distribution of the first story columns, and the building performance level in residential type reinforced-concrete buildings with different openings and number of stories were investigated. In the study conducted by Tekin et al. [17], the strengths of the filled and unfilled four-storey three-span planar reinforced-concrete frames were compared with the capacity curves. In the study conducted by Sivri [18], a reinforced concrete structure with different infill wall placements was taken into consideration and the results were compared in order to examine the effect of infill walls and wall layout on the building behavior. In a

study by Paripour et al. [19] investigated the effect of infill walls on the risk of progressive collapse in reinforced-concrete (RC) frames. Layadi et al. [20] investigated the infill wall effect experimentally in their study. In this and similar studies, the positive contributions of the infill walls used in reinforced concrete structures to the earthquake behavior of the building have been revealed.

Within the scope of this study, the infill wall effect for a reinforced-concrete frame consisting of three different openings was tried to be revealed by static pushover and eigenvalue analysis on five different structural models. For each structural model, period, seismic capacity, elastic stiffness value and target displacement values for structural performance were obtained separately. Suggestions were made by comparing the results obtained with the study.

2. Material and Method

Within the scope of the study, eigenvalue and static pushover analyzes were performed for the reinforced concrete frame consisting of three different spans. Model analysis is a dynamic analysis method that enables the determination of free vibration periods, frequency values, mass participation rates and mode shapes of the structure [21]. Another method used in generating performance estimates is pushover analysis. This method is a practical way of demonstrating the behavior of a building in the inelastic region. This type of analysis gives the base shear force and the peak displacement capacity curve of the building. To obtain this curve, the lateral forces are monolithically increased until the displacement of the top of the building reaches a predetermined value [22-26]. To obtain the pushover curve, it is necessary to geometrically combine the intersection points on an interaction diagram of the roof displacement values corresponding to the base shear forces under the applied load, raising the structure from zero to unstable. The limit states given in the worldwide used damage estimation Eurocode-8 (Seciton 3) are taken into account in the structural analysis [27,28]. Three different cases are specified for damage cases in the software. These states are considered near collapse (NC), significant damage (SD), and damage limitation (DL). These cases are calculated for all structural models.

Table 1. Limit states in Eurocode 8 (Part 3) [27,28].

Limit State	Description	Return Period (year)	Probability of exceedance (in 50 years)
Limit state of damage limitation (DL)	Only lightly damaged, damage to non-structural components economically repairable	225	0.20
Limit state of significant damage (SD)	Significantly damaged, some residual strength and stiffness, non-structural components damaged, uneconomic to repair	475	0.10
Limit state of near collapse (NC)	Heavily damaged, very low residual strength & stiffness, large permanent drift but still standing	2475	0.02

The behavior of building materials under loads can be determined by using some mathematical models that have an important place in building design and evaluation [29]. For the concrete and steel material, the nonlinear concrete model [30] and steel model [31] were used. The stress-strain relationship of these material models is shown in Figure 1.

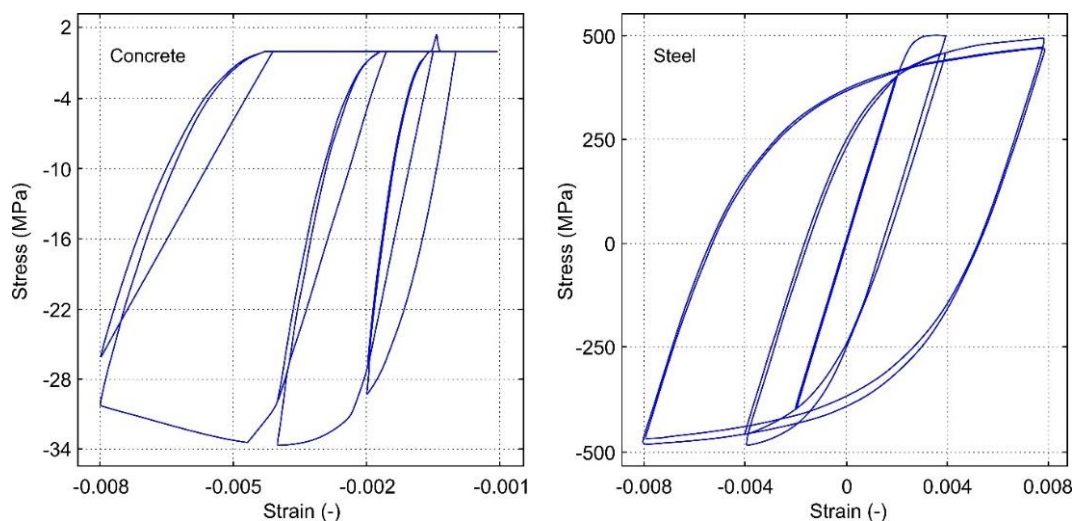


Figure 1. Material models for concrete and steel considered in this study [32]

The story heights were chosen as 2.7 m, being equal to each other. The reference structure model is shown in Figure 2.

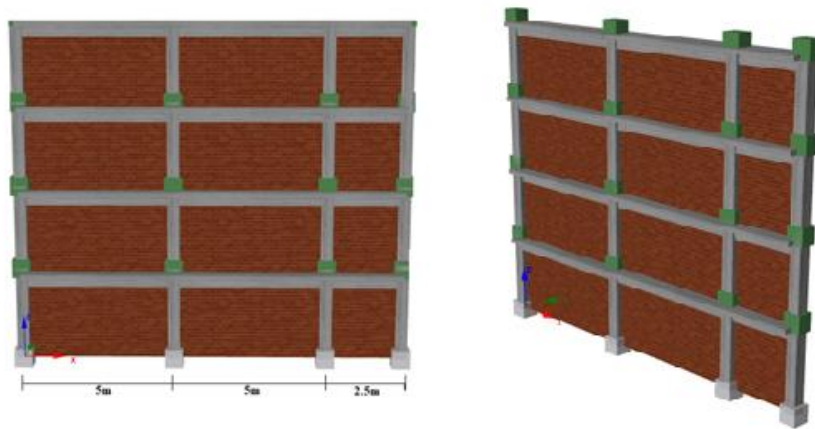


Figure 2. Structural models of the reference building model considered in the study.

The load cases applied in all structural models considered within the scope of this study are shown in Figure 3.

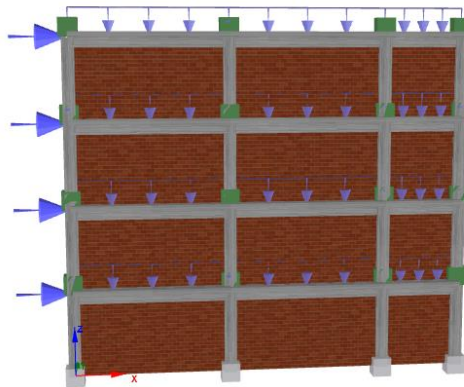


Figure 3. Applied loads

Within the scope of this study, the columns and beams used in the reinforced-concrete frame were created by using the same size and material in all structural models. C25-S420 was taken into consideration for all RC buildings model. In order to reveal the infill wall effect more clearly, no changes were made to these load-bearing elements. The cross-sections of the beams and columns used are given in Figure 4. While the columns were chosen as 40*40 cm, the beams were taken into account as 25*50 cm.

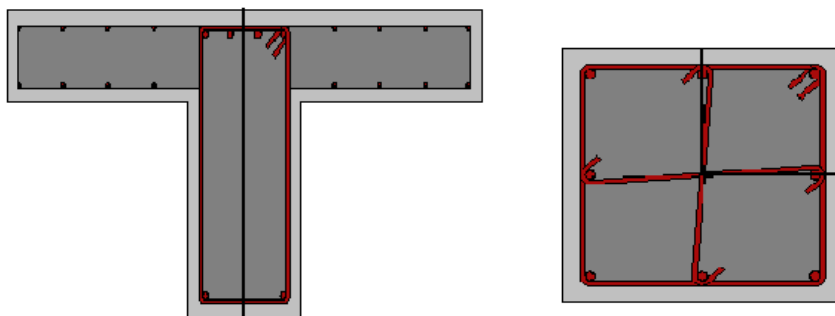


Figure 4. Cross-sections of columns and beams used in the RC frame

Other structural models considered in the study are shown in Figure 5. The reference building was rated as Model 1. The target displacement was chosen as 0.10 m in order to make comparisons in all structural models.

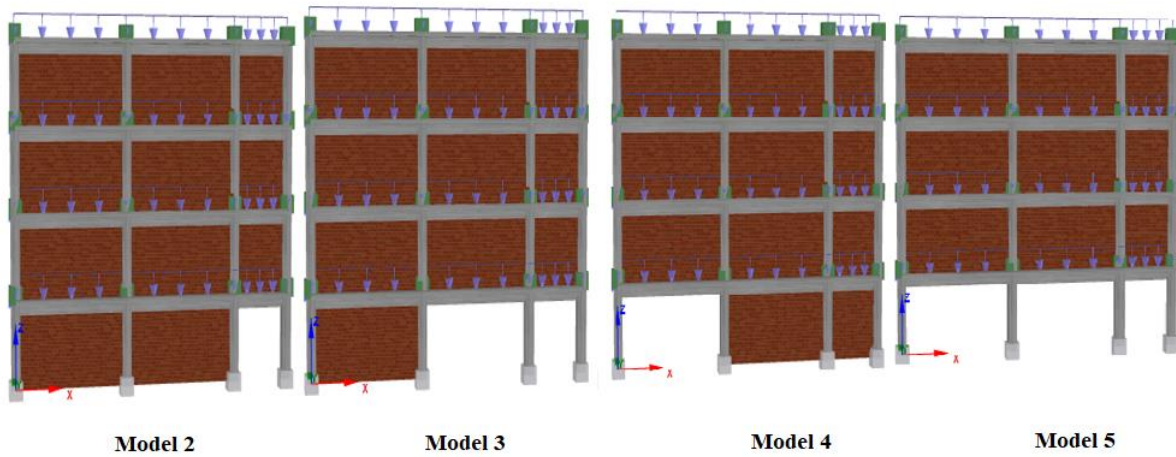


Figure 5. Structural models obtained for the infill wall effect

Within the scope of the study, only the changes of the infill walls on the ground floor were examined. Structural models were created in this context are shown in [Table 2](#).

Table 2. Structural models

Model No	Description
Model 1	Completely filled
Model 2	One gap in the corner
Model 3	Double gap in the left corner
Model 4	Double gap in the right corner
Model 5	Completely bare (No infill)

While making earthquake resistant design and performance evaluation, the natural vibration period of the buildings is an important parameter. The equivalent seismic lateral force is determined using the static design method from a design spectrum that is a function of the fundamental vibration period of a building [33,34]. By using eigenvalue analysis, fundamental natural periods can be obtained. The results were shown in [Table 3](#).

Table 3. The natural periods for structural models

Model	Model 1	Model 2	Model 3	Model 4	Model 5
1	0.199634	0.208785	0.225426	0.228301	0.308856
2	0.069151	0.071214	0.074129	0.074455	0.08129
3	0.06244	0.062441	0.062452	0.062463	0.062476
4	0.05144	0.051469	0.051482	0.051442	0.051485
5	0.047596	0.047619	0.047668	0.047647	0.047815
6	0.044667	0.045209	0.045829	0.045872	0.046776
7	0.036328	0.036436	0.036547	0.036534	0.036694
8	0.033518	0.033533	0.033536	0.033521	0.033539
9	0.022823	0.022823	0.022827	0.02283	0.022834
10	0.022244	0.022293	0.022336	0.022369	0.022555

The stiffness values of reinforced concrete elements differ from the stiffness values estimated under the effect of earthquakes. Therefore, effective cross-sectional stiffness values are used when designing and analyzing such structural elements. In order to determine the performance of reinforced concrete structural systems under earthquake loads, the stiffness of the cracked sections is taken into account. The effective stiffness value of the cracked sections is obtained using the stiffness reduction coefficients predicted from the elastic stiffness value [35-37]. The elastic stiffness (K_{elas}) and effective stiffness (K_{eff}) values for the structural models are directly obtained using the stiffness reduction coefficients estimated in the algorithm. All results were shown in [Figure 3](#).

Table 4. Comparison of values obtained values

Model	Base Shear (kN)	Kelas (kN/m)	Keff (kN/m)	DL (m)	SD (m)	NC (m)
Model 1	913.61	193954.2	130170.6	0.003017	0.00387	0.009665
Model 2	881.71	173653.5	117333.4	0.003435	0.004406	0.010996
Model 3	554.87	145838.0	88925.6	0.004605	0.007061	0.015233
Model 4	524.43	143538.4	87404.39	0.007618	0.01079	0.021345
Model 5	396.36	62842.24	44267.62	0.014845	0.019238	0.033857

3. Results and Discussion

In most cases, only the weight of the infill walls is taken into account and other strength parameters are ignored. In the scope of this study, the effect of infill wall for reinforced concrete structures was investigated. Eigenvalue and static pushover analyze were performed for five different structural models. The lowest period was obtained in Model 1, where the reinforced-concrete frame was completely infilled, while the highest period was obtained for the ground story without a completely infilled wall. As the amount of infill wall decreased, the period value became higher. The results obtained for Model 2 and Model 4 show that the period value increases as the infill wall opening increases. The seismic capacities obtained for the reinforced-concrete frame were obtained in full compliance with these values. In the case of a full infill wall, the seismic capacity increased by 2.3 times compared to the case of no infill wall. The seismic capacity decreased as the opening increased in the sections without infill walls. The lowest seismic capacity was obtained for the fully hollow frame model. Completely similar results were obtained for elastic and effective stiffness values. The presence and length of infill walls directly affect these values. With the study, target displacement values were also obtained for the expected performance levels from the building. While the smallest values were obtained for Model 1 with a fully infill wall, the largest values were obtained for Model 5, which is a fully hollow model.

All the result values obtained were fully compatible with each other. The results showed once again that infill walls make very important contributions to the seismic behavior of reinforced concrete frames. Therefore, it is clear that considering the effect of infill walls in the calculations will allow the structural analyzes to be more realistic. In future studies, the type of infill wall material, the use of infill walls with different openings and heights, or the examination of the effects of door and window gaps will also be beneficial.

Acknowledgement

This paper was partly presented in 1st Advanced Engineering Days (AED) held on Thursday, December 23, 2021 in Mersin/Turkey [38].

Funding

This research received no external funding.

Author contributions

Ercan Işık: Conceptualization, Methodology, Software **Mehmet Cihan Aydın:** Data curation, Writing-Original draft preparation, Validation. **Ali Emre Ulu:** Visualization, Investigation, Writing-Reviewing and Editing.

Conflicts of interest

The authors declare no conflicts of interest.

References

- Gazić, G., & Sigmund, V. (2016). Cyclic testing of single-span weak frames with masonry infill. *Grđevinar*, 68(08), 617-633.
- Timurağaoğlu, M. Ö., Doğangün, A., & Livaoğlu, R. (2019). Comparison and assessment of material models for simulation of infilled RC frames under lateral loads. *Grđevinar*, 71(01.), 45-56.
- Hak, S., Morandi, P., & Magenes, G. (2013). Evaluation of infill strut properties based on in-plane cyclic tests. *Grđevinar*, 65(6), 509-521.
- Pul, S., & Arslan, M. E. (2019). Cyclic behaviors of different type of hollow brick infill walls: A hinged rigid frame approach. *Construction and Building Materials*, 211, 899-908.
- Choi, S. W., Park, S. W., & Park, H. S. (2017). Multi-objective design model for retrofit of reinforced concrete frames with infilled walls using FRP bracings. *Construction and Building Materials*, 140, 454-467.

6. Ozkaynak, H., Yuksel, E., Yalcin, C., Dindar, A. A., & Buyukozturk, O. (2014). Masonry infill walls in reinforced concrete frames as a source of structural damping. *Earthquake Engineering & Structural Dynamics*, 43(7), 949-968.
7. Isik, E., Aydin, M. C., & Buyuksarac, A. (2020). 24 January 2020 Sivrice (Elazığ) earthquake damages and determination of earthquake parameters in the region. *Earthquakes and Structures*, 19(2), 145-156.
8. Latifi, R., & Hadzima-Nyarko, M. (2021). A comparison of structural analyses procedures for earthquake-resistant design of buildings. *Earthquakes and Structures*, 20(5), 531-542.
9. Hadzima-Nyarko, M., Ademović, N., & Krajnović, M. (2021, December). Architectural characteristics and determination of load-bearing capacity as a key indicator for a strengthening of the primary school buildings: Case study Osijek. In *Structures* (Vol. 34, pp. 3996-4011). Elsevier.
10. Tabrizikahou, A., Hadzima-Nyarko, M., Kuczma, M., & Lozančić, S. (2021). Application of shape memory alloys in retrofitting of masonry and heritage structures based on their vulnerability revealed in the Bam 2003 earthquake. *Materials*, 14(16), 4480.
11. Kaplan, H., Bilgin, H., Yilmaz, S., Binici, H., & Öztas, A. (2010). Structural damages of L'Aquila (Italy) earthquake. *Natural Hazards and Earth System Sciences*, 10(3), 499-507.
12. Işık, E. (2014). The effects of 23.10. 2011 Van earthquake on near-field and damaged on structures. *International Anatolia Academic Online Journal, Scientific Science*, 2(2), 10-25.
13. Bilgin, H., Shkodrani, N., Hysenlliu, M., Ozmen, H. B., Isik, E., & Harirchian, E. (2022). Damage and performance evaluation of masonry buildings constructed in 1970s during the 2019 Albania earthquakes. *Engineering Failure Analysis*, 131, 105824.
14. Kaplan, S.A. (2008). Dolgu Duvarların Betonarme Taşıyıcı Sistem Performansına Etkisi. *TMH*, 452, 49-62.
15. Korkmaz, A. & Uçar, T., (2006). Betonarme Binaların Deprem Davranışında Dolgu Duvar Etkisinin İncelenmesi. *Dokuz Eylül Üniversitesi Mühendislik Fakültesi Fen ve Mühendislik Dergisi*, 8(1), 101-108.
16. Akyürek, O., Tekeli, H., & Demir, F. (2018). Plandaki dolgu duvar yerleşiminin bina performansı üzerindeki etkisi. *International Journal of Engineering Research and Development*, 10(1), 42-55.
17. Tekin, M., Alsancak, E., & Murat, A. Y. (2007). Betonarme çerçevelerde dolgu duvar etkisinin incelenmesi. *Celal Bayar University Journal of Science*, 3(1), 95-104.
18. Sivri, M., Demir, F., & Kuyucular, A. (2006). Dolgu duvarlarının çerçeve yapının deprem davranışına ve göçme mekanizmasına etkisi. *Süleyman Demirel Üniversitesi Fen Bilimleri Enstitüsü Dergisi*, 10(1).
19. Paripour, M. B., Budak, A., & Düzgün, O. A. (2021). A Parametric Study on Progressive Collapse in Reinforced Concrete Frames with Infill Walls. *Journal of Failure Analysis and Prevention*, 1-14.
20. Layadi, I., Messabhia, A., Plassiard, J. P., & Olivier, P. L. E. (2020). The effect of masonry infill walls on the reinforced concrete frames behavior under lateral load. *Journal of Materials and Engineering Structures JMES*, 7(1), 125-140.
21. Mutlu Ö., & Şahin A. (2016). Investigating the Effect of Modeling Approaches on Earthquake Behavior of Historical Masonry Minarets-Bursa Grand Mosque Case Study, *Sigma*, 7 (2), 123-136.
22. Inel, M., & Ozmen, H. B. (2006). Effects of plastic hinge properties in nonlinear analysis of reinforced concrete buildings, *Engineering Structures*, 28(11), 1494-1502.
23. Chopra, A. K., & Goel, R. K. (2002). A modal pushover analysis procedure for estimating seismic demands for buildings, *Earthquake Engineering and Structural Dynamics*, 31(3), 561-582.
24. Fajfar, P. (1999). Capacity spectrum method based on inelastic demand spectra, *Earthquake Engineering and Structural Dynamics*, 28(9), 979-993.
25. Korini, O., & Bilgin, H. (2013, July). A new modeling approach in the pushover analysis of masonry structures. *International Student Conference of Civil Engineering*.
26. Ademovic, N., Hrasnica, M., & Oliveira, D. V. (2013). Pushover analysis and failure pattern of a typical masonry residential building in Bosnia and Herzegovina. *Engineering Structures*, 50, 13-29.
27. EN 1998-3, (2005). Eurocode-8: Design of Structures for Earthquake Resistance-Part 3: Assessment and Retrofitting of Buildings; European Committee for Standardization: Bruxelles, Belgium.
28. Pinto, P. E., & Franchin, P. (2011). Eurocode 8-Part 3: assessment and retrofitting of buildings. In: *Proceedings of the Eurocode 8 Background and Applications, Dissemination of Information for Training*, Lisbon, Portugal.
29. Işık, E., Özdemir, M., Karaşin, İ. B., & Karaşin, A. (2019). Betonarme yapılarda kullanılan malzeme modellerinin karşılaştırılması. *Bitlis Eren Üniversitesi Fen Bilimleri Dergisi*, 8 (3), 968-984.
30. Mander, J. B., Priestley, M. J., & Park, R. (1988). Theoretical stress-strain model for confined concrete. *Journal of Structural Engineering*, 114(8), 1804-1826.
31. Menegotto, M., & Pinto, P. E. (1973). Method of analysis for cyclically loaded RC plane frames including changes in geometry and non-elastic behavior of elements under combined normal force and bending. Symposium on the resistance and ultimate deformability of structures acted on by well-defined repeated loads. In *International Association for Bridge and Structural Engineering*, Zurich, Switzerland, 15-22.
32. Antoniou, S., & Pinho, R. (2003). Seismostruct-seismic analysis program by Seissoft. *Technical Manual and User Manual*.

33. Aksoylu, C., & Arslan, M. H. (2019). Çerçeve türü betonarme binaların periyod hesaplarının farklı ampirik bağıntılara göre irdelenmesi. *Bitlis Eren Üniversitesi Fen Bilimleri Dergisi*, 8(2), 569-581.
34. Kutanis, M., Boru, E. O., & Işık, E. (2017). Alternative instrumentation schemes for the structural identification of the reinforced concrete field test structure by ambient vibration measurements. *KSCE Journal of Civil Engineering*, 21(5), 1793-1801.
35. Caglar, N., Demir, A., Ozturk, H., & Akkaya, A. A. (2015). Simple formulation for effective flexural stiffness of circular reinforced concrete columns. *Engineering Applications of Artificial Intelligence*, 38, 79-87.
36. Wilding, B.V., & Beyer, K. (2018). The effective stiffness of modern unreinforced masonry walls. *Earthquake Engineering & Structural Dynamics*, 47(8), 1683-1705.
37. Ugalde, D., Lopez-Garcia, D., & Parra, P. F. (2020). Fragility-based analysis of the influence of effective stiffness of reinforced concrete members in shear wall buildings. *Bulletin of Earthquake Engineering*, 18(5), 2061-2082.
38. Işık, E., Aydın, M. C., & Ulu, A. E. (2021). Effect of infill walls on limit states in reinforced-concrete frames. *Advanced Engineering Days (AED)*, 1, 35-37.



© Author(s) 2022. This work is distributed under <https://creativecommons.org/licenses/by-sa/4.0/>



Evaluation of the soil conditions in Alikahya Region (Izmit)

Talas Fikret Kurnaz*¹ 

¹Mersin University, Department of Transportation Services, Türkiye, fkurnaz@mersin.edu.tr

Cite this study: Kurnaz, T. F. (2022). Evaluation of the soil conditions in Alikahya Region (İzmit). Advanced Engineering Science, 2, 87-92

Keywords

Soil investigation
Geotechnic
Geophysic
Liquefaction
Alikahya

Research Article

Received: 16.01.2022
Revised: 25.02.2022
Accepted: 01.03.2022
Published: 14.03.2022



Abstract

In this study, the soil conditions of Alikahya region (Izmit) were investigated by the results of geological, geophysical and geotechnical survey results. Alikahya region is almost entirely located on sub-mid-upper Eocene aged rocks and Quaternary aged sediments. The alluvium thickness is nearly 300 m. According to seismic studies, P-wave velocities are between 277-2562 m / sec, and S-wave velocities are between 110-1427 m / sec in the study area. The determined local soil classes are Z-3 on the clay stones and Z-4 on the Quaternary aged alluvium, respectively. The ground water level varies between 1-2 m depths in the alluvium. Alikahya region located on first degree earthquake risk zone and liquefaction analysis results indicated that the existence of local liquefiable areas in the study area.

1. Introduction

Since Turkey is located on an active tectonic belt, it has a suitable topography for natural disasters such as earthquakes and landslides. This reveals the necessity of determining safe and risky areas in terms of soil properties in the planning of residential areas. Especially the losses and damages experienced in the Izmit and Düzce earthquakes in 1999 have contributed to the development of earthquake awareness and sensitivity about the precautions to be taken against possible earthquakes in our country.

Local soil conditions also play an important role in the assessment of earthquake risk for residential areas, as well as features such as the probability of an earthquake, its magnitude and distance from the study area. While seismic waves pass through the soil layers, their properties can change according to the local soil conditions and can decrease or increase the earthquake forces acting on the structures located on the ground surface [1]. Likewise, during the propagation of earthquake waves, the properties of the soil layers can also change. Generally, young and thick sedimentary areas deposited on old rock units and creating a significant density difference with the rock units amplify the amplitudes of seismic waves. The amplification effect of such different ground behaviors on seismic waves has been clearly demonstrated by studies on the significant earthquakes in 1985 Mexico City (Mexico), 1989 Loma Prieta (USA) and 1999 Kocaeli (Turkey) earthquakes [2-4]. Based on this, detailed investigation of local soil conditions in areas with high earthquake risk is of great importance in terms of developing earthquake resistant structure design and minimizing the damages that may occur.

During earthquakes, pore water pressure increases that occur under cyclic loading in saturated soil layers can cause liquefaction in the soil, which can be described as the transformation from solid phase to liquid phase. The liquefaction of soils depends on seismic factors such as the size and duration of the earthquake, as well as properties such as grain size and distribution, geological age and precipitation conditions, initial density and water permeability [5]. The looseness of the ground together with the closeness of the groundwater level in the ground

to the surface is one of the conditions that are effective for the liquefaction of the ground. Although the liquefaction phenomenon developed in many earthquakes, it started to be taken into consideration with the 1992 Erzincan earthquake in Turkey, and the importance of this phenomenon gained importance by attracting the attention of all segments with the liquefaction events that occurred in the 1999 Marmara earthquake.

Geotechnical studies to be completed prior to any civil engineering design process; it requires an appropriate soil survey program that covers drilling, sampling, laboratory and field tests. Laboratory and field tests are the most important tools that allow the determination of soil properties in geotechnical science. In this study, the soil properties of the Alikahya region of Izmit province were examined with the research results of geological, geophysical and geotechnical methods and the suitability of the region for settlement was investigated. In this direction, field studies such as drilling, seismic refraction, and laboratory results on soil samples were examined in detail. Considering the earthquake hazard of the region, the liquefaction risk of the soils was also investigated.

2. Geological and Tectonical Features

Alikahya Region is located in the eastern part of Izmit province. According to the geological data, the Izmit Basin extending from Izmit Bay to Sapanca consists of Quaternary and Pliocene aged sediments, and a transition towards older and solid soils is observed towards the north and south of the Izmit Basin. In the parts close to Izmit Bay, transitions to Lower-Middle Eocene aged sandstone, conglomerate, shale and mudstone are observed. In the Alikahya Region, Quaternary aged alluvium is generally formed by consecutive clay-sand-silt. The unit observed in the northern parts of the study area has a medium-hard rock quality in terms of engineering. The unit is may described as cracked and fractured. The waters seeping into these cracks and fractures decomposed the rock. Alteration is observed in the surface sections of the unit where it comes into contact with water.

The study area is located on the North Anatolian Fault (NAF). NAF is approximately 1500 km long and is one of the most active faults in Turkey and the world. The NAF splits into two branches from the Mudurnu Stream valley in the west of Izmit Bay. The northern branch forms the Izmit-Sapanca segment, and the southern branch forms the Geyve-Iznik branch (Figure 1). Different structural models have been proposed for this branch of the NAF. The first of these is the right-sided strike-slip system model with a vertical slip component of the NAF in the Gulf of Izmit and the Sea of Marmara [6]. In another model, in which seismological data are also used, it is suggested that the trough areas in the Gulf of Izmit and the Sea of Marmara are grabens developed due to gravitational forces [7]. In the third model, it is assumed that the northern branch of the NAF zone is represented by many fault segments and that there are pull-apart basin structures between these stepped segments [8, 9].

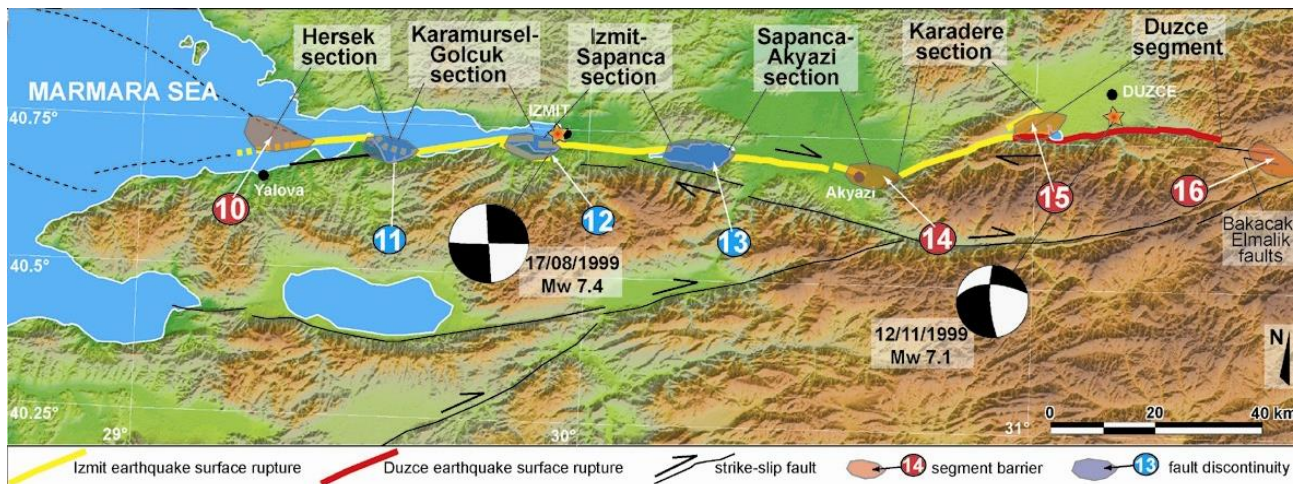


Figure 1. General tectonics map of Eastern Marmara Region [10]

3. Geophysical Research

Field study results of 18 seismic refraction measurements were used to determine the geophysical properties of the soils in the study area. Based on these measurements, layer thicknesses, underground velocity structure, dynamic-elastic engineering parameters of the soils were determined. Table 1 contains the information about the seismic refraction measurement results taken in all profiles. In the seismic refraction measurements performed along 18 profiles, the longitudinal wave velocities of the soils V_p were measured between 277 – 2562 m/sec and shear wave velocities V_s between 110 – 1427 m/sec.

Table 1. Dynamic parameters determined by the seismic surveys

Profile No/ Layer No	Vp (m/s)	Vs (m/s)	Pre. Period (sec)	Thickness (m)	Bulk M. (kg/cm ²)	Density (gr/cm ³)	Elasticity M. (kg/cm ²)	Poisson Rate	Shear M. (kg/cm ²)
P-1/L1	384	129	0.70	2.09	1719	1.37	656	0.43	228
P-1/L2	963	401	"	7.79	12312	1.73	7748	0.73	2776
P-1/L3	1593	782	"		33730	1.96	32127	1.96	11976
P-2/L1	376	150	0.48	2.12	1520	1.37	863	0.40	307
P-2/L2	1323	627	"	9.10	22924	1.87	19920	0.35	7349
P-2/L3	1894	961	"		48179	2.05	50111	0.32	18886
P-3/L1	351	130	0.68	1.92	1350	1.34	644	0.42	226
P-3/L2	873	410	"	8.71	9065	1.69	7696	0.35	2832
P-3/L3	1688	910	"		34677	1.99	42622	0.29	16454
P-4/L1	339	120	0.66	1.81	1273	1.33	547	0.42	191
P-4/L2	956	452	"	7.10	11058	1.72	9551	0.35	3521
P-4/L3	1859	977	"		44439	2.04	50875	0.30	19429
P-5/L1	277	110	0.40	1.99	766	1.26	430	0.40	153
P-5/L2	1274	627	"	4.29	20352	1.85	19515	0.34	7280
P-5/L3	2010	1123	"		48956	2.08	66651	0.27	26177
P-6/L1	385	155	0.43	2.59	1595	1.37	925	0.40	329
P-6/L2	1514	747	"	9.82	29937	1.93	28898	0.33	10790
P-6/L3	2562	1427	"		84883	2.21	114533	0.27	44911
P-7/L1	474	205	0.40	3.42	2478	1.45	1610	0.40	578
P-7/L2	1980	1054	"		50439	2.07	59833	0.30	22972
P-8/L1	424	155	0.44	2.51	2078	1.41	961	0.42	337
P-8/L2	1836	898	"		46584	2.03	43945	0.34	16363
P-9/L1	353	140	0.48	1.65	1323	1.34	740	0.40	263
P-9/L2	1295	622	"	6.00	21593	1.86	19426	0.35	7194
P-9/L3	2487	1310	"		85312	2.19	98279	0.30	37568
P-10/L1	460	200	0.51	1.59	2272	1.44	1588	0.38	574
P-10/L2	923	461	"	5.30	9715	1.71	9687	0.33	3631
P-10/L3	2121	1210	"		53572	2.10	77542	0.25	30801
P-11/L1	414	170	0.47	1.52	1857	1.40	1130	0.39	404
P-11/L2	1372	687	"	5.42	23641	1.89	23734	0.33	8904
P-11/L3	2510	1386	"		82036	2.19	107962	0.28	42150
P-12/L1	369	130	0.51	2.85	1543	1.36	656	0.42	229
P-12/L2	1581	720	"		35349	1.95	27748	0.36	10133
P-13/L1	380	140	0.48	2.55	1618	1.37	762	0.42	268
P-13/L2	1513	750	"		29758	1.93	29083	0.33	10875
P-14/L1	415	180	0.46	1.75	1805	1.40	1254	0.38	453
P-14/L2	1333	642	"	9.80	22989	1.87	20829	0.34	7720
P-14/L3	2247	1210	"		66097	2.13	80984	0.29	31248
P-15/L1	458	185	0.49	1.69	2353	1.43	2353	0.40	490
P-15/L2	1432	714	"		26142	1.91	26141	0.33	9721
P-16/L1	432	170	0.40	1.98	2092	1.41	1150	0.40	408
P-16/L2	2249	1215	"		65959	2.13	81555	0.29	31514
P-17/L1	303	116	0.71	1.49	955	1.29	492	0.41	174
P-17/L2	756	354	"	4.63	6574	1.63	5539	0.36	2037
P-17/L3	1621	854	"		32558	1.97	37525	0.30	14345
P-18/L1	284	110	0.50	2.03	821	1.27	434	0.41	153
P-18/L2	1378	636	"	4.73	25678	1.89	20851	0.36	7639
P-18/L3	2000	1141	"		46938	2.07	67945	0.25	26989

4. Geotechnical Research

14 drilling studies and laboratory test results of the samples obtained from the drillings were used in determining the geotechnical properties of the soils in the study area, Groundwater level in the study area varies between 1 and 3 m according to the drilling data, Average of the number of SPT blows determined during drilling is 16 for the study area. The soil classes are determined as predominantly ML and CH in the region [11]. Statistics of the index properties of soils in the study area are given in the Table 2. According to the classification for local soil classes; in the sections with rock units, the soil class is Z-3 soil group B, and in the alluvial region with low slope, the soil class Z-4 soil group is D [12]. Average cohesion values (c) vary between 0.22 – 0.56 kg/cm², and internal friction angle (Ø) vary between 5.20° and 33.4°, according to the results of the triaxial pressure test performed especially for loose soil zones in the study area.

Table 2. Statistics of the index properties

	Minimum	Maximum	Average
Gravel Content %	9.27	36.21	18.25
Sand Content %	11.36	39.52	25.18
Fine Content %	21.52	79.64	56.57
LL	NP	67	21.42
PL	NP	36	9.36
PI	NP	45	12.74
Wn %	16.84	22.30	19.76

5. Liquefaction Risk

The serious decrease in shear strength in parallel with the increase in the pore water pressure of the soil can be accepted as the most general definition of soil liquefaction. Liquefaction occurs in saturated cohesionless soils, when the effective stress is zero, with the increase in pore water pressure during shaking. Thus, the layer behaves like a liquid; cannot support the structure, the structure tilts, sinks, overturns or turns. It is known that liquefaction does not occur in all soil layers in the field. For this reason, in liquefaction hazard analyzes, it is necessary to examine whether the necessary conditions for liquefaction to occur are primarily required. It can be stated that the most important ones among these conditions are the earthquake magnitude and the distance from the center of the earthquake, the composition of the soil layer and its geological history, and the stress and compactness of the soil.

The liquefaction susceptibility of soils is evaluated by the calculated liquefaction safety number using simplified procedures. In this approach, the cyclic shear stresses caused by the earthquake and the cyclic resistance of the soil to liquefaction are compared. The most common field test used to evaluate the resistance of soils to liquefaction is the standard penetration test (SPT). SPT, which is a dynamic penetration test, is one of the most frequently used tests in soil investigations in our country. SPT results are used in liquefaction analysis as well as successfully predicting the firmness and shear resistance properties of especially granular soils. SPT-based liquefaction analysis was first proposed by Seed and Idriss, [13] and has been improved over time. Today, especially with the procedure proposed by Youd [14], it has become a widely used method to determine the liquefaction sensitivity of sands in Turkey as well as in many countries of the world.

In determining the liquefaction potential of the soils in the study area, liquefaction analyzes based on SPT results were carried out in accordance with the purpose of the study with the obtained drilling information. In this context, the simplified procedure proposed by Seed and Idriss [13] was used (Equation 1);

$$FS = \frac{CRR}{CSR} \quad (1)$$

FS is the safety coefficient, CRR is the cyclic rate of resistance and defined on the clean sand curve by Youd et al. [14], CSR is the ratio of cyclic stress generated during earthquakes and calculated as (Equation 2);

$$CSR = 0.65 \times \frac{a_{max}}{g} \times \frac{\sigma_v}{\sigma'_v} \times r_d \quad (2)$$

Here is, *g*, gravitational acceleration; σ_v and σ'_v , total and effective stress; a_{max} , the peak horizontal acceleration; r_d , stress reduction coefficient.

Considering the earthquake hazard of the region and previous studies, the maximum horizontal ground acceleration (a_{max}) was evaluated as 0.40g and the earthquake magnitude (M_w) as 7.5, in the study. The safety coefficients obtained as a result of the calculations were used to determine the levels with and without liquefaction

potential. Levels with a factor of safety less than 1 are considered liquefiable, while levels greater than 1 are considered non-liquefiable. The results of the liquefaction analysis of soils in the study area are given in Table 3.

Table 3. Liquefaction analysis results in the study area

Drilling No	Z (m)	Water Level (m)	FC (%)	Unit Weight kN/m ³	N ₁₆₀	CSR	CRR	FS
D1	3.00	2.44	45.08	19.57	16.50	0.281	0.176	0.63
D1	6.00	2.44	43.27	19.59	34.10	0.354	0.425	1.20
D1	7.50	2.44	40.29	19.61	45.20	0.370	0.489	1.32
D1	9.00	2.44	32.22	19.81	48.00	0.378	0.453	1.20
D3	3.00	1.9	35.18	19.75	36.00	0.311	0.374	1.20
D3	4.50	1.9	24.15	19.99	19.50	0.353	0.209	0.59
D4	3.00	2.2	46.36	19.56	18.50	0.294	0.197	0.67
D4	4.50	2.2	41.44	19.59	24.30	0.339	0.278	0.82
D4	9.00	2.2	48.67	19.53	37.10	0.386	0.464	1.20
D7	7.50	2	46	19.56	43.60	0.388	0.465	1.20
D7	12.00	2.1	7	20.41	21.70	0.369	0.238	0.64
D7	14.50	2.1	5	20.43	24.20	0.343	0.277	0.80
D8	3.00	2.8	45	20.10	32.20	0.265	0.318	1.20
D8	14.50	2.8	8	20.39	39.00	0.338	0.405	1.19
D9	6.00	2.5	15.5	20.26	24.00	0.347	0.274	0.79
D9	9.00	2.5	17.3	20.23	41.10	0.369	0.443	1.20
D9	12.00	2.5	14.8	20.26	45.20	0.361	0.455	1.26
D10	1.50	1.2	10	20.50	14.80	0.285	0.158	0.55
D10	3.00	1.2	11	20.34	16.80	0.358	0.178	0.50
D10	4.50	1.2	7	20.41	21.00	0.389	0.229	0.59
D10	6.00	1.2	10	20.36	26.80	0.405	0.332	0.82
D10	9.00	2	44.2	29.30	5.00	0.393	0.426	1.08
D11	3.00	2.1	3	20.46	13.80	0.297	0.148	0.50
D11	4.50	2.1	2.3	20.47	15.70	0.339	0.167	0.49
D11	6.00	2.1	3.1	20.45	17.40	0.362	0.185	0.51
D11	9.00	2.1	3	20.46	25.00	0.379	0.292	0.77
D11	12.00	2.1	2.9	20.46	20.50	0.368	0.222	0.60
D11	14.50	2.1	3.5	20.45	24.20	0.343	0.277	0.80
D13	3.00	2.1	47	19.56	42.50	0.304	0.395	1.30
D13	4.50	2.1	48	19.55	45.40	0.351	0.421	1.20
D13	6.00	2.2	8	20.39	27.70	0.358	0.361	1.01

6. Discussion and Conclusions

In building design, the behavior of the ground in response to the general characteristics of the ground and the loads acting on it is of great importance. As a result of the seismic loads that the ground is exposed to, the parameters based on the building safety should be determined correctly. Considering the fact that our country is located in an earthquake zone, the importance of the situation increases even more. The liquefaction in the soil layers can cause significant damage to the surface and buried structures during the earthquakes. Therefore, it is very important to determine the factors that cause liquefaction in soils and the liquefaction hazard and to predict their possible harmful effects in geotechnical earthquake engineering.

In this study multiple research data were used together to determine the soil properties and liquefaction potential of Alikahya region (Izmit). Despite the presence of sandstone, conglomerate, shale and mudstone units in the north of the study area, the remaining areas are represented by Quaternary aged alluvium. Seismic velocities and SPT blow numbers were found to be low, especially at near-surface depths throughout the study area. According to the liquefaction analyzes performed considering the earthquake hazard and loose soil structure of the region, it has been determined that some local areas in the study area are at risk of liquefaction (Table 3). It will be beneficial to use the necessary soil improvement methods for new constructions to be made in areas with liquefaction risk in the region.

Funding

This research received no external funding.

Conflicts of interest

The authors declare no conflicts of interest.

References

1. Safak, E. (2001). Local site effects and dynamic soil behavior. *Soil Dynamics and Earthquake Engineering*, 21 (5), 453-458.
2. Singh, S. K., Mena E., & Castro, R. (1988). Some aspects of source characteristics of the 19 September 1985 Michoacan earthquake and ground motion amplification in and near Mexico City from strong motion data, *Bulletin of Seismological Society of America*, 78, 451-477
3. Ozel O., Cranswick E., Meremonte M., Erdik M., Şafak E. (2002). Site effect in Avcılar, west of Istanbul, Turkey from strong and weak motion data. *Bulletin of Seismological Society of America*, 92, 499-508
4. Ergin M., Özalaybey S., Aktar M., & Yalçın M. N. (2004). Site Amplification at Avcılar, İstanbul. *Tectonophysics*, 391, 335-346.
5. Özaydın, K. (2007). Liquefaction in Soils. Sixth National Earthquake Engineering Conference, Istanbul, 231-255
6. Saroğlu, F., Emre, Ö., & Boray, A. (1987). Active faults and seismicity of Turkey. MTA, Report No: 8174.
7. Crampin, S., & Evans, R. (1986). Neotectonic of the Marmara Sea region in Turkey. *J. Geol. Soc.*, 143, 343 - 348.
8. Barka, A., & Kandinsky-Cade, K. (1988). Strike-slip fault geometry in Turkey and its influence on earthquake activity. *Tectonics*, 7, 663-684.
9. Barka, A., & Gülen, L. (1988). New constraints on age and total offset of the North Anatolian fault zone; Implications for tectonics of the Eastern Mediterranean region: In "1987 Melih Tokay Symp., Spec. Publ. METU. Ankara, Turkey, 39-65.
10. Pantosti, D., Pucci, S., Palyvos, N., Zabcı, C., De Martini, P.M., Uçarkuş, G., Dikbaş, A., Meghraoui, M., Akyüz, H.S., & Collins P. (2004). Paleoearthquakes along the Düzce fault segment of the North Anatolian Fault Zone (Turkey). 32nd IGC, Florence 2004 - Abstracts, p. 1215.170
11. Soil Classification Handbook: Unified Soil Classification System. Denver, Colo.:Geotechnical Branch, Division of Research and Laboratory Services, Engineering and Research Center, Bureau of Reclamation, 1986
12. Regulation on Buildings to be Constructed in Disaster Areas. (1998). Ministry of Public Works and Settlement, Ankara, p. 37.
13. Seed H. B., & Idriss I. M. (1971). Simplified procedure for evaluating soil liquefaction potential. *Journal of Soil Mech. Foundation Div., ASCE*, 97 (9), 1249-73.
14. Youd T. L., Idriss, I. M., Andrus, R. D., Arango, I., Castro, G., Christian, J. T., Dobry, R., Liam Finn W. D., Harder L.F.Jr., Hynes M.E., Ishihara K., Koester J.P., Laio S.S.C., Marcuson WF III., Martin, G. R., Mitchell J.K., Moriwaki Y., Power M.S., Robertson P. K., Seed, R. B., Stokoe K.H. (2001). Liquefaction resistance of soils: summary report from the 1996 NCEER and 1998 NCEER/NSF workshops on evaluation of liquefaction resistance of soils. *Journal of Geotechnical and Geoenvironmental Engineering*, 127 (10), 817-833.





Assessment of the artificial fiber contribution on the shear strength parameters of soils

Özgür Lütfi Ertuğrul *¹, Furkan İnal ¹

¹Mersin University, Department of Civil Engineering, Türkiye, ertugrul@mersin.edu.tr; furkaninal@mersin.edu.tr

Cite this study: Ertugrul, O. L., & Inal, F. (2022). Assessment of the artificial fiber contribution on the shear strength parameters of soils. *Advanced Engineering Science*, 2, 93-100

Keywords

Soil improvement
Soil reinforcement
Fiber
Regression Analysis

Research Article

Received: 16.01.2022
Revised: 26.02.2022
Accepted: 02.03.2022
Published: 14.03.2022



Abstract

Soil stabilization is one of the methods of soil improvement that has been used since ancient times in human history. Soil mass reinforced with randomly distributed discrete fibers is one of the techniques for improving the properties of soils. Reinforcing the soil with randomly distributed discrete fibers has attracted the attention of many researchers over the past few decades. For this purpose, many studies have been carried out with fibers obtained from synthetic, natural and waste materials. Studies on soil reinforced with discrete fibers have revealed the effect of fibers are beneficial to strength parameters of soils. In this study multivariate regression analysis were performed by using data from literature to formulate the effect of fibers on the soil. The formulas obtained from multivariate regression analyses are in harmony with the values of unconfined compression and shear strength.

1. Introduction

As is known, almost all types of structures, from high-rise buildings to the construction of roads, railways, tunnels and viaducts, are built either on the soil or in the soil. In this regard, the structures are in constant interaction with the soil. Unfortunately, the soil that is supposed to carry the constructed structure may not always have sufficient engineering properties. The fact that the soil has insufficient engineering properties may cause the existing soil to be discarded and a new filling to be made or it can bring up the construction of deep foundation. But it may not be possible to implement these solutions for economic reasons. At this point, engineers go to ways to improve the soil on the site.

Soil stabilization is one of the methods of soil improvement that has been used since ancient times in human history. The stabilization of soils has been performed for millennia. For instance, the Mesopotamians and Romans separately discovered that it was possible to improve the ability of pathways to carry traffic by mixing the weak soils with a stabilizing agent like pulverized limestone or calcium [1]. Random distribution of fibers on the ground also improves the strength parameters of the soil by simulating the behavior of plant roots [2]. Also in ancient civilizations, straw was a material used for reinforcing building blocks obtained from slurry [1]. At present, the reinforcing of the soil to improve its properties is attributed to the Vidal [3]. One of the methods of reinforcing the soil is use of fiber. Reinforcing the soil with randomly distributed discrete fibers has attracted the attention of many researchers over the past few decades. For this purpose, many studies have been carried out with fibers obtained from synthetic [4-9], natural [10-19] or recycled/waste materials [20-25] in order to study the effect of fibers on the engineering properties of the soil.

2. Literature Review

Uysal, carried out a laboratory study by mixing sand samples having different relative density values (20%, 30% and 40%) with kapolymer and virgin homopolymer fibers in ratios of 0.50%, 1.0% and 1.50% of the dry weight of the soil. Shear box tests were conducted in order to observe the effect of relative density and fiber content on the shear strength. It was observed that the samples having a high relative density has a higher shear strength, and the angle of internal friction also increases as the fiber ratio increases [9].

Wei et al. performed laboratory tests by mixing a silty clay soil with both lime and fibers to investigate the mechanical properties of the soil. Wheat straw, rice straw, hemp and polypropylene fibers were added to the soil-lime mixtures. Unconfined compression and triaxial compression tests were performed on samples in order to examine the shear strength properties. The optimum fiber content was found to be 0.2% or 0.25% and the optimum fiber length was found to be 30%-40% of the sample diameter. Fiber reinforcement has significantly increased cohesion and slightly improved the angle of internal friction. When the performance of fiber varieties in cohesion increases was compared, it was determined that polypropylene, jute, rice straw and wheat straw were from the best to the lowest [18].

Özdemir, investigated the consistency limits, compaction characteristics, unconfined compression and freeze-thaw properties of fiber-clay samples obtained by adding natural (straw, hemp) and synthetic (polyester) fibers to a cohesive soil sample. It was observed that the unconfined compression strength of the samples increased with an increase in the percentage of fiber, and improvements in the unconfined compression strength after freezing and thawing also occurred when compared to natural clay. The samples with hemp additives exhibited superior behavior against freezing and thawing [15].

Pradhan et al. investigated the effect of polypropylene fiber contribution on the shear strength and unconfined compression strength of cohesive soils. They observed that the addition of fibers increased the peak and residual shear strength as well as unconfined compression strength and CBR values [26].

Consoli et al. carried out a study to determine the differences in the strength of artificially cemented sandy soil with and without fiber reinforcement. The controlling parameters evaluated were the amount of cement, porosity, moisture content, and voids/cement ratio. A series of unconfined compression tests were performed. Results show that the fiber addition increased the unconfined compression strength of the samples at all cement ratios [27].

Nezhad et al. in their study, aimed to investigate the effect of natural fibers on the strength behavior of clayey soils as sustainable fibers containing basalt (BS) and bagasse (BG) and synthetic polyester (PET) fibers. For this purpose, the effects of various fiber contents (0.5%, 1% and 2%) and lengths (2.5 mm, 5 mm and 7.5 mm) were evaluated experimentally. By performing indirect tensile strength (ITS) and CBR tests, it was found that increased fiber content and length had a significant effect on CBR and values. In addition, the CBR and ITS values obtained by mixing the 7.5 mm long fibers with the soil at 2% density caused the highest values [14].

Valipour et al. have investigated the effects of recycled tire polymer fibers (RTFP) and glass fibers (GF) on improving the strength/deformation properties of clays. A series of compaction, unconfined pressure and shear box tests were carried out on clay soils with RTFP and GF, with various lengths (5 mm and 10 mm) and fiber ratios (0.5, 1.0 and 1.5%). It was seen that the fiber addition was more effective on the cohesion value, while the changes in the internal friction angle values remained at a minimum level. The highest shear stress values were obtained at 0.5% for RTPF and 1.0% for GF. It has been observed that fiber reinforced soils show higher ductility and load bearing capacity compared to non-reinforced soils [25].

Bao et al. studied the mechanical performance of clayey soil (fiber density: 1.0%, 2.0% and 3.0% fiber lengths: 3 mm, 6 mm and 12 mm) reinforced with carbon fibers (CF). Unconfined compressive strength tests were performed on soil samples under optimum water content. The unconfined compressive strength of the soil samples improved significantly with increasing fiber content. The samples reinforced with 3% CF content of 6 mm have reached the highest unconfined pressure value [5].

Yetimoglu and Salbas investigated the shear strength of sands reinforced with randomly distributed fiber by shear box test. The test results showed that the peak shear strength and stiffness did not change significantly with the addition of fiber. Horizontal displacements during failure under equal stresses in the vertical direction were found to be comparable in fiber-reinforced and unreinforced sands. Fiber reinforcement reduced the brittleness of the soils and reduced post-peak strength losses. Thus, fiber reinforcement to the sandy soil led to an increase in the residual strength [28].

Çetinkaya used clay, fly ash and polypropylene fiber materials in his study. CBR and free pressure experiments were performed on mixtures prepared by mixing clay and fly ash samples with polypropylene fibers. According to the results of the experiments, it was observed that the CBR value increased by 100% and the unconfined compression strength increased by 48% in the mixtures prepared with fiber additives at a rate of 1.0% by weight of the clay-fly ash mixture [6].

In his study, Fındıkçı homogeneously mixed 3, 6, 12 mm long glass fibers into bentonite clay at 1%, 2%, and 3% ratios in his study. As a result of the unconfined compression experiments, the optimum values were obtained from samples containing 12% fiber with a length of 12 mm [7].

Ayraçma carried out shear box experiments by mixing 0.25% and 0.5% glass fiber into white silica sand with different relative density values (20% and 60%). During the experiments, due to the difficulties in ensuring the homogeneous distribution of the glass fiber in the sample, material changes were made and sand-polypropylene fibers were used in the rest of the study. Shear box tests were carried out on sand-polypropylene fiber blends mixed at 0.25%, 0.5% and 1.0% ratios. The shear box results performed on the fiber-reinforced samples showed that the peak internal friction angle of the fiber-reinforced soils increased. Also, the post-peak strength loss after fracture decreased [4].

Consoli et al. applied unconfined compression tests, split tensile tests and drained triaxial pressure tests to fine grained sand classified as SP. The inclusion of PET fiber increased the peak and ultimate strength and energy absorption capacity. While the cohesion did not change, the internal friction angle increased with the inclusion of the fiber and the length of the fiber. The addition of fiber did not affect the initial stiffness or ductility. The unconfined compressive strength and tensile strength of cemented sand significantly increased by fiber reinforcement [20].

Terzi, has added basalt fiber in certain proportions to soil samples classified as high plasticity clay (CH), shear box tests were applied under different vertical stresses after the samples were first consolidated under 45 kPa load for 7 days. The samples were prepared by slurry method by adding 6 mm, 12 mm and 24 mm long basalt fiber at 0%, 1%, 1.5%, 2% and 2.5% by weight of the clay sample. According to the results of 39 experiments; As the basalt fiber ratio and length increased, a non-linear increase was observed in the internal friction angle, while peak values were observed at different basalt fiber ratios depending on the basalt fiber length in the cohesion value. While the cohesion value peaked at 2% fiber in the samples worked with 6 mm fiber length, the highest improvements were obtained in the cohesion value of 1.5% in the samples worked with 12 mm fiber length, and the cohesion value at 1% fiber in the samples worked with 24 mm fiber length [29].

Sevencan, investigated the unconfined compressive strength of the samples by mixing them with different ratios of fly ash (10.0%, 20.0% and 30.0%) and polypropylene fibers of different ratios (0.50% and 1.0%) and lengths (6 mm and 19 mm) on the clayey soil. As a result of standard proctor tests of clayey soils with fly ash additive, it was observed that the dry unit volume weight values increased and the optimum water content decreased with the increase in the fly ash content. The use of fiber alone (without adding fly ash) reduces the unconfined compressive strength somewhat. Only 1.0% M19 fiber reinforced sample increases the strength slightly. A similar behavior is observed for mixtures containing 10% fly ash. On the other hand, it was observed that the unconfined compressive strength of the mixtures containing 30% fly ash decreased slightly with 0.5% fiber content, while the unconfined compressive strength of the mixture was increased with 1.0% fiber content [8].

Prabakar and Sridhar, applied sisal fibers to soil samples in four different densities (0.25, 0.5, 0.75 and 1%) and 4 different lengths (10, 15, 20, 25 mm) on low plasticity clayey soils, which they classified as CL in their study. have supplemented. Compaction and triaxial compression tests were applied to the prepared samples. According to the test results, the shear stress of the fiber reinforced soil is improved by the addition of sisal fiber. Shear stress increases non-linearly with increasing fiber length up to 20 mm and beyond, where an increase in length decreases shear stress. The shear stress of the reinforced soil also increases with the increase in cell pressure (σ_3). The percentage of fiber content also affects shear strength as shear stress develops non-linearly with increase in fiber content. But beyond 0.75% fiber content, shear stress decreases with increase in fiber content. The cohesion value is increased due to the inclusion of sisal fiber. The maximum cohesion value is achieved as 66 kPa versus 18 kPa (unreinforced soil). Up to 20 mm long, the increase in fiber length increases the cohesion value. There is no particular trend for the internal friction angle to change with fiber length. It has been determined that the cohesion improves linearly with the increase in fiber content, thanks to the fiber content of up to 0.75%. But for the same fiber content of different lengths, the amount of increase in cohesion is less [16].

Ahmad et al. conducted triaxial compression tests to evaluate the response of randomly distributed fibers on the strength of silty sand. In this study, palm fiber (OPEFB) was mixed with silty sand soil to investigate the increase in shear strength during triaxial compression. Samples were tested under drained and undrained conditions with different lengths (i. e. 15mm, 30mm and 45mm) and different ratios (0.25% and 0.5%). In addition, OPEFB fibers coated with acrylic butadiene styrene thermoplastic were also tested to determine the effect of the coating on reinforcement. The inclusion of randomly dispersed discrete fibers significantly increased the shear strength of the silty sand. Coated OPEFB fibers increased the shear strength of silty sand much more than uncoated fibers. The coating increased the surface area of the fibers, increasing the interface friction between the fiber and soil particles. Reinforced silty sand containing 0.5% coated fiber with a length of 30 mm showed approximately 25% increase in internal friction angle and 35% increase in cohesion under undrained loading conditions compared to that of unreinforced silty sand. The results show that the shear strength parameters of the soil-fiber mixture can be significantly improved [10].

Wu et al. aim to determine the behavior of randomly distributed sisal fiber reinforced soil in silty clay in their study. The fibers were cut in different lengths (5, 10 and 15 mm) and randomly mixed with the soil at different percentages (0.5%, 1.0% and 1.5%). In this article, the researchers evaluated the effect of sisal fiber on the engineering properties of silty clay soil using the triaxial shear test. As a result of the test results, the cohesion of

the fiber-reinforced soil and the peak of the principal stress difference improved after the fiber reinforcement to the soil. With increasing fiber content, the peak of the principal stress difference increases. When the fiber content reached 1.0%, the increase in the bearing capacity of the soil body was limited by mixing more fiber. Compared to the 5 mm long fiber, a significant improvement in cohesion values and the peak of the principal stress difference was observed for the 10 mm long fiber. The level of recovery occurred at about 20% [19].

Kaniraj and Gayathri, conducted an experimental study to investigate the effect of randomly oriented fiber additives on the geotechnical behavior of two different (DA, RA) fly ash. In the experiments, two different types of polyester fiber and 1% fixed fiber content (based on dry weight) were chosen as the fiber ratio. The polyester fibers used in the experiments were produced from 100% recycled plastic waste. This article presents the results of unconfined compression tests and triaxial compression tests on fiber-reinforced fly ash. In all triaxial compression tests, fiber reinforcement had a significant effect on the stress-strain behavior of the samples. In the unconfined pressure tests, when the lean fly ash samples reached the axial deformation values of 1.5-2.5%, the samples collapsed. However, fiber-reinforced samples exhibited a highly ductile behavior. F6DA and F6RA samples reached peak axial stresses at relatively higher axial strain values than raw fly ash samples and then continued to deform under decreasing axial stress. In unconsolidated and undrained tests, the deviator stress reached a peak in the range of 11-14% for DA specimens and 6-10% for RA specimens as axial deformation, after which it remained almost constant. In the F6DA and F6RA samples, the peak deflection stress could not be reached even at 20% axial deformation. The behavior of fly ash and fly ash-fiber samples in the drained tests were similar to the behaviors in the unconsolidated and undrained tests. The fiber additive increased the strength of the raw fly ash samples and changed the brittle behavior to ductile behavior [30].

Muntohar et al. investigated the engineering behavior of stabilized (rice husk ash blended with lime) clayey/silty soil reinforced with randomly distributed discrete plastic waste fibers. 12% lime, 12% ricehusk ash and plastic waste fibers in different proportions (0.1%, 0.2%, 0.4%, 0.8% and 1.2%) were mixed into the highly plastic silty soil. unconfined compression test, split tensile test, triaxial compression test and CBR tests were applied to the prepared samples. The results show that the proposed method further improves the engineering properties, stability and durability of the clayey-silty soil. Depending on compressive strength, California strength ratio (CBR), shear strength and failure properties, optimum fiber content in soil-lime-rice ash mixtures was determined to vary between 0.4-0.8% of dry mass [24].

Babu and Vasudevan (2008) tried to present the results of the strength and stiffness behavior of soil reinforced with coconut fibers in their study. Cylindrical soil samples reinforced with coconut fibers mixed with soil of different sizes (10 cm, 15 cm, 25 cm, 30 cm) and densities (0.5%, 1.0%, 1.25%, 1.5%, 2.0%, 2.5%) to determine the strength and stiffness of the samples. It was tested on a triaxial shear device and the results were compared with unreinforced soils. The stress-strain behavior of the soil was improved by incorporating coconut fibers into the soil, the deviator stress at failure was observed to increase up to 3.5 times compared to the unreinforced soil with fiber inclusion. In fiber-reinforced soils, the deviator stress increased as the fiber diameter increased. The maximum stress increase was observed when the fiber length was between 15 and 25 mm and the length was between 40 and 60% of the smallest lateral dimension of the sample. As the fiber content increased, the energy absorption capacity of the fibrous samples increased. The results show that the addition of 1-2% coconut as a random reinforcement material increases both the strength and stiffness of the clayey soil studied in the study [12].

Mirzababaei et al. conducted comprehensive research on the use of carpet waste fibers in the reinforcement of clay soils in their study. The effects of adding two different types of shredded carpet waste fibers in proportional amounts to clayey soils (i. e., 1, 3 and 5% according to the dry weight of the soil) were investigated and evaluated. The research was carried out on samples prepared with maximum dry unit weight and optimum water content, and samples prepared under variable dry unit weight and water content conditions. A comparison was also made on the samples prepared at the same fiber content by changing the dry unit weight while keeping the water content unchanged or by changing both the dry unit weight and the water content. The research revealed that the incorporation of carpet waste fibers into prepared clayey soils at the same dry unit weight can significantly increase the unconfined compression strength (UCS), reduce the post-peak strength loss, and change the failure behavior from brittle to ductile. It has been observed that the benefit of the fiber to increase the unconfined compression strength of clay soils is highly dependent on the initial dry unit weight and water content of the soil [23].

3. Material and Method

Current state of the art on fiber addition to soils shows that synthetic fiber reinforcement of soils has positive effects on the unconfined compressive strength and shear strength parameters of soils.

In this study, the effects of synthetic fiber addition on the unconfined compression strength, cohesion and internal friction angle of soils were formulated by multivariate regression analysis method. In order to formulate the fiber effects with multivariate regression analysis, the relative density and fiber percent in sandy soils, and the fiber percent and length parameters in cohesive soils were selected from the data in the previous studies and the

unconfined compressive strength and shear strength parameters were tried to be determined by regression analysis. The data used in the analyses are given in Table 1.

Table 1. A summary of the data used from literature

Soil Type	Dr (%)	Fiber Percent (%)	Fiber Length (mm)	Φ (°)	Soil Type	Fiber Percent (%)	Fiber Length (mm)	q_u (kPa)
SP	20	0	0	28	CL	0	0	157
SP	30	0	0	31	CL	0,5	2	340
SP	40	0	0	33	CL	1	2	380
SP	20	0,5	15	31	CL	1,5	2	397
SP	20	1	15	33	CL	0,5	5	301
SP	20	1,5	15	34	CL	1	5	340
SP	30	0,5	15	33	CL	1,5	5	345
SP	30	1	15	34	Soil Type	Fiber Percent (%)	Fiber Length (mm)	c (kPa)
SP	30	1,5	15	36	CL	0	0	291
SP	40	0,5	15	36	CL	0,2	12	301
SP	40	1	15	38	CL	0,25	12	331
SP	40	1,5	15	39	CL	0,3	12	307
SP	20	0,5	15	29	CL	0,2	19	326
SP	20	1	15	30	CL	0,25	19	358
SP	20	1,5	15	32	CL	0,3	19	344
SP	30	0,5	15	32	Soil Type	Fiber Percent (%)	Fiber Length (mm)	Φ (°)
SP	30	1	15	33	CL	0	0	32
SP	30	1,5	15	35	CL	0,2	12	32
SP	40	0,5	15	34	CL	0,25	12	33
SP	40	1	15	35	CL	0,3	12	31
SP	40	1,5	15	37	CL	0,2	19	32
SP	40	0,5	15	36	CL	0,25	19	33
SP	40	1	15	38	CL	0,3	19	33

The soil used to determine cohesion has a salt content of 2.64%, was collected from coastal area, and was air dried and sieved (2 mm). The physical properties indices of soil are presented in Table 2 [18].

Table 2. Physical properties of soil used to determine cohesion (c, kPa) [18].

Properties	Value
Specific gravity	2.72
Grain size distribution	
Gravel (%)	0
Sand (%)	2.2
Silt (%)	62.6
Clay (%)	35.2
Atterberg limits	
Liquid limit (%)	32.6
Plastic limit (%)	16.8
Plasticity index	15.8
Optimal moisture content (%)	18
Maximum dry density (g/m ³)	1.81

Sand sample was used for the calculation of the internal friction angle and the percentage of sand was found to be 99% according to the results of the sieve analysis. The parameters of the soil are given in Table 3 [9].

Table 3. Physical properties of soil used to calculate internal friction angle (Φ , °) [9].

Properties	Value
Gravel (%)	0
Sand (%)	99
Clay and Silt (%)	1
D ₆₀	0,315
D ₃₀	0,256
D ₁₀	0,215
C _c	0.968
C _u	1.465
USCS	SP

To determine the free compressive strength, the researchers used a sample of natural clay. After drying the sample in the laboratory for 24 hours, they pulverize it in the Los Angeles abrasion device until it was crumbly enough. The soil parameters are given in Table 4 [15].

Table 4. Physical properties of soil used to determine unconfined compression strength (q_u) [15]

Properties	Value
< 0,002 mm (%)	42
Unit volume of grain, (kN/m ³)	25,9
Liquid limit, (%)	60,8
Plastic limit, (%)	26,5
Plasticity Index, (%)	34,3
USCS	CH

4. Results and Discussion

Based on the multiple variate regression analyses, the following equations were obtained for the relationship between fiber percent, fiber length and relative density with the internal angle of friction (Φ , °), cohesion (c , kPa) and undrained compressive strength:

$$q_u = a + bF_p + cF_L + d(F_p^2) + e(F_p \cdot F_L) + f(F_L^2) \quad (1)$$

In this equation, q_u represents undrained compressive strength in kPa whereas F_p , and F_L denotes fiber percent and fiber length. The constant parameters of a , b , c , d , e and f will be taken as 157, 179.7 81.67, -57, -4.333 and -13.13, respectively. For the relationship between fiber percent and relative density with the internal angle of friction (Φ , °) of cohesionless soils:

$$\Phi = g + hF_p + iD_r \quad (2)$$

where F_p , and D_r denotes fiber percent and soil relative density (divided by 100). The constant parameters of g , h , i will be taken as: 22.95, 26.57, and 3.106, respectively. The coefficient of determination is found as 0.90 for the suggested formula. For the relationship between fiber percent and fiber length with the cohesion (c , kPa) of cohesive soils:

$$c = j + kF_p + lF_L + m(F_p^2) + n(F_L^2) \quad (3)$$

The constant parameters of j , k , l , m and n will be taken as: 291, 5120, -86.48, -1e+04, 2.926 respectively. The coefficient of determination is found as 0.99 for the suggested formula.

5. Conclusion

Researchers conducted laboratory tests in order to investigate the mechanical behavior of fiber reinforced soils. Based on the carried-out tests, it was observed that reinforcing soil with fibers, the peak strength loss is decreased, and thus the behavior of the material changed from brittle to ductile, the swelling pressure and desiccation cracks decreased, in short, the behavior of the soil improved in the desired direction. When compared

to classical soil improvement techniques, the main advantage of mixing randomly distributed fibers is the maintenance of strength isotropy and absence of potential failure plane that can develop parallel to the oriented reinforcement [16]. By using the results of the previous laboratory tests reported in the literature, multivariate regression analyses were performed. Formulas were suggested to be used for the practical purposes for the site engineers and designers.

Acknowledgement

This study was partly presented in 1st Advanced Engineering Days [31].

Funding

This research received no external funding.

Author contributions

Özgür Lütü Ertuğrul: Data curation, Validation, Writing-Reviewing and Editing. **Furkan İnal:** Investigation, draft preparation

Conflicts of interest

The authors declare no conflicts of interest.

References

1. Hejazi, S. M., Sheikhzadeh, M., Abtahi, M. S., & Zadhoush, A. (2012). A simple review of soil reinforcement by using natural and synthetic fibers. *Construction and Building Materials*, 100-116.
2. Wu, T. H., McOmber, R. M., Erb, R. T., & Beal, P. E. (1988). Study of soil-root interaction. *Journal of Geotechnical Engineering*, 114(12), 1351-1375.
3. Vidal, H. (1969). *The Principle of Reinforced Earth*. Highway Research Board, Geology and Foundations, 1-16.
4. Ayraçma, B. B. (2015). *Sentetik Fiber ve Çimento Katkılı Kumların Mukavemet Özellikleri*. İstanbul Teknik University, Institute of Science and Technology, Master's Thesis.
5. Bao, X., Jin, Z., Xiao, X., Tang, W., Cui, H., & Chen, X. (2021). Experimental investigation on mechanical properties of clay soil reinforced with carbon fiber. *Construction and Building Materials*, 1-9.
6. Çetinkaya, M. (2012). *Polipropilen Liflerin Uçucu Kül Zemin Karışımlarında Geoteknik Özelliklere Etkisi*. İstanbul Teknik University, Institute of Science and Technology, Master's Thesis.
7. Fındıkçı, B. (2020). *Bentonit Kilinin Cam Fiber ile İyileştirilmesi*. Kocaeli University, Institute of Science and Technology, Master's Thesis.
8. Sevecan, Ü. (2009). *Polipropilen Fiber ve Uçucu Kül Katkılı Ankara Kilinin Geoteknik Özelliklerinin Araştırılması*. Kırıkkale University, Institute of Science and Technology, Master's Thesis.
9. Uysal, N. (2014). *Polimer ile Stabilize Edilmiş Kumların Kayma Mukavemetinin Laboratuvar Deneyleri ile Belirlenmesi*. İstanbul Teknik University, Institute of Science and Technology, Master's Thesis.
10. Ahmad, F., Bateni, F., & Azmi, M. (2010). Performance evaluation of silty sand reinforced with fibres. *Geotextiles and Geomembranes*, 93-99.
11. Al Adili, A., Azzam, R., & Spagnoli, G. (2012). Strength of soil reinforced with fiber materials (Papyrus). *Soil Mechanics and Foundation Engineering*, 241-247.
12. Babu, G. S., & Vasudevan, A. K. (2008). Strength and Stiffness Response of Coir Fiber-Reinforced Tropical Soil. *Journal of Materials in Civil Engineering*, 571-577.
13. Dang, L. C., Fatahi, B., & Khabbaz, H. (2016). Behaviour of Expansive Soils Stabilized with Hydrated Lime and Bagasse Fibres. *Procedia Engineering*, 658-665.
14. Nezhad, M. G., Tabarsa, A., & Latif, N. (2021). Effect of natural and synthetic fibers reinforcement on California bearing ratio and tensile strength of clay. *Journal of Rock Mechanics and Geotechnical Engineering*, 1-17.
15. Özdemir, B. (2019). *Doğal/Sentetik Lif ve Uçucu Kül Katkılı Killerin Bazı Geoteknik Özelliklerinin Araştırılması*. Atatürk University, Institute of Science and Technology, Master's Thesis.
16. Prabakar, J., & Sridhar, R. S. (2002). Effect of random inclusion of sisal fibre on strength behaviour of soil. *Construction and Building Materials*, 123-131.

17. Wang, Y. X., Guo, P. P., Ren, W. X., Yuan, B. X., Yuan, H. P., Zhao, Y. L., & Cao, P. (2017). Laboratory Investigation on Strength Characteristics of Expansive Soil Treated with Jute Fiber Reinforcement. *International Journal of Geomechanics*, 1-12.
18. Wei, L., Chai, S. X., Zhang, H. Y., & Shi, Q. (2018). Mechanical properties of soil reinforced with both lime and four kinds of fiber. *Construction and Building Materials*, 300-308.
19. Wu, Y. K., Li, Y. B., & Niu, B. (2014). Investigation of mechanical properties of randomly distributed sisal fibre reinforced soil. *Materials Research Innovations*, 953-959.
20. Consoli, N. C., Montardo, J. P., Prietto, P. M., & Pasa, G. S. (2002). Engineering Behavior of a Sand Reinforced with Plastic Waste. *Journal of Geotechnical and Geoenvironmental Engineering*, 462-472.
21. Edinçliler, A., & Cagatay, A. (2013). Weak subgrade improvement with rubber fibre inclusions. *Geosynthetics International*, 39-46.
22. Kalkan, E. (2013). Preparation of scrap tire rubber fiber-silica fume mixtures for modification of clayey soils. *Applied Clay Science*, 117-125.
23. Mirzababaei, M., Miraftab, M., Mohamed, M., & McMahon, P. (2013). Unconfined Compression Strength of Reinforced Clays with Carpet Waste Fibers. *Journal of Geotechnical and Geoenvironmental Engineering*, 483-493.
24. Muntohar, A. S., Widiyanti, A., Hartono, E., & Diana, W. (2013). Engineering Properties of Silty Soil Stabilized with Lime and Rice Husk Ash and Reinforced with Waste Plastic Fiber. *Journal of Materials in Civil Engineering*, 1260-1270.
25. Valipour, M., Shourijeh, P. T., & Mohammadina, A. (2021). Application of recycled tire polymer fibers and glass fibers for clay reinforcement. *Transportation Geotechnics*, 1-14
26. Pradhan, P. K., Kar, R. K., & Naik, A. (2012). Effect of Random Inclusion of Polypropylene Fibers on Strength Characteristics of Cohesive Soil. *Geotechnical and Geological Engineering*, 15-25.
27. Consoli, N. C., Bassani, M. A., & Festugato, L. (2010). Effect of fiber-reinforcement on the strength of cemented soils. *Geotextiles and Geomembranes*, 344-351.
28. Yetimoglu, T., & Salbas, O. (2003). A study on shear strength of sands reinforced with randomly distributed discrete fibers. *Geotextiles and Geomembranes*, 103-110.
29. Terzi, S. (2021). Killi Zeminlerin Kayma Direncine Bazalt Fiberin Katkısı. Sakarya University Institute of Science and Technology, Master's Thesis.
30. Kaniraj, S. R., & Gayathri, V. (2003). Geotechnical behavior of fly ash mixed with randomly oriented fiber inclusions. *Geotextiles and Geomembranes*, 123-149.
31. Ertuğrul, Ö. L., & İnal, F. (2021). Assessment of the artificial fiber contribution on the shear strength parameters of soils. *Advanced Engineering Days (AED)*, 1, 114-117.



© Author(s) 2022. This work is distributed under <https://creativecommons.org/licenses/by-sa/4.0/>



Determination of water quality in Hadim District of Konya (Turkey) and the investigation of disinfection efficiency

Sukru Dursun ^{*1}, Abdurrahman Sarcan ¹

¹Konya Technical University, Environmental Engineering Department, Türkiye, sdursun@ktun.edu.tr; asarcan_31@hotmail.com

Cite this study: Dursun, S., & Sarcan, A. (2022). Determination of water quality in Hadim district of Konya (Turkey) and the investigation of disinfection efficiency. *Advanced Engineering Science*, 2, 101-108

Keywords

Hadim
Konya
Drinking Water
Bacteria
Disinfection
Chlorination
Water quality

Research Article

Received: 17.01.2022
Revised: 27.02.2022
Accepted: 03.03.2022
Published: 14.03.2022



Abstract

Drinking and usage water of Hadim Town (Konya, Turkey) has been provided from underground water. For this reason, there is no any treatment method but only disinfection with chlorine is applied. In the scope of this study, it is intended to determine the characteristic of the water quality via some analysing method of the drinking and usage water and to explore the effectiveness of the existing disinfection method which is applied at present. Water has been analysed collected 200 water samples from 5 points selected in the central district of Hadim water mains system. Subsequently, analyses, which are intended for characterizing the drinking and usage water of Hadim district, have been conducted both in the territory and in the public health laboratories of Konya province. Furthermore, analyses have been conducted in order to determine to what extent and at what point is effective the selected disinfection method (chlorination). Consequently, it has been determined that, on account of its chemical specialties, drinking water of the Hadim district is suitable for the standards stipulated for our country. Nevertheless, bacteriologically, it has been determined that the quality of the water is low owing to coinciding with coliform type bacteria from time to time.

1. Introduction

There is no doubt that water, which has a very important place in the life and life of people and other living things, is an indispensable substance. Early humans chose areas where they could easily obtain water and protect themselves easily to settle. Throughout history, civilizations have developed more in areas with water resources. In order to benefit from these waters better and more, they seized the resources and built dams and dams on the river beds. The fact that the surface waters, which are easy and cheap to use, cannot meet the needs and become polluted quickly, have led people to benefit from underground waters by making galleries, wells and drillings. Increasing population, rapidly developing industry and rapidly increasing number of factories have caused people to turn their attention to regions with low population density. People settle, process, set up facilities, etc. While searching for lands for various purposes, they aimed to find water in such regions first of all. This means that the surface waters in the distance are tunnels, canals, etc. It is possible by transporting the groundwater in various ways and bringing it to the surface by making it possible to transport it in very costly ways such as for this reason, the phrase "water is life" has not been said in vain [1].

Only less than 1% of the total amount of water on earth can be used as drinking water. Existing drinking water resources, increasing population, rapidly developing industry and disappearing natural environment limit underground and surface drinking water resources. While groundwater is generally directly drinkable, surface waters, streams, streams, lakes and dams are generally not of directly potable quality. Their chemical structures

mostly depend on the lands they pass through and on which they are located, on the nearby factories and settlements. Especially those close to large settlements are significantly polluted [2]. All water sources can be used both as drinking water and for industrial purposes. The natural water resources that are widely used in the industry by applying the appropriate treatment process are surface and underground waters. Despite this, it is expected that the ground waters that filter through a thick soil layer are cleaner than the surface waters, but the dissolved salt content is higher [3]. The best waters are spring waters, which are not sufficient in terms of quantity. Well water is also generally of good quality. However, these are not enough to meet the water needs of big cities. Therefore, river, stream and lake waters are used to meet the water needs. Such waters are sufficient in terms of quantity but not sufficient in terms of quality [4].

Sönmez [5], in his study, took samples in three different periods, in November-2002, April-2003 and August-2003, in order to examine the existing quality, pollution dimensions and sources of Incesu-Dokuzpinar underground cold-water sources and whether they comply with the standards. made analyses to reflect its quality and pollution status. As a result of the study, according to the Water Pollution Control Regulation of Dokuzpinar groundwater, in November I. It has seen that the class provides quality water values, but some parameters exceed the limits in April and August. In order to improve the water quality and maintain its usability as drinking water, it is recommended to provide training for the creation of protection areas around the source and for the local people to carry out their activities more consciously. The most important harm of organic matter accumulation is that it causes oxygen deficiency [6]. As a result of wastewater from factories related to agriculture and food and domestic discharges, they carry a large amount of organic substances to the aquatic environment [7].

Since the presence of pathogenic microorganisms that cause disease in drinking water is not continuous, it is not a sure and safe way to investigate them. Coliform bacteria and *Escherichia coli* are searched for because their search is difficult, requires a long time, and the chance of detecting these pathogens is not always high enough. In other words, in bacteriological water examination, "indicator" bacteria living in the intestines of humans and warm-blooded animals and mixed with faeces and polluted waters are investigated. These bacteria, which are an indicator of pollution, are called "coliform bacteria" [8]. The absence of coliform bacteria in a water indicates that it is clean, and the presence of more than a certain number indicates that it is dangerous. Although coliforms do not pose a great danger directly, they inform the danger [9].

It is aimed to disinfect drinking water by any method and to prevent the spread of infectious diseases that spread through water. Disinfection process is very important especially for public health. The most well-known disinfection process is chlorination. Chlorine and chlorine derivatives are the most commonly used disinfectants. Since the chlorine demand of a water may vary under the influence of other factors, the amount of chlorine for bacteria in the water should be measured with the orthotolidin test from time to time and the presence of coliform bacteria should be checked [10]. The presence of *E. coli* in waters is a sign of the presence of harmful organisms. There are 10⁸ – 10⁹ *E. coli* in one gram of stool. For this reason, if *E. coli* is found when a drinking water source is analysed, it is understood that this source is contaminated with the faeces of humans, mammals and birds. The drinking water standard accepted for Turkey is the TSE TS 266 Drinking Water Standard and the Regulation on Water Intended for Human Consumption, which came into force after being published in the Official Gazette dated 17.02.2005 and Official numbered as 25730 [11].

This study is to determine the conformity of drinking and utility water quality to standards by examining some properties of drinking and utility water in the centre of Hadim district of Konya, which has a population of approximately 4000 people, in terms of chemical and bacteriological aspects. In addition, it is to investigate the effectiveness of the disinfection method used by the district municipality and used in the warehouses and distribution network and the disinfectant substance used in disinfection.

2. Material and Method

Hadim district center covers the drinking water network. On-site measurement and sampling points were selected according to the distribution of the areas covering the study area. At selected points, the physical, chemical and bacteriological parameters of the drinking water of Hadim district centre were measured both in the field and in the laboratory. Since Hadim district centre is small and accordingly the distribution network is short, it was deemed appropriate to choose 5 stations. For this reason, a total of 10 samples were taken, once a month for chemical analysis, and a total of 50 samples were taken from 5 points, once a month for bacteriological analyses, in order to monitor the quality changes in drinking water. In addition, in order to determine the residual chlorine ratio, a total of 200 samples were taken from 5 points, 4 times a month, once a week.

2.1. Study area

In this study, which was started on the basis of shopping centres located in Selçuklu district of Konya province, Hadim is one of the districts of Konya, located in the Central Anatolian region of our country, and is at the intersection of 37 degrees north parallel and 33 degrees east meridian in the northern hemisphere. Eunuch; It was established in a valley in the centre of the Central Taurus Mountains of Konya province, and its distance from Konya is 128 km. is at the same time, it falls within the borders of the Mediterranean region. Eunuch; It is in the

south of Konya. There is Karaman province in the east, Taşkent district in the south, Bozkır in the west and Alanya lands in the south-west of the district. The altitude of the district from sea level is 1500-1700 m [12].

Hadim drinking and utility water is supplied from Akdağ Spring in Akdağ location outside the district and Küçüksu spring in Gevne road junction area. The water coming from here is taken to various 6 collection areas in the district and collected in 3 main reservoirs that distribute to the network from here. While 15 L of water per second enters these tanks during the winter months, it drops to 8 L/sec in the summer months. Taşpınar meets the water needs of the district with its 370 m³, Hocalar 110 m³ and Lower hadim 90 m³ reservoirs. Only chlorination is carried out in these warehouses, which distribute through network pipes made of PVC, cast iron and asbestos material. The physical, chemical and bacteriological properties of water are not known exactly, both at the source where it originates and at the points where it is used in Hadim district. It has been determined that there is no previous study based on analysis on this subject. The warnings made by the health institutions in certain periods against the fact that it is not bad in taste and smell cause some people to obtain drinking water from small sources in the environment or ready-made. For this reason, with this study, it is aimed to reveal the situation of drinking water, which is important for public health, in Hadim and to ensure that necessary precautions are taken [12].

2.2. Water Sampling Method

The standards of TS 266 Drinking Water, TS 5089 Water Quality-Sampling Part-1: TS 5090 Water Quality-Sampling Part-2: Sampling Techniques were complied with in the collection [11, 13, 14], transportation and preservation of the samples. Containers used for bacteriological analysis; Black, sterile and capped glass bottles were used. While taking the sample, the mouth of the faucet from which the water will be taken was sterilized by burning with a flame. Afterwards, the tap was opened to the end and flowed for a few minutes, and after making sure that the water representing the mains water came, the sample cups were rinsed with tap water and filled so that there was no air gap.

2.3. Organic Matter

Calcium and magnesium carbonate in the soil's composition turns into bicarbonate and dissolves in water. For this reason, there is more dissolved matter in the calcareous layers than in the previous ones. The excess of acids in the waters is formed by the decomposition of organic matter. Ammonia and iron are also high in waters passing through layers rich in organic matter. Generally, in places where water passes, chlorides, alkali sulphates, calcium and magnesium sulphates and their carbonates, iron and manganese compounds dissolve first, respectively. As the water passes underground, dissolved and soluble substances increase, and other substances gradually decrease with the filtering function of the ground. This is especially important for microbes. The water that passes through the layers that act as a good filter is cleaned from bacteria very quickly. Since the water passing through the cracks is not well filtered, it has not been purified by bacteria [15]. The water that evaporates into the air in nature is naturally clean when it is in the form of steam in the air. But this water rain, snow, etc. As it falls to the earth, it becomes more or less polluted according to the degree of pollution of the atmosphere by taking the gases, dust, fumes, radioactive sprinkles and microbes in the air layers. From the moment it comes into contact with the soil surface, its load begins to increase in terms of microorganisms, organic and inorganic substances, depending on the characteristics of these places. It also absorbs human, animal and plant organic wastes, agriculture, industry, sewage and nuclear pollution while flowing on the earth or passing into the depths [16].

The most important harm of organic matter accumulation is that it causes oxygen deficiency [6]. As a result of the deterioration and decomposition of aquatic flora and fauna, dissolved organic substances are mixed into the lake waters. However, these substances have been found in large quantities in the aquatic environment, especially as a result of the growth and development of industry and cities, and the increase in tourism. As a result of wastewater from factories related to agriculture and food and domestic discharges, they carry a large level of organic substances to the aquatic environment [7]. Organic materials can enter waters from a variety of sources, including humans, animals, and plants. Organic substances of plant origin are unimportant as they are not harmful. Those of animal origin are also transmitted to the water by birds, fish and aquatic animals. Of these, the most dangerous are organic substances contaminated by humans and other cattle. Especially in the waters that come into contact with places such as sewage cesspools, cemeteries, manures, barns, poultry houses, organic materials are high. Organic materials are relatively less in spring waters. The oxygen required to burn organic substances in one liter of water does not exceed 1.5 mg. When this figure is less than 1 mg, the water is considered chemically clean [16].

For Determination of Organic Matter, it is based on the oxidation of organic substances in water by using permanganate in an acid medium. The oxidation ability of water is expressed by the mg of potassium permanganate or the corresponding mg of oxygen consumed to oxidize the oxidisable substances in 1 liter of water. 100 mL sample is taken. 10 mL of dilute sulfuric acid solution and 10 mL of adjusted potassium permanganate solution are added and left in the water bath for 30 minutes (The sample is placed in the water bath so that the water level in the flask and the water level in the water bath are the same). The sample is removed from

the water bath and 10 mL of ammonium oxalate solution is immediately added. While it is hot, it is titrated with the adjusted potassium permanganate solution until a light pink is obtained. The result is found in mg of oxygen per liter.

2.4. Coliform and E. coli Determination

Drinking water is usually disinfected using chlorine or ozone. For disinfection to be successful, all pathogens must be exposed to the chemical disinfectant used. Most harmful organisms are exposed to disinfectant in turbid waters. However, in case of turbidity due to domestic wastewater solids, it is highly likely that harmful microorganisms can survive in the flocs. Therefore, excessive use of disinfectant is required. This is also expensive. For these and similar reasons, it is desirable to have very low turbidity values in water to be used as drinking water.

The 'Standard Methods' method was used in the search and counting of Coliform and E. coli bacteria from bacteriological analyses. Estimation Experiment, Confirmation Experiment, Completion Experiment were carried out. First of all, for the estimation experiment, 0.1 ml, 1 ml and 10 ml water samples were placed in three tubes with Lactose Broth medium containing Durham Tubes, and kept in an oven at 37 °C for 24/48 hours. If there is gas at the end of the waiting period, it is said that it can be Coliform, and if there is no gas, it is said that there is no Coliform. For the confirmation experiment, Brilliant Green-Laktose medium was cultivated. As a result of sowing, it is kept in an oven at 37 °C for 48 hours. If there is gas, it is said that there is coliform. If there is no gas, it is said that there is no coliform [17].

The presence of E. coli was tested for the completion assay. For this, EMB (Eosin-Methylene Agar) medium was cultivated and incubated in an oven at 37 °C for 24 hours. E. coli is said to be present or absent depending on whether it gives the metallic green colour or not. Counting coliforms; It is made according to the Most Probable Number (MPN) method in 100 ml. By diluting the sample at 10% rate 3 times, 3 tubes of 10 ml, 1 ml and 0.1 ml are prepared [17]. Sowing is done in these three prepared tubes. Reproductive results are evaluated according to the table below.

Table 1. Coliform bacteria count calculation according to the MPN method [17].

10 ml sample	1 ml sample	0,1 ml sample	Results MPC/100ml
+	+	+	>240
+	+	-	240
+	-	+	95
+	-	-	23
-	+	+	19
-	-	+	9
-	-	-	1>

2.5. Evaluation of residual chlorine analysis results

The first option for testing uses a liquid chemical OTO (orthotolidine) that causes a color change to yellow in the presence of total chlorine. You simply fill a tube with water, add 1-5 drops of the solution, and look for the colour change. These kits are sold in many stores as a way to test the concentration of total chlorine in swimming pool water. This method does not measure free chlorine. Whether you use chlorine gas or sodium hypochlorite to disinfect the wastewater, both have one thing in common – in solution they are reactive and very unstable. The chlorine wants to change from a high oxidizing level to a more stable reduced one. Because of this it is impossible to preserve a sample for residual chlorine. Any sample taken for residual chlorine analysis must be tested immediately. According to EPA, this means the sample must be tested within fifteen minutes of collection [18].

As a result of the analyses made, in the 3rd week of June, 1st and 2nd week of July, 3rd and 4th week of August, 4th week of September, 1st, 2nd and 3rd week of November, December, no chlorine was found in the mains water in January, February and March. In the 1st week of September, it was found only in the 1st sampling point, but not in the others. In the 2nd week of September, it was absent in the 1st sampling point, while it was found in the others. In the 3rd week of September, it was found in the 5th sampling point, but could not be found in other points. It was found in the first 4th sampling point in the 1st and 2nd week of October, but it could not be found in the 5th sampling point. The amount of chlorine required in the samples taken at all other points was determined. According to the results and as a result of the researches, the disinfection method in the mains water of Hadim district is carried out randomly and far from scientific techniques.

3. Results and Discussion

Some physical-chemical and bacteriological properties of drinking and utility water of Hadim district (district centre) were examined and sampling and analyses were carried out in a 10-month period in order to determine its quality. The results of the analysis of the samples taken from 5 sampling points determined in the study area were arranged separately for each month. Among the chemical analyses, pH, conductivity, total hardness, chloride and organic matter parameters were evaluated separately and their graphs were drawn. Bacteriological analyses were also evaluated separately. The residual chlorine parameter, which is used to control the disinfection, was evaluated alone. Organic Matter analysis results between June-2007 and March-2008 were evaluated. In the drinking water network of Hadim district centre, the results of the organic matter analysis made in the 10-month period were found even at low values in certain periods. While organic matter was not found in July, November, December and February, it was found at low rates in other months. However, since these values are below the normal values; The drinking water of Hadim District centre is at the desired drinking water quality level in terms of organic matter.

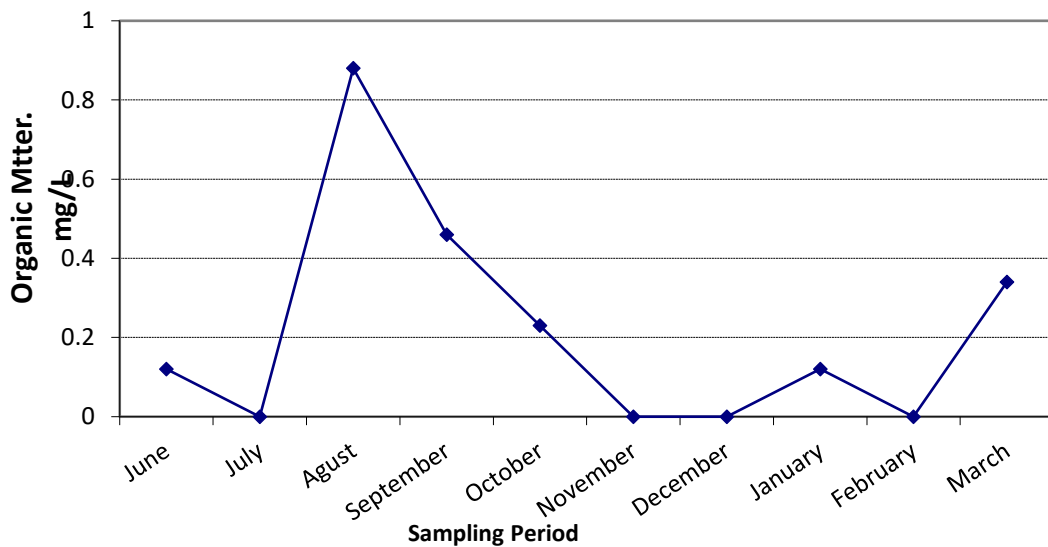


Figure 1. This is the example of table formatting

3.1. Bacteriological Analysis Results of Hadim Drinking Water Network Regarding Monthly E. Coli

The numbers of E. coli in 100 ml determined as a result of the bacteriological examination of the monthly water samples taken from 5 points are given in Table 2.

Table 1. E. coli results per 100 ml counted at points from June 2007 to March 2008

Sampling period	Sampling point-1 Prefecture	Sampling point-2 Central Pri. Sch.	Sampling point-3 Belediye Hotel	Sampling point-4 Hospital	Sampling point-5 A. Hadim Mosq
June	240 +*	240 +	240 +	240 +	240 +
July	240 -**	-	-	23	-
August	-	-	-	23 -	-
September	-	-	-	-	-
October	-	-	-	-	-
November	240 +	240 -	240 -	240 -	240 -
December	-	-	-	-	-
January	-	-	-	-	-
February	-	-	23 -	-	23 +
March	240 -	240	23+	23 +	240

* + sign indicates that reproduction continues; ** - sign indicates uraemia has stopped.

No bacteriological findings were found in the analyzes performed in September, October, December and January. In June and March, *E. coli* was found at all sampling points in the drinking water network. In the remaining months, while *E. coli* was detected at some points, it was not detected at some points. This suggests that the drinking water network was subsequently contaminated at some points. While the hospital point is the most polluted point bacteriologically, since five of the 10 measurements made, there is a pollution indicator, while the Central Primary School point was determined as the cleanest point with 3 pollution indicators.

As a result of the analyzes made, in the 3rd week of June, 1st and 2nd week of July, 3rd and 4th week of August, 4th week of September, 1st, 2nd and 3rd week of November, December, no chlorine was found in the mains water in January, February and March. In the 1st week of September, it was found only in the 1st spot, but not in the others. In the 2nd week of September, it was absent in the 1st point, while it was found in the others. In the 3rd week of September, it was found in the 5th position, but could not be found in other points. It was found in the first 4 spots in the 1st and 2nd week of October, but it could not be found in the 5th spot. The amount of chlorine required in the samples taken at all other points was determined. According to the results and as a result of the researches, the disinfection method in the mains water of Hadim district is carried out randomly and far from scientific techniques.

4. Conclusions and Recommendations

microorganisms. Depending on the occurrence of this decomposition event in an oxygenated and anaerobic environment, various decomposition substances are formed. If this decay event occurs in an oxygenated environment, odourless decay occurs. Here, carbon dioxide from carbon, sulfuric acid from sulphur, nitrite and nitrate acids from nitrogen are formed [15]. Calcium and magnesium carbonate in the soil's composition turns into bicarbonate and dissolves in water. For this reason, there is more dissolved matter in the calcareous layers than in the previous ones. The excess of acids in the waters is formed by the decomposition of organic matter. Ammonia and iron are also high in waters passing through layers rich in organic matter. Generally, in places where water passes, chlorides, alkali sulphates, calcium and magnesium sulphates and their carbonates, iron and manganese compounds dissolve first, respectively. As the water passes underground, dissolved and soluble substances increase, and other substances gradually decrease with the filtering function of the ground. This is especially important for microbes. The water that passes through the layers that act as a good filter is cleaned from bacteria very quickly. Since the water passing through the cracks is not well filtered, it has not been purified by bacteria [15].

The importance of reliable and quality drinking water for public health is known by everyone. Providing a quality drinking water for use is possible by showing the necessary attention and sensitivity at every stage, from the quality of the water at the source, to the proper disinfection and treatment process, to the storage and distribution of the water. However, if necessary, attention is paid to these issues, drinking water can be safely offered to the use of consumers. Relevant public institutions have important duties in this regard. In the studies carried out, samples were taken from 5 points determined within a 10-month period of the drinking water of Hadim district, and the results obtained as a result of the analyses are given below:

While evaluating the mains water in Hadim as drinking water, the TS-266 drinking water standards in force in our country are taken as basis. Accordingly, it was determined in accordance with the standards in terms of chemical parameters. According to the results, it can be called 1st class water since it will be given to drinking water without any treatment other than disinfection. According to TS-266, while there should be 0 coliform bacteria in 100 ml, it is seen that this is not achieved in most of the samples. The presence of *E. coli* at some points in the samples taken on the same day indicates that there is wastewater leakage into the network. Coliform bacteria, which is an indicator of pollution, is another important parameter in terms of public health. The absence of coliform bacteria in a water indicates that it is clean, and the presence of more than a certain number indicates that it is dangerous. Although coliforms do not pose a great danger directly, they do signal danger. Accordingly, the health of the people who use tap water in some periods may be in danger. According to the results of the analysis and the presence of coliform bacteria in the network, the disinfection process is not performed properly and remains insufficient.

The absence of disinfection in warehouses and networks in December, January, February and March carries a great risk for the public. The presence of chlorine in the samples taken from the points in some weeks indicates that the disinfection was carried out irregularly and uncontrolled during the months. According to the results, it is understood that the current disinfection system used is insufficient and ineffective in terms of protecting the health of the public. We can list the reasons why many water samples taken from the mains could not meet the drinking water standards in terms of bacteriology as follows:

Water resources are dirty or polluted in the area where they originate. Disinfection (Chlorination) is not done in accordance with scientific techniques. Since the network is very old and not constructed properly, there is leakage into the drinking water pipes either from the sewerage or wastewater puddles.

5. Suggestions

Suggestions to be considered in order to improve the drinking and utility water quality of Hadim district are given following:

In accordance with the Water Pollution Control Regulation [19-21]; Class AGW I and Class UGW II group wells, springs and infiltration galleries, from which groundwater is taken, are used for drinking water supply, no structures, solid and liquid waste discharge and passage are allowed at distances closer than 50 meters. In order to achieve this, the surrounding of the sources, which are completely unprotected, is 50 m. surrounded by barbed wire. When necessary, a second protection band should be created and construction, agriculture and animal husbandry should not be allowed. The increase in cherries in recent years also brings some chemical pollution. For this reason, awareness raising studies should be carried out for agricultural activities carried out in places close to the source and suggestions should be made for the use of natural fertilizers. Otherwise, the deterioration of high-quality water will not be prevented. Disinfection should be done in accordance with scientific rules. The purpose of disinfection is the destruction of pathogenic organisms and the prevention of water-borne diseases. Success in disinfection with chlorine; It depends on the type, density, contact time of the microorganism, pH value of the water, temperature of the water, and the presence of organic matter in the water. For a good disinfection, the turbidity should be low. For this reason, all these factors should be taken into account when chlorinating the mains water. In normal times, the minimum initial dose of chlorine to be given is 1.0 mg/L. If ammonium ions are present in the water, 6 mg/L chlorine is needed for 1 mg/L NH₄⁺. Studies have shown that 0.5–1 mg/L hypochlorous acid residue is effective for a contact time of 30 minutes [22]. Again, according to this information, the amount of chlorine added to the network is not always the same, and changes should be observed by observing. At least, chlorination doses should be adjusted by constantly monitoring ammonium ion analysis.

Persons responsible for disinfection application must be qualified and at least trained. Permanent staff should be assigned. Chemical, physical and bacteriological analyses should be done continuously and precautions to be taken for changes should be planned in advance. Urgent solutions should be sought for chlorination, which is not done in the face of freezing and excess water in winter. Necessary thermal insulation must be provided for the chlorinator. In addition, chlorination techniques should be investigated and a more effective technique and device suitable for the warehouse and network should be used. Extra new tanks should be made in order to remove chlorination and turbidity.

Acknowledgement

This paper has been prepared a part of Absdurrahman Sarcan Master Sc. Thesis, and presented at 1st Advanced engineering Days, Mersin-2021 [23].

Funding

There is no Research Found for this work.

Author contributions

Sukru Dursun: Conceptualization, Methodology, -Reviewing and Editing; **Abdurrahman Sarcan:** Investigation, Experimental work, Writing-Original draft preparation, Conclusion.

Conflicts of interest

The authors declare no conflicts of interest.

References

1. Canik, B. (1998). Hidrojeoloji. Ankara Üniversitesi Fen Fakültesi Jeoloji Müh. Böl. Yayını, Ankara
2. Gündüz, T. (1994). Çevre sorunları, Ankara Üniversitesi, Fen Fakültesi, Bilge Yayıncılık, Ankara.
3. Yalçın H., & Gürü M., (2002). Su Teknolojisi, Palme Yayıncılık, Ankara.
4. Uslu O., & Türkman, A. (1987). Su kirliliği ve Kontrolü, T.C Başbakanlık Çevre Genel Müdürlüğü Yayınları, Eğitim Dizisi 1, 360, Ankara.
5. Sönmez, G. (2004). Kayseri-İncesu-Dokuzpınar Su Kaynaklarının Kalitesi Ve Çevresel Etkilerinin İncelenmesi, Niğde Üniversitesi Fen Bilimleri Enstitüsü Çevre Mühendisliği Anabilim Dalı, Yükseksek Lisans Tezi, Niğde.
6. Egemen, Ö., & Sunlu, U. (1999). Su kalitesi. Ege Üniv. Su Ürünleri Fakültesi Yayınları, Yayın
7. Şengül, F., & Türkman, A. (1998). Su ve Atıksu Analizleri, TMMOB., Çevre Mühendisleri Odası Yayını, 285-6, 152 pp, İzmir, Turkey.


8. Özçelik, S. (1998). Gıda Mikrobiyolojisi Uygulama Kılavuzu, Süleyman Demirel Üniversitesi Ziraat Fakültesi, Isparta.
9. Kıvanç, M., Kunduhoğlu, B., Atik, S., & Malkaçoğlu, B. (1996). Eskişehir İçme ve Kullanma Sularının Bakteriyolojik Kirliliği, Ekoloji Çevre Dergisi, Sayı 19, Ankara.
10. Şengül, B., & Şengül, Ü. (1998). İçme Ve Kullanma Suyu Klorlama Teknikleri, Kayseri 1. Atıksu Sempozyumu Bildiri Kitabı, Kayseri.
11. TS 266 Drinking Water, Turkish Standard Institution, Ankara, Turkey
12. Isık, I. (2018). Lykaonia Bölgesi Kuzeydoğu Kesimi Tarihi ve Yerleşim Yerleri. SEFAD, 2018 (40): 191-206. DOI: 10.21497/sefad.515307
13. TS 5089 Water Quality-Sampling Part-1: Turkish Standard Institution, Ankara, Turkey
14. TS 5090 Water Quality-Sampling Part-2: Sampling Techniques, Turkish Standard Institution, Ankara, Turkey
15. Gamsız, E., & Ağacık, G. (1978). Su ve Analiz Metotları, Devlet Su İşleri Genel Müdürlüğü, Ankara.
16. Demirer, M. A. (1988). Besin Hijyeni- Su Hijyeni, Ankara Üniversitesi, Ankara.
17. UNEP/WHO (1996). Water Quality Monitoring - A Practical Guide to the Design and Implementation of Freshwater Quality Studies and Monitoring Programmes. Chapter 10 - Microbiological Analyses. Edited by Jamie Bartram and Richard Balance Published on behalf of United Nations Environment Programme and the World Health Organization, Geneva
18. Blokkera, M., Vreeburga, J. & Speight, V. (2014). Residual chlorine in the extremities of the drinking water distribution system: the influence of stochastic water demands. Procedia Engineering, 70(1), 172 - 180
19. Anonim, (2005). Water intended for human consumption, TS 266, Türk Standartları Enstitüsü (TSE). 17.Şubat.2005 tarihli Resmi Gazete, Ankara.
20. WHO (1984). Guidelines for Drinking - Water Quality, Volume II-III, Geneva.
21. Baltacı, F. (1998). Su Kalite Standartları, Devlet Su İşleri Genel Müdürlüğü Seminer Notları, Ankara.
22. Uslu, G., Ünlü, A., & Arslan, E. I. (1998). Elazığ Kenti Şebeke Suyu Kalitesinin Araştırılması, I. Atıksu Sempozyumu, Kayseri.
23. Dursun, S., & Sarcan, A. (2021). Determination of water quality in Hadim district of Konya (Turkey) and the investigation of disinfection efficiency. *Advanced Engineering Days (AED)*, 1, 75-77.



© Author(s) 2022. This work is distributed under <https://creativecommons.org/licenses/by-sa/4.0/>



The effects of the EU Green Deal harmonization policies in Turkey

Aziz Cumhur Kocalar*¹ 

¹Niğde Ömer Halisdemir University, Urban and Regional Planning Department, Türkiye, azizcumhurkocalar@gmail.com

Cite this study: Kocalar, A. C. (2022). The effects of the EU Green Deal harmonization policies in Turkey. Advanced Engineering Science, 2, 109-117

Keywords

Climate change
Economics
European Green Deal
Regional integration
Environment and Growth

Research Article

Received: 21.03.2022
Revised: 16.04.2022
Accepted: 22.04.2022
Published: 28.04.2022



Abstract

This study examines the highlights related to the adaptation process to the EU Green Reconciliation, and it deals with the economic findings related to the process. The method of the study is based on the interdisciplinary findings about process. The current steps of the process had been visualized, then conveyed in a simple and understandable way. The study also deals with the economic findings related to the same process on the literature of the economic with graphics. The study focuses on issues such as the results of environmental pollution created by the cement sector on a sectoral basis for international trade. It examines the affections of sectoral environmental pollution on the economy and its reflections on carbon pricing at the border and make predictions about the near future. The research is important in terms of illuminating the critical points of the compliance process of the EU Green Consensus on the reflections of our country.

1. Introduction

This study first examines the highlights related to the adaptation process to the EU Green Reconciliation. The research deals with the economic findings related to the process.

2. Material and Method

The highlights related to the adaptation process to the EU Green Reconciliation are process steps. The study first examines this developing process. The method of the study is based on the interdisciplinary findings about process. The current steps of the process had been visualized, then conveyed in a simple and understandable way.

The study deals with the economic findings related to the same process on the literature of the economic with graphics. The first material of the study is historical agreements on the process. These are international and national documents.

Paris Agreement has entered into force on 5 October 2016 after signing in 2015 [1]. The European Green Reconciliation (EGD) can only be put into effect in 2019 [2]. Turkey has published the Green Reconciliation Action Plan in 2021 [3]. The Paris Agreement of Turkey Paris has signed in 2021 again [4].

Turkey is now in this final process involving EGC and must speed up their preparation for transition. Turkey's participation in the party in the immediate past such as the following way in the following way (Figure 1).

In this final process from the Paris Agreement to Europe, the digital conversion will be determinant in this final process. The solutions that the process will provide is particularly important for the future. For this purpose, new moves must be seen in Turkey's policies.

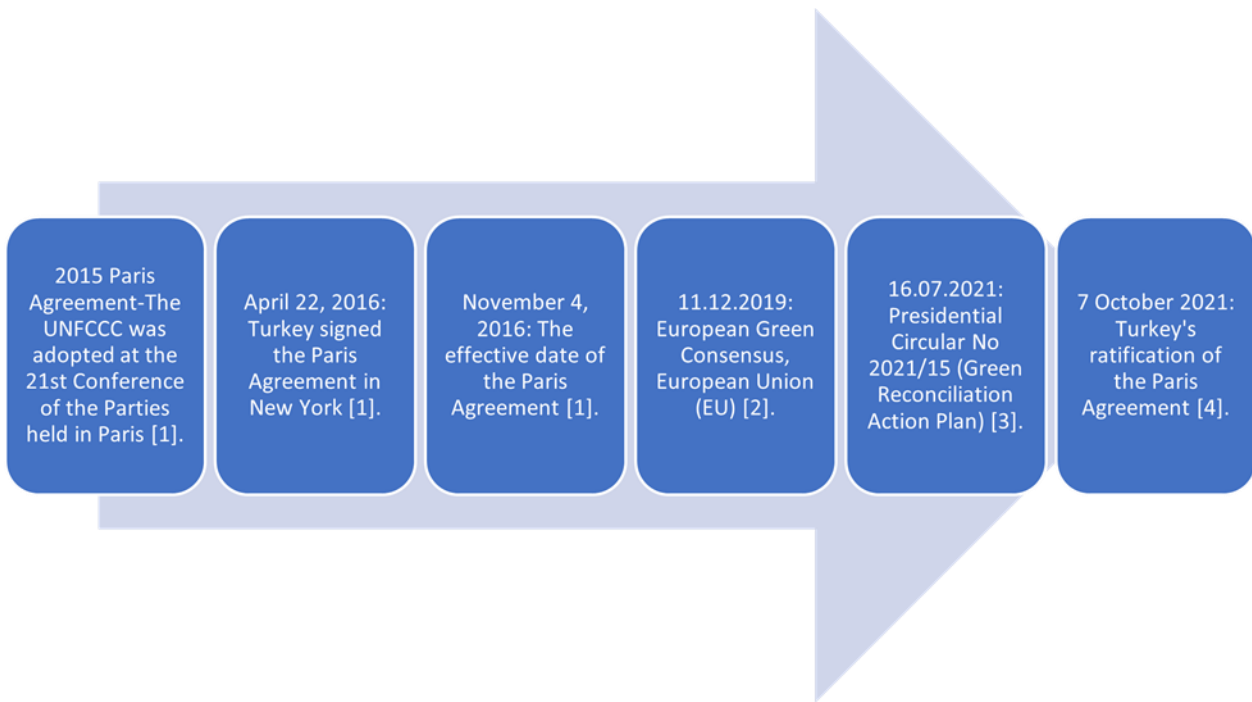


Figure 1. Turkey's accession to the party countries in the Historical Process from the Paris Agreement to the European Green Consensus.

Economic data is visualized with tables and graphs to facilitate clarity and country-product comparisons in findings part below. Besides process steps are also collected in a figure again for 2021 year (Figure 2).

3. Findings

Turkey's some tasks and events in 2021 are given in Figure 2.



Figure 2. Turkey's some tasks and events in 2021.

The Climate Council is also completed after serial meetings. This and another process summary also explained with the sub-titles.

3.1. Emissions reduction plan in long-term

Minister (Ministry of Environment, Urbanization and Climate) said that “There is a critical threshold in front of the world: to limit global warming to 1.5°C. To achieve the 1.5°C target, it is required that global emissions be reduced by 45% by 2030 and that net zero is achieved by 2050. The way to achieve this goal is for all countries to reduce by 7.6% each year by 2030” [5].

Countries join process promising dated to be carbon neutral and emission reduction (%) before (Table 1). Australia, Switzerland and Norway also promised date outside of EU, Turkey, China.

Table 1. Carbon Neutral Promise dated for Countries

Countries	Promise dated	% Emission reduction	Carbon Neutral
EU		50-55	2030
EU			2050
Turkey			2053
China	22.09.2020		2060

3.2. The COP26

Turkey attended the 26th COP (Conference of Parties). It held in Glasgow. Turkey attended it as a party to the Paris Agreement in December and we also hosted 21 Mediterranean countries in Antalya. At the same time, Türkiye have taken over the Presidency of the Secretariat of the Barcelona Convention for 2 years.

3.3. Climate Change and Adaptation Coordination Board Meeting

We held the Climate Change and Adaptation Coordination Board Meeting with members to determine plans, policies, strategies, and actions regarding climate change on January 11. There are members from different institutions, private sector, and civil society representatives in meeting.

3.4. The Climate Council 2022 Committees

The Climate Council 2022 committees established in line with the specified aim and their working subjects are as given in Figure 3.

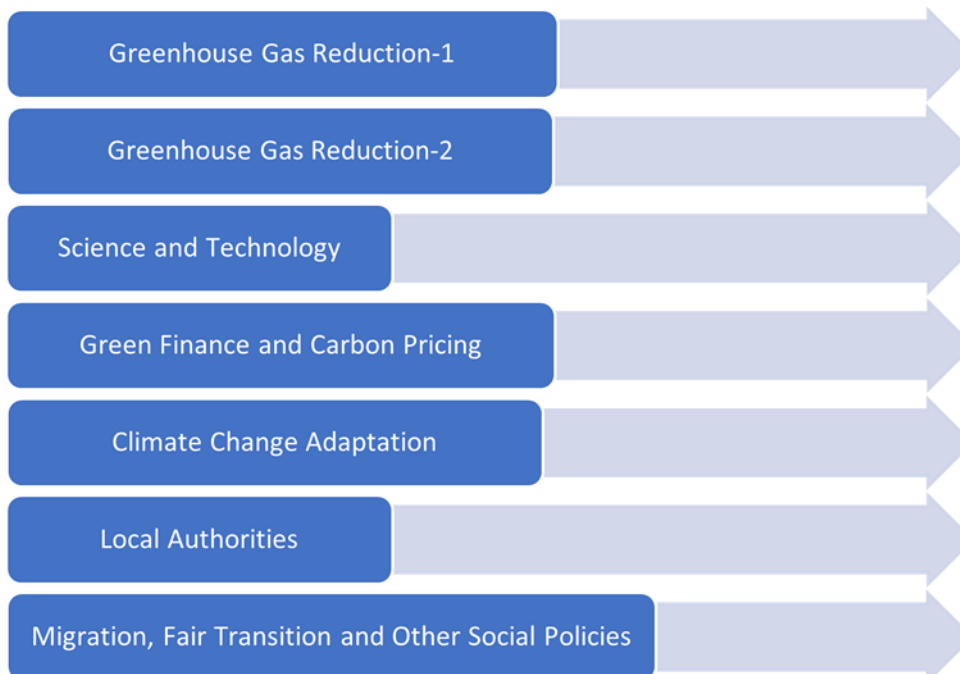


Figure 3. The Climate Council 2022 Committees Derived by the author, taken from the relevant source [6].

3.5. Turkey's Green Development Revolution

We held the Consultation Meeting, “Türkiye on the Road to Green Development” in Antalya. We shared our 11-point final declaration with our nation on the fields (Figure 4).

11-point final declaration	Climate change
	Zero waste
	Energy
	Finance
	Green technology
	Circular economy
	Low emission zones
	Social housing
	Urban transformation
	Green buildings
	Youth employment
Education mobilization	

Figure 4. 11-point final declaration with our nation on the fields.

3.6. 2053 Target for Turkey: Carbon Neutral

T.R. President announced our 2053 Carbon Neutrality target for Turkey at the UN General Assembly. Our roadmap and primary policies have been setting yet.

For GD (2021-2050); Expected cost of all conversions totalling €28 trillion (5% of annual EU national income) (included Energy, Transportation, Building Housing Industry Agriculture Infrastructure) [7-8].

3.7. New Strategies (Action Plan for 2022)

Nationally Determined Contribution and Long-Term Strategy and Action Plan for 2022 should be prepared immediately together. We will finish all consultations by the end of this year. We will also submit it to the Secretariat of the UN Framework Convention on Climate Change (UN FCCC) like that (Figure 5).

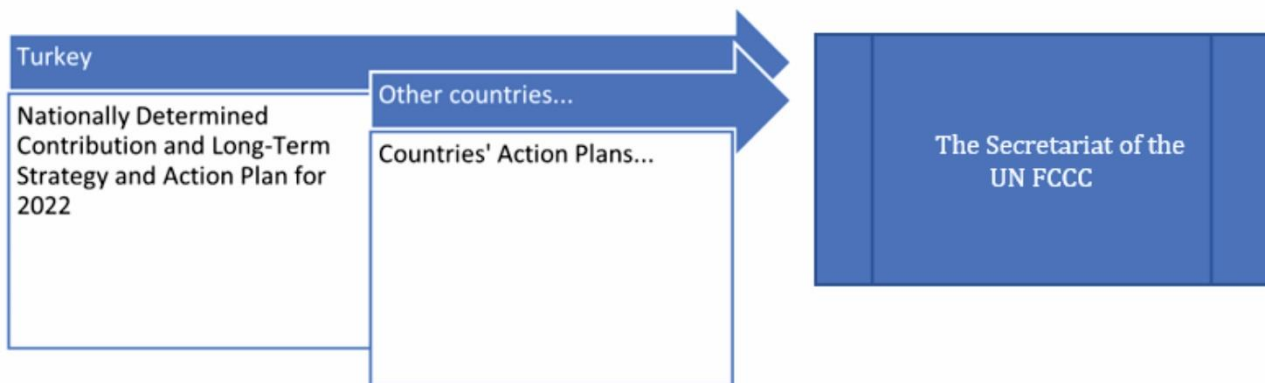


Figure 5. Turkey Strategy and Action Plan 2022 with Countries' Action Plans.

3.8. The Border Carbon Adjustment (BCA)

The European Union adopted a new growth strategy under the EU Green Agreement in 2021. In this case, the Border Carbon Adjustment is a vital issue for Turkey. Turkey's exports 45% to EU countries.

3.9. Draft of Climate Law Preparations

The council members and committees will reflect the scientific bases filtered from perspectives on 7 different fields on our Climate Law. Draft of Climate Law can be prepared after they will present all their studies to our assembly in detail.

3.10. Carbon Pricing with Statistical Data for Sectors (24#)

It is stated that if Turkey does not take precautions, it will be isolated in the extremely near future. According to 2018 data, Turkey is 4 times more polluting than the EU average (EU27 region) as shown in Figure 6.

$$17,5 \text{ (kg CO}_2\text{e/€)} = \sim 4 \times 4,5 \text{ (kg CO}_2\text{e/€)}$$

(CO₂e/€: Emission Pricing in €: Amount of CO₂e/€ released into the air per ton of product)



Figure 6. Turkey is 4 times more polluting than the EU average (2018) for electric energy sector emission density (CO₂e/Added Value) (kg CO₂e/€) Derived by the author, taken from the relevant source [8].

2# Bar: Blue: 2017; Orange: 2018.

In the Turkish economy, the electricity generation sector is seen as the sector with the highest emission density with 154.9 Mt CO₂e, which corresponds to a 34% share in total greenhouse gas emissions.

Statistical data cover 24# sectors and two categories for the carbon pricing in EU trade (million €) with a bar graphics below (Figure 7).

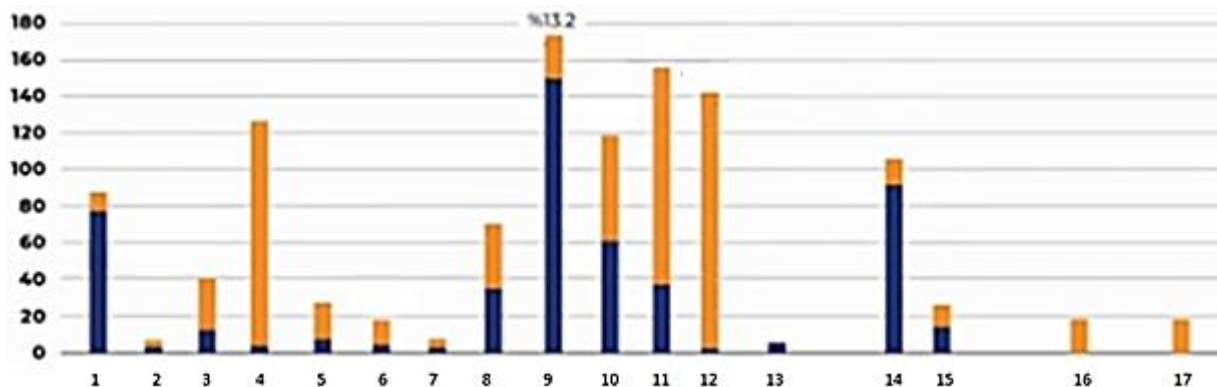


Figure 7. Carbon Pricing (Derived by the author) from the relevant source [8].

There are two categories in this graphic (Figure 7).

Categories:

Blue: Carbon cost (million €, EUA=30€) (directly affect) For example, Cement sector (9.bar), etc.

Orange: Carbon cost (million €, EUA =30€) (indirectly effect)

There are also some of 24# categories in this graphic (Figure 7). Cement sector is the biggest one between these 24# sectors (Table 2).

Table 2. Sector list in Figure 5 [8].

Sectors				
1.Agriculture	6.Paper	11.Machine	16.Transportation	21.Finance
2.Mine	7.Oil	12.Automotive	17.Airline	22.Tourism
3.Food	8.Chemistry	13.Electricity	18.Mail	23.Education
4.Textile	9.Cement	14.Construction	19.Accommodation	24.Health
5.Other	10.Iron-Steel	15.Retail	20.Service	

Scenario-A: Total carbon cost also defines with two categories sum in all sectors. It is **1085** million € (Table 3).

Scenario-B: Total carbon cost also defines with two categories sum in all sectors. It is **1809** million € (Table 3).

Scenario-A: If the tax per ton (EUA) is 30 Euros, 478 million Euros - **1085** million Euros

Scenario-B: €797 million – €**1809** million even if the tax per tonne (EUA) is €50

Total carbon pricing with two categories (1, 2) in all sectors are shown in Table 3.

Table 3. Total carbon pricing with two categories (1, 2) in all sectors.

	Scenario-A	Scenario-B
Categories	Million €	Million €
EUA €	30	50
1	478	797
2	607	1012
1+2	1085	1809

Derived by the author, taken from the relevant source [8].

GDP (billion TL) graphs for 30 and 50 categories with 2018 price in Border Carbon Regulation (BCA) is given by figure below (Figure 8).

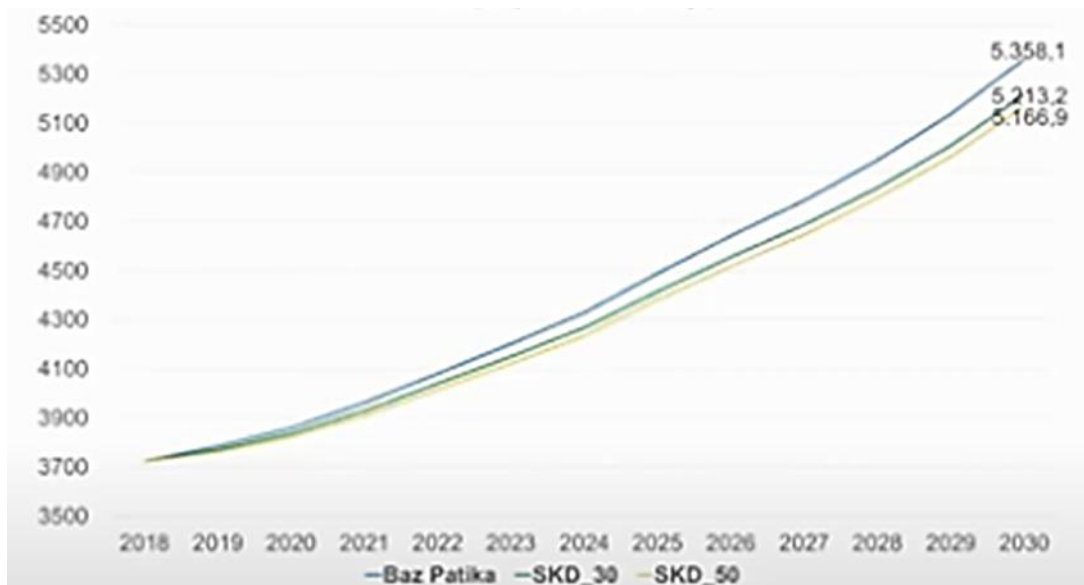


Figure 8. 3# GDP (billion TL) * graphs for 30-50-Base categories with 2018 price in Border Carbon Regulation (BCA) [8].

Total Carbon (CO₂) Emission graphs (million ton) for €30- €50-Base categories are given in Figure 9.

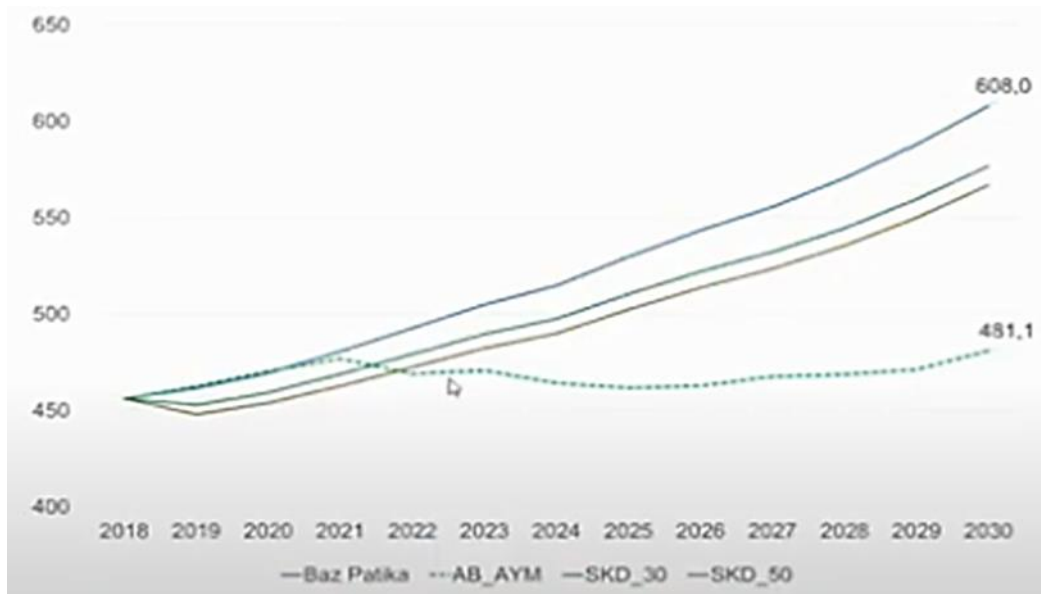


Figure 9. Total Carbon (CO₂) (million ton) Emission graphs for 30-50-Base categories [8].

4. Results

The study focuses on issues such as the results of environmental pollution created by the cement sector on a sectoral basis for international trade. It examines the affections of sectoral environmental pollution on the economy and its reflections on carbon pricing at the border and make predictions about the near future.

For the EU, since carbon regulation will partially shift production abroad, it is a loss of production and employment. However, when the sectors that must reduce emissions in the EU go abroad, this obligation will not be eliminated, so they will be able to keep their current emissions at a global level and keep them low (carbon leak). In an analysis, the weighted effects of the sectors on each other were also discussed with a network structure modelling [8]. The effects of the regulations in Turkey were also analysed numerically with this modelling.

The data will also be fully equipped with time in concrete and relational context in time. As can be foreseen from field examples in Turkey, the general situation is quite thought provoking. Especially in recent years, increased immigration from rural areas to metropolis continued to develop rapidly and irregularly.

On the other hand, measurement processes are rapidly approaching according to EGC criteria. Countries that supply products from Turkey to abroad will also comply with EGC criteria. In 2023, carbon footprint calculations will be started at 2023. Activities are known to be evaluated in this context. For example, wastewater, renewable energy etc. Therefore, the concrete and accurate measured documents will be revealed. First, models based on these measurements should be determined.

It is a fact that tax items to be paid for carbon emissions have also begun to gain visibility. For this purpose, the institutions, and organizations of the state acted (Ministry of Commerce and so on).

The action plan was prepared and published. In this process, the stakeholder institutions and their related tasks need to become clear. Thus, the relevant activities will be executed within the areas of more definite responsibility.

5. Discussion

EU-Green Deal (GD) is aimed:

- Don't leave anyone behind.
- Financial support.
- New targets and investments.
- Alignment with EU climate policies.

Today is entered into a smart transformation process. After the EGC approval, this interaction should be increased through the existing trade with the EU. Therefore, digital transformation approaches should be confirmed and verified. This transformation in institutional structures started in the 2000s and continues to increase to the present day.

What should be done?

- Smart approaches will be very important.
- Realism and analysis of country realities will be at the forefront.
- Follow and adapt developments
- Constantly re-evaluating opportunities and threats
- Recognize and better use flexibility mechanisms
- Developing new scenarios by prioritizing national interests

6. Conclusion

The need to increase global efforts for a sustainable world by all stakeholders at all levels has become increasingly evident in recent years. The reflections of the social and economic crisis created by the COVID-19 pandemic in 2020 further reinforced this process. In the recovery period after the COVID-19 crisis, the building of a sustainable and inclusive global economy is the priority agenda of the international community. In addition to all these, it is seen that an increasing number of international companies and investors are aiming to accelerate the transition to a low-carbon, green economy by determining green transformation roadmaps. Among these initiatives are the Zero Emission Race [9], to which 1397 companies and 74 investors have participated under the umbrella of the United Nations, and RE1002 (Renewable Energy 100) [10], to which 280 companies have participated. The research is important in terms of illuminating the critical points of the compliance process of the EU Green Consensus on the reflections of our country.

Capacity increases in all action categories in developing commercial activities in the world and Turkey are also highly evident. This complexity of commercial processes is increasing. Recent commercial processes have also made mixed professional groups stakeholders. This constantly increases the interaction between stakeholders. Therefore, the coordination of processes must be facilitated by utilizing information and communication technologies.

Problems with the issues drawn in the study can only be overcome by effective and timely plans. The difficulties arising from increasing competition in international trade are the most important of these problems. For this purpose, Turkey's economic planning, public administration and politics were required to start making new moves.

Other technical details exceeding the boundaries of the work will be the subject of recent studies.

Acknowledgement

This study was partly presented in 2nd Advanced Engineering Days [11].

Funding

This research received no external funding.

Conflicts of interest

The authors declare no conflicts of interest.

References

1. Paris Agreement of 2015, 21st United Nations Climate Change Meeting (COP21), Paris. (Effective on November 4, 2016).
2. European Green Consensus dated 11.12.2019, European Union (EU).
3. Presidential Circular dated 16.07.2021 and numbered 2021/15 (Green Reconciliation Action Plan) (O.G. dated 16.07.2021 and numbered 31543).
4. Turkey's becoming a party to the Paris Agreement upon its approval by the Grand National Assembly of Turkey on 7 October 2021.
5. The Climate Council (2022). Internet Web Site, <https://iklimsurasi.gov.tr/en/sayfa/opening-remarks-of-mr-minister>, Access date: 10.04.2022.
6. The Climate Council (2022) Internet Web Site, <https://iklimsurasi.gov.tr/en/sayfa/the-aim-and-goals-of-the-council>, Access date: 10.04.2022.

7. TÜSİAD, (2020). New Climate Regime Report from the Lens of TÜSİAD Economic Indicators, (Ekonomik Göstergeler Merceğinden Yeni İklim Rejimi Raporu), 21 September 2020.
<https://tusiad.org/tr/tum/item/10634-tusi-ad-in-ekonomi-k-gostergeler-mercegi-nden-yeni-i-kli-m-reji-mi-raporu-tanitildi>, Access date: 10.04.2022.
8. Yeldan, E., Aşıcı, A. A. & Acar, S. (2020). TÜSİAD New Climate Regime Report Launch Webinar from the Lens of TÜSİAD Economic Indicators, Mod. Fatih Özkadı, 22 September 2020,
https://www.youtube.com/watch?v=ZtJ_3thifZY, Access date: 10.04.2022.
9. Race to Zero Campaign, <https://unfccc.int/climate-action/race-to-zero-campaign#eq-4> , 2 Ocak 2020, Access date: 10.04. 2022.
10. RE100, <https://www.there100.org/>, 2 January 2020, Access date: 10.04. 2022.
11. Kocalar, A. C. (2022). The effects of the climate crisis and adaptation policies: The Green Consensus. *Advanced Engineering Days (AED)*, 2, 96-98.



© Author(s) 2022. This work is distributed under <https://creativecommons.org/licenses/by-sa/4.0/>



On behalf of an intelligent approach based on 3D CNN and multimodal remote sensing data for precise crop yield estimation: Case study of wheat in Morocco

Khadija Meghraoui ^{*1}, Imane Sebari ^{1,2}, Saloua Bensiali ³, Kenza Ait El Kadi ^{1,2}

¹Unit of Geospatial Technologies for Smart Decision, Hassan II Institute of Agronomy and Veterinary Medicine. Morocco, k.meghraoui@iav.ac.ma, i.sebari@iav.ac.ma, k.aitelkadi@iav.ac.ma

²Cartography and Photogrammetry Department, School of Geomatics and Surveying Engineering, Hassan II Institute of Agronomy and Veterinary Medicine. Morocco, i.sebari@iav.ac.ma, k.aitelkadi@iav.ac.ma

³Department of Applied Statistics and Computer Science, Hassan II Institute of Agronomy and Veterinary Medicine. Morocco, s.bensiali@iav.ac.ma

Cite this study: Meghraoui, K., Sebari, I., Bensiali, S. & Ait El Kadi, K. (2022). On behalf of an intelligent approach based on 3D CNN and multimodal remote sensing data for precise crop yield estimation: Case study of wheat in Morocco. *Advanced Engineering Science*, 2, 118-126

Keywords

Crop yield
Yield estimation
Deep learning
Remote sensing
CNN

Research Article

Received: 09.07.2022

Revised: 22.09.2022

Accepted: 30.09.2022

Published: 11.10.2022



Abstract

Agriculture is a key sector in the global economy, and crop yield is a primary element in this field. Its estimation represents a troublesome task considering its link to market planning. Different techniques have been tested to estimate crop yield. However, they present several limits in terms of human effort and time. The agricultural world is now experiencing a digital revolution, for example the utilization of UAV (Unmanned Aerial Vehicle) provides high-resolution images of crops. Besides this, artificial intelligence techniques namely, DL (Deep Learning) enables today a revolution of the flow processing and improves the resulting information. This paper presents a case study of wheat yield estimation in Morocco using UAV multimodal remote sensing data and 3D CNN (3D Convolutional Neural Network). Our data was acquired during the growth season, and predicted yield was compared to in situ data. Based on our results, the RMSE value was 0.175 qx/ha. Our conclusions highlight the efficient role of convolutional neural network in capturing features in raw image data and the importance to improve resulting predictions by acquiring data over the entire period of growth, and the necessity to choose a temporal architecture, which is able to process temporal variations.

1. Introduction

Agriculture provides food, fuel, and natural substances, which are all fundamental for human life [1]. To meet this demand, farmers and policymakers are working hard to improve crop yield. Despite the existence of many possibilities of cropland extension [2], the accentuation ought to be on increasing the production within the actual agricultural lands to avoid harmful effects on the environment. Recent advances in sensor technology have infiltrated agriculture, so different remote sensing systems are now available and allow generating data and providing relevant results to optimize a variety of agricultural products. These systems provide temporally relevant spatial data on land surfaces at different scales [3]. Generally, the main objective of precision farming is improving the quality and optimizing the production processes of crops [4] and this by reducing environmental pollution and costs. The utilization and application of new technologies has resulted in a transformation of crop management from a qualitative science based primarily on observations to a more quantitative science based on measurements, including a variety of production factors such as soil, climate conditions, and irrigation

management, that all have a significant impact on potential yield and growth, leading to the optimization of agricultural production. Total population is estimated to be more than 9 billion by 2050 [5], also current agricultural yields should increase up to 50% per unit in order to ensure food security. So as to achieve food safety and security, several stakeholders including national and international authorities, farmers, and other business units, expressed appreciation for timely and reliable information about crop management, production, and yield [6].

For a long time, yield squares have been among the conventional techniques for estimating agricultural yield. The principle of this method is the exploitation of a sample with square geometric shape which is placed at random in a plot to count all the plants that are in it [7]. To lay these squares, we determine the area of the plot as well as identify diagonals and location of samples. For a plot of minimum 1ha, each diagonal must have 5 plots while avoiding the edges, whereas plots having an area of less than 1 ha, it is necessary to place 2 to 3 squares per diagonal, without having less than 4 squares in total. In the end, to calculate the yield using the square, we divide the total amount of harvest weighted by the area of the considered yield square. Crop models aim to simulate the growth of agricultural crops [8]. They can work at different scales and help replicate key plant growth processes as well as the development in detail, and could therefore be used to determine crop yield [9] without forgetting the quantification and impact of individual factors in determining agricultural yield. To make future estimates and determinations, statistical models have been mainly used to develop an empirical relationship, combining a large number of current season yield characteristics with historical yield data [10]. More than a linear regression approach for predicting crop yield has been developed and used by studies dealing with estimating crop yields.

Remote sensing has facilitated crop monitoring by providing continuous data over large areas [11]. It offers the advantages of non-destructive, rapid and more profitable surveillance [12]. Satellite systems such as Sentinel and Landsat provide temporally interesting spatial data on visible land surfaces at very large scales [3]. Even though satellite images have been used extensively in estimating crop yield, we are facing many issues that still require resolution. For example, satellite images with high spatial and temporal resolution are rarely obtained at the same time [12], and sometimes it is not possible to obtain valid data during the critical phase of growth due to bad weather conditions. Remote sensing is now witnessing the expansion of UAV systems that have been rapidly developed and applied in the estimation of crop yield at the farm-scale over the past few years [13]. UAV platforms provide a cost effective and efficient way to meet the increasing demands of spatial, temporal and spectral resolution. Unlike satellites, Unmanned Aerial Vehicles are able to carry sensors at low cost and operate on very flexible schedules [14]. Drones data have been widely tested for agricultural monitoring of sugarcane, sunflower, soybean and triticale [12], as well as for forecasting yields of rice, wheat [15] and barley. Remote sensing sensors mounted on drones include RGB, NIR and multispectral cameras. With the advancement of imaging technology, hyperspectral cameras have gradually been equipped on drones to acquire remote sensing data which will make it possible to obtain more spectral bands and precise spectral information, and consequently improve the precision of the monitoring.

In recent years, deep learning has proven to have a significant advantage in agriculture, especially in estimating yield. Mu et al. [16] reported that deep learning, specifically the convolutional neural network, has the ability to extract specific characteristics of crop growth, and used it with multitemporal MODIS (MODerate resolution Imaging Spectroradiometer) data to predict winter wheat yield. Their results showed that winter wheat yield based on remote sensing time series images correlates strongly with yield, having Pearson R and RMSE values of 0.82, 724.72 kgh.m⁻², they conclude that CNN represents an essential technical reference for the large-scale crop yield while Wang et al. [17] estimated the winter wheat yield using LSTM (Long Short-Term Memory) networks for meteorological data with AVHRR (Advanced Very High Resolution Radiometer) inputs and convolutional neural networks for static soil characteristics inputs. Their model performed well, with an overall R² and an RMSE of 0.77 and 721 kg/ha, respectively. Garcia et al. [18] determined corn yield using UAV images with different multispectral vegetation indices, RGB, canopy cover and plant density in a multilayered perceptron model, their results demonstrated that neural networks had a high correlation coefficient and the spectral data collected by remote sensors mounted on UAV and processed into vegetation indices, canopy cover and plant density data is extremely useful and have more sense for agricultural characterization and estimation. Other authors tested deep learning approaches to predict rice yield, for instance Yang et al. [19] explored the ability of high resolution RGB images from drones with convolutional neural network and a new deep learning architecture with deep feature decomposition. Results demonstrate that the proposed network is more robust than the network without in-depth decomposition of the characteristics.

Through our study, we want to focus on methods for an intelligent estimation of agricultural yield, and present a case study carried out in Morocco, especially to estimate wheat yield, and the precision application of artificial intelligence, more particularly CNN architecture. Our study will present the results of 2D (two-dimensional) CNN applied to multispectral UAV data acquired during the season, and propose another architecture that can explain more yield variability, which is the third dimension of convolutional neural network.

2. Material and Method

In this section, we will present the area where our study was conducted and the main steps of our methodological workflow, starting from the UAV used for our acquisition, the followed methodology, and a description of the deep learning architecture used and our proposed model with its different layers.

2.1. Study Area

Our study area is located in the heart of Morocco, more precisely the region of Rabat Sale Kenitra ($34^{\circ}02'N$, $6^{\circ}50'W$), which is known for its cereal production. It is one of the best-ranked regions for the annual production of this type of crops.

This region has several important natural resources, in particular those of the forest, in this case we have the Maamora forest, as well as an activity and a large-scale agricultural sector. It alone holds almost 11% of the useful agricultural area of the country with a greater contribution to the national cereal production. [Figure 1](#) indicates the location of the considered region in Morocco country.

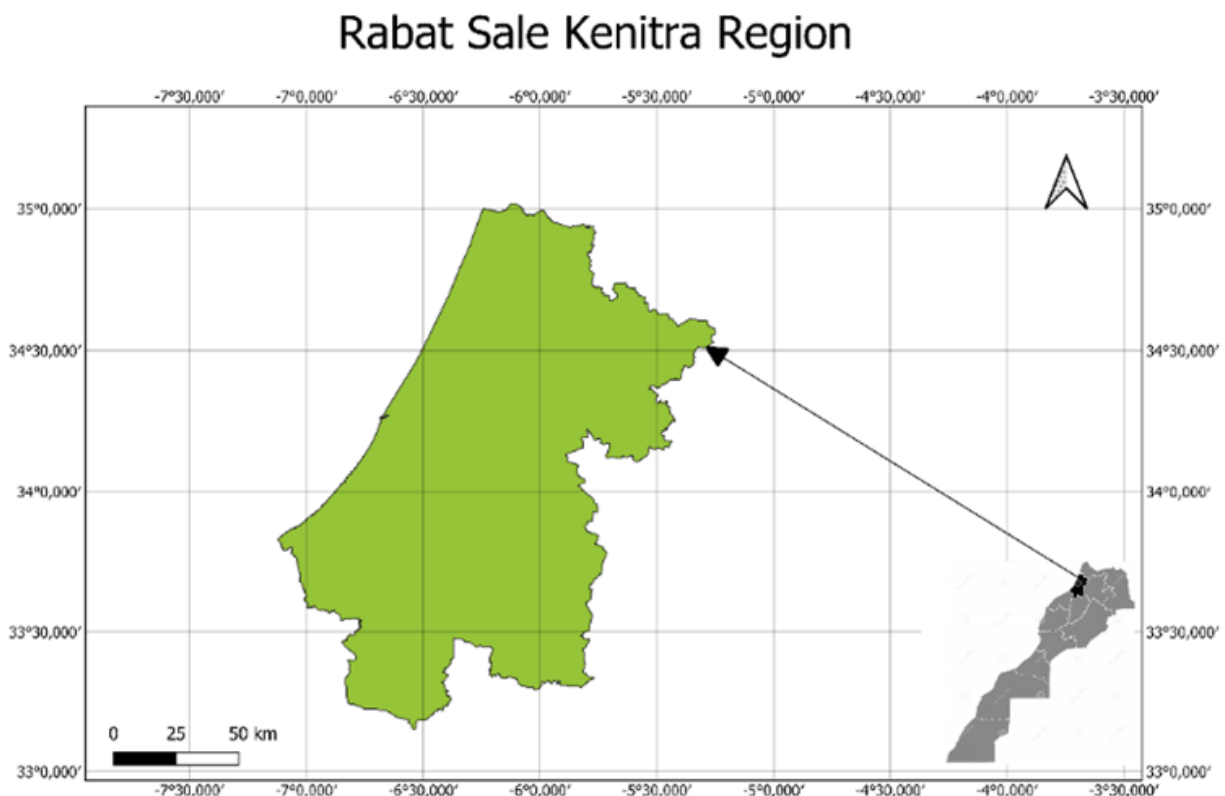


Figure 1. Localization map of the study area

2.2. Data acquisition and processing

Our study focused on estimating wheat yield in Morocco by exploiting remote sensing data. We started our methodology by acquiring UAV imagery with a HAGL (Height Above the Ground Level) of 60 m, and the processing of resulting images, then the extraction of necessary informations. Ground field yield collection was done, with a view to calibrating the model. The use of deep learning is especially proposed to capture the non-linearity that exists between yield data and predictors; in particular, convolutional neural network is proposed to process and extract features from our input images. A detailed methodological diagram is presented in [\(Figure 2\)](#). Remote sensing data was collected by a multispectral drone during the growth period, a single flight was performed, and a total of twenty plots were captured. All the plots considered in our study include wheat. Multispectral data was generated using the eBee Classic with MultiSPEC 4C as a camera, it is a special drone developed for precision agriculture [\(Figure 3\)](#). Almost hundred images covering all the plots have been acquired. Data processing was done in Pix4Dmapper, which allow us to generate orthomosaics by spectral band and also DSM (Digital Surface Model), and other special products especially for precision agriculture, for example reflectance maps and vegetation index maps.

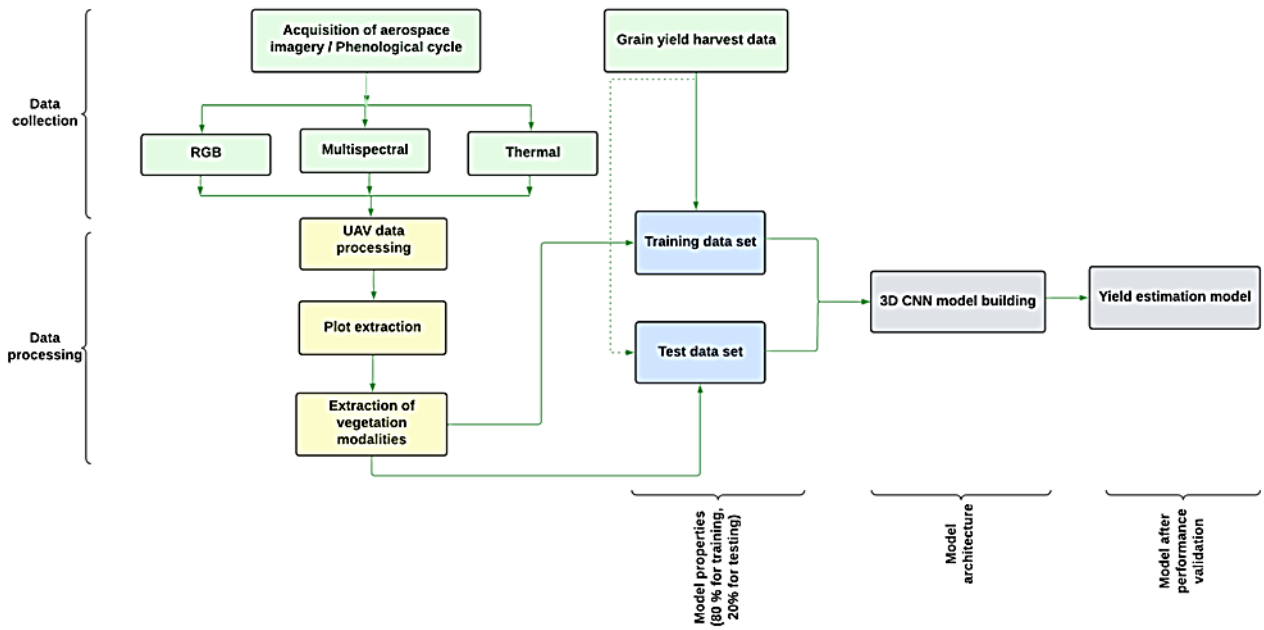


Figure 2. Methodological workflow of our study

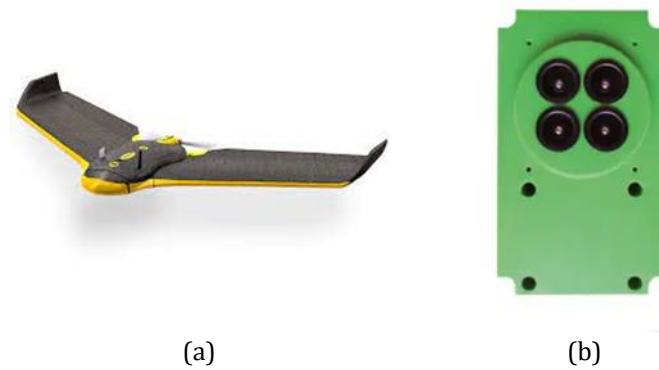


Figure 3. (a) eBee Classic UAV. (b) MultiSPEC 4C camera used

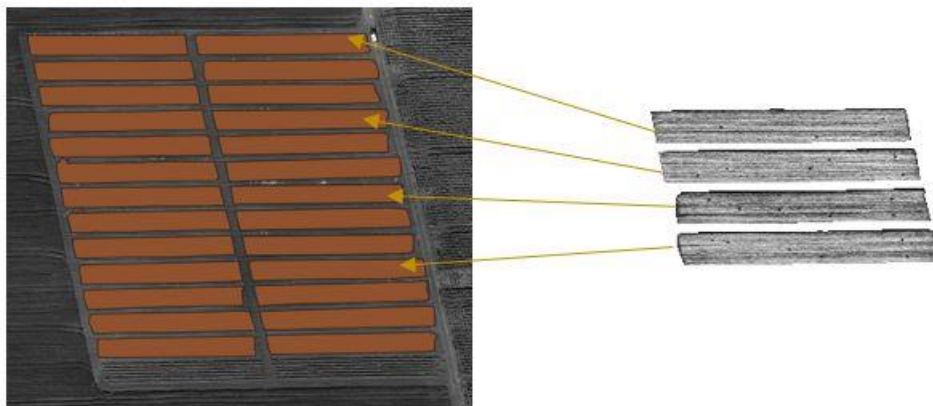


Figure 4. Shape of extracted plots

2.3. Convolutional neural network model

Artificial intelligence is an emerging technology that makes it possible to imitate human intelligence. It is based on the creation of applications and executable algorithms in computers and dynamic environments. It also makes it possible to meet a main goal, which is making computers able to act like human in terms of decisions in front of a special task.

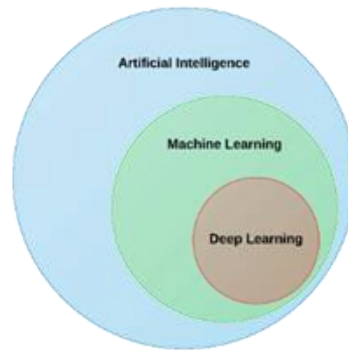


Figure 5. Artificial intelligence, machine learning and deep learning [20]

Machine learning is a branch of artificial intelligence that allows computers to solve tasks without having to be programmed in detail.

Deep learning another field of AI (Artificial Intelligence) is a sub-branch of machine learning, and a particular form of ANN (Artificial Neural Networks) which has the particularity of being deep [21]. It is generally composed of an input layer, two or more hidden layers and an output layer. Figure 6 shows us the structure of this architecture. Here the depth is represented by the number of hidden layers. DL is one of the fields that have shown a great revolution through the different architectures, in particular convolutional neural networks [7], recurrent networks [22] and other more advanced architectures [23].

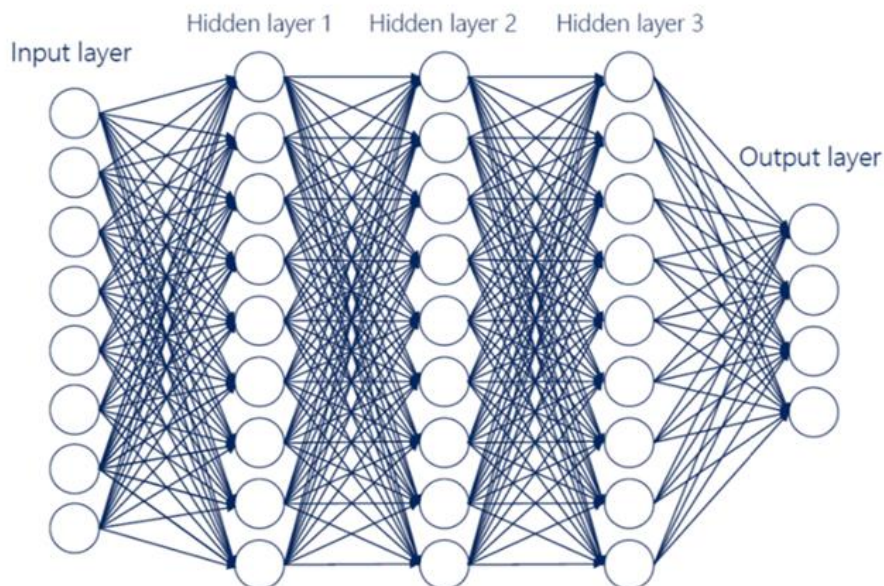


Figure 6. Deep Neural Network architecture [24]

The convolutional neural network architecture is one of the very advanced revolutions of this technology. Indeed, it allows an extraction of what is called features from images. A CNN model mainly comprises several layers of different natures namely [25]:

Convolution layer: which perform convolution operations on the input images and generate nonlinear activation maps.

Pooling layer: which aim to decrease the size and dimensions of the feature map and keep the main changes from feature maps. It is much more a compression role of this layer.

Flatten layer: A flatten layer has the role of creating a one-dimensional output from its inputs, and this to allow its use by the next layer which is the fully connected layer.

Fully connected layer: This layer is placed at the end of the CNN architecture; it allows to generate results relating to the tasks of classification or regression on the basis of its inputs.

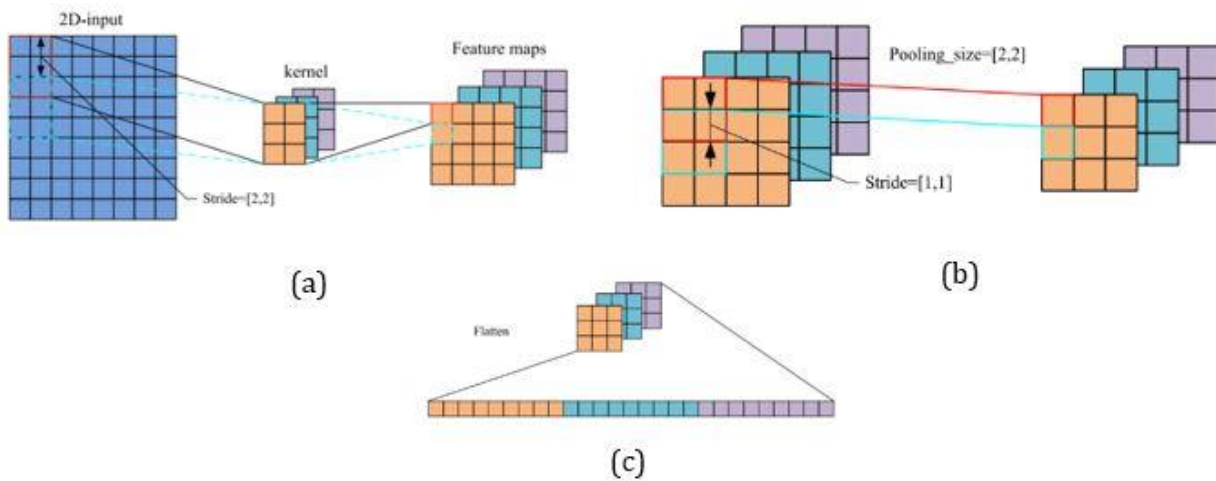


Figure 7. (a) Convolution layer (b) Pooling layer (c) Flatten layer [26]

3D convolutional neural network is an architecture generally characterized by a capacity for processing both spatial and temporal data [27], and this thanks to the addition of a dimension allowing the processing of time series. Using three-dimensional filters, 3D CNN performs a convolution on images while considering their appearance in different temporal resolutions. In the case of a 3D CNN architecture, the results are 3D maps, which will be the input of the next layer of pooling as in a simple convolution neural network. Figure 8 shows us this architecture.

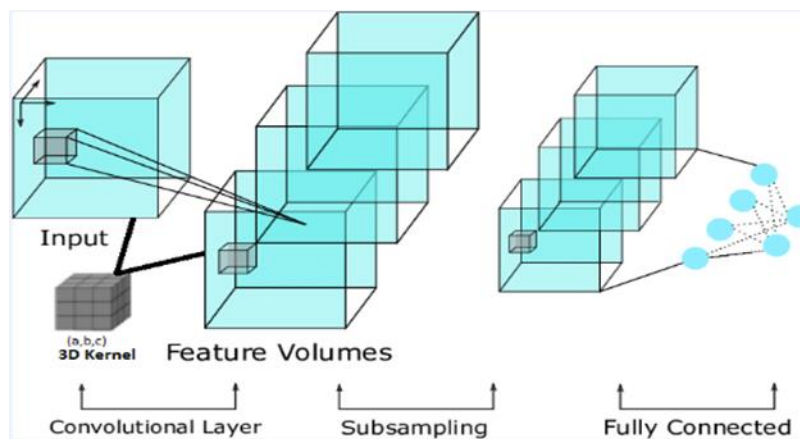


Figure 8. Convolutional neural network architecture used (modified from [28])

For the parameterization and the configuration of our convolutional neural network, we worked on the environment of jupyter. We used two convolution layers, each of them is connected to a max pooling layer, then an average pooling layer was used, and finally flatten and fully connected layers. The first convolution layer has 32 kernels while the second one has 64. The activation function used was ReLU (Rectified Linear Unit), and for the last layer we chose a linear function, since we are dealing with a regression application.

3. Results

In this section, we will present the results of an intelligent approach based mainly on the use of high-resolution aerospace images, particularly data from a multispectral camera. We will also present the results of crop yield estimation using the red edge spectral band, which is well-known for its sensitivity to agricultural applications, in particular those related to the estimation of crop yield. It often improves the results of processing [29]. Results presented in the following paragraphs concern the convolutional neural network architecture, more particularly the second dimension, and this given the availability of aerospace images of a single phenological stage. We were able to implement our deep learning model by using python programming language with its various libraries. Figure 9 shows us the variation of the loss function related to training data with increasing epochs. The agricultural yield estimates established by our convolutional neural network were compared with the results of yield values estimated by in situ methods. The generated RMSE was 0.175 qx/ha and the coefficient of determination was 0.4. Table 1 shows us the in-situ values and the predicted values. Our results confirm that a deep neural network is able to predict yield even before harvest and this by using non-destructive methods that can help farmers to obtain informations about their crops and their production.

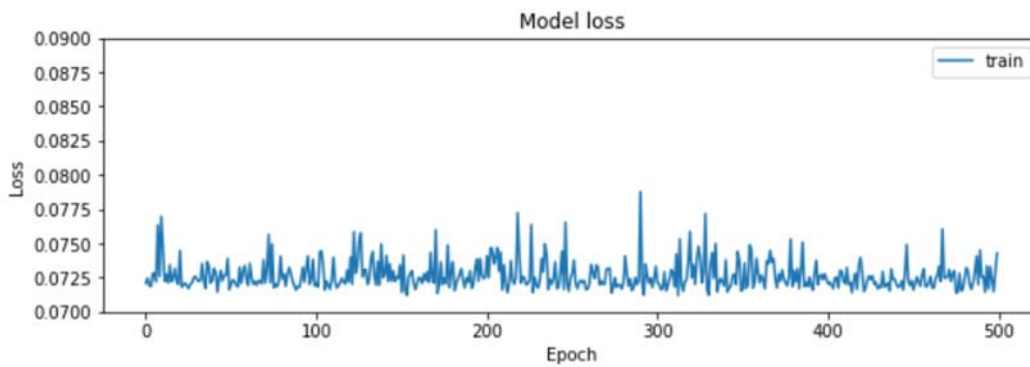


Figure 9. Variation of the loss function of our convolutional neural network

Table 1. Estimation results of DL model compared to in-situ data

N° plot	Difference between actual and predicted yield (Qx/ha)
1	0.34
2	2.11
3	3.78
4	3.44
5	5.14
6	4.46
7	1.61
8	14
9	12.73
10	1.57
11	19.24
12	7.27
13	4.94
14	8.89
15	0.53
16	14.11
17	4.31
18	4.06
19	0.06
20	4.66
21	0.11
22	2.07
23	3.78
24	3.66
25	5.54
26	4.78

4. Discussion

Through our study, we focused on estimating agricultural yield, more specifically that of wheat in Morocco. we opted for aerospace imagery first, for its ease of acquisition as well as the spectral and also the spatial richness it provides. Our study focused on the spectral band of the red edge from a multispectral camera, as long as it presents a great importance in remote sensing of agricultural crops, particularly with regard to the classification but also the prediction of physical and biological parameters of crops.

We have also chosen to manipulate our images by using deep learning, and this in order to capture all the non-linearities that may exist between our input data and the resulting output. Regarding the chosen architecture, we have opted for convolutional neural networks. It is one of the most powerful architectures that have revolutionized the deep learning field, given their ability to process unstructured data, including images.

The two-dimensional CNN architecture and drone images acquired only during one stage of the growth period were used. This explains on the one hand, the value of the correlation coefficient which was about half. We can say it was due mainly to the fact that, plants during the same growth period can have the same spectral characteristics, and other variations will appear and exist after the date of acquisition of our images. Moreover, choosing plots that are close and do not have a great variability explains the point of having very similar estimates by the model.

All this leads us to propose new possibilities for improving the results of this study, these are mainly:

- * Using several spectral information describing a specific agricultural crop.
- * Identifying more information of different natures and which can enrich the developed model, in particular texture information.
- * Using drone images acquired throughout the wheat growth cycle to allow a detailed description of the plants and their yield as a result.

* Using deep learning architectures that allow capturing both spatial and temporal variations and, in this sense, 3D CNN is one of the architectures that can respond to this point.

5. Conclusion

This study explored the precise estimation of agricultural yield by exploiting remote sensing imagery. Our methodology is mainly based on acquiring images from multispectral UAV sensor, more precisely the red edge spectral band and ground field data, and this in the middle season of growth. We chose to obtain our data in the region of Rabat, which is a well-known territory for its annual wheat yield production. Our project was focused on exploring the convolutional neural network architecture as an algorithm to process spatial variations. Our results highlight the importance of such architecture in capturing features from raw image data and before harvest. However, more input images should be considered and this by acquiring data over the entire period of growth and not only in one stage. Furthermore, more advanced architectures should be used, namely temporal networks, which will process different aspects and specificities of an agricultural crop. Based on this, in our future work, we will apply similar architectures for estimating the yield of wheat and also other crops.

Acknowledgement

We would like to thank the company “Les Domaines Agricoles” for providing the UAV equipment as well in situ data to accomplish our project.

This study was partly presented at the 3rd Advanced Engineering Days [30].

Funding:

This research received no external funding.

Author contributions:

Khadija Meghraoui: Conceptualization, Methodology, Software, Data curation, Writing-Original draft preparation, Validation. **Imane Sebari:** Conceptualization, Methodology, Software, Data curation, Writing-Original draft preparation, Validation, Visualization, Investigation, Writing-Reviewing and Editing. **Saloua Bensiali:** Visualization, Investigation, Writing-Reviewing and Editing. **Kenza Ait El Kadi:** Methodology, Visualization, Investigation, Writing-Reviewing and Editing.

Conflicts of interest:

The authors declare no conflicts of interest.

References

1. Weiss, M., Jacob, F., & Duveiller, G. (2020). Remote sensing for agricultural applications: A meta-review. *Remote Sensing of Environment*, 236, 111402.
2. Sagan, V., Maimaitijiang, M., Bhadra, S., Maimaitiyiming, M., Brown, D. R., Sidike, P., & Fritschi, F. B. (2021). Field-scale crop yield prediction using multi-temporal WorldView-3 and PlanetScope satellite data and deep learning. *ISPRS journal of photogrammetry and remote sensing*, 174, 265-281.
3. Nevavuori, P., Narra, N., Linna, P., & Lipping, T. (2020). Crop yield prediction using multitemporal UAV data and spatio-temporal deep learning models. *Remote Sensing*, 12(23), 4000.
4. Livieris, I. E., Dafnis, S. D., Papadopoulos, G. K., & Kalivas, D. P. (2020). A multiple-input neural network model for predicting cotton production quantity: a case study. *Algorithms*, 13(11), 273.
5. Alzadjali, A., Alali, M. H., Veeranampalayam Sivakumar, A. N., Deogun, J. S., Scott, S., Schnable, J. C., & Shi, Y. (2021). Maize tassel detection from uav imagery using deep learning. *Frontiers in Robotics and AI*, 136.
6. Martos, V., Ahmad, A., Cartujo, P., & Ordoñez, J. (2021). Ensuring agricultural sustainability through remote sensing in the era of agriculture 5.0. *Applied Sciences*, 11(13), 5911.
7. Zannou, J. G. N., & Houndji, V. R. (2019, April). Sorghum yield prediction using machine learning. In 2019 3rd International Conference on Bio-engineering for Smart Technologies (BioSMART) (pp. 1-4). IEEE.
8. Zhang, L., Zhang, Z., Luo, Y., Cao, J., & Tao, F. (2019). Combining optical, fluorescence, thermal satellite, and environmental data to predict county-level maize yield in China using machine learning approaches. *Remote Sensing*, 12(1), 21.
9. Gao, Y., Wang, S., Guan, K., Wolanin, A., You, L., Ju, W., & Zhang, Y. (2020). The ability of sun-induced chlorophyll fluorescence from OCO-2 and MODIS-EVI to monitor spatial variations of soybean and maize yields in the Midwestern USA. *Remote Sensing*, 12(7), 1111.

10. Wang, Y., Zhang, Z., Feng, L., Du, Q., & Runge, T. (2020). Combining multi-source data and machine learning approaches to predict winter wheat yield in the conterminous United States. *Remote Sensing*, 12(8), 1232.
11. Espinosa, C. E., Velásquez, S., & Hernández, F. L. (2020, March). Sugarcane Productivity Estimation Through Processing Hyperspectral Signatures Using Artificial Neural Networks. In 2020 IEEE Latin American GRSS & ISPRS Remote Sensing Conference (LAGIRS) (pp. 290-295). IEEE.
12. Wang, F., Wang, F., Zhang, Y., Hu, J., Huang, J., & Xie, J. (2019). Rice yield estimation using parcel-level relative spectral variables from UAV-based hyperspectral imagery. *Frontiers in plant science*, 10, 453.
13. Han, X., Wei, Z., Chen, H., Zhang, B., Li, Y., & Du, T. (2021). Inversion of winter wheat growth parameters and yield under different water treatments based on UAV multispectral remote sensing. *Frontiers in plant science*, 639.
14. Zheng, C., Abd-Elrahman, A., & Whitaker, V. (2021). Remote sensing and machine learning in crop phenotyping and management, with an emphasis on applications in strawberry farming. *Remote Sensing*, 13(3), 531.
15. Astaoui, G., Dadaiss, J. E., Sebari, I., Benmansour, S., & Mohamed, E. (2021). Mapping wheat dry matter and nitrogen content dynamics and estimation of wheat yield using UAV multispectral imagery machine learning and a variety-based approach: Case study of Morocco. *AgriEngineering*, 3(1), 29-49.
16. Mu, H., Zhou, L., Dang, X., & Yuan, B. (2019, August). Winter wheat yield estimation from multitemporal remote sensing images based on convolutional neural networks. In 2019 10th International Workshop on the Analysis of Multitemporal Remote Sensing Images (MultiTemp) (pp. 1-4). IEEE.
17. Wang, X., Huang, J., Feng, Q., & Yin, D. (2020). Winter wheat yield prediction at county level and uncertainty analysis in main wheat-producing regions of China with deep learning approaches. *Remote Sensing*, 12(11), 1744.
18. García-Martínez, H., Flores-Magdaleno, H., Ascencio-Hernández, R., Khalil-Gardezi, A., Tijerina-Chávez, L., Mancilla-Villa, O. R., & Vázquez-Peña, M. A. (2020). Corn grain yield estimation from vegetation indices, canopy cover, plant density, and a neural network using multispectral and RGB images acquired with unmanned aerial vehicles. *Agriculture*, 10(7), 277.
19. Yang, Q., Shi, L., & Lin, L. (2019, July). Plot-scale rice grain yield estimation using UAV-based remotely sensed images via CNN with time-invariant deep features decomposition. In IGARSS 2019-2019 IEEE International Geoscience and Remote Sensing Symposium (pp. 7180-7183). IEEE.
20. <https://www.codesofinterest.com/2016/11/difference-artificial-intelligence-machine-learning-deep-learning.html> , [last accessed: July 02 2022].
21. Kim, N., & Lee, Y. W. (2016). Machine learning approaches to corn yield estimation using satellite images and climate data: a case of Iowa State. *Journal of the Korean Society of Surveying, Geodesy, Photogrammetry and Cartography*, 34(4), 383-390.
22. Tian, H., Wang, P., Tansey, K., Han, D., Zhang, J., Zhang, S., & Li, H. (2021). A deep learning framework under attention mechanism for wheat yield estimation using remotely sensed indices in the Guanzhong Plain, PR China. *International Journal of Applied Earth Observation and Geoinformation*, 102, 102375.
23. Gavahi, K., Abbaszadeh, P., & Moradkhani, H. (2021). DeepYield: A combined convolutional neural network with long short-term memory for crop yield forecasting. *Expert Systems with Applications*, 184, 115511.
24. Merenda, M., Porcaro, C., & Iero, D. (2020). Edge machine learning for ai-enabled iot devices: A review. *Sensors*, 20(9), 2533.
25. Alibabaei, K., Gaspar, P. D., & Lima, T. M. (2021). Crop yield estimation using deep learning based on climate big data and irrigation scheduling. *Energies*, 14(11), 3004.
26. Li, J., Li, X., & He, D. (2019). A directed acyclic graph network combined with CNN and LSTM for remaining useful life prediction. *IEEE Access*, 7, 75464-75475.
27. Fernandez-Beltran, R., Baidar, T., Kang, J., & Pla, F. (2021). Rice-yield prediction with multi-temporal sentinel-2 data and 3D CNN: A case study in Nepal. *Remote Sensing*, 13(7), 1391.
28. Roy, A., & Mishra, D. (2019, October). ECNN: Activity Recognition Using Ensembled Convolutional Neural Networks. In TENCON 2019-2019 IEEE Region 10 Conference (TENCON) (pp. 757-760). IEEE.
29. Kang, Y., Meng, Q., Liu, M., Zou, Y., & Wang, X. (2021). Crop classification based on red edge features analysis of GF-6 WFV data. *Sensors*, 21(13), 4328.
30. Meghraoui, K., Sebari, I., El Kadi, K. A., & Bensiali, S. (2022). Towards 3D CNN for precise crop yield estimation using multimodal remote sensing data: Case study of wheat in Morocco. *Advanced Engineering Days (AED)*, 3, 79-81.





Gabion structures and retaining walls design criteria

Esra Uray*¹ 

¹KTO Karatay University, Faculty of Engineering and Natural Sciences, Department of Civil Engineering, Konya, Türkiye
esra.uray@karatay.edu.tr

Cite this study: Uray, E., (2022). Gabion structures and retaining walls design criteria. Advanced Engineering Science, 2, 127-134

Keywords

Gabion retaining wall
Gabion application areas
Design criteria
Highways application
Railways application

Research Article

Received: 09.07.2022
Revised: 08.10.2022
Accepted: 14.10.2022
Published: 19.10.2022



Abstract

Retaining structures, which are utilized as a solution to meet the horizontal soil pressures between two different soil levels, have a very common usage area in geotechnical engineering. Gabions, which have found application with the developments in material production and coating technologies, are also applied as a type of retaining structure. Gabions, which are especially economical and environmentally friendly solutions, are engineering structures with many advantages. Gabion structures are built by placing these baskets in a specific order and these structures are used in many applications of civil engineering like retaining walls in highways, railways, erosion prevention, slope stability, stream bed improvement, shoreline survey, bridge approach, etc. In this study, gabion-type structures and their main application areas, advantages, design criteria, and comprehensive literature summary are given.

1. Introduction

The stability problem due to lateral soil loads between distinct soil levels is a widespread problem in civil engineering. Structures that connect these different soil levels by keeping them stable against the horizontal soil pressure created by static or dynamic loads are defined as retaining structures. Although there are a lot of types of retaining walls, gabion walls have been commonly begun to utilize in many applications of geotechnical engineering around the world. Gabion walls are preferable to stone retaining walls whose materials cannot be obtained easily, labor costs are high, and performance in the case of earthquakes is low. As the gabion has a cellular structure, these gaps fill with soil naturally over time. Also, it is possible to green gabion baskets artificially by adding bio textiles. Gabion structures are eco-environment friendly structures thanks to vegetation formation and are durable to environmental impact.

Gabion is originally an Italian word that means big cage. A gabion basket is a rectangular cage obtained from hexagonal double-twisted and zinc-coated steel wire mesh and filled with stone or rock of certain size and mechanical characteristics. Gabion structures are built by placing these baskets in a specific order and these structures are used in many applications of civil engineering like retaining walls in highways, railways, erosion prevention, slope stability, stream bed improvement, shoreline survey, bridge, or tunnel approach, etc. Gabion baskets adopted in composing the retaining wall have been seen as commonly utilized for different purposes according to historical ruins or structures from past to present. Gabions were primarily employed along the Nile River in 5000 BC in Egypt and along the Yellow River in China in 1000 BC, protection against coastal floods. Gabions were constructed as temporary walls for military purposes during Roman times and as a foundation for San Marco Castle designed by Leonardo Da Vinci. A gabion design was created by Egidio Palvis (1880–1929), one of the engineers of the Royal Union of Civil Engineers of Italy. The application of the gabion retaining wall, which is

accepted as the first engineering design, was made by the Maccaferri company in 1893, with sack gabions in the Reno River in Italy [1] (Figure 1).

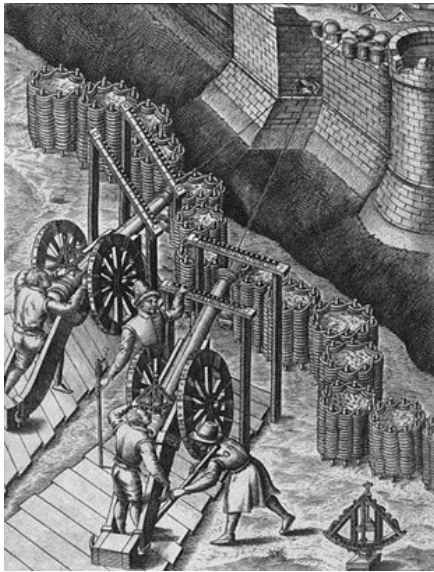


Figure 1. History of gabion structures [1]

Some of the analytical and experimental studies of gabion structures are tabulated as a literature review in Table 1.

Table 1. Literature review of gabion wall

Study	Explanation
Flexible gabion structures in earth-retaining works [2]	The mechanical behavior of the gabion basket under the load and calculations of the gabion retaining wall were given in the study conducted by Agostini and Maccaferri which was thought of as the first experimental investigation.
Analytical study for the stability of gabion walls [3]	The effects of parameters such as wall height, wall inclination, the slope of backfill, and surcharge load on the stability of the gabion retaining wall were examined analytically for different values of the parameters.
The stability of gabion walls for earth-retaining structures [4]	The durability of the gabion wall against lateral loads, which is used effectively to prevent erosion in flood areas, was investigated experimentally in terms of gabion wall basket arrangement and gabion basket geometry change.
Settlement behavior of new reinforced earth retaining walls under loading-unloading cycles [5]	Elastic and plastic deformation for different types of reinforced soil structures under load was examined experimentally by exposing the loading-unloading cycle at different loading values.
Dynamic deformation behavior and life analysis of green reinforced gabion retaining wall [6]	Lateral and vertical deformation behaviors of green reinforced gabion retaining walls were investigated experimentally by imposing the dynamic loads with different frequencies and amplitudes to be able to estimate fatigue damage and fatigue life with train load and speed.
Multibody modeling of gabion beams for impact applications [7]	Shear and bending deformation for a multibody of gabion blocks which are likely to be used as a roadside impact absorption device were investigated experimentally and analytically.
Failures of gabion walls [8]	It is a review study which is presented failures and defects of gabion walls due to failure types like bulging, corrosion, stone erosion, backfill cracks, or erosion foundation soil obtained by observing walls in different sites.
Investigation of design criteria for the type of gabion walls [9]	The effect of parameters like the wall height, base length, angle of internal friction, wall angle, and backfill slope on the gabion retaining wall design was investigated analytically based on statistics.
Optimization of a slope-stabilization system combining gabion-faced geogrid-reinforced retaining wall with embedded piles [10]	A gabion-faced geogrid-reinforced retaining wall system has been applied for the protection of the road against slope stability and parametric studies of the height of the slope, the ratio of the embedded length of the pile to the thickness of the unstable soil layer, and the ratio of the spacing to the diameter of the pile have been performed for the optimum slope stabilization infrastructure.
Numerical modeling of gabion retaining wall under loading and unloading [11]	A real-scale gabion retaining wall with a 4.5m wall height was analyzed using the finite element method under the effect of water pressure in a loaded-unloaded case and its crest displacement was measured for comparing the experimental one.

2. Material and Method

Today, the necessity of constructing new highways and railways for passenger, freight transportation, or individual use has come to the fore under the influence of the increasing population and developing technology. Structures such as tunnels, viaducts, and bridges are widely used in transportation, especially in covering large distances in a short time because it allows for crossing great mountains and wide valleys. To serve safely this kind of road structure, it should be designed according to the possible dangers on the route like landfall or rockfall. In this scope, retaining structures that resist the lateral soil loads which are occurred in different soil levels are widely used in applications of filling and splitting works, deep excavation, slope stability, approach fill of tunnels, bridges, viaduct foundations, etc. In Figure 2, some of the applications for retaining structures are demonstrated.

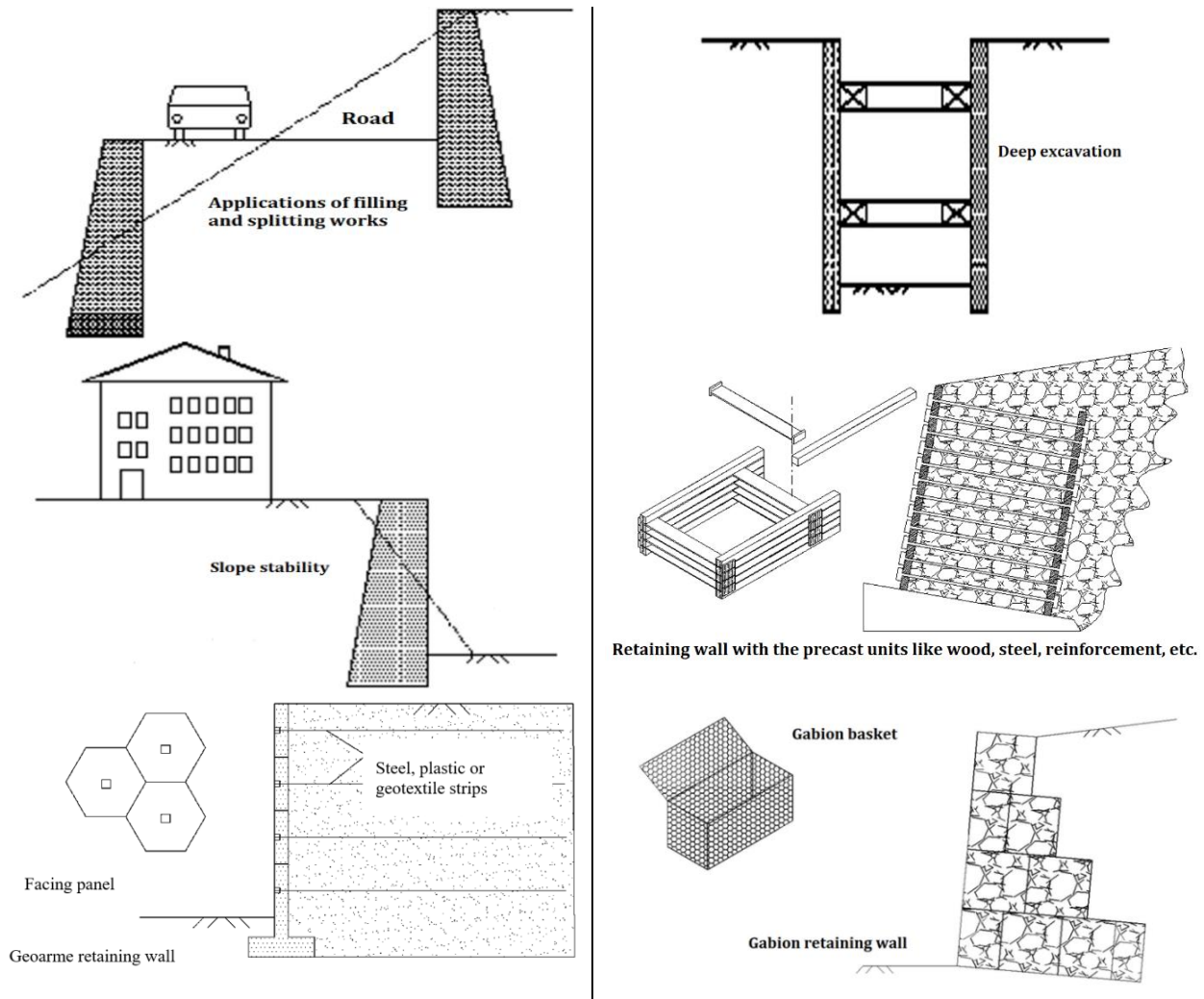


Figure 2. Retaining structures applications [12]

Gabion retaining walls which are retaining structures are an alternative and economic solution since they provide gabion basket filling material from the quarry or environment close to the site area and are a factory-produced material. Although it is possible to construct retaining walls as different types like stone, concrete, or reinforced concrete retaining wall, gabion retaining walls are more advantageous in terms of many criteria like flexible structure, economic, easily buildable, no needing drainage precaution, adaptive with the natural, durable, eco-friendly, and so on. Gabion retaining walls are favorable more than the other type of retaining walls (gravity) as the others require excess labor and manufacturing costs and periodical maintenance to prevent engorged. Also, tolerance of occurring failure due to a different settlement of soil is more acceptable for gabion retaining walls according to other retaining wall types. As gabion retaining walls are flexible in various settlements of the foundation soil and do not require an additional drainage system, thanks to their hollow structures, using these walls is advantageous compared to other retaining wall types. Gabion walls are economical as qualified workers are not necessary for assembling the gabion baskets packed and transported from the factory. Gabions are eco-friendly as allow the growth of vegetation and release less carbon dioxide into the atmosphere for transportation from the factory to the site and during construction, as well.

The comparison between a gabion retaining wall and other retaining walls like concrete or gravity retaining walls is tabulated in [Table 2](#).

Table 2. Comparison of retaining walls [\[13\]](#)

Comparison	Gabion retaining wall	Other retaining walls
Flexibility	flexible	rigid
Cellular structure	has	has not
Drainage precaution	is not necessary	is necessary
Employment cost	low	high
Time	can be constructed in a short time	takes a long time to construct
Settlement	adapts to different settlements	does not tolerate different settlements much
Environmental impact	suitable for vegetation growth	not compatible with the environment
Weight of the wall	light	heavy

3. Applications of Gabion

Gabion baskets have been produced by using zinc-coated steel wire mesh covered with PVC, galvanic, galfan, polymer, etc., and double-twisted in various hexagonal aperture sizes [\(Figure 3\)](#). As the abovementioned cover of wire mesh provides resistance to environmental conditions, the gabion retaining wall has a long life like 30-100 years depending on covering materials compared with other types of retaining walls. Gabion baskets, which have a specific geometric form, are filled with small rocks and stones having suitable mechanical properties.

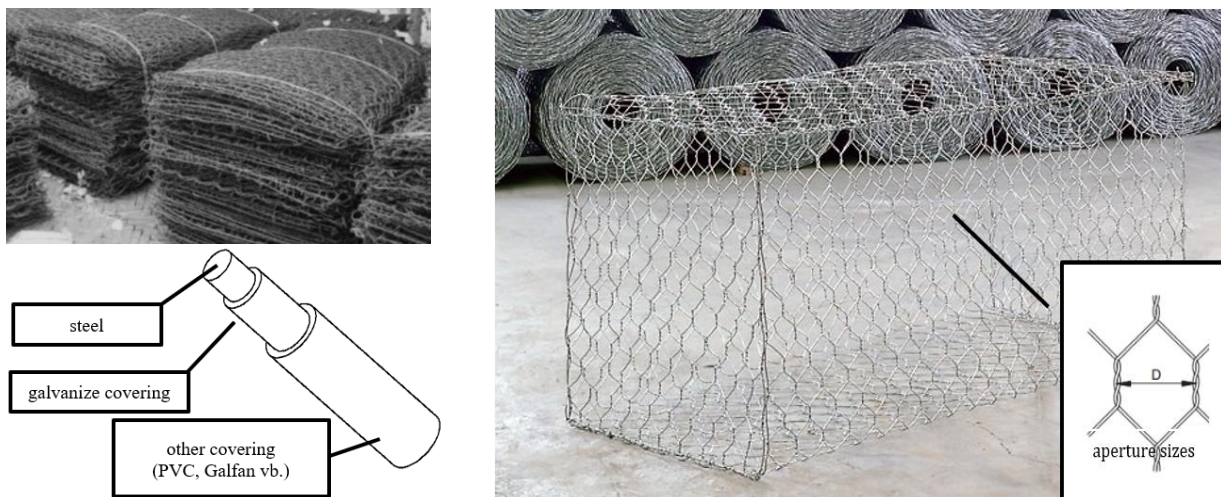


Figure 3. Gabion basket and wire mesh coating [\[12\]](#)

Gabion products like baskets, mattresses, sacks, or wire mesh have been commonly utilized in retaining walls, highways-railways, prevention of erosion, sediment transportation in rivers, falling rock or stone from slopes, remediation of a stream bed, shore protection as a breakwater, supporting of slopes, approach fill of tunnel and bridge and so on. Gabion products like baskets, mattresses, sacks, or wire mesh have been commonly utilized in retaining walls, highways-railways, prevention of erosion, sediment transportation in rivers, falling rock or stone from slopes, remediation of a stream bed, shore protection as a breakwater, supporting of slopes, approach fill of tunnel and bridge and so on. Gabion types like the basket, the mattress, the sack, and their different engineering applications are demonstrated in [Figure 4](#).

The gabion structure which is widely used as a retaining wall is obtained by placing the gabion baskets of appropriate sizes in a certain order and connecting them to each other with suitable fasteners [\(Figure 4.a\)](#). Thus, soil which prone to lateral expansion is kept with a gabion retaining wall, and possible soil slipping problems solve on a natural or artificial slope near highways and railways. Gabion wire mesh is used to prevent the damage of large stones and rock fragments from natural slopes to the living creatures and structures in the vicinity. Since the wire mesh limits the movements of the rocks and ensures that the broken pieces are collected at the top of the slope, it creates a precaution against possible damages that may occur in the environment [\(Figure 4.b\)](#). The gabion mattress is an important and environmentally friendly alternative in the erosion solution to the desertification problem, which is encountered due to the movement of the soil mainly by the effects of rivers and seasonal precipitation [\(Figure 4.c\)](#). Gabion baskets are used in the bridge or tunnel approach to provide proper route in highways and railways [\(Figure 4.d\)](#). In contrast to reinforced concrete structures, mattress gabion is widely used in stream bed improvement. It is less damaged by hydraulic forces thanks to its flexible and hollow structure and is constructed quickly. In this way, it prevents the erosion and scouring of the riverbanks and ensures a smoother flow of the riverbed [\(Figure 4.e\)](#).



Embankment Manufacturing of Kozcağız Dam-Gabion Basket with Terramesh System [14]



Rock Barrier and Steel Grid Application of Kavşakbendi Project- Gabion Wire Mesh [15]



Application of Reno Mattress for Slope Erosion Prevention within the Scope of Ankara-Istanbul 2nd Stage High-Speed Train Project [16]



Construction of Terramesh System Retaining Wall within the Scope of Ankara-Istanbul 2nd Stage High-Speed Train Project [17]



Turkey, Astaldi Bolu Mountain Crossing Stream Bed Improvement Work for the Protection of Viaduct Foundations with Gabion Basket Reno Mattress [18]

Figure 4. Type of gabion products and some applications

4. Design Criteria

When the retaining wall with the gabion retaining wall are compared, it is commented that the gabion retaining wall is more flexible and is more reliable with its performance on different settlements and against earthquake loads. In design of gabion retaining wall design criteria is differ from conventional retaining wall. The design criteria of the gabion retaining wall have been presented as the following [12];

Stability check: In the design of the gabion retaining wall, it is necessary to inspect the structure in terms of stability problems caused by lateral soil pressure and perform a check of safety factors of sliding, overturning, bearing capacity, and slope stability according to proper safety factor limits in literature [19]. The active horizontal soil pressure coefficients according to Rankine [20] or Coulomb [21] theory etc. that are effective in the design are determined.

Backfill material: Due to the permeability of the gabion retaining wall, soil type is used in a wider area as filling material. While clayey soils that swell with water are not preferred as the backfill of the other type of retaining wall due to no possibility of draining the water in the reinforced concrete retaining wall, it is not a problem for backfill of the gabion retaining wall. Backfill soil is selected by evaluating factors such as the proximity of the place where the gabion retaining wall will be built to the quarries, the groundwater situation, and the excavation area.

Foundation soil: After the examination of the ground on which the gabion retaining wall will be built, the engineer designing the foundation should consider criteria such as soil bearing capacity, wall dimensions, drainage condition and ground settlement condition. During the preparation of the foundation, the upper ground is excavated until the solid load-bearing ground is reached and the foundation is formed with granular stone material in layers of 15-45 cm to increase the bearing capacity and reduce different settlements. Depending on the condition of the soil and the construction area, in some cases, the foundation is prepared by compressing the filling material with a compression ratio of 95%.

Backfill soil: By compression of the backfill soil placed behind the gabion retaining wall, the sliding resistance of the soil increases, the swelling-shrinkage behavior is controlled, the compressibility decreases, and the liquefaction problem is brought under control. In terms of the long-term performance of the gabion retaining wall, the filling material of the backfill soil should have a compression ratio of 95% on the condition that it is placed and compacted following local standards. Uncompacted or poorly compacted weak backfill soil may cause horizontal wall movement, structural settlement, and insufficient shear strength, reducing wall performance.

Filling material of gabion basket: Due to the permeability of the gabion retaining wall, soil type is used in a wider range for filling material of the gabion basket. Appropriate filling soil type should be placed and compacted by considering factors such as the proximity of the place where the gabion retaining wall will be built to the quarries, the groundwater situation, and the excavation area. The gabion fills in the hollow structure placed in the gabion basket provides free drainage to the ground behind the wall (Figure 5).

Filter fabric: The gabion retaining wall built without filter fabric placement is dragged on by the effect of free drainage, causing the loss of the soil and a decrease in the soil height. Therefore, filter fabric should be used to prevent soil loss (Figure 5).

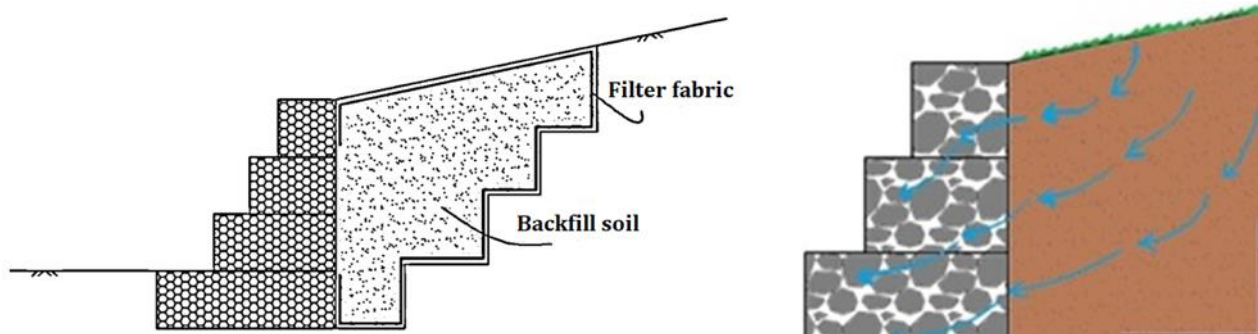


Figure 5. Application of filter fabric and permeability of gabion retaining wall [12-13]

5. Conclusion

In this study, the application case, advantages, and design criteria of the gabion structures have been presented with literature studies. Gabion structures are solutions for the problems meeting in many areas of civil engineering that provide safe, economical, and environmentally friendly. It is thought that the design and construction of gabion retaining walls without requiring any drainage measures, especially in soil environments where the groundwater level changes with the seasonal effect, will be a solution to the problem of demolition of retaining walls. Demolition of retaining wall may be due to the blocking of barbacane which is used for draining the water in time when the water accumulated if essential maintenance of the barbacane does not conduct.

The design criteria of gabion structures, whose use is becoming more and more widespread today, have not been fully developed. The design criteria and software utilized in the current situation are largely based on the experimental and analytical results obtained by the research and development studies of the manufacturers and the efforts of some researchers. Comprehensive finite element-based analyzes and experimental studies are required to fully develop the design criteria of gabion retaining walls, which are distinguished from stone, concrete, or reinforced concrete retaining walls with different properties like their porous structure and water permeability.

Consequently, the route can serve safely with reliable and effective gabion applications such as slope support, protection against rock or stone falls, tunnel approach filling in highways and railways. In addition, it is possible to make gabion structures that serve for many years due to their low cost and environmentally friendly solution.

Acknowledgement

In this study, some of the parts from the master thesis about “Investigation of design criteria for the type of gabion walls” have been presented. I express my deepest gratitude to my dear advisor of master thesis, Prof. Dr. Özcan Tan, who passed away on 6 January 2020.

Funding:

This research received no external funding.

Conflicts of interest:

The authors declare no conflicts of interest.

References

1. Gabion-Wikipedia. (n.d.). What is the gabion? Retrieved December 20, 2021, from <https://en.wikipedia.org/wiki/Gabion>
2. Agostini, R. (1978). Flexible gabion structures in earth retaining works. In *Officine Maccaferri*. Retrieved from <https://www.worldcat.org/title/flexible-gabion-structures-in-earth-retaining-works/oclc/20688526#borrow>
3. Peerdawood, C. T., & Mawlood, Y. (2010). Analytical Study for Stability of Gabion Walls. *Journal of Pure and Applied Sciences*, 22(5).
4. Ramli, M., Karasu, T. J. R., & Dawood, E. T. (2013). The stability of gabion walls for earth retaining structures. *Alexandria Engineering Journal*, 52(4), 705–710. <https://doi.org/10.1016/j.aej.2013.07.005>
5. Lin, Y., & Fang, Y. (2013). Settlement Behavior of New Reinforced Earth Retaining Walls under Loading-Unloading Cycles. *Applied Mechanics and Materials*, 256–259(PART 1), 215–219. <https://doi.org/10.4028/www.scientific.net/AMM.256-259.215>
6. Lin, Y., & Yang, G. (2013). Dynamic Deformation Behavior and Life Analysis of Green Reinforced Gabion Retaining Wall. *Applied Mechanics and Materials*, 256–259(PART 1), 251–255. <https://doi.org/10.4028/www.scientific.net/AMM.256-259.251>
7. Amato, G., Obrien, F., Simms, C. K., & Ghosh, B. (2013). Multibody modelling of gabion beams for impact applications. *International Journal of Crashworthiness*, 18(3), 237–250. <https://doi.org/10.1080/13588265.2013.775739>
8. Chikute, G. C., & Sonar, I. P. (2019). Failures of gabion walls. *International Journal of Innovative Technology and Exploring Engineering (IJITEE)*, 8(11), 1384–1390. <https://doi.org/10.35940/ijitee.J9731.0981119>
9. Uray, E., & Tan, O. (2015). Investigation of design criteria for the type of gabion walls. *Digital Proceeding of The International Conference on Civil and Environmental Engineering ICOCEE*, 1571–1581. <https://doi.org/https://doi.org/10.13140/RG.2.1.1185.5845>
10. Wang, Y., Smith, J. V., & Nazem, M. (2021). Optimisation of a Slope-Stabilisation System Combining Gabion-Faced Geogrid-Reinforced Retaining Wall with Embedded Piles. *KSCE Journal of Civil Engineering*, 25(12), 4535–4551. <https://doi.org/10.1007/s12205-021-1300-6>
11. Grodecki, M. (2021). Numerical modelling of gabion retaining wall under loading and unloading. *Archives of Civil Engineering*, 67(2), 155–164. <https://doi.org/10.24425/ACE.2021.137160>
12. Uray, E. (2014). Investigation of Design Criteria for The Type of Gabion Walls. The Graduate School of Natural and Applied Science of Selçuk University, The Degree of Master of Science in Civil Engineering, Master's Thesis.

13. Uray, E., & Tan, O. (2015). Gabion tipi dayanma yapıları. *Türkiye Mühendislik Haberleri*, 60(2), 19–29. Retrieved from https://www.imo.org.tr/resimler/ekutuphane/pdf/17070_03_49.pdf
14. Maccaferri Turkey Case History. (2017). Embankment manufacturing of Kozcagız Dam. Retrieved February 15, 2021, from <https://maccaferri.com.tr/kozcagiz-baraji-terramesh-sistem-ile-sedde-imalati/>
15. Maccaferri Turkey Case History. (2013). Rock barrier and steel grid application of Kavsakbendi project. Retrieved February 15, 2021, from <https://maccaferri.com.tr/kavsakbendi-baraji-hes-projesi-kaya-bariyeri-ve-celik-grid-uygulamasi/>
16. Maccaferri Turkey Case History. (2012). Application of Reno Mattress for Slope Erosion Prevention within the Scope of Ankara-Istanbul 2nd Stage High Speed Train Project. Retrieved March 20, 2014, from <https://maccaferri.com.tr/en/case-history/>
17. Maccaferri Turkey Case History. (2012). Construction of Terramesh System Retaining Wall within the Scope of Ankara-Istanbul 2nd Stage High Speed Train Project. Retrieved March 20, 2014, from <https://maccaferri.com.tr/en/case-history/>
18. Maccaferri Turkey Case History. (2005). Astaldi Bolu Mountain Crossing Stream Bed Improvement Work for the Protection of Viaduct Foundations. Retrieved March 20, 2015, from teknomaccaferri.com.tr/cozum-konulari/istinat-yapilari/referanslar
19. Braja, M. Das, & Sivakugan, N. (2017). *Principles of Foundation Engineering (9th Edition)*. Cengage Learning. Retrieved from <http://thuvienso.hau.edu.vn:8888/dspace/handle/hau/5215>
20. Rankine, W. (1857). Earth pressure theory. *Phil. Trans. of the Royal Soc.* rankine.
21. Coulomb, C. (1773). *Essai sur une application des regles de maximis et minimis a quelques problemes de statique relatifs a l'architecture* (essay on maximums and minimums of). Retrieved from <https://trid.trb.org/view/124803>



© Author(s) 2022. This work is distributed under <https://creativecommons.org/licenses/by-sa/4.0/>



Integration of 2D mapping, photogrammetry and virtual reality in documentation of material deterioration of stone buildings: Case of Mardin Şeyh Çabuk Mosque

Lale Karataş*¹

¹Mardin Artuklu University, Department of Architecture and Urban Planning, Türkiye, karataslale@gmail.com

Cite this study: Karatas, L. (2022). Integration of 2D mapping, photogrammetry and virtual reality in documentation of material deterioration of stone buildings: Case of Mardin Şeyh Çabuk Mosque. *Advanced Engineering Science*, 2, 135-146

Keywords

Photogrammetry
Virtual Reality
Stone Material
Deteriorations
Historic Buildings
Cultural Heritage

Research Article

Received: 22.08.2022
Revised: 19.10.2022
Accepted: 25.10.2022
Published: 01.11.2022



Abstract

Today, various methods are used in documenting the cultural heritage with the development of technology. However, it is seen that 3-dimensional (3D) documentation technologies have some disadvantages. For instance, ground laser scanning techniques are not used widely due to their high costs and the expertise required. Although photogrammetry can create point clouds with lower costs, it has large data files, which require allocating more time for data management. Within this context, the aim of this study is to present a method, which integrates the photogrammetry and virtual reality technologies in order to obtain 3D model of a stone building with a reasonable cost and in a short time; and to research the stone material deteriorations over the 3D model obtained. The study is significant in terms of systematically presenting the methods how the material deterioration maps are obtained over the 3D model of a stone building in a virtual environment. Mardin Şeyh Çabuk Mosque, which shall be investigated as case analysis under the study, was investigated on-site, and 360 degree panoramic images were taken related with the building. 3D virtual environment was created from the panoramic images on Mozilla Hubs programme, which is an open web-sourced platform. Stone material deteriorations were determined over the model in the virtual environment, and determinations regarding the stone building deterioration types were entered into the schedules prepared. As a result of the study, it was concluded that the virtual 3D environment regarding the building can be created from the global panoramic photographs with the suggested method on Mozilla Hubs platform, which is an open-sourced website, with a reasonable cost and in a very short time; and stone material deteriorations regarding the building can be determined easily on this virtual environment.

1. Introduction

Stone buildings are the works of art that occupy the largest ratio in cultural heritage field in the world. However, the stone buildings are defaced by being exposed to various impacts [1-4]. The types of stone material deteriorations are classified and mapped under various names from past to present in literature. For this purpose, documents were presented in order to establish standard methods for investigating the stone material changes and tracking the interventions carried out in stone material conservation field in also various countries, primarily in Italy.

The most important of these documents is the Italian Standard Normal 1/88, which was published in Italy in 1990 and is called "Alterazioni macroscopiche dei materyali lapidei: lessico" that may be used in mapping the stone deteriorations. Each of 27 terms provided in this dictionary was shown with photographs and a graphical

schedule [5]. Another document is a document written by Jose Delgado Rodrigues, which is consisted of 26 terms, intended for the terminology of stone deterioration forms on monuments, and was created within the framework of ICOMOS Stone Committee's Petrography Group. This suggestion, was used as a base to publish a dictionary in Portuguese in 2004, which includes short definitions, including the terms related with stone, masonry and plaster deteriorations and each term is linked with a graphical table [6]. Another illustrated document, which was written by Fitzner et al. [7] and updated by Fitzner & Heinrichs in 2002, classifies the deterioration models per type and intensity. "Verein Deutscher Ingenieure" is a list of German terms comprised of 14 terms together with the definitions and drawings meaning Union of German Engineers [8]. As in the Italian Standard and in Fitzner's system, it has presented a suggestion for the graphical representation of deterioration models. Another document is an illustrated dictionary drawn up by Queen's University of Belfast (England), which is consisted of 30 terms. On its website (<http://www.qub.ac.uk>), comprehensive segregation characteristics, which both include the deterioration models of the monuments and refer to the anthropogenic damages, are presented. In 2008, with the 'ICOMOS-ISCS: Illustrated glossary on stone deterioration patterns', which was published by ICOMOS, ICOMOS International Scientific Committee of Stone (ISCS) has created a scientific language on stone deterioration incidents and processes [9].

Various countries, institutions, and authors made various classifications on the types of deteriorations over the years in order to ease the determination of stone material deteriorations as explained. Based on these documents, the method of material deterioration mapping on the buildings has been used in many studies in literature over the years, and its positive contribution into the determination of material problems is known [7, 10, 11, 12-17]. However, many of these studies emphasize that the studies, which document the stone material deteriorations as 3-dimensional (3D), are needed to diagnose the stone material deteriorations, which vary in geographic areas [12, 18-19]. Franković et al. [12], which is a significant example, have compared the stone material damage maps carried out on Belgrade Castle, and demonstrated that deterioration type damage maps, which are prepared in detail, are important diagnosis instruments in restoration projects, and it was suggested that the maps, which are created utilizing these classifications, must be carried to the 3D environments in future studies. Napolitano et al. [19] emphasized that while two-dimensional (2D) mapping is reasonable in terms of time and cost, at the same time it has various disadvantages when compared with 3D methods. They have mentioned that the surface contamination, which is among the stone material deteriorations seen on a historical building, may be caused by erroneous drainage system on the roof of the building or by various factors such as air pollution; it causes failing to document the diagnosis of the problem completely, since it fails to demonstrate the link between the damages on more than one sides of the building in the determinations made by considering the samplings at standards; and the material deteriorations of the buildings must absolutely be documented as 3D, since the 2D documentations enable only the treatment of instantaneous symptoms.

However, when 3D documentation technologies are considered, they have also some disadvantages [20-22]. Some technologies such as ground laser scanning techniques are not used widely due to the high costs and required expertise [23-25]. Although photogrammetry can create point clouds with lower costs, it has large data files, which require allocating more time for data management [26-27]. Within this context, various studies, which present methods intended for creating virtual reality environments to close the disadvantages of the gap between 2D mapping, photogrammetry and laser scanning and to determine the material deteriorations, have been conducted in the literature. These studies may be classified under two headings: those produced from 3D models and those produced from 360-degree panoramic images. Virtual reality environments, which are produced from 3D models, are costly, since they require time and knowledge of 3D. However, the virtual reality environments, which are produced from panoramic images, have the advantage of creating rapidly. It is seen that the use of global panoramic images provides great convenience in 3D documentation procedure to the user in terms of time and cost [19]. A significant example by Mah et al. [23] is consisted of the hard data used in creating the virtual tour, which is produced for the temple structure built from stone material, global images collected via 360° camera and 2D high resolution images obtained via digital single-lens reflex camera. It is determined that this method is advantageous because of increasing the accessibility for heritage practitioners through a 360° camera, which does not require high levels of technical specialty when compared with the other digital and visualization technologies, and the relatively low pricing of the 360-degree camera; and facilitating the future practices. Within this context, it is seen that besides 2D documentations, 3D documentation is a new and effective way of preserving and using culture. It is necessary to combine different techniques to obtain a representation of the historical buildings [28].

In summary, today 3D documentation of cultural heritage through digital archiving became a global objective. In this respect, use of digital and visualization technologies to document the cultural heritages is increasing [29-30]. Many of these approaches require the introduction of new data collecting and processing systems [31-32]. Remote sensing technologies enable us to model the object without touching it [33-35]. Within this context, the aim of this study is to present a method, which integrates the photogrammetry and virtual reality technologies in order to obtain 3D model of a stone building with a reasonable cost and in a short time; and to research the stone material deteriorations over the 3D model obtained. The study is significant in terms of systematically presenting the methods how the material deterioration maps are obtained over the 3D model of a stone building in a virtual environment. Mardin Şeyh Çabuk Mosque, which shall be investigated as case analysis under the study, was firstly

investigated on-site, and 360-degree panoramic images were taken related with the building. 3D virtual environment was created from the panoramic images on Mozilla Hubs programme, which is an open web-sourced platform. Stone material deteriorations were determined over the model in the virtual environment, and determinations regarding the stone building deterioration types were entered into the schedules prepared. As a result of the study, it was concluded that the virtual 3D environment regarding the building can be created from the global panoramic photographs with the suggested method on Mozilla Hubs platform, which is an open-sourced website, with a reasonable cost and in a very short time; and stone material deteriorations regarding the building can be determined easily on this virtual environment. The presented method enables to display a stone building as 3D with a reasonable cost and in a short period by eliminating the cost caused by the laser scanning to create a 3D model and the data burden regarding the 3D point cloud obtained through photogrammetric methods. Furthermore, the presented method eliminates the disadvantages of 2D documentation by enabling complete documentation of the diagnosis of the material problem on the building, since it displays the link between the damages on more than one side as 3D in virtual environment.

In line with the aim identified, initially information on the building is provided under the study, and in the second section the method, which was followed to be able to create the virtual environment of the building, is described. In the following stage, images from the virtual environment, which are the findings of the study and the determination schedules of material deterioration are provided, and suggestions are made for future studies.

1.1. Location and History of the Building

Şeyh Çabuk Mosque is in Mardin Province, Çubuk Neighbourhood and on the South of the 1st Avenue (Figure 1).

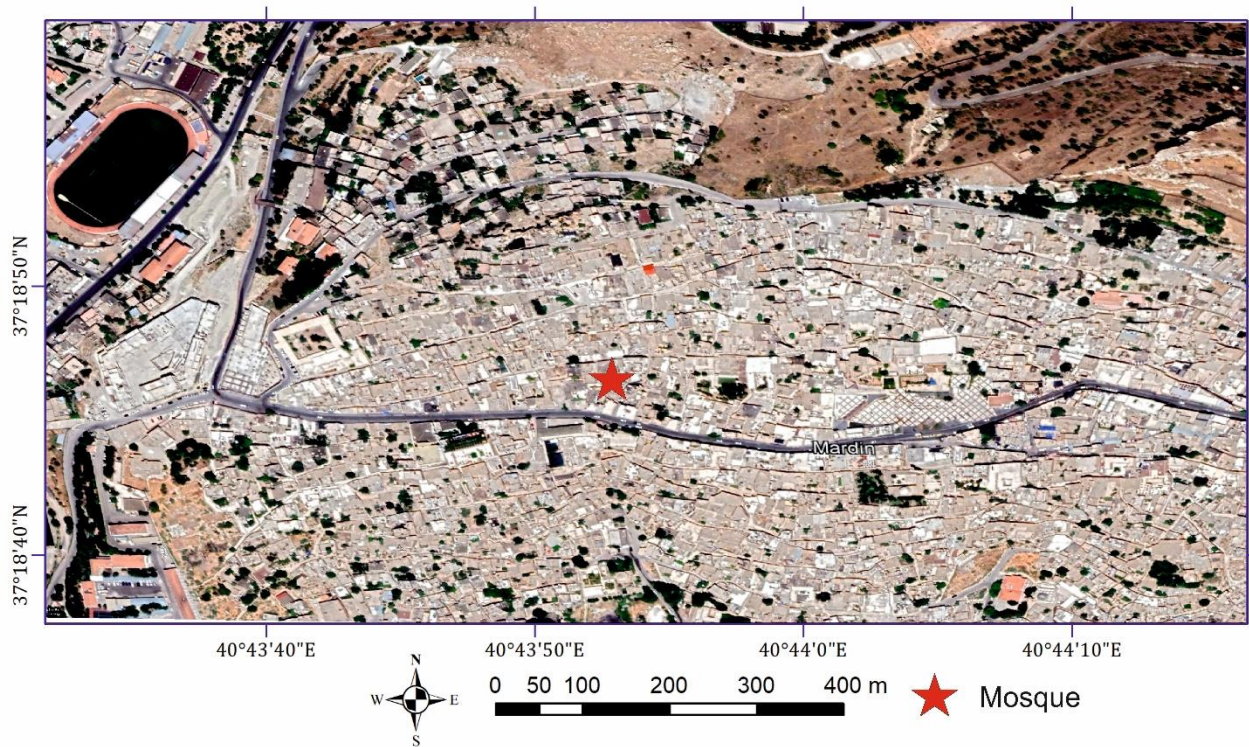


Figure 1. Location of Şeyh Çabuk Mosque within the city

The year of construction of Şeyh Çabuk Mosque is unknown and it has been repaired two times in the 19th century. The building has been mentioned as masjid in the 16th century Ottoman records and it is estimated that the part on the south of the entrance was tersanctus place. It is estimated that the building has been converted into masjid from zawayah and to a mosque afterwards. The delubrum located within the mosque belongs to Abdullah Bin Enes El Cüheyri, who has been the messenger of Mohammed. It is written on the epigraph on its door that it has been repaired in 1843. Women's section, which has a separate entrance, was added afterwards on the North side of the mosque. West part of the building has been changed, as the building is under the risk of collapsing frequently due to the gap underneath. The women's section of the building, which was separated in 1967, is opened today, and added into the main sanctuary section [36] (Figure 2 and 3).

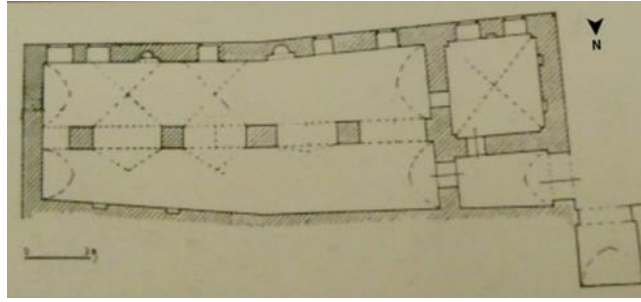
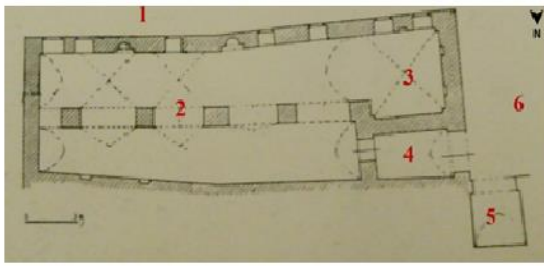


Figure 2. Plan according to the status in November 1967 [36]

1.2. Spatial Characteristics of the Building

In Şeyh Çabuk Mosque, a transverse rectangular plan scheme is seen and the main venue is consisted of two naves covered by two barrel vaults parallel to the mihrab wall. The entrance to the building is provided by the north-west iwan (space nr. 4) opening to the main courtyard (space nr. 6). The main sanctuary is consisted of the spaces nr. 2 and 3, and there is an iwan (space nr. 5), which is used as lumination place today on the North side of the building (Figure 3).



Space Nr	Original Function	Current Function
1	Back courtyard	Back courtyard
2	Men's Section	Main sanctuary
3	Women's Section	Main sanctuary
4	Iwan	Iwan
5	Iwan	Lumination place
6	Front Courtyard	Front Courtyard

Figure 3. Plan scheme of Şeyh Çabuk Mosque Ground Floor

2. Material and Method

Mardin Şeyh Çabuk Mosque, which shall be investigated as case analysis under the study, was investigated on-site, and 360 degree panoramic images were taken related with the building. 3D virtual environment was created from the panoramic images on Mozilla Hubs programme, which is an open web-sourced platform. Stone material deteriorations were determined over the model in the virtual environment, and determinations regarding the stone building deterioration types were entered into the schedules prepared.

2.1. Obtaining 360 degree panoramic images

Initially, 360 degree panoramic images of the buildings were taken with NCTech iris360^o Model Panoramic Imaging by visiting the building, in order to create the 3D environments (Figure 4).



Figure 4. NCTech iris360^o Model

The panoramic images obtained shall be used in 3D virtual environment on Mozilla Hubs, which is an open source platform in internet environment (Figure 5).



Figure 5. 360 degree panoramic image of Mardin Şeyh Çabuk Mosque taken by NCTech iris360° Model Panoramic Imaging Device

Mozilla Hubs platform is a free platform, which may be accessed by everyone at any place with internet connection, and may be used without downloading any software or programme onto the computer environment. The buildings are transformed into 3D environments, where the insides can be toured, utilising the feature of transforming the panoramic images into 3D environments, provided by Mozilla Hubs platform.

Furthermore, if it is desired to add other 3D models into the venue, again 3D point clouds may be obtained by importing the 360 degree panoramic photograph of the selected building into the photogrammetric modelling programme "Agisoft Photoscan", which supports 360° image infrastructure. The use of these models may be downloaded into the environment, which is created through uploading into sketchfab open source, which is a feature of Mozilla hubs site. In addition, sketchfab is a source, which is open-sourced and in which the individuals all around the world may upload their 3D models, and every model created as such and uploaded into sketchfab is a data source for the students and other interdisciplinary professions involved in cultural heritage.

2.2. Stages of obtaining 3D virtual environment

First, login in Mozilla Hubs internet site (<https://hubs.mozilla.com>). Then, 'Join Room' tab is clicked on the screen opened (Figure 6).

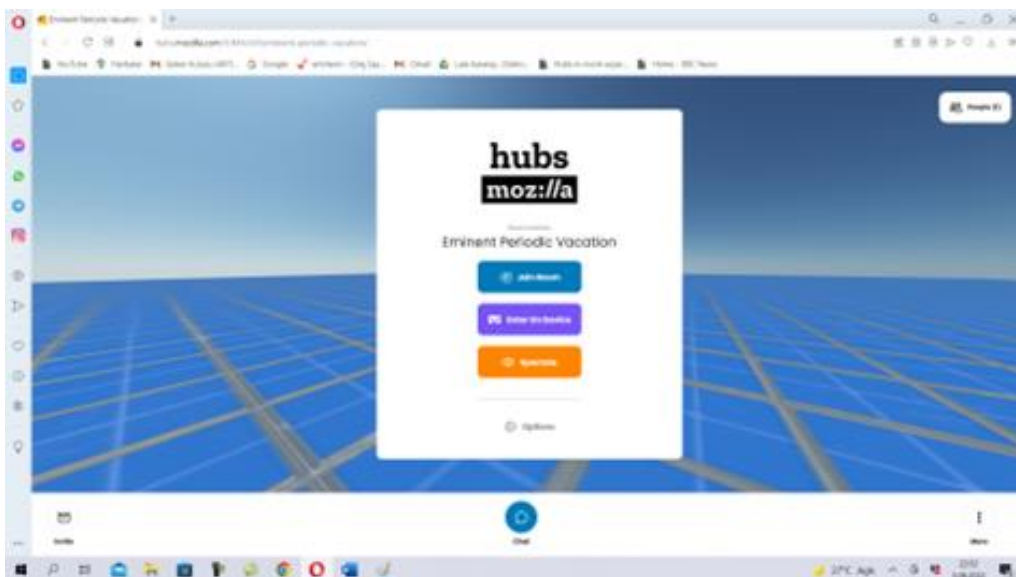


Figure 6. Mozilla Hubs login screen

Afterwards, the “place” tab is clicked on the screen opened and “scene” is clicked on the window opened. Then, the environment is entered in by clicking ‘new project’ tab on the new window opened (Figure 7).

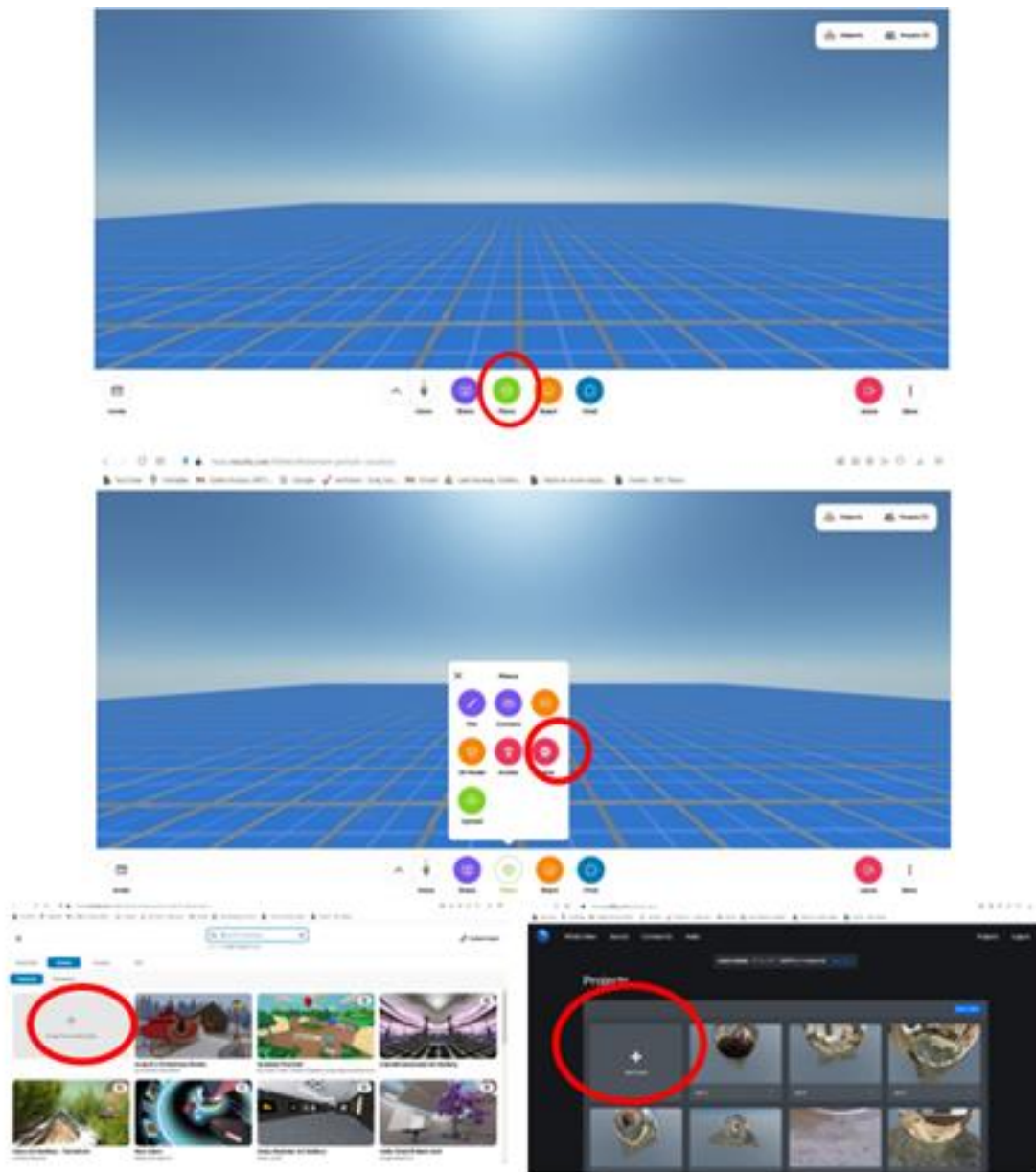


Figure 7. Creating scene on Mozilla Hubs platform

360 degree panoramic picture taken by Panoramic Imaging Device relating to structure, for which 3D image required to be taken, is uploaded by clicking on “image” section on the page appears. The uploaded picture shall come to the scene as flat. “360 degree tangular” button, which is on the tab next side, is clicked in order to transform this picture into 3D environment. When we enter into the environment, in order to walk around in a comfortable position, the “spawn point” tab again on the next side, that is the scale of the picture of the mosque imported into it with the scale of human eye, is adjusted and saved with the “image size” dimension again on the next tab. And, environment may be entered as 3D by clicking the “publish the hubs” tab placed on the rightmost upper side. In the section below, the screenshots of the steps that have to be followed in order to obtain 3D environment from a 360 degree panoramic picture in Mozilla Hubs environment are presented stage by stage (Figure 8).

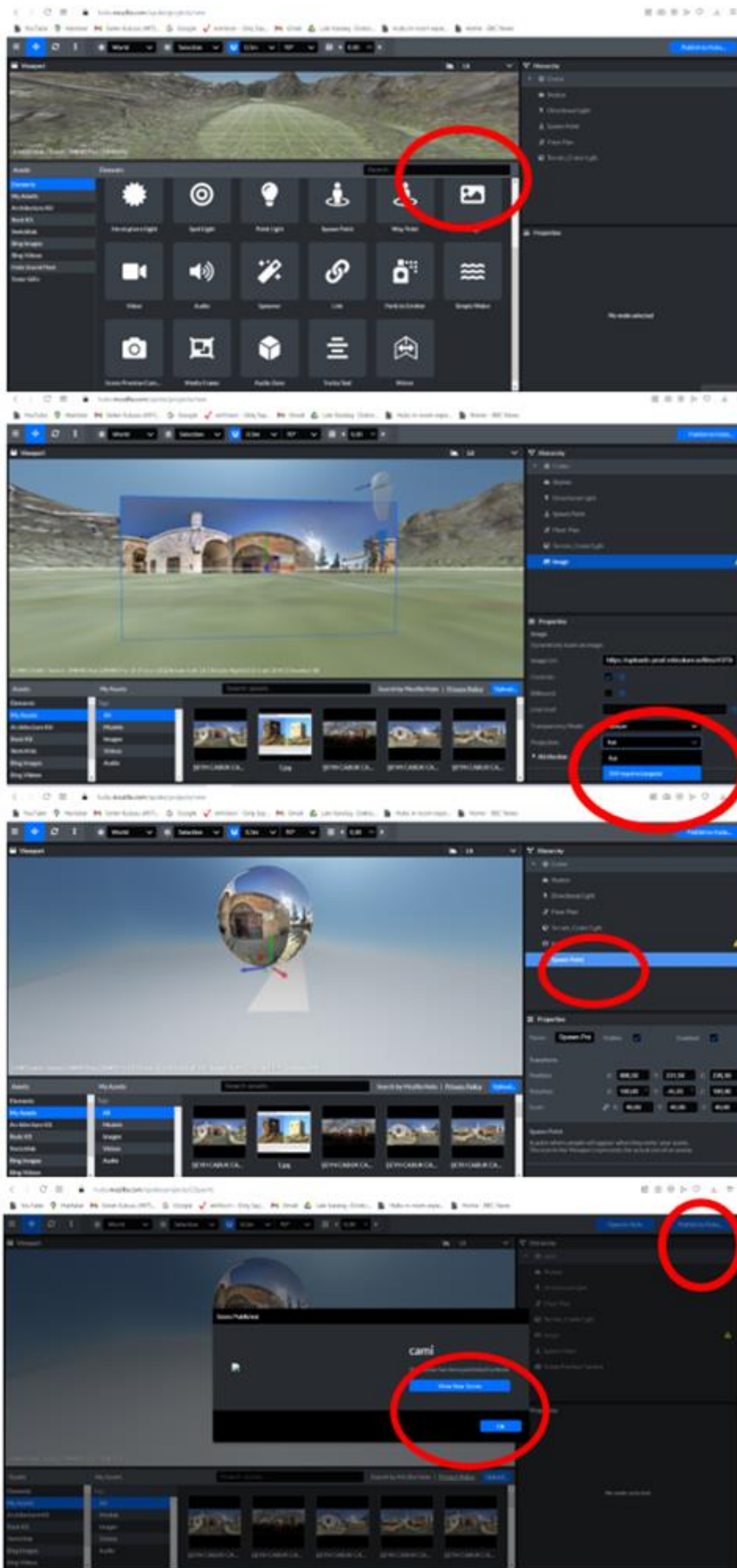


Figure 8. Transformation of 360 degree panoramic images into 3D virtual environment on Mozilla Hubs platform

3. Results

3D virtual environment was obtained regarding the building from the 360 degree panoramic photographs under the study and deterioration maps were defined over this virtual environment.

3.1. Obtaining 3D virtual environment of the building

Virtual environment of Melik Mahmut Mosque was obtained from 360 degree panoramic photographs in Mozilla Hubs programme. The building can be perceived clearly, toured in the virtual environment and the information on its materials and material deteriorations can be displayed in detail by zooming in and out thanks to the avatars. The images of the building in the virtual environment are presented in the figures below (Figure 9).

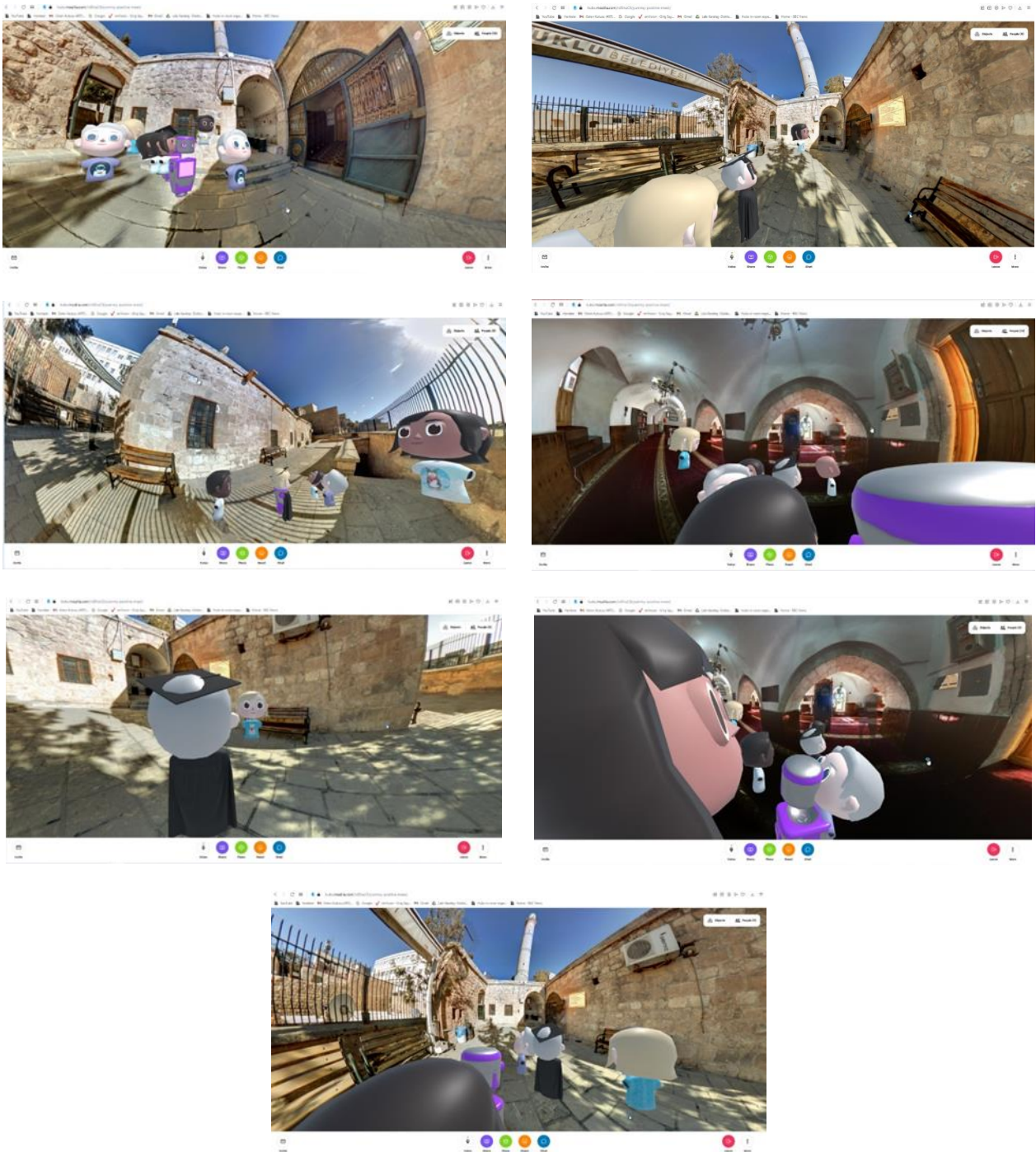


Figure 9. Images of 3D Model of Mardin Şeyh Çabuk Mosque on Mozilla Hubs Environment

4. Discussion

The aim of this study is to present a method, which integrates the photogrammetry and virtual reality technologies in order to obtain 3D model of a stone building with a reasonable cost and in a short time; and to research the stone material deteriorations over the 3D model obtained. The method presented within the scope of the study enables to display a stone building as 3D with a reasonable cost and in a relatively short period, such as 2 minutes, by eliminating the cost caused by the laser scanning to create a 3D model [22-25] and the data burden regarding the 3D point cloud obtained through photogrammetric methods [26], which are the disadvantages emphasized in the literature. Material deteriorations can be investigated in detail by zooming in and out with the avatars on the building, with the advantage of touring the building in the virtual environment. Thus, it enables the complete documentation of the diagnosis of the material problem on the building, since it displays the link between the damages on more than one sides of the building in the virtual environment. This conclusion demonstrates that the method presented in this study may eliminate the disadvantage [19] that 2D documentation enables only the regional focusing, which is emphasized in various studies in the literature.

In the study, the virtual environment could be obtained from the global panoramic images rapidly. This result supports the finding obtained by Napolitano et. al [19] that the virtual reality environments are obtained from the panoramic images rapidly and the use of global panoramic images provide great convenience in 3D documentation procedure to the user in terms of time and cost. Furthermore, the study results verify the finding obtained by Mah et. al [23] in their study results that this method is advantageous because of increasing the accessibility for heritage practitioners through a 360° camera, which does not require high levels of technical specialty when compared with the other digital and visualization technologies, and the relatively low pricing of the 360 degree camera; and facilitating the future practices.

5. Conclusion

With the study conducted, a method is presented, which integrates the photogrammetry and virtual reality technologies in order to obtain 3D model of a stone building with a reasonable cost and in a short time; and the detectability of the stone material deteriorations over the 3D model obtained is researched. Within this scope, as a result of the study it is concluded that the virtual 3D environment regarding the building can be created from the global panoramic photographs with the suggested method on Mozilla Hubs platform, which is an open-sourced website, with a reasonable cost and in a very short time; and stone material deteriorations regarding the building can be determined easily on this virtual environment.

As a result of the study, it is seen that it is possible to add other 3D models into the venue in, Mozilla Hubs environment. Another finding is that these models can be uploaded easily into the media that is created by uploading into the sketchfab open source, which is a feature available in Mozilla Hubs website, after the 360 degree panoramic photograph of the selected building is imported into the "Agisoft Photoscan" programme, which is a photogrammetric modelling programme supporting the 360° image infrastructure, and the 3D point clouds of the buildings are obtained. Besides, it is seen that it is possible to upload the 3D historical building models we made and their materials free of charge on Mozilla Spoke page by clicking the 'custom url or file' button located on the rightmost upper part on sketchfab tab. It is seen that with this method it is possible to create an open data library, where the materials of the buildings and the material deteriorations may be investigated closely and determined, as Sketchfab is a source, which is open-sourced and in which the individuals all around the world may upload their 3D models, and every model created as such and uploaded into sketchfab is a data source for the students and other interdisciplinary professions involved in cultural heritage. As a result of increasingly growth of these open data clusters, it shall be possible to create a material library.

It is suggested to create the virtual environments of the historical buildings in different countries with the systematic followed in our study, in order to obtain a library regarding the stone material deteriorations in future studies. Thus, an open data library shall be created and every individual in another place of the world shall have the chance to view, tour and investigate all historical buildings, which are documented in this environment, free of charge.

Acknowledgement

I would like to thank to the people of Mardin Şeyh Çabuk Mosque.

Funding

This research received no external funding.

Conflicts of interest

The authors declare no conflicts of interest.

References

1. Alptekin, A., Çelik, M. Ö., & Yakar, M. (2019). Anıtmezarın yersel lazer tarayıcı kullanarak 3B modellenmesi. *Türkiye Lidar Dergisi*, 1(1), 1-4.
2. Alptekin, A., & Yakar, M. (2021). 3D model of Üçayak Ruins obtained from point clouds. *Mersin Photogrammetry Journal*, 3(2), 37-40.
3. Kanun, E., Alptekin, A., & Yakar, M. (2021). Cultural heritage modelling using UAV photogrammetric methods: a case study of Kanlıdivane archeological site. *Advanced UAV*, 1(1), 24-33.
4. Rives, V., & Talegon, J. G. (2006). Decay and conservation of building stones on cultural heritage monuments. In *Materials science forum* (Vol. 514, pp. 1689-1694). Trans Tech Publications Ltd.
5. Normal, R. (1990). 1/88: Alterazioni macroscopiche dei materiali lapidei: Lessico. *CNRICR, Roma*.
6. Henriques, F. M. A., Rodrigues, J. D., Aires-Barros, L., & Proença, N. (2005). Materiais pétreos e similares- Terminologia das formas de alteração e degradação. *LNEC, Lisboa, Portugal*.
7. Fitzner, B., Heinrichs, K., & Kownatzki, R. (1995). *Weathering Forms, Classification and Mapping: Verwitterungsformen-Klassifizierung und Kartierung*. Ernst and Sohn.
8. VDI, 3798 (1998). Untersuchung und Behandlung von immissionsgeschädigten Werkstoffen, insbesondere bei kulturhistorischen Objekten. Die Graphische Dokumentation. VDIRichtlinien, 1-27.
9. Vergès-Belmin, V. (2010). ICOMOS-ISCS: Illustrated glossary on stone deterioration patterns= Ilustrovaný glosar projevu poskozeni kamene.
10. Adamopoulos, E., & Rinaudo, F. (2021). Combining multiband imaging, photogrammetric techniques, and FOSS GIS for affordable degradation mapping of stone monuments. *Buildings*, 11(7), 304.
11. Bozdağ, A., İnce, İ., Bozdağ, A., Hatır, M. E., Tosunlar, M. B., & Korkaç, M. (2020). An assessment of deterioration in cultural heritage: The unique case of Eflatunpınar Hittite Water Monument in Konya, Turkey. *Bulletin of Engineering Geology and the Environment*, 79(3), 1185-1197.
12. Franković, M., Novaković, N., & Matović, V. (2015). Damage quantification of built stone on Dark Gate (Belgrade, Serbia): sample of damage index application for decay rate evaluation. *Environmental Earth Sciences*, 73(10), 6181-6193.
13. Hatır, M. E., İnce, İ., & Korkaç, M. (2021). Intelligent detection of deterioration in cultural stone heritage. *Journal of Building Engineering*, 44, 102690.
14. Kramar, S., Mladenović, A., Pristacz, H., & Mirtič, B. (2011). Deterioration of the black Drenov Grič limestone on historical monuments (Ljubljana, Slovenia). *Acta Carsologica*, 40(3), 483-495
15. Patil, S. M., Kasthurba, A. K., & Patil, M. V. (2021). Characterization and assessment of stone deterioration on heritage buildings. *Case Studies in Construction Materials*, 15, e00696.
16. Steiger, M., Charola, A. E., & Sterflinger, K. (2011). Stone in architecture. *Stone in Architecture: Properties*, 225-315.
17. Rodrigues, J. D. (2015). Defining, mapping and assessing deterioration patterns in stone conservation projects. *Journal of Cultural Heritage*, 16(3), 267-275.
18. Smith, B. J., Curran, J. M., Warke, P. A., Adamson, C., Stelfox, D., & Savage, J. (2013). Stone-built heritage inventory and 'performance in use' condition assessment of stonework. *Quarterly Journal of Engineering Geology and Hydrogeology*, 46(4), 391-404.
19. Napolitano, R. K., Scherer, G., & Glisic, B. (2018). Virtual tours and informational modeling for conservation of cultural heritage sites. *Journal of Cultural Heritage*, 29, 123-129.
20. Yakar, M., Yılmaz, H. M., & Mutluoğlu, Ö. (2010). Close range photogrammetry and robotic total station in volume calculation.
21. Taşdemir, Ş., Yakar, M., Ürkmez, A., & İnal, Ş. (2008, June). Determination of body measurements of a cow by image analysis. In *Proceedings of the 9th International Conference on Computer Systems and Technologies and Workshop for PhD Students in Computing* (pp. V-8).
22. Yakar, M. (2009). Digital elevation model generation by robotic total station instrument. *Experimental Techniques*, 33(2), 52-59.
23. Mah, O. B. P., Yan, Y., Tan, J. S. Y., Tan, Y. X., Tay, G. Q. Y., Chiam, D. J., ... & Feng, C. C. (2019). Generating a virtual tour for the preservation of the (in) tangible cultural heritage of Tampines Chinese Temple in Singapore. *Journal of Cultural Heritage*, 39, 202-211.
24. Murphy, M., McGovern, E., & Pavia, S. (2009). Historic building information modelling (HBIM). *Structural Survey*, 27(4), 311-327.
25. Percy, K., Ward, S., Quintero, M. S., & Morrison, T. (2015). Integrated digital technologies for the architectural rehabilitation & conservation of Beinn Bhreagh Hall & surrounding site, Nova Scotia, Canada. *ISPRS Annals of the Photogrammetry, Remote Sensing and Spatial Information Sciences*, 2(5), 235.
26. Barazzetti, L., Binda, L., Scaioni, M., & Taranto, P. (2011). Photogrammetric survey of complex geometries with low-cost software: Application to the 'G1' temple in Myson, Vietnam. *Journal of Cultural Heritage*, 12(3), 253-262.

27. Alptekin, A., & Yakar, M. (2020). Heyelan bölgesinin İHA kullanarak modellenmesi. *Türkiye İnsansız Hava Araçları Dergisi*, 2(1), 17-21.
28. Haddad, N. A. (2011). From ground surveying to 3D laser scanner: A review of techniques used for spatial documentation of historic sites. *Journal of King Saud University-Engineering Sciences*, 23(2), 109-118.
29. Economou, M. (2015). Heritage in the digital age. *A companion to heritage studies*, 15, 215-228.
30. Erener, A., & Yakar, M. (2012). Monitoring coastline change using remote sensing and GIS technologies. *Lecture Notes in Information Technology* 30, 310-314
31. Campanaro, D. M., Landeschi, G., Dell'Unto, N., & Touati, A. M. L. (2016). 3D GIS for cultural heritage restoration: A 'white box' workflow. *Journal of Cultural Heritage*, 18, 321-332.
32. Doğan, Y., & Yakar, M. (2018). GIS and three-dimensional modeling for cultural heritages. *International Journal of Engineering and Geosciences*, 3(2), 50-55.
33. Yılmaz, H. M., Yakar, M., Mutluoğlu, O., Kavurmacı, M. M., & Yurt, K. (2012). Monitoring of soil erosion in Cappadocia region (Selime-Aksaray-Turkey). *Environmental Earth Sciences*, 66(1), 75-81.
34. Unal, M., Yakar, M., & Yildiz, F. (2004, July). Discontinuity surface roughness measurement techniques and the evaluation of digital photogrammetric method. In *Proceedings of the 20th international congress for photogrammetry and remote sensing, ISPRS* (Vol. 1103, p. 1108).
35. Yakar, M., Yılmaz, H. M., & Mutluoğlu, H. M. (2009). Hacim Hesaplamalarında Laser Tarama ve Yersel Fotogrametrinin Kullanılması, TMMOB Harita ve Kadastro Mühendisleri Odası 12. *Türkiye Harita Bilimsel ve Teknik Kurultayı, Ankara*.
36. Altun, A. (1971). *Turkish Era Architecture in Mardin*. Acar Basım, İstanbul, 168 s.



© Author(s) 2022. This work is distributed under <https://creativecommons.org/licenses/by-sa/4.0/>



Mineralogy and geochemical signatures of the Mn mineralization in Taşdemir (Pazarcık, Kahramanmaraş, Türkiye)

Cihan Yalçın ¹, Mustafa Tekin Akkütük ², Yusuf Uras ²

¹ Ministry of Industry and Technology, General Directorate of Industrial Zones, Ankara, Türkiye, cihan.yalcin@sanayi.gov.tr

² Kahramanmaraş Sütçü İmam University, Department of Geological Engineering, Türkiye, mtekinakkutuk@gmail.com; yuras@ksu.edu.tr

Cite this study: Yalçın, C., Akkütük, M. T. & Uras, Y. (2022). Mineralogy and geochemical signatures of the Mn mineralization in Taşdemir (Pazarcık, Kahramanmaraş, Türkiye). *Advanced Engineering Science*, 2, 147-153

Keywords

Karadut Complex
Radiolarite
Pyrolusite
Manganite
Taşdemir

Research Article

Received: 23.09.2022

Revised: 22.10.2022

Accepted: 28.10.2022

Published: 21.11.2022



Abstract

Along the Southeast Anatolian Orogenic Belt, units on the Arabian plate and a series of Ophiolitic Melange overlain by tectonic contact are observed. In the Upper Cretaceous thrust belt, the Koçali Complex is situated at the base and the Karadut Complex at the top, respectively. Throughout this belt, Mn mineralization is identified in the lithologies of the Karadut Complex. Around Taşdemir Village (Pazarcık-Kahramanmaraş), units existing in the Koçali and Karadut Complex are frequently observed. Haydar and Germav formations overlie these units with angular unconformity. All units are consequently covered with Middle-Upper Eocene aged limestones existing to the Midyat Group with angular unconformity. In this district, Mn mineralizations linked with the radiolarites of the Karadut Complex are observed. Stratiform-type Mn mineralization is observed through lenses between the layers. Reddish brown and dark grey forms have been identified. Pyrolusite and manganite minerals are identified in XRD analysis. Major oxide and trace element analyses of samples gathered from the ore zone were carried out. As a result of the analysis, the MnO range was detected as 7.42-32.76% (average 20.65), and the SiO₂ range was detected as 60.68-83.52% (average 72.88). Fe/Mn rate is considerably lower than 0.1. On average, the MnO/TiO₂ ratio of Taşdemir Mn mineralization is 483.65, indicating a pelagic environment. In addition, the Fe₂O₃-Al₂O₃/(Al₂O₃+Fe₂O₃) diagram supports this conclusion. Major and trace elements are evaluated in the diagrams to highlight the origin of manganese mineralization. These evaluations indicate that the mineralization is of hydrothermal origin.

1. Introduction

In addition to being a strength-enhancing substance in the iron and steel industry, manganese is also widely used in battery technology concerning green energy growth in recent years. The need for manganese, which contains significant physical and chemical properties, is increasing daily. For this reason, mineral deposit exploration is also widespread.

Mn deposits observed in many geological environments correspond to their geological, tectonic, mineralogical, and geochemical properties. These are; (1) hydrogenous, (2) hydrothermal, and (3) diagenetic deposits, respectively [1-3]. In these classifications, Fe/Mn contents also offer significant clues about the origin of the deposit [4]. Since manganese deposits in Turkey are related to the evolution of the Tethys Ocean, the deposits have been described in different geological environments [5-9]. The belts that stand out from these deposits are the İzmir-Ankara-Erzincan Suture Belt and the Southeastern Anatolian orogenic belt. These belts contain hydrothermal and hydrogenetic manganese deposits associated with radiolarian cherts [7, 9]. There are many manganese

mineralizations in the Southeastern Anatolian Orogenic Belt, where the study area is located, in the literature [10-11].

Kahramanmaraş has attracted the attention of many geoscientists due to its geological features. Important geological structures are observed in the Kahramanmaraş region, an important area where the Taurus Orogenic Belt and the Arabian Plate are sutured. Because of this complex structure, Gül [12] defined these regions as the Orogenic belt and the Arabian plate belt and divided the units belonging to these two belts into sub-belts. Taşdemir (Pazarcık, Kahramanmaraş) manganese mineralization is orogenically located in two important tectonic units, the Southeast Fold Belt and the Eastern Taurus Orogenic Belt (Figure 1a). According to Gül [12], the study area is located in the margin fold belt at the northern end of the Arabian plate (Figure 1b). Mn mineralization is observed in the sedimentary rocks outcropping in the Taşdemir (Pazarcık) region. This paper reveals the geological, mineralogical, and geochemical characteristics of mineralization.

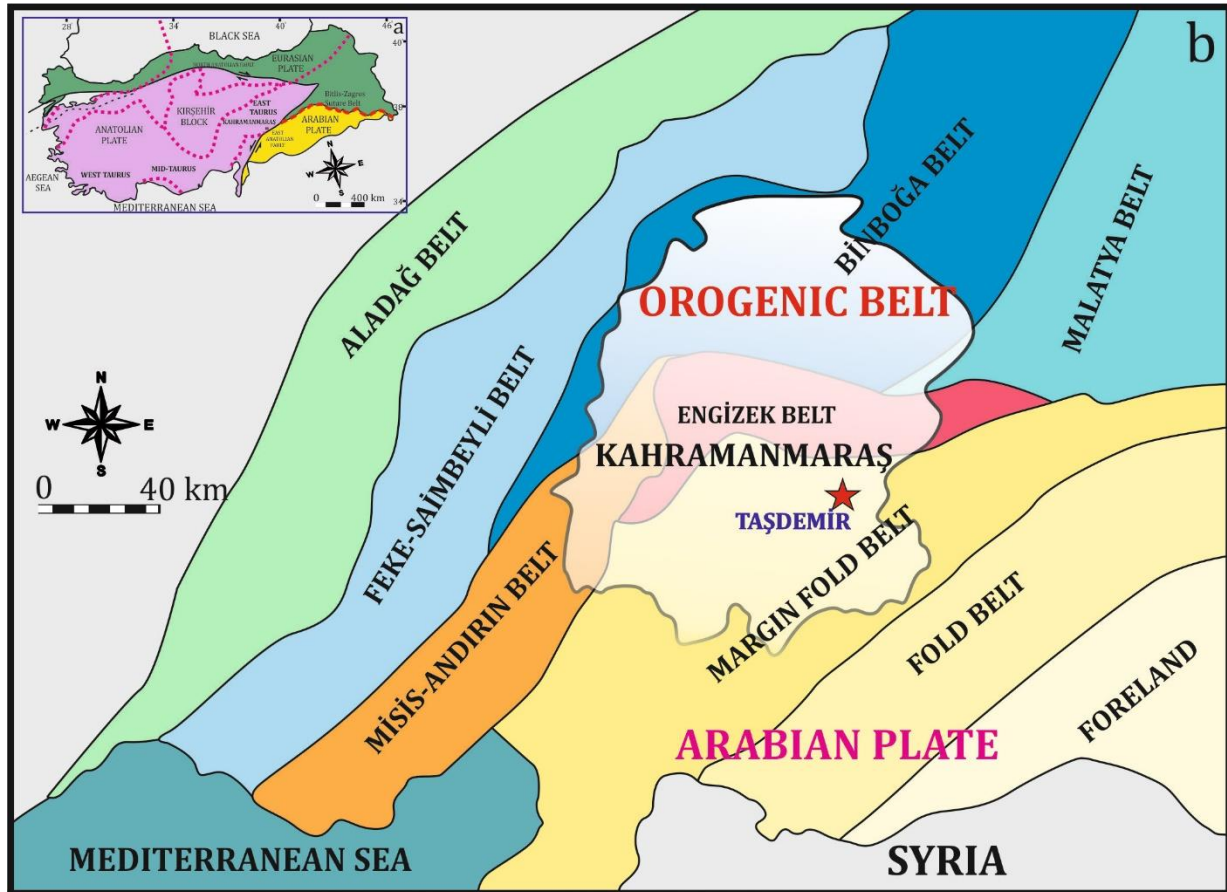


Figure 1. a. Tectonic location of the Kahramanmaraş (modified from Işık [13]), b. Tectonic location of the study area according to Gül [12].

2. Material and Method

The 1/25,000 scaled geological map of the study area prepared by MTA on the M39d4 sheet was used. The geological structures in the region were evaluated based on this map. Samples were collected from a 50-meter-long trench opened in the study area for ore work.

Observational geological investigations were carried out in the ore zone. As a result of the observations, sampling was made in the ore zone to conduct mineralogical and geochemical studies. These samples' major oxide and trace element analyses were performed at ITU-JAL using XRF and ICP-MS methods. XRD analyses were also performed for mineralogical identification.

2.1. Geological Background

Around Taşdemir Village (Pazarcık-Kahramanmaraş), units belonging to the Koçali and Karadut Complexes are commonly observed (Figure 2). Haydar and Germav formations overlie these units with angular unconformity. All units are covered with Middle-Upper Eocene aged limestones belonging to the Midyat Group with angular unconformity (Figure 2). The contacts of the melange in the study area are generally tectonic. Dip-slip faults cut thrust zones in places and strike-slip faults in places. In this region, Mn mineralization associated with the radiolarites of the Karadut Complex are observed.

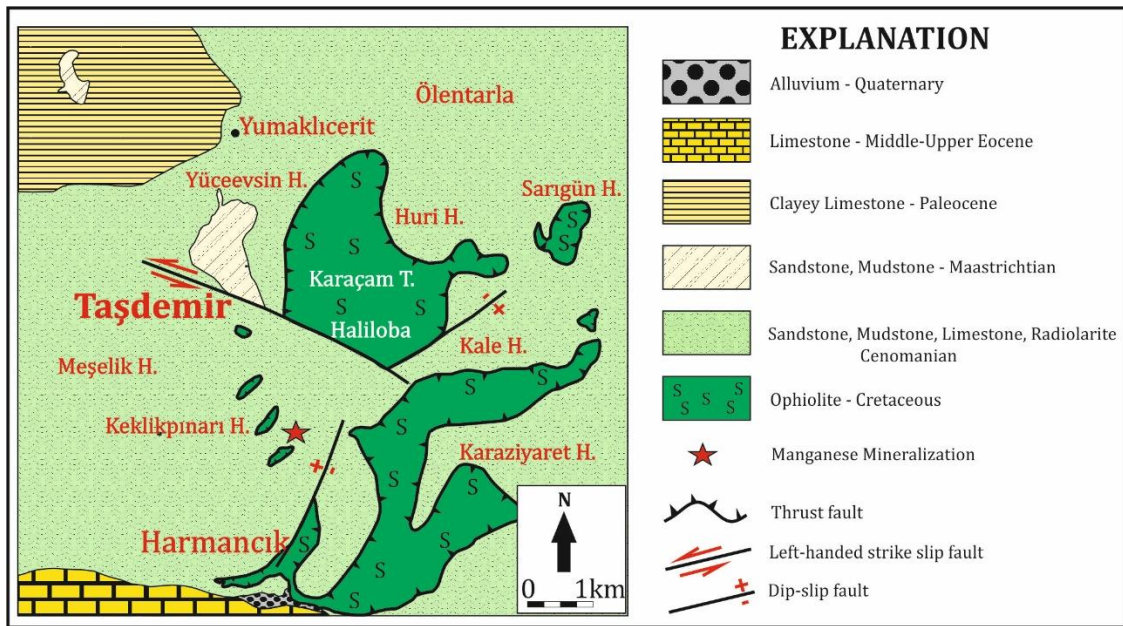


Figure 2. Geological map of the study area [14]

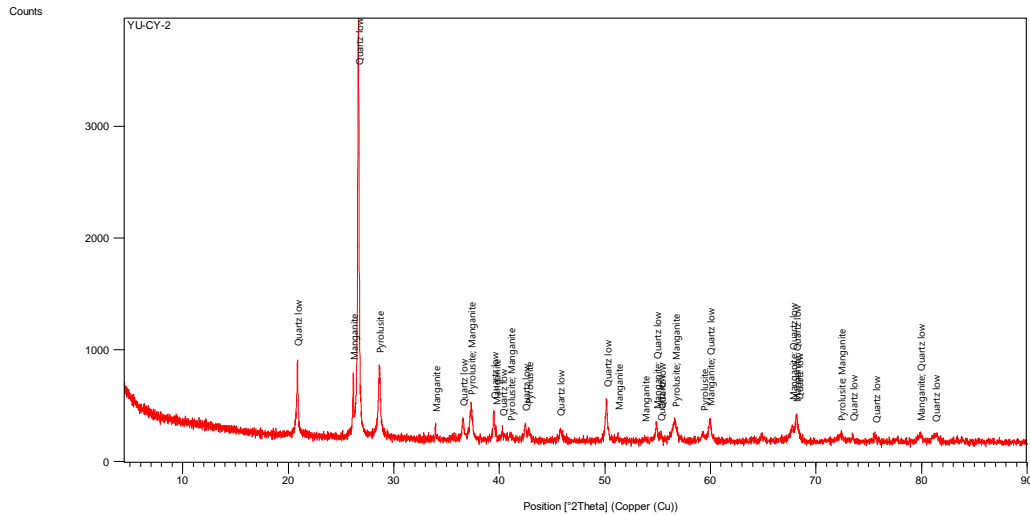
2.2. Ore Geology

The mineralization consists of short and medium-sized lenses conforming with the layers (Figure 3). It is commonly exposed at different levels of the layers of the succession. This formation continues along a zone of approximately 250 m. The ore lenses, which can be identified in the field with their blackish colour, have also been altered in places (Figure 3). The host rock is Cenomanian aged radiolarite, the upper layers of succession.

XRD study was carried out for the mineralogical identification of the samples taken from this ore zone. As a result of the analysis, pyrolusite and manganite minerals were determined (Figure 4).



Figure 3. General view of radiolarite-hosted manganese mineralization



Ref. Code	Mineral Name	Chemical Formula
98-000-5737	Pyrolusite	Mn1 O2
98-003-9931	Manganite	H1 Mn1 O2

Figure 4. XRD analysis of manganese mineralization

3. Geochemistry

Geochemical analyses of the samples collected from the ore zone were carried out (Table 1). According to the analysis, the amount of SiO₂ is rather rich. The reason for this is the intense exposure to radiolarites. MnO values at ore levels are between 7.42-32.76%. There is no substantial anomaly when the other major oxide values are examined. No alternative metallic enrichment is observed in samples with high manganese.

In the Si–Al discrimination diagram [15], the mineralization is distributed within the hydrothermal field due to low Al and high Si content (Figure 5). Likewise, in the triangular diagram [16], a different diagram in which trace elements such as Co, Zn, and Ni are compared relative to each other shows the distribution in the hydrothermal area (Figure 6).

Table 1. Major oxide concentration (%) of the manganese mineralization

SAMPLE	T 2	T 7	T 15	T 17	T 19	T 20	T 23
SiO ₂	67,96	86,18	64,74	65,11	83,52	82,00	60,68
Al ₂ O ₃	0,36	0,46	1,28	0,72	2,90	1,47	0,92
Fe ₂ O ₃	0,15	0,21	0,73	0,34	1,43	0,63	0,44
MgO	0,01	0,04	0,42	0,15	0,59	0,28	0,19
CaO	0,22	0,15	0,41	0,19	0,42	0,31	0,22
Na ₂ O	0,01	0,08	0,06	0,04	0,12	0,09	0,05
K ₂ O	0,00	0,07	0,17	0,09	0,47	0,21	0,09
TiO ₂	0,02	0,02	0,10	0,05	0,16	0,06	0,06
P ₂ O ₅	0,14	0,05	0,10	0,00	0,08	0,09	0,10
MnO	27,12	8,88	27,30	29,05	7,42	12,09	32,76
Cr ₂ O ₃	0,01	1,57	0,02	0,01	0,00	0,00	0,01
LOI	3,87	2,10	4,46	4,10	2,82	2,67	4,32
TOTAL	99,86	99,83	99,80	99,87	99,94	99,90	99,85
Co	59,79	110,04	40,39	41,79	26,04	37,42	38,42
Ni	58,00	823,69	59,22	30,74	25,07	28,86	39,57
Zn	54,24	20,98	50,59	31,77	21,89	24,00	41,64
MnO/TiO ₂	1233,82	501,54	272,06	611,29	47,73	206,27	512,85
Fe/Mn	0,00	0,02	0,02	0,01	0,17	0,05	0,01

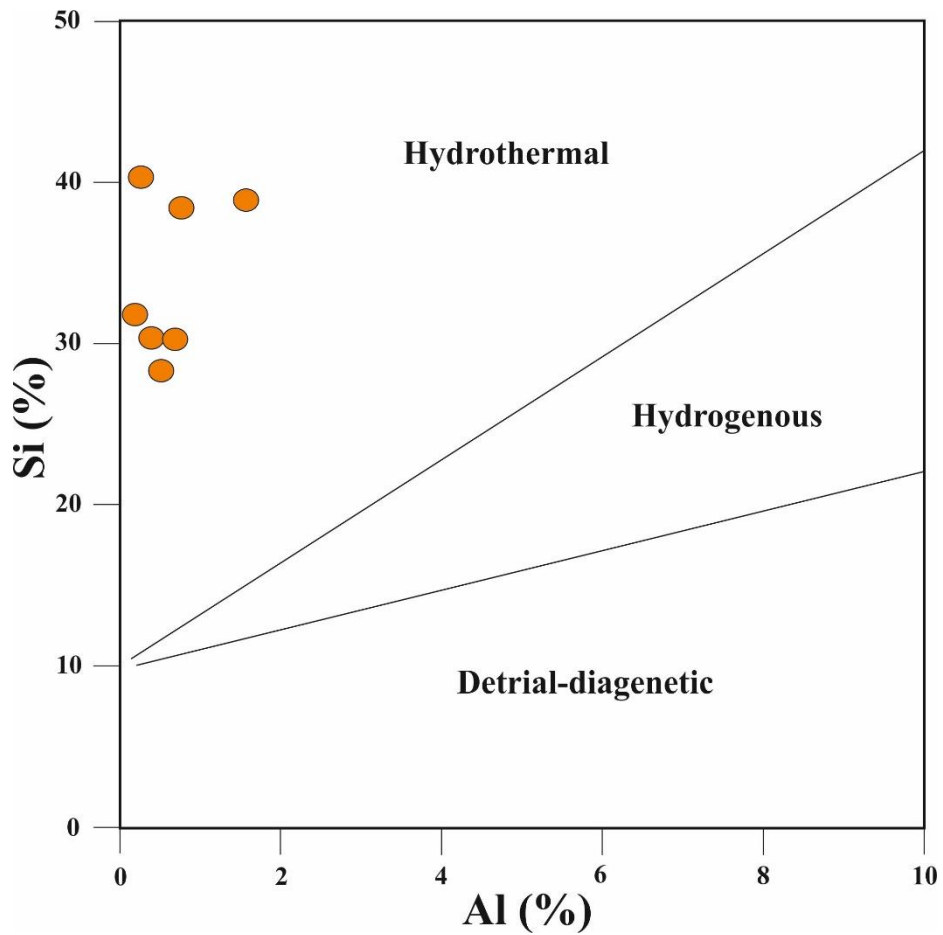


Figure 5. Si-Al discrimination diagram [15]

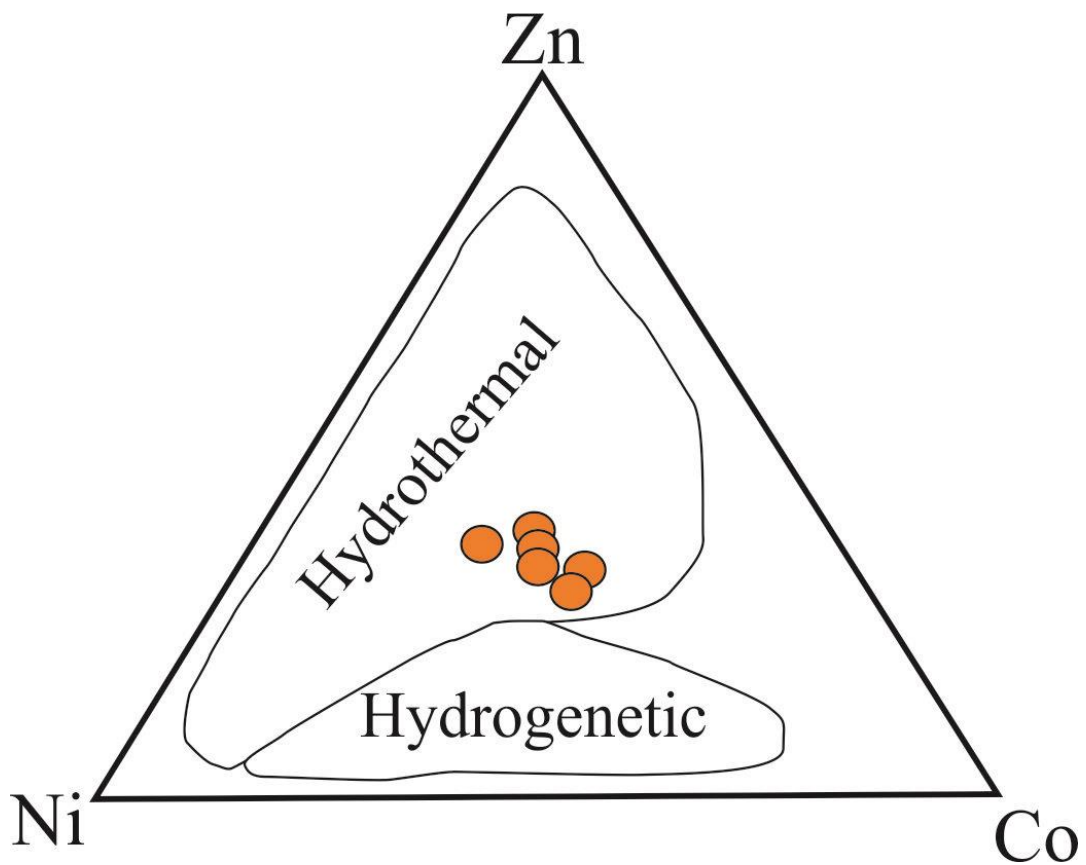


Figure 6. Zn-Ni-Co discrimination diagram [16]

In manganese formations associated with marine sedimentary rocks, the deposition environment is near the Spread ridge, pelagic (open ocean), and continental margin [17]. In order to explain the deposition environments of manganese formations associated with chert, radiolarian chert, and shale, the MnO/TiO₂ ratio is checked [18-19]. MnO/TiO₂ ratio < 0.5 indicates continental margin sedimentation environment and > 0.5 indicates pelagic environment. On average, the MnO/TiO₂ ratio of Taşdemir Mn mineralization is 483.65, indicating a pelagic environment. In addition, the Fe₂O₃-Al₂O₃/(Al₂O₃+Fe₂O₃) diagram (Figure 7) used to reveal the storage environment still supports the above ratio [20].

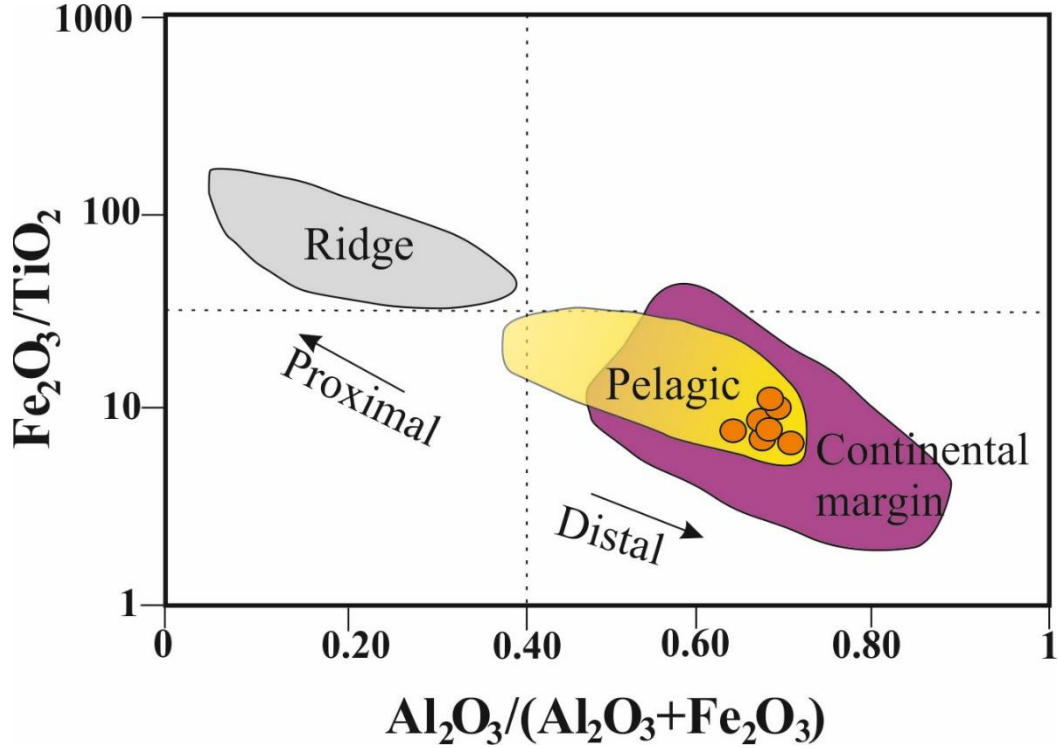


Figure 7. Plots of Fe₂O₃-Al₂O₃/(Al₂O₃+Fe₂O₃) diagram [20]

4. Conclusion

One of the basic approaches for identifying manganese deposits is the Fe/Mn ratio of the ore. In studies on manganese mineralizations of various types [21-22], the Fe/Mn ratio of mineralization (Table 1) is 1 in hydrogenetic deposits that slowly precipitate from seawater. In the submarine hydrothermal deposits around the region, <0.1 (manganese-rich) and >10 (rich in iron) were determined. Very low Fe/Mn ratios are explained by the rapid precipitation of hydrothermal solutions in submarine hydrothermal centers. Fe/Mn ratios in this study are considerably lower than 0.1 and resemble submarine hydrothermal deposits.

The data obtained in this study determined that Taşdemir Mn mineralization is related to Cenomanian-aged radiolarites, and pyrolusite and manganite are found as manganese minerals. According to the results of geochemical analysis, mineralization characterizes a hydrothermal deposit associated with volcanism in the pelagic environment.

Acknowledgement

This study was supported by Kahramanmaraş Sütçü İmam University Scientific Research Projects Coordination Unit. Project No: 2020/6-2 YLS.

This study was partly presented at the 4th Advanced engineering Days [23] on 21 September 2022.

Funding

This research received no external funding.

Author contributions

Cihan Yalçın: Data curation, Methodology, Writing-Original draft preparation, Editing. **Mustafa Tekin Akkütük:** Petrography, Geochemistry. **Yusuf Uras:** Software, Visualization, Investigation.

Conflicts of interest

The authors declare no conflicts of interest.

References

1. Roy, S. (1992). Environments and processes of manganese deposition. *Economic Geology*, 87(5), 1218-1236.
2. Hein, J. R., Koschinsky, A., Halbach, P., Manheim, F. T., Bau, M., Kang, J. K., & Lubick, N. (1997). Iron and manganese oxide mineralization in the Pacific. *Geological Society, London, Special Publications*, 119(1), 123-138.
3. Polgári, M., Hein, J. R., Vigh, T., Szabó-Drubina, M., Főrizs, I., Bíró, L., ... & Tóth, A. L. (2012). Microbial processes and the origin of the Úrkút manganese deposit, Hungary. *Ore Geology Reviews*, 47, 87-109.
4. Hein, J. R., Gibbs, A. E., Clague, D. A., & Torresan, M. (1996). Hydrothermal mineralization along submarine rift zones, Hawaii. *Marine georesources & geotechnology*, 14(2), 177-203.
5. Özgür, V. (1990). The Views on Geology. *Deposition and Genesis of Manganese Deposit in Cayırlı (Ankara-Haymana) Bulletin of MTA*, 110, 29-43.
6. Öztürk, H., & Frakes, L. A. (1995). Sedimentation and diagenesis of an Oligocene manganese deposit in a shallow subbasin of the Paratethys: Thrace Basin, Turkey. *Ore Geology Reviews*, 10(2), 117-132.
7. Öztürk, H. (1993). Manganese mineralizations in Turkey: Processes of formation and types. *Istanbul University Eng. Fac. Geological Engineering Pub*, 43, 24.
8. Öztürk, H. (1993). Characteristics and formations of fossil manganese nodules in the Koçali Komplex, Adıyaman, Turkey. *Geol Bull Turk*, 36, 159-169.
9. Öztürk, H., Kasapçı, C., & Özbaş, F. (2019). Manganese deposits of Turkey. In *Mineral Resources of Turkey* (pp. 261-281). Springer, Cham.
10. Altunbey, M., & Sağıroğlu, A. (1995). Properties and origins of Koçkale-Elazığ manganese mineralizations. *Bulletin of the Mineral Research and Exploration*, 117, 139-148.
11. Şaşmaz, A., Türkyılmaz, B., Öztürk, N., Yavuz, F., & Kumral, M. (2014). Geology and geochemistry of Middle Eocene Maden complex ferromanganese deposits from the Elazığ-Malatya region, eastern Turkey. *Ore geology reviews*, 56, 352-372.
12. Gül, M.A., (2000). Kahramanmaraş yöresinin jeolojisi. Hacettepe Üniversitesi, Fen Bilimleri Enstitüsü, Doktora Tezi, 304 s.
13. Işık, V. (2016). Torosların Jeolojisi; Türkiye Jeolojisi Ders Notu. *Ankara Üniversitesi, Jeoloji Mühendisliği Bölümü, Ankara*.
14. MTA. 1/25.000 Scaled geology map of the m39d4
15. Peters, T. (1988). Geochemistry of manganese-bearing cherts associated with Alpine ophiolites and the Hawasina formations in Oman. *Marine Geology*, 84(3-4), 229-238.
16. Choi, J. H., & Hariya, Y. (1992). Geochemistry and depositional environment of Mn oxide deposits in the Tokoro Belt, northeastern Hokkaido, Japan. *Economic Geology*, 87(5), 1265-1274.
17. Murray, R. W., Buchholtz ten Brink, M. R., Jones, D. L., Gerlach, D. C., & Russ III, G. P. (1990). Rare earth elements as indicators of different marine depositional environments in chert and shale. *Geology*, 18(3), 268-271.
18. Sugisaki, R., Yamamoto, K., & Adachi, M. (1982). Triassic bedded cherts in central Japan are not pelagic. *Nature*, 298(5875), 644-647.
19. Kunimaru, T., Shimizu, H., Takahashi, K., & Yabuki, S. (1998). Differences in geochemical features between Permian and Triassic cherts from the Southern Chichibu terrane, southwest Japan: REE abundances, major element compositions and Sr isotopic ratios. *Sedimentary geology*, 119(3-4), 195-217.
20. Murray, R. W. (1994). Chemical criteria to identify the depositional environment of chert: general principles and applications. *Sedimentary Geology*, 90(3-4), 213-232.
21. Bonatti, E., Zerbi, M., Kay, R., & Rydell, H.S., (1976). Metalliferous deposits aphenine ophiolites. *Geological Society of American Bulletin*, 87, 83.
22. Crerar, D. A., Namson, J., Chyi, M. S., Williams, L., & Feigenson, M. D. (1982). Manganiferous cherts of the Franciscan assemblage; I, General geology, ancient and modern analogues, and implications for hydrothermal convection at oceanic spreading centers. *Economic Geology*, 77(3), 519-540.
23. Yalçın, C., Akkütük, M. T., & Uras, Y. (2022). Geological and Geochemical characterization of the radiolarite hosted Mn mineralization in Taşdemir (Pazarçık, Kahramanmaraş, Turkey). *Advanced Engineering Days (AED)*, 4, 93-95.

